

H24/3692

MONASH UNIVERSITY
THESIS ACCEPTED IN SATISFACTION OF THE
REQUIREMENTS FOR THE DEGREE OF
DOCTOR OF PHILOSOPHY

ON..... 26 August 2003

Sec. Research Graduate School Committee

Under the Copyright Act 1968, this thesis must be used only under the normal conditions of scholarly fair dealing for the purposes of research, criticism or review. In particular no results or conclusions should be extracted from it, nor should it be copied or closely paraphrased in whole or in part without the written consent of the author. Proper written acknowledgement should be made for any assistance obtained from this thesis.

ERRATA

- p 9 para 3, line 6: "pressurised" for "pressurized"
- p 11 para 3, first sentence: add "The" as in "The experimental part..."
- p 18 para 4, line 1: remove "in the"
- p 58 section 2.4.1, line 1: remove "a"
- p 62 line 5: "Yates (1996)" for "(Yates, 1996)"
- p 86 section 3.9, line 3: insert "of" as in "the motion of particles..."
- p 123 line 4: "Halow (1997)" for "(Halow, 1997)"

ADDENDUM

- p 4 figure 1-1: insert "0.1" at the origin of the Y-axis
- p 9 para 3, line 6: replace "to enable" with "in order to contribute to"
- p 18 line 4: replace "density of bed material" with "the particle density of the bed material"
- p 30 section 2.2.5.1, line 3: after "carbon dioxide" insert "in a 100mm-diameter and 1.9m-high column with a porous plate distributor"
- p 30 section 2.2.5.1, line 4: after "found" insert "by visual observation"
- p 30 para 2, line 4: after "who found" insert "in a similar experimental setup"
- p 30 para 3, line 3: after "with nitrogen" insert "in a small 45mm-diameter column with a sintered steel and a perforated steel distributors"
- p 30 para 3: add at the end: "According to Sobreiro and Monteiro (1982), at each flow rate, the pressure drop and the bed height were recorded and special care was taken while determining the minimum bubbling velocity. However, it is not clear how the minimum bubbling velocity was measured."
- p.32 para 3: comment: Varadi and Grace (1978) reported these interesting results of their preliminary study in a two-dimensional fluidized bed at a Fluidization conference, however further search for other publications based on their work produced no results.
- p 33 para 2, line 5: after "Later" insert "in a preliminary study,"
- p 34 para 1: comment: The minimum bubbling velocity was determined by Piepers et al. (1984) from a graph of the bed height versus the superficial velocity.
- p 34 para 2, line 3: after "range of particle sizes and" insert "determined the minimum bubbling velocity visually or graphically from the bed expansion curve when there was a transition from non-bubbling to bubbling fluidization."
- p 34 para 2, line 4: before "found" insert "They" as in "They found that in the majority..."
- p 34 para 3: comment: Jacob and Weimer (1987) established the minimum bubbling velocity graphically from the bed expansion curve.
- p 34 para 3, line 3: replace "an industrial pilot-scale fluidized bed" with "a 97mm-diameter and 2.8m-high fluidized bed with a porous metal distributor and"
- p 39 para 1: after "conditions" insert "due to excessive scattering of the experimental data in various researchers' reports"
- p 53: replace the last sentence with "Assuming the absence of bubble-bubble interactions and wall effects in a 130mm-diameter and 2.7m-high fluidized bed, Weimer and Quarderer (1985) inferred the mean bubble diameter from bubble rise velocity measured by statistical techniques and known bed operating parameters, and found the decrease in bubble size to be strongly dependent on particle size with greater bubble size decrease for smaller particles."
- p 54 para 2, line 1: after "examined" insert "using X-rays"
- p 54 para 4, line 1: after "King and Harrison (1980)" insert "investigated the slugging and bubbling behavior of a wide-size range of powders in a tall 100mm-diameter bed by X-ray photography and"
- p 55, line 3: after "other researchers" insert "used X-ray photography and"
- p 55, line 6: after "consistent with the" insert "capacitance probe"

p 59 para 3: insert "indirect" as in "possible indirect pressure influence..." and add at the end: "by virtue of the change in bubble characteristics".

p 61 para 3, second sentence: remove "available in the literature"

p 87 para 1: add at the end: "The video camera was mounted on a tripod in front of the observation window as described further in Section 6.2.1."

p 88 para 2: add at the end: "The particle size distribution data are presented in Appendix C."

p 126 para 4: comment: When emptying the fluidized bed vessel with a vacuum cleaner, attempts were made to remove as much bed material as possible. However, a very small amount of fine solids could not be removed completely from the plastic bed walls. Bed material was weighted before the bed charging and after the removal, and the material loss was found to be negligible. Further tests suggested that the calibration was unaffected by the constant presence of some solids on the empty vessel's walls.

p 202: insert appendix

"Appendix C. Particle size distribution of bed materials used in experiments"

Size range (μm)	Volume distribution (%)				
	FCC Catalyst	Silica sand	Pigment A	Pigment B	Vermiculite
22 - 31	1.02		3.11		
31 - 41	4.41		8.46		
41 - 48	5.00		8.07		
48 - 56	7.49		13.00		
56 - 76	23.64		29.20		
76 - 89	13.28		13.82		
89 - 104	13.23		10.73	4.74	
104 - 121	12.00	1.40	7.63	2.00	
121 - 141	8.43	2.88	4.54	3.34	
141 - 164	5.85	8.35	1.44	5.21	
164 - 191	3.65	19.56		7.61	
191 - 222	2.00	30.54		10.31	
222 - 259		22.76		12.83	
259 - 302		11.90		14.75	6.77
302 - 351		2.61		13.63	1.53
351 - 409				11.01	2.58
409 - 477				7.83	4.84
477 - 556				4.86	10.78
556 - 647				1.88	20.16
647 - 879					53.34

RESPONSE TO QUESTIONS RAISED BY T. PUGSLEY (EXAMINER A)

Associate Professor Pugsley feels that there is a great opportunity to use the existing experimental setup for obtaining and presenting bubble diameter data as function of pressure using the electrical capacitance tomography (ECT).

Without doubt, the role of bubbles in fluidized beds is important when prolonged contact between the gas and the bed solids is required for chemical reactions. With large bubbles, substantial amount of gas can pass through the fluidized bed without sufficient contact with solids. Because of the importance of bubbles to an industrial process performance, determining the bubble characteristics, such as size and rise velocity, has been a major topic for fluidization research.

It is known that bubble characteristics vary with the type of bed material, gas properties and, therefore, operating pressure, the fluidized bed diameter, and the position in the bed. The analogy with visible gas bubbles in liquids has been often used to describe gas-solid fluidized beds by applying the simple two-phase theory. While the simple two-phase model is convenient, it has serious limitations in conveying the view that bubbles are stable and rise through the fluidized bed at steady rates. It has been observed that bubbles in fluidized beds are very dynamic and are constantly

changing in size, shape and position (Gilbertson et al., 1998). Gas-solid fluidized beds are not transparent, and it has been difficult to experimentally test the simple two-phase theory.

It is widely accepted that the tomographic images, reconstructed from the capacitance measurements using the standard linear back-projection algorithm, are of low resolution and suffer from blurring (Byars, 2001). Previous work at Monash University supported this view. Visual analysis of several image frames was tried in this work and confirmed that the ECT images were not accurate enough to justify the bubble size analysis. Image resolution and accuracy can be improved by employing an iterative linear back-projection algorithm, which is still under development (Dyakowski et al., 2000; Isaksen, 1996). However, image improvement based on this algorithm and further frame-by-frame image analysis is very time consuming, especially for large number of image files (16000 per each velocity setup). Due to the level of financial and technical support for the ECT system used in this work, further image improvement and analysis was not feasible.

A novel method to extract bubble properties from ECT data has been recently published (McKeen & Pugsley, 2003), but was not known of when the present work was carried out. According to McKeen & Pugsley (2003), Halow et al. (1993) instead of using the bubble contours available from the tomographic images obtained in a METC multi-plane system, used average cross-sectional voidages from ECT data to calculate bubble diameters. As early as 1990, Halow et al. (1990) reported the first preliminary observations of a bubbling bed using ECT and described the average voidage plots method they used for extracting the bubble characteristics. With this method, an average cross-sectional voidage at each of four levels was determined for each frame. When plotted against time, the average voidages for some bed materials showed peaks corresponding to the passage of bubbles. Determination of the voidage peaks provided a measure of the maximum cross-sectional area of the bubble, from which Halow et al. (1990) calculated a bubble diameter assuming that the single present bubble was hemispherical in shape. From the known spacing of the four imaging electrode levels and the time shifts of the peaks, the rise velocity was determined. The volume of the bubble at each level was determined by integrating the data to obtain the area under the voidage vs time curve and knowing the bubble rise velocity.

However, Halow et al. (1993) pointed out that characterizing the fluidization in terms of the two-phase model and a single bubble rising had serious limitations and directed their further research to the image analysis of the ECT data. They rarely observed the circular cross section of spherical bubbles and had more success in observing and characterizing slugs when using 3mm-diameter nylon spheres as bed solids. Halow et al. (1990) conducted eight experiments with the 70 μ m FCC catalyst in the range of velocities from the minimum fluidization velocity to $4U_{mf}$ and observed a large number of small bubbles with much overlapping. Because of this overlap Halow et al. (1990) could not calculate bubble volumes for both FCC catalyst and 700 μ m plastic.

In this high-pressure work, several bubbles were observed when the FCC catalyst was fluidized. The ECT system was a single-plane with the 50mm-high sensors and the bubble rise velocity could not be established. Much more than eight experiments were carried out in this study, and in the further image analysis for several experiments no distinct voidage peaks were identified. Considering some differences in the experimental setup and the limitations of the method originally proposed by Halow et al. (1990) in processing the average cross-sectional voidage with several assumptions (simple two-phase theory and single spherical bubble, for example), a decision was made to present the findings of this research in the form of voidage fluctuations and not bubble diameters.

ADDITIONAL BIBLIOGRAPHY

- Byars, M. (2001). *Developments in Electrical Capacitance Tomography*. Paper presented at the 2nd World Congress on Industrial Process Tomography, Hannover.
- Dyakowski, T., et al. (2000). Applications of electrical tomography for gas-solids and liquid-solids flows - a review. *Powder Technology*, 112, 174-192.
- Gilbertson, M. A., et al. (1998). Observations and measurements of isolated bubbles in a pressurized gas-fluidized bed. In L. S. Fan & T. M. Knowlton (Eds.), *Fluidization IX* (pp. 61-68). New York: Engineering Foundation.
- Halow, J. S., et al. (1990). Preliminary capacitance imaging experiments of a fluidized bed. *AIChE Symposium Series*, 86(276), 41-50.
- Halow, J. S., et al. (1993). Observations of a fluidized bed using capacitance imaging. *Chemical Engineering Science*, 48(4), 643-659.
- Isaksen, O. (1996). A review of reconstruction techniques for capacitance tomography. *Measurement Science and Technology*, 7(3), 325-337.
- McKeen, T., & Pugsley, T. (2003). Simulation and experimental validation of a freely bubbling bed of FCC catalyst. *Powder Technology*, 129, 139-152.

Pressure Effects on Fluidized Bed Behaviour

by

Igor Sidorenko

Honours Degree in Mechanical Engineering
Ural State Technical University, Russia

A thesis submitted in fulfilment of the
requirements for the degree of
Doctor of Philosophy

Department of Chemical Engineering
Monash University
Australia

© 2003

Declaration

To the best of my knowledge and belief this thesis contains no material that has been accepted for the award of any other degree or diploma in any University, and contains no material previously published or written by another person, except where due reference is given in the text.



I. Sidorenko

Department of Chemical Engineering

Monash University

April 2003

Acknowledgements

I gratefully acknowledge the financial support from the Department of Chemical Engineering offered by my supervisor Prof. M. J. Rhodes in my first year at Monash University in Clayton, and from the Cooperative Research Centre for Clean Power from Lignite in the subsequent years.

After several years of rewarding industrial experience in Russia, Switzerland and Australia my return to university life was extremely easy and my stay at Monash University was enjoyable and enlightening thanks to friendly academic and general staff, and fellow postgraduate students, of whom there are too many to mention.

I very much appreciate friendly and helpful manner and much technical support and assistance given in my research by everyone in the Technical Services of the Department. The departmental chemist John Barnard and Alfi Zakhari (formerly from CSIRO Division of Minerals) were especially helpful in performing size analysis of the materials used in this work.

Special thanks are given to Dr Mao Qi Ming from the Department of Chemical Engineering for his guidance and assistance during the whole research project and his help in designing and manufacturing the fibre optic probe. I am very grateful to Dr Seng Lim and Tim Barton from CSIRO Division of Minerals for allowing me to use equipment at their site and their help in agglomerating the luminescent pigment. Also I appreciate constructive feedback and remarks given to me by Dr Seng Lim over the period of my research.

I would also like to acknowledge former fellow students Dr Belinda Mathers for her assistance with video processing, and Dr John Sanderson for his assistance with the electrical capacitance tomography, and Dr Ian Harper

from Monash Micro Imaging for his help and guidance in performing image analysis of my experimental results.

In returning to university and completing the research project I have always been supported by my family which has grown since the commencement of the project. I thank my wife Olga for her moral and financial support and assistance with some of the figures in the thesis; and my son Alexci for his assistance in converting hundreds of thousand computer files from one software programme to another, and for being a trouble-free son. I am glad that our twins Michael and Andrew are also rather trouble-free.

Enormous gratitude is given to my parents for babysitting Michael and Andrew and allowing me to painlessly complete this thesis.

Abstract

With much interest in developing processes for coal combustion and gasification in fluidized beds under pressure, both academic and industrial researchers from many countries have investigated various aspects of the pressurised operation of fluidized beds. Previously, many researchers commented on the improvement of fluidization at elevated pressures and on the smoothness of fluidization compared with atmospheric pressure. However, it seems that many of the pressure effects have not been adequately explained and properly quantified, and they differ depending on physical characteristics of fluidized particles. Although some data on the effect of pressure on the behaviour of fluidized beds have been obtained, areas remain where further experimental work and analysis would be valuable.

This study was undertaken as a part of the research programme of the Cooperative Research Centre (CRC) for Clean Power from Lignite which primary objective is developing technologies to reduce greenhouse gas emissions from lignite-based power generation by improving efficiency while maintaining low costs of electricity. Advanced coal-based power generation technologies involve pressurised fluidized bed coal gasification, followed by combustion of the product gas in a gas turbine. It is expected that commercial lignite gasification will be carried out in a bubbling fluidized bed.

Present understanding of flow processes, found in pressurised fluidized beds is far from complete with great concern for the lack of good quality physical data. The overall aim of the study was to determine relevant hydrodynamic data for the pressurized fluidized bed operation to enable the design of large demonstration and commercial scale reactors for the coal gasification and combustion processes and to prepare a comprehensive review of literature on the subject.

The objective of the project was to study the influence of pressure on fluidization phenomena, such as minimum fluidization velocity, minimum bubbling velocity, bed expansion and voidage, and particle motion near to the bed wall. Experiments were conducted in a bubbling fluidized bed apparatus at operating pressures up to 2500kPa with several Geldart A and B materials.

The pressure vessel was 2.38m-high and was equipped with 5 glass observation ports. A 15cm-diameter plastic fluidized bed vessel was inserted into the pressure vessel and used to study physical behaviour of gas-fluidized beds. Pressure probe, visual observation and the electrical capacitance tomography (ECT) were used for characterising the fluidized bed behaviour at elevated pressure. Although the electrical capacitance tomography has been already used for research in the area of fluidization, it has not been previously used to study the fluidized bed behaviour in a pressurised environment.

It was found that the minimum fluidization velocity decreased only slightly with pressure increase for both Geldart A and Geldart B materials, and the minimum bubbling velocity for the Geldart A materials was practically unaffected by the pressure increase. Voidage at the minimum fluidization conditions was hardly affected by pressure for most of the materials. Voidage at the minimum bubbling conditions increased slightly with the pressure increase. The experimental results were compared to the predictions from several simplified correlations available in the literature. It was found that the correlations did not predict the experimental values with sufficient accuracy.

The tomographic images obtained from the capacitance measurements were of relatively low resolution and suffered from blurring so, that no conclusion on the volume or size of individual bubbles could be reached. The dynamic ECT results were processed by the software specifically designed to analyse experimental time series fluctuation in fluidized beds. The solids volume fraction time series were analysed to determine the average, the average absolute deviation and the average cycle frequency. This provided an overall

picture of the bed behaviour, indicated the magnitude of the fluctuations and the time scale of the signal.

For the Geldart B material, over the range of pressures studied, increasing operating pressure caused an increase in the average bed voidage, but had no influence on both the amplitude and frequency of voidage fluctuations. For the Geldart A material, however, increasing operating pressure caused in general a decrease in all the average bed voidage, amplitude and frequency of voidage fluctuations.

The influence of operating pressure on the motion of Geldart A and B particles near the fluidized bed wall surface, which permits better understanding of the effect of pressure on wall-to-bed heat transfer, was studied using luminescent pigment as bed solids. The luminescent pigment was available in the form of spherical Geldart A particles, and the larger Geldart B particles were produced from these by agglomeration.

A pulse of bright light was transmitted from outside of the pressure vessel via fibre optics and illuminated a small region of the bed material adjacent to a transparent vessel wall. The illuminated particles showed an afterglow for several seconds, which was digitally recorded on video and analysed. Typically the illuminated particles remained visible as a bright spot decreasing in intensity with time. In a bubbling fluidized bed the spot shifted along the wall surface. Digital image analysis of the movement of the spot provided its statistically determined velocity along the surface, and the luminosity decay defined the particle exchange frequency in the direction perpendicular to the wall surface.

In a bubbling bed, significant pressure effect on the mean residence time of illuminated particles near to the wall was not observed when using both Geldart A and B materials implying the independence of the particle convective heat transfer coefficient on pressure in fluidized beds of small particles.

Table of Contents

Declaration.....	ii
Acknowledgements.....	iii
Abstract	v
Table of Contents	viii
List of Figures.....	xii
List of Tables.....	xvii
Notation.....	xviii
Chapter 1 Introduction	1
1.1 Background.....	1
1.2 Pressurised fluidized bed processes.....	3
1.2.1 Pressurised fluidized bed combustion.....	3
1.2.2 Pressurised fluidized bed gasification	5
1.2.3 Polymerisation	8
1.3 Project aim.....	8
1.4 Thesis structure	10
Chapter 2 Literature Review.....	13
2.1 Introduction	13
2.2 Non-bubbling fluidization at elevated pressure	15
2.2.1 Minimum fluidization velocity	16
2.2.2 Pressure effects on minimum fluidization velocity.....	19
2.2.3 Prediction of minimum fluidization velocity at high pressure	23
2.2.4 Minimum bubbling velocity	28
2.2.5 Pressure effects on minimum bubbling velocity	29
2.2.6 Fluidized bed stability.....	35
2.2.7 Effect of pressure on non-bubbling bed expansion	37
2.3 Bubbling fluidization at elevated pressure	45
2.3.1 Dense phase expansion in pressurised bubbling beds	46
2.3.2 Effect of pressure on bubbling bed expansion	50

2.3.3 Bubble characteristics	52
2.4 Other studies of pressurised fluidized beds.....	58
2.4.1 Bed-to-surface heat transfer	58
2.4.2 Bed penetration by gas jets.....	61
2.4.3 Solids mixing.....	62
2.4.4 Particle entrainment	62
2.4.5 Transition from bubbling to turbulent fluidization	63
2.5 Conclusions	66
Chapter 3 Experimental.....	67
3.1 Experimental facility	67
3.2 Fluidized bed apparatus.....	68
3.3 Process and instrumentation	73
3.4 Measuring gas flow.....	74
3.5 Control of operating pressure.....	78
3.6 Ensuring safe operation.....	79
3.7 Bed pressure drop measurement.....	81
3.8 Electrical capacitance tomography.....	83
3.8.1 Electrical capacitance tomography system	83
3.8.2 Capacitance sensor design.....	83
3.8.3 Connecting leads	85
3.9 Equipment used for studying particle motion	86
3.10 Fluidising gases and bed materials	87
Chapter 4 Minimum Fluidization and Minimum Bubbling Conditions.....	94
4.1 Experimental determination of the minimum fluidization velocity	94
4.1.1 Overview	94
4.1.2 Experimental method.....	96
4.1.3 Experimental results	98
4.2 Influence of pressure on minimum fluidization.....	101
4.2.1 Influence of pressure on the minimum fluidization velocity	101
4.2.2 Bed voidage at minimum fluidization at elevated pressure	109
4.3 Experimental determination of the minimum bubbling velocity	110
4.3.1 Overview	110
4.3.2 Experimental method.....	111

4.4 Influence of pressure on minimum bubbling.....	111
4.4.1 Pressure effect on the minimum bubbling velocity.....	111
4.4.2 Bed expansion and voidage at minimum bubbling at elevated pressure	116
4.5 Summary.....	120
Chapter 5 Experimental Observation of Voidage in a Pressurised Bubbling Fluidized Bed	121
5.1 Experimental determination of the bed voidage.....	121
5.1.1 Measuring dense phase voidage.....	121
5.1.2 Non-invasive techniques.....	122
5.2 Electrical capacitance tomography.....	123
5.2.1 PTL300 ECT system	123
5.2.2 Principle of operation.....	124
5.2.3 Experimental method.....	126
5.2.4 Experimental results	129
5.2.5 Quantitative analysis	131
5.3 Influence of pressure on voidage fluctuations	135
5.3.1 Experimental results at elevated pressure	135
5.3.2 Bed voidage at elevated pressure	136
5.4 Bed collapse experiments	150
5.4.1 Collapse test technique	150
5.4.2 Experimental method.....	152
5.4.3 Experimental results at various operating pressures	154
5.4.4 Influence of pressure on the dense phase voidage.....	157
5.5 Summary.....	158
Chapter 6 Experimental Observation of the Motion of Particles near the Wall Surface in a Pressurised Bubbling Fluidized Bed	161
6.1 Overview	161
6.2 Motion of particles	162
6.2.1 Experimental method.....	162
6.2.2 Data analysis.....	164
6.3 Particle motion observation at similar fluidization velocities	167
6.4 Particle motion observation at various pressures	171

6.4.1 Decay of mean luminosity	171
6.4.2 Analysis of the experimental data	174
6.4.3 Mean residence times at the wall	176
6.4.4 Relating wall contact time to heat transfer	179
6.5 Particle motion velocity	181
6.5.1 Observation of particle motion parallel to the wall	181
6.5.2 Axial particle motion velocity at elevated pressures	182
6.6 Summary	185
Chapter 7 Conclusions and Recommendations	186
Appendix A Operating procedures	195
Appendix B Curriculum Vitae	199

List of Figures

Figure 1-1. Relative bed area of fluidized bed combustors at different operating pressures (from Roberts et al., 1983).....	4
Figure 2-1. Effect of operating pressure on minimum fluidization velocity for spherical particles in a size range from 100 μ m to 10mm and density of 1250kg/m ³ (from Rowe, 1984)	20
Figure 2-2. Changes in U_{mb}/U_{mf} ratio with pressure for alumina of different sizes according to Sobreiro and Monteiro (1982)	31
Figure 2-3. Changes in U_{mb}/U_{mf} ratio with pressure for ballotini of different sizes and iron sulfide particles according to Sobreiro and Monteiro (1982).....	32
Figure 2-4. Changes in U_{mb}/U_{mf} ratio with pressure for sand of similar sizes according to Varadi and Grace (1978), and King and Harrison (1982).....	33
Figure 2-5. Effect of pressure on minimum bubbling voidage for solids with particle size in the range 40 - 300 μ m as predicted by the Hydrodynamic Forces Stability Theory (from Gibilaro et al., 1988).....	40
Figure 2-6. Variation of bed voidage at minimum bubbling with pressure as reported by (a) Guedes de Carvalho et al. (1978) and (b) King and Harrison (1982)	43
Figure 2-7. Variation of bed voidage at minimum fluidization (ϵ_{mf}) and minimum bubbling (ϵ_{mb}) with pressure as reported by King and Harrison (1982).....	45
Figure 2-8. Effect of pressure and particle size on superficial dense phase gas velocity as reported by (a) Piepers et al. (1984), (b) Weimer and Quarderer (1985) and (c) Foscolo et al. (1989).....	50
Figure 3-1. General view of the high-pressure cold fluidized bed facility built for this work	68
Figure 3-2. Expanded view of the plenum chamber and distributor assembly, where 1 - clear plastic fluidized bed, 2 - rubber gaskets, 3 - intermediate steel collar, 4 - steel collar for sealing the distributor. 5 - rubber O-rings, 6 - distributor plate, and 7 - steel plenum chamber	70
Figure 3-3. Pressure drop versus superficial gas velocity for sintered bronze distributor	71
Figure 3-4. Pressure drop versus superficial gas velocity for paper based distributor	71
Figure 3-5. Process and instrumentation diagram of the pressurised fluidized bed apparatus used in this study.....	73
Figure 3-6. Verification of rotameter R1 calibration at atmospheric and 600kPa operating pressures	77

Figure 3-7. Verification of rotameter R2 calibration at atmospheric and 400kPa operating pressures	77
Figure 3-8. Verification of rotameter R4 calibration at various operating pressures (100, 300, 500, 700, 1100, 2100 and 2500kPa)	78
Figure 3-9. Calibration curve for the differential pressure transmitter DP1.....	82
Figure 3-10. Capacitance sensor with the earth screen open, fitted to the fluidized bed vessel and connected to the DAM200 data acquisition unit.....	84
Figure 3-11. Experimental setup for studying particle motion along the wall.....	87
Figure 3-12. Location of solids used in experiments on powder classification diagram by Geldart (1973)	88
Figure 3-13. Particles of FCC catalyst under 10x magnification (full scale is 1mm).....	89
Figure 3-14. Particles of silica sand under 10x magnification (full scale is 1mm).....	89
Figure 3-15. Particles of luminescent pigment A under 10x magnification (full scale is 1mm).....	90
Figure 3-16. Particles of agglomerated in V-blender luminescent pigment B under 5x magnification (full scale is 1mm).....	90
Figure 3-17. Particles of vermiculite under 5x magnification (full scale is 1mm).....	91
Figure 4-1. Bed pressure drop as a function of increasing and decreasing superficial gas velocity for FCC catalyst at atmospheric pressure.....	99
Figure 4-2. Bed pressure drop as a function of increasing and decreasing superficial gas velocity for pigment A at atmospheric pressure	99
Figure 4-3. Bed pressure drop as a function of increasing and decreasing superficial gas velocity for silica sand at atmospheric pressure.....	100
Figure 4-4. Bed pressure drop as a function of increasing and decreasing superficial gas velocity for pigment B at atmospheric pressure	100
Figure 4-5. Bed pressure drop as a function of increasing superficial gas velocity for vermiculite at atmospheric pressure	101
Figure 4-6. Variation of the minimum fluidization velocity with pressure for FCC catalyst (EXP - experimental values, E - (Ergun, 1952; Werther, 1977), W-Y - (Wen & Yu, 1966a), T - (Thonglimp et al., 1984), S-V - (Saxena & Vogel, 1977), C - (Chitester et al., 1984), N - (Nakamura et al., 1985), and B - (Borodulya et al., 1982))	104
Figure 4-7. Variation of the minimum fluidization velocity with pressure for silica sand (EXP - experimental values, E - (Ergun, 1952; Werther, 1977), W-Y - (Wen & Yu, 1966a), T - (Thonglimp et al., 1984), S-V - (Saxena & Vogel, 1977), C - (Chitester et al., 1984), N - (Nakamura et al., 1985), and B - (Borodulya et al., 1982)).....	104
Figure 4-8. Variation of the minimum fluidization velocity with pressure for pigment A (EXP - experimental values, E - (Ergun, 1952; Werther, 1977), W-Y -	

(Wen & Yu, 1966a), T - (Thonglomp et al., 1984), S-V - (Saxena & Vogel, 1977), C - (Chitester et al., 1984), N - (Nakamura et al., 1985), and B - (Borodulya et al., 1982)).....	105
Figure 4-9. Variation of the minimum fluidization velocity with pressure for pigment B (EXP - experimental values, E - (Ergun, 1952; Werther, 1977), W-Y - (Wen & Yu, 1966a), T - (Thonglomp et al., 1984), S-V - (Saxena & Vogel, 1977), C - (Chitester et al., 1984), N - (Nakamura et al., 1985), and B - (Borodulya et al., 1982)).....	105
Figure 4-10. Variation of the minimum bubbling velocity with pressure for FCC catalyst (EXP - experimental values and A-G - (Abrahamsen & Geldart, 1980a))	113
Figure 4-11. Variation of the minimum bubbling velocity with pressure for pigment A (EXP - experimental values and A-G - (Abrahamsen & Geldart, 1980a))	113
Figure 4-12. Variation of the minimum bubbling to minimum fluidization velocity ratio with pressure for FCC catalyst (EXP - experimental values and A-G - (Abrahamsen & Geldart, 1980a))	115
Figure 4-13. Variation of the minimum bubbling to minimum fluidization velocity ratio with pressure for pigment A (EXP - experimental values and A-G - (Abrahamsen & Geldart, 1980a))	115
Figure 4-14. Variation of the maximum bed expansion ratio with pressure for FCC catalyst (EXP - experimental values and A-G - (Abrahamsen & Geldart, 1980a))	117
Figure 4-15. Variation of the maximum bed expansion ratio with pressure for pigment A (EXP - experimental values and A-G - (Abrahamsen & Geldart, 1980a))	117
Figure 4-16. Variation of bed voidage at minimum fluidization (ϵ_{mf}) and minimum bubbling (ϵ_{mb}) with pressure for FCC catalyst	118
Figure 4-17. Variation of bed voidage at minimum fluidization (ϵ_{mf}) and minimum bubbling (ϵ_{mb}) with pressure for pigment A.....	119
Figure 5-1. Variation in average bed voidage with gas velocity for FCC catalyst over a range of operating pressures from 300 to 1900kPa (lines are used to guide the eye)	138
Figure 5-2. Variation in average bed voidage with gas velocity for silica sand over a range of operating pressures from atmospheric to 1700kPa	140
Figure 5-3. Variation in average absolute deviation in bed voidage with gas velocity for FCC catalyst over a range of operating pressures from 300 to 1900kPa (lines are used to guide the eye)	142

Figure 5-4. Variation in average absolute deviation in bed voidage with gas velocity for silica sand over a range of operating pressures from atmospheric to 2100kPa	143
Figure 5-5. Variation in average cycle frequency with gas velocity for FCC catalyst over a range of operating pressures from 300 to 1900kPa (lines are used to guide the eye)	144
Figure 5-6. Variation in average cycle frequency with gas velocity for silica sand over a range of operating pressures from atmospheric to 2100kPa (lines are used to guide the eye)	145
Figure 5-7. Kolmogorov entropy as a function of gas velocity for FCC catalyst over a range of operating pressures from 300 to 1900kPa (lines are used to guide the eye)	148
Figure 5-8. Bed surface collapse curves for FCC catalyst at various operating pressures ...	155
Figure 5-9. Variation of the dense phase expansion with pressure for FCC catalyst (EXP - experimental values and A-G - (Abrahamsen & Geldart, 1980a))	156
Figure 5-10. Variation with pressure of dense phase voidage (ϵ_{fl}), settled bed voidage (ϵ_s), minimum fluidization voidage (ϵ_{mf}) and minimum bubbling voidage (ϵ_{mb}) for FCC catalyst.....	158
Figure 6-1. An example of the illuminated cluster of particles as seen on a video camera (actual size)	163
Figure 6-2. Decay of maximum image luminosity on a greyscale in packed bed of pigment A compared to fluidized bed at atmospheric pressure (fluidization gas velocity $U = 0.012\text{m/s}$)	166
Figure 6-3. Image trajectory for pigment A at atmospheric pressure and gas velocity of 0.012m/s (actual size).....	167
Figure 6-4. Image trajectory for pigment A at 500kPa and gas velocity of 0.011m/s (actual size).....	168
Figure 6-5. Image trajectory for pigment A at 1100kPa and gas velocity of 0.011m/s (actual size).....	168
Figure 6-6. Image trajectory for pigment A at 1500kPa and gas velocity of 0.011m/s (actual size).....	168
Figure 6-7. Image trajectory for pigment A at 2000kPa and gas velocity of 0.011m/s (actual size).....	168
Figure 6-8. Difference between mean image luminosities on a greyscale for pigment A at different operating pressures and similar fluidization velocities.....	170
Figure 6-9. Variation in exponential luminosity decay constant k for pigment A with superficial gas velocity in the pressure range 101 - 2100kPa	171
Figure 6-10. Image trajectory for pigment A at atmospheric pressure and gas velocity of 0.023m/s	172

Figure 6-11. Image trajectory for pigment A at atmospheric pressure and gas velocity of 0.029m/s	172
Figure 6-12. Image trajectory for pigment A at atmospheric pressure and gas velocity of 0.041m/s	173
Figure 6-13. Image trajectory for pigment A at atmospheric pressure and gas velocity of 0.046m/s	173
Figure 6-14. Variation in exponential luminosity decay constant k for pigment B with superficial gas velocity in the pressure range 101 - 1100kPa	174
Figure 6-15. Mean time between pigment A particle illumination and departure from the wall versus gas velocity at various operating pressures	177
Figure 6-16. Mean time between pigment B particle illumination and departure from the wall versus gas velocity at various operating pressures	178
Figure 6-17. Particle motion velocity in vertical direction versus superficial gas velocity at various operating pressures for pigment A	182
Figure 6-18. Particle motion velocity in vertical direction versus superficial gas velocity at various operating pressures for pigment B	183
Figure 6-19. Particle motion velocity in horizontal direction versus superficial gas velocity at various operating pressures for pigment A	184

List of Tables

Table 1. Comparison of constants C_1 and C_2 in Wen and Yu correlation (Eq.(2.2.5)) with constants proposed for similar correlations for predicting minimum fluidization velocity at elevated pressure.....	22
Table 2. List of equipment and instruments used in experimental set-up.....	73
Table 3. Typical characteristics of bed materials used in experiments.....	91
Table 4. The mass of bed solids, static bed height and the experimental pressure range for different materials used in the experiments to establish the minimum fluidization and minimum bubbling velocities and bed expansion	96

Notation

The S. I. system of units has been used. Abbreviations and symbols are defined in the text as they arise and appropriate units are given, for example mean particle diameter d_p is expressed in μm as being more convenient. **Unless specified otherwise, absolute pressure units are used in this thesis, i.e. typical atmospheric pressure is 101kPa.** The equations indicated refer to the location where the symbol is first used or first defined.

A	cross-sectional bed area (m^2)
AC	flow meter accuracy class (dimensionless), Eq.(3.4.1)
C_1	constant (dimensionless), Eq.(2.2.5)
C_2	constant (dimensionless), Eq.(2.2.5)
C_D	drag coefficient (dimensionless), Eq.(2.2.12)
$C_{D,\varepsilon}$	modified drag coefficient (dimensionless), Eq.(2.2.12)
$C_{D,mf}$	drag coefficient at minimum fluidization (dimensionless), Eq.(2.2.10)
c_g	specific heat capacity of gas (J/kgK), Eq.(2.4.3)
c_p	specific heat capacity of particles (J/kgK), Eq.(2.4.3)
D	bed diameter (m)
D_o	illuminated spot diameter (m), Eq.(6.4.3)
d_b	bubble size diameter (m), Eq.(2.3.5)
d_o	jet nozzle diameter (m), Eq.(2.4.5)
d_p	mean particle diameter (m)
E_a	actual flow meter error (%), Eq.(3.4.1)
E_{mb}	elasticity modulus at minimum bubbling (N/m^2), Eq.(2.2.19)
F	mass fraction of fines less than $45\mu\text{m}$ (dimensionless), Eq.(2.2.16)
F	percentage of the flowmeter full-scale flow (%), Eq.(3.4.1)

f	sampling frequency (Hz)
f	particle exchange frequency (Hz), Eq.(6.4.1)
f_c	average cycle frequency (Hz)
g	gravitational acceleration (m/s^2)
Ga	Galileo (or Archimedes Ar) number (dimensionless), Eq.(2.2.4)
H	bed height (m)
H_c	critical (collapse) bed height (m)
H_d	dense phase height (m), Eq.(2.3.1)
H_f	expanded bed height (m), Eq.(2.3.5)
H_{mb}	bed height at minimum bubbling (m), Eq.(2.2.22)
H_{mf}	bed height at minimum fluidization (m), Eq.(2.2.22)
H_o	packed bed height (m), Eq.(5.2.1)
H_s	settled bed height (m)
h	heat transfer coefficient (W/m^2K), Eq.(2.4.1)
h_{gc}	interphase gas convective component of bed to surface heat transfer coefficient (W/m^2K), Eq.(2.4.1)
h_{pc}	particle convective component of bed to surface heat transfer coefficient (W/m^2K), Eq.(2.4.1)
h_{max}	maximum heat transfer coefficient (W/m^2K), Eq.(2.4.2)
h_r	radiative component of heat transfer coefficient (W/m^2K), Eq.(2.4.1)
K	Kolmogorov entropy (bits/s), Eq.(5.2.4)
k	constant (dimensionless), Eq.(2.4.8)
k	exponential decay rate constant (1/s), Eq.(6.3.1)
L	bed height (m), Eq.(2.2.1)
L	image luminosity on a greyscale (0 - 255) (dimensionless), Eq.(6.3.1)
L_0	initial image luminosity on a greyscale (0 - 255) (dimensionless), Eq.(6.3.1)
L_{max}	maximum jet penetration length (m), Eq.(2.4.5)
$L_{threshold}$	image threshold luminosity on a greyscale (0 - 255) (dimensionless), Eq.(6.3.1)
m	mass of bed solids (kg)

n	expansion parameter (dimensionless), Eq.(2.2.20)
n_p	number of the illuminated particles at the wall (dimensionless), Eq.(6.4.4)
n_{p0}	initial number of the illuminated particles at the wall (dimensionless), Eq.(6.4.3)
Nu	Nusselt number (dimensionless), Eq.(2.4.2)
p	pressure (Pa)
Δp	bed pressure drop (Pa), Eq.(2.2.1)
Δp_{max}	maximum bed pressure drop (Pa), Eq.(4.1.1)
Pr	Prandtl number (dimensionless), Eq.(2.4.4)
R_{cf}	ratio of complete fluidization velocity at elevated pressure over that at atmospheric pressure (dimensionless), Eq.(2.4.5)
Re	particle Reynolds number (dimensionless), Eq.(2.2.3)
Re_c	modified Reynolds number (dimensionless), Eq.(2.2.13)
Re_{mf}	particle Reynolds number at minimum fluidization (dimensionless), Eq.(2.2.2)
t	time (s)
Δt	time interval (s)
U	superficial gas velocity (m/s)
U_0	superficial gas velocity (m/s), Eq.(2.4.5)
U_b	bubble rise velocity (m/s), Eq.(2.3.7)
U_{br}	single bubble rise velocity (m/s), Eq.(2.3.6)
U_C	regime transition velocity (m/s), Eq.(2.4.7)
U_c	bed collapse velocity (m/s), Eq.
U_d	dense phase gas velocity (m/s)
U_1	superficial gas velocity at a voidage of unity (m/s), Eq.(2.2.21)
U_{mb}	minimum bubbling velocity (m/s)
U_{mf}	minimum fluidization velocity (m/s)
U_o	average jet nozzle velocity (m/s), Eq.(2.4.5)
U_t	particle terminal fall velocity (m/s), Eq.(2.2.20)
U_x	particle motion velocity along the wall in the horizontal direction (m/s)

U_v	particle motion velocity along the wall in the vertical direction (m/s)
W	probability (dimensionless), Eq.(6.4.1)
(X_0, Y_0)	initial coordinates of the illuminated spot centre of gravity (m)
(X_n, Y_n)	final coordinates of the illuminated spot centre of gravity (m)
X	average solids volume fraction (dimensionless), Eq.(5.2.2)
ΔX	average absolute deviation (dimensionless), Eq.(5.2.3)

Greek symbols

δ	bed expansion ratio (dimensionless), Eq.(2.3.3)
δ	bed height fluctuation ratio (dimensionless), Eq.(2.3.4)
δ	gap between the wall and the particles (m), Eq.(6.4.5)
ε	voidage (dimensionless)
ε_d	voidage of dense phase (dimensionless), Eq.(2.3.1)
ε_{mb}	voidage at minimum bubbling (dimensionless)
ε_{mf}	voidage at minimum fluidization (dimensionless)
ε_o	voidage in packed bed (dimensionless), Eq.(5.2.1)
ε_s	voidage in settled bed (dimensionless)
ϕ	particle shape factor (sphericity) (dimensionless), Eq.(2.2.1)
λ_g	gas thermal conductivity (W/mK), Eq.(2.4.2)
λ_p	particle thermal conductivity (W/mK), Eq.(6.4.5)
μ	gas viscosity (Pa s)
$\mu_{(ref)}$	gas viscosity at atmospheric pressure and temperature of 293K (Pa s), Eq.(2.4.7)
ν	kinematic gas viscosity (m ² /s)
ρ_g	gas density (kg/m ³)
$\rho_{g(ref)}$	gas density at atmospheric pressure and temperature of 293K (kg/m ³), Eq.(2.4.7)
ρ_p	solids (particle) density (kg/m ³)
τ	mean residence time at the wall (s), Eq.(6.4.5)

Chapter 1

INTRODUCTION

This chapter provides some background information about the previous research on the influence of pressure on fluidization, briefly discusses uses of industrial processes based on fluidized bed technology and operating at elevated pressure, and outlines the aim and approach of the present study.

1.1 BACKGROUND

Fluidized bed¹ technology originated as the Winkler process for lignite gasification developed in Germany in the 1920s. However, the fluidization technique as it is known now was born from the successful development of the fluidized bed catalytic cracking process in the USA in the early 1940s. Since then the application of fluidization has spread to metallurgical ore roasting, calcination, coal combustion and gasification, coating, granulation and drying, freezing and roasting food products, olefin polymerisation, and even to the design of nuclear reactors and radioactive waste solidification (Zenz, 1997).

Until the 1970s, there was very little published information dealing with the influence of pressure on the operation of fluidized bed processes. One of the reasons for that was, and still is, the high cost of building and operating of the high-pressure laboratory research rigs and pilot plants. Also, a certain number of measuring techniques, common at ambient conditions, cannot be used under severe conditions of high pressure.

The earliest work on fluidization under pressurised conditions was carried out independently in the United States (May & Russell, 1953), the Soviet

¹ Australian English (which is generally similar to British English) spelling is used in this thesis with only two fixed term exceptions - "fluidization" and "fluidized bed"

Union (Altshuler & Sechenov, 1963) and the United Kingdom (Godard & Richardson, 1968).

The behaviour of fluidized beds at high pressures is of much interest from both practical and theoretical points of view. It is important for optimal design and operation of the high pressure fluidized bed reactors such as those used in coal gasification and combustion processes including advanced hybrid gasification and combustion cycles that are particularly important for future clean technologies for power generation.

Pioneer pilot plant investigations into the potential benefits of coal combustion in pressurised fluidized bed began in the UK in 1968. The early 1970s saw much interest in developing processes for coal combustion and gasification in fluidized beds under pressure. Since then both academic and industrial researchers from many countries including the UK, USA, Japan, Germany, Russia, Sweden, Italy, France, and the Netherlands have investigated many aspects of pressurised operation of fluidized beds.

However, fundamental research quite often is too complicated or too idealised for industrial use, while industrial research, if published, has tendency to finish with empirical correlations explaining only particular experimental data with minimal theoretical basis. Although some data on the effect of pressure on the behaviour of fluidized beds have been obtained during the past 50 years, areas remain where further experimental work and analysis would be valuable.

From early work published in Russian it is known that the use of higher operating pressures increases the rate of processes in fluidized beds and improves fluidization quality (Fridland, 1963). Since then many scientists have commented on the improvement of fluidization at elevated pressures and on the smoothness of fluidization compared with atmospheric pressure.

The usual explanation is that increase in pressure causes the reduction in bubble size. This is proven to be true for fine particles but evidence is conflicting for operation of fluidized beds of coarse particles that are more appropriate for the pressurised fluidized bed combustors (PFBC).

High operating pressure results in an increase of bed expansion, heat transfer coefficients and apparently solid entrainment; and in a decrease of minimum fluidization velocity and solid segregation. However, it seems that all these pressure effects have not been adequately explained and properly quantified, and they differ depending on size of fluidised particles.

A number of industrial processes based on fluidized bed technology and operating at elevated pressure have been developed in the past 35 years. The status of these different technologies varies considerably, with some fully commercial and some still under development and demonstration.

1.2 PRESSURISED FLUIDIZED BED PROCESSES

1.2.1 PRESSURISED FLUIDIZED BED COMBUSTION

In the industry, a fluidized bed coal combustion process can operate either at atmospheric pressure or at elevated pressures, usually in the range from 500 to 2000 kPa. Atmospheric pressure fluidized bed combustors are commercially available as bubbling or circulating bed systems in the capacity range $1\text{MW}_{\text{thermal}}$ to $250\text{MW}_{\text{electric}}$. Several hundred units of both types are in operation in developed countries, and over 2500 bubbling beds are operational in China and India together (UK Department of Trade and Industry, 1999).

The advantages of fluidized bed combustion are in using a wider range of waste-derived fuels than conventional pulverised fuel combustion, and emitting less nitrogen oxides (NO_x) because of lower combustion temperatures and less oxides of sulphur (SO_x) when crushed limestone is continuously added with coal. Although, the efficiency of fluidized bed combustors used for power generation is similar to that of conventional plant (averaging around 38%), this technology provides better environmental performance when utilising lower grade coal.

Pressurised bubbling fluidized bed combustors (PFBC), which can achieve efficiencies of up to 45%, are now commercially available. The major

advantage of PFBC is that the hot combustion gases leave the combustor under pressure and can be expanded through a gas turbine to generate additional electricity.

Other advantages include fuel flexibility, enhanced heat and mass transfer, modularity and suitability for retrofit applications (UK Department of Trade and Industry, 2000). The elevated pressure increases the power output per area unit, and hence reduces the size and the capital cost of equipment (Figure 1-1).

In combined cycle power applications, combustion takes place at a pressure of 1200 to 1600kPa and 75-80% of the electricity is generated in a conventional steam turbo-alternator. The pressurised combustion gases after a cleaning process can be expanded through a gas turbine to generate remaining 20-25% of electricity. A limitation of the technology is in requirement to use either a proprietary "ruggedised" gas turbine or special high-temperature filters.

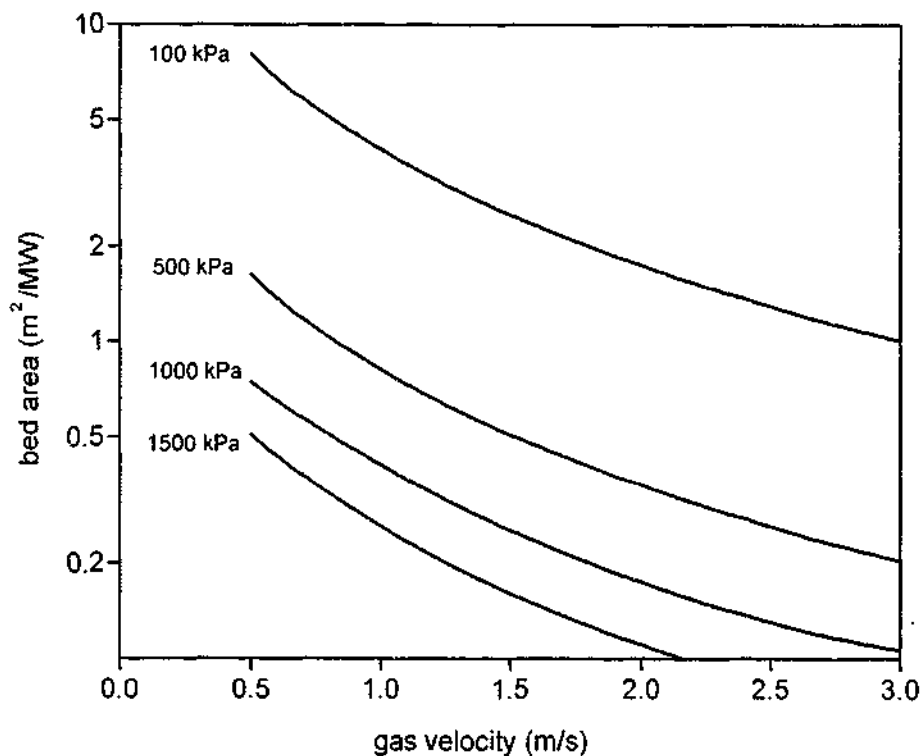


Figure 1-1. Relative bed area of fluidized bed combustors at different operating pressures (from Roberts et al., 1983)

Compared to hundreds of atmospheric fluidized bed combustors in use worldwide, only a small number of PFBC based on the bubbling bed concept have been installed in the world. The initial monopoly supplier, Alstom Power (formerly ABB Carbon), has supplied seven out of nine installations. These installations in Sweden, Spain, Japan, Germany and the USA initially functioned as demonstration units, and most of them are now operating on a commercial basis.

The highest level of current large-scale activity is in Japan (Komatsu et al., 2001), where a long tradition of technical innovation and willingness to take risks, a very strong heavy industry manufacturing base and scarcity of fuel for power generation have created a favourable commercial and technological conditions for PFBC deployment.

Pressurised circulating fluidized bed combustion (PCFBC) is the alternative technology variant, which can offer several significant advantages over the bubbling bed arrangement. These are higher combustion efficiency, lower sorbent consumption and higher sulphur removal efficiency, better NO_x control, and smaller in diameter and lighter units for the same capacity.

However, PCFBC processes remain at an earlier stage of development with a number of pilot-scale investigations. There is an ongoing project to develop a hybrid gasification/PCFBC system at Foster Wheeler Development Corporation and supported by the US Department of Energy. This hybrid system is usually referred to as the advanced, or second-generation, or topping cycle, pressurised circulating fluidized bed combustion and can result in very high efficiency of 44–50% (Pai, 1995; US Department of Energy, 1999).

1.2.2 PRESSURISED FLUIDIZED BED GASIFICATION

Coal gasification is a well-proven technology and commercial coal gasification plants are used in many countries for the production of gas and chemicals. However, commercial fluidized bed gasifiers are very rare nowadays. There were around 70 conventional bubbling fluidized bed, atmospheric pressure

Winkler gasifiers in operation but they were superseded by the entrained flow and fixed bed gasifiers (Scott & Carpenter, 1996).

Rheinbraun AG, which owns and operates several lignite mines in Germany, started to develop the Winkler process under pressure in 1975 and completed research and development in 1997 (Adlhoch et al., 2000). If the original Winkler process was based on a bubbling bed, the modified version could be operated as an expanded bubbling bed or in circulating mode.

The basic idea for the development of so-called high temperature Winkler (HTW) process was to increase the specific capacity, optimise the carbon conversion and increase the gas quality. The HTW process is based on the gasification of lignite and was originally developed to produce reducing gas for iron ore. Further development switched to the production of synthesis gas, then to power generation and later to the gasification of waste plastics.

Rheinbraun built several pilot and demonstration plants in Germany and Finland with the operating pressure varying between 1000kPa for synthesis gas production and 2500-3000kPa for the integrated gasification combined cycle (IGCC).

In recent years with the development of large and efficient gas turbines, there has been much interest in using gasification to generate electricity. Gasification enables the advantages of gas turbine technology to be accessed using any fuel. The combination of a coal gasification plant and a gas turbine could generate power as efficiently as the most modern conventional coal-fired power plant, but with much lower emissions (UK Department of Trade and Industry, 1998). Biomass and different types of pre-treated residual waste can also be successfully gasified.

At one stage the HTW process combined with a fluidized bed steam dryer has been proposed as the most attractive option for power generation from German brown coal and Australian lignite. However, economic considerations intervened as it became more difficult to secure an adequate return from the capital expenditure to improve thermal efficiency, based on expensive capital and cheap coal.

In 1988 – 1996 several Finnish companies and universities had undertaken significant process development work related to biomass-based IGCC technology (Kurkela, 2001). The whole IGCC process was demonstrated by Foster Wheeler Energia in Sweden in 1993 – 1999. The process was based on a small demonstration pressurised air-blown circulating fluidized bed gasifier and carried out at 2000kPa. Although tests carried out with a range of fuels were successful and the process was considered to be technically ready, no plans to build industrial plants were made for economical reasons.

In Japan, Ebara and UBE Industries have jointly developed the process to generate syngas (a gas mixture of hydrogen and carbon monoxide) from plastic packaging waste, which serves as the feedstock for the ammonia synthesis process. This system is a two-stage pressurised gasifier and a slag combustion system. The first stage gasifier uses the twin internal circulating fluidized bed furnace, developed by Ebara, as a pressurised low temperature (873 – 1073K) gasifier and the second stage reactor is a high temperature (1573 – 1773K) gasifier. Both reactors are operated under elevated pressure in the range from 700 to 1000kPa. After an extensive test program in 2000, the first demonstration plant with capacity of 30 tonnes per day was commissioned for commercial operation in 2001 to recycle plastic packaging waste (Steiner et al., 2002).

The Clean Coal Technology Demonstration Program is co-funded by the US Government and industry in order to provide the energy marketplace with advanced, more efficient and environmentally clean coal-based technologies. Among the technologies being demonstrated is the IGCC process. A 42-month demonstration project based on a Kellogg Rust Westinghouse (KRW) pressurised fluidized bed gasifier was completed in the USA in 2001. The KRW gasifier is the product of 13 years of development and operating experience on a process development unit and bench scale studies at the Westinghouse Research Laboratory, and can operate at the pressure of 2000kPa (US Department of Energy, 1996).

The current status of the IGCC technology is that it is clean and efficient but very expensive (20–30% more than that of conventional power plant),

and unreliable with availability 25% less than that of conventional coal-fired plant, fitted with flue gas desulphurisation.

1.2.3 POLYMERISATION

In 1968 Union Carbide developed and commercialised an industrial process used to transform ethylene into high-density polyethylene (HDPE). The "UNIPOL" process enabled the reaction of polymerisation to occur in a bubbling fluidized bed at the operating pressure of 2000kPa. In the early 1980s this process was successfully applied to the gas-phase polymerisation of linear low-density polyethylene (LLDPE), and later to manufacturing polypropylene (PP) (Brockmeier, 1987).

For more than 30 years the inventor of the process has held a monopoly position in the pressurised fluidized bed polymerisation. The "UNIPOL" process has been accepted and licensed to more than 20 companies worldwide. The technology has been proved in use with more than 80 fluidized bed reactors operating in the world.

Recently a new process to manufacture vinyl acetate monomer (VAM) has been patented ("BP makes leap to VAM fluidised bed process," 1998). The new technology replaces the currently used fixed bed reactors with a more efficient fluidized bed system operating at pressures between 800 and 1000kPa. The advantage of fluidized bed reactors is mainly the savings in fixed capital investment with expected investment cost reduction of about 30% compared to fixed bed technology.

1.3 PROJECT AIM

This experimental project was undertaken as a part of the research programme of the Cooperative Research Centre (CRC) for Clean Power from Lignite. The primary objective of the Centre is developing technologies to reduce greenhouse gas emissions from lignite-based power generation by improving efficiency while maintaining low costs of electricity.

Since the majority of advanced lignite-based power generation processes use fluidized beds as their major reactors, one of the Centre's research areas is fluidized bed process development. Present understanding of flow processes found in pressurised fluidized beds is far from complete with great concern for the lack of good quality physical data.

This study is expected to contribute to the development of gasification-based fluidized bed technologies to generate syngas and electric power from lignite, which is currently underway at the Centre.

Many experiments have been carried out in the field of fluidization under pressure since the 1950s; however no consistent conclusions have been drawn in many cases. The overall aim of this project was to provide a comprehensive and current review of what was known about the effect of pressure on fluidized bed behaviour; and to study experimentally relevant hydrodynamic data for pressurized fluidized bed operation to enable the design of large demonstration and commercial scale reactors for the coal gasification and combustion processes.

The objective of the project was to study the influence of pressure on fluidization phenomena, such as minimum fluidization velocity, minimum bubbling velocity, bed expansion and voidage, and particle motion near to the bed wall; as well as to test a novel diagnostic technique suitable for online monitoring of fluidized bed behaviour.

To achieve this goal, experiments were conducted in a bubbling fluidized bed at operating pressures up to 2500kPa and ambient temperature with Geldart A and B materials² (Geldart, 1973). Pressure probe, visual observation and the electrical capacitance tomography (ECT) were used for characterising the fluidized bed behaviour at elevated pressure. The electrical capacitance tomography is still relatively new and promising technique, which being non-invasive does not interfere with the processes taking place in

² The Geldart classification of particles is widely used in the area of fluidization, with the solids simply called *Geldart A solids*, and so forth (Kunii, D., & Levenspiel, O. (1991). *Fluidization Engineering* (2nd ed.). Boston: Butterworth-Heinemann.). This practice is followed here.

fluidized beds. Although it has been used in fluidization research, it has not been previously used to study the fluidized bed behaviour in a pressurised environment.

The influence of operating pressure on the motion of Geldart A and B particles near the fluidized bed wall surface, which permits better understanding of the effect of pressure on wall-to-bed heat transfer and solids mixing, was studied using luminescent pigment as bed solids. The luminescent pigment was available in the form of spherical Geldart A particles, and the larger Geldart B particles were produced from these by agglomeration.

A pulse of bright light was transmitted from outside of the pressure vessel via fibre optics and illuminated a small region of the bed material adjacent to a transparent vessel wall. Illuminated particles showed an afterglow for several seconds, which was digitally recorded on video and analysed.

1.4 THESIS STRUCTURE

Following this introductory chapter, the thesis is divided into a number of interconnecting chapters:

- Literature review
- Experimental
- Minimum fluidization and minimum bubbling conditions
- Experimental observation of bed voidage in a pressurised bubbling bed
- Experimental observation of particle motion near the wall surface in a pressurised bubbling bed

The literature review for this research project was conducted over a period of several years and involved an examination of numerous book and encyclopaedia texts, refereed journal publications in various disciplines,

conference proceedings, theses and trade journals and magazines. The objective of this review was to gain an understanding of the current state of knowledge in the field in which the research has been undertaken since the 1950s; and to identify key researchers and seminal authors.

The research findings, presented by each of the authors cited in the review, were attempted to be balanced against each other, so that a basis for the current research could be established. This approach provided a reference by which any contributions to knowledge in the area of fluidization in a pressurised environment, presented in this thesis, could be measured.

Experimental part of the thesis starts with a chapter describing the experimental high-pressure facility erected at Monash University for this project. The experimental chapter provides detailed information about the fluidized bed vessel including gas distributors, flow and pressure measuring instruments and high-pressure safety measures.

Further, the experimental chapter describes the electrical capacitance tomography (ECT) system used in this work to study the bed voidage; and provides details about special arrangements made for using the ECT system in a pressurised environment. The chapter continues with describing the equipment and instruments used in the experimental study of the influence of pressure on the motion of particles near to the fluidized bed wall; and concludes with the information about the Geldart A and B solids used in this study.

Since discussion on accurate prediction of the minimum fluidization velocity still appears to remain of much interest, the present experimental programme started with determining this fluidization parameter for several Geldart A and B materials at various operating pressures; and comparing the experimental results with predictions from various available correlations.

The experimental methodology and the results of experiments to study the effect of pressure on the minimum fluidization velocity, minimum bubbling velocity, and the voidage at minimum fluidization and minimum bubbling are reported in the chapter dealing with those conditions.

The subsequent chapter is on experimental observation of bed voidage in a pressurised bubbling fluidized bed. Two methods described in this chapter were used to measure the bed voidage. For a Geldart A material, the bed collapse technique was used to measure the dense phase voidage in a bubbling bed at several elevated pressures. For the first time in fluidization research at elevated pressure, the electrical capacitance tomography was used to measure the overall bed voidage in bubbling beds of Geldart A and B solids.

The final experimental chapter describes and discusses the observation of the influence of pressure on particle motion near to the wall of a fluidized bed. Digital image analysis of the movement of the illuminated cluster of luminescent Geldart A and B particles was applied in this chapter and provided statistically determined velocity of the cluster along the wall surface and the particle exchange frequency in the direction perpendicular to the wall, determined from the decay in luminosity.

The thesis is concluded with the final chapter which summarises the findings of the research.

Chapter 2 LITERATURE REVIEW

With the development of coal combustion and gasification fluidized bed processes in the early 1970s the need for investigations of fluidization at elevated pressure became evident. Since then many academic and industrial researchers have studied the effect of pressure on fluidized bed behaviour. This chapter provides a review covering literature on effects of elevated operating pressure on fluidization, published before August, 2002.

2.1 INTRODUCTION

Pressure affects the operation of gas-solid fluidized beds because it affects gas density in a system. If system pressure is increased at constant temperature, according to the perfect gas law the gas density is increased by the same factor as the pressure increase ratio. Gas viscosity, however, increases only weakly with pressure and it is customary to neglect the pressure variation in most engineering work (White, 1994).

For example, at constant temperature of 300K an increase in pressure from atmospheric to 2000kPa will change air density from 1.161 to 23.365kg/m³ and air viscosity from 0.0185 to 0.0187mPa·s ("Table 2-229 Thermophysical properties of compressed air," 1997).

In a well-known textbook on fluidization (Kunii & Levenspiel, 1991) the authors only briefly summarized the experimental findings on effect of pressure on behaviour of fluidized beds of porous carbon powder, coal, char and uniformly sized glass beads (ballotini) at pressures up to 8000kPa as follows:

voidage at minimum fluidization ε_{mf} increases
slightly (1-4%)

minimum fluidization velocity U_{mf} decreases, however, this decrease is negligible for beds of fine particles less than $100\mu\text{m}$ in diameter, and becomes significant (up to 40%) for larger particles ($\approx 360\mu\text{m}$)

the ratio of the minimum bubbling velocity to the minimum fluidization velocity U_{mb}/U_{mf} for coarse alumina ($450\mu\text{m}$) increases up to 30% which suggests that an increase in pressure widens the range of non-bubbling fluidization

Further the authors summarized the experimental findings on effect of pressure on bed properties of bubbling fluidized beds:

voidage fraction in the emulsion ε_d increases by 20-40% in pressure range from 100 to 7000kPa for Geldart A particles (Geldart, 1973) and does not change for particles on the A/B boundary

bubbles become flatter, smaller and less stable for Geldart A particles and do not change for Geldart B particles

bubble splitting is from below and more frequent for Geldart A particles, and from the roof and not more frequent for Geldart B particles

Geldart B materials change to Geldart A with smoother fluidization, less slugging and sharp increase in entrainment

The aim of this review was to extend on the textbook's brief summary and provide an overall picture of more than 40 years of research in pressure

effects on fluidized bed behaviour. One of the objectives of the review was to acquire an understanding of the current state of knowledge in the field of fluidization in pressurised conditions.

In preparing the present review a number of comprehensive and valuable review papers have been drawn on (Botterill, 1989; Gogolek & Grace, 1995; Knowlton, 1999; Yates, 1996). Early Russian research in the pressurised fluidized beds has been somewhat summarised in English by Creasy (1971) and Botterill (1975).

Many workers have noted that the influence of pressure cannot be explained in terms of change in gas density only and fluidized beds consisting of solids of different types and sizes behave differently at similar operating conditions. In this regard information about materials used in various studies will be given when required.

2.2 NON-BUBBLING FLUIDIZATION AT ELEVATED PRESSURE

When gas is passed upwards through a packed bed of particles, several types of fluidization behaviour are possible. Fluidized beds behave differently as gas velocity, gas properties and solids properties are varied. The state of fluidization starts at the point of minimum fluidization when the drag force on the particles becomes equal to the weight of the bed.

At the onset of fluidization the bed is more or less uniformly expanded and as the gas velocity is increased further, bubbles appear in the bed. The gas velocity at which the first bubbles appear on the surface of the bed is the minimum bubbling velocity.

The regime of non-bubbling fluidization is bounded by the minimum fluidization velocity U_{mf} and the minimum bubbling velocity U_{mb} . In this regime all the gas passes between the particles without forming bubbles and the bed smoothly expands with a more or less uniform bed structure. The operational range of the non-bubbling fluidization regime is quite narrow and at ambient conditions the non-bubbling regime exists only in fluidized beds with Geldart A powders.

In fluidized beds of coarse solids bubbles tend to appear as soon as gas velocity reaches the minimum fluidization velocity. At elevated pressures or with gases of high density the range of non-bubbling regime expands as was observed by several researchers (e.g. Rietema & Piepers, 1990; Rowe et al., 1982; Varadi & Grace, 1978; Vogt et al., 2002).

2.2.1 MINIMUM FLUIDIZATION VELOCITY

It is common knowledge that the minimum fluidization velocity is the basic information required for the design and development of fluidized bed processes; however in industrial practice fluidized bed reactors are mostly operated at superficial gas velocities well above the minimum fluidization velocities and, therefore, the minimum fluidization velocity is not a quantity with a precise significance for industrial applications.

From the point of view of engineering practice even inaccuracies of up to 40% in the prediction of the minimum fluidization velocity values are more or less acceptable (Molerus & Wirth, 1997b). Despite that and many earlier works, discussion on accurate prediction of the minimum fluidization velocity still seems to remain of much scientific interest.

2.2.1.1 Determination by experiment

A standard method of determination of minimum fluidization velocity by experiment is by measuring the dependence of bed pressure drop on gas velocity. At minimum fluidization velocity the weight of the bed is fully supported by the gas flow and the pressure drop becomes constant.

Usually the gas flow rate is gradually reduced in increments from a vigorously fluidized state (e.g. Barnea & Mednick, 1975), although according to Svarovsky (1987) better reproduction of results can be obtained by allowing the bed to mix first by bubbling freely before turning the gas flow rate down to zero and then taking pressure drop measurements, while increasing gradually the gas flow rate. The minimum fluidization velocity is taken as the intersection point of extrapolated straight line of the packed bed

region and fluidized bed isobar as described elsewhere (e.g. Hartman & Svoboda, 1986; Howard, 1989; Kunii & Levenspiel, 1991; Rhodes, 1998; Svarovsky, 1987).

2.2.1.2 Estimation and computation

It is generally accepted that the best method to determine the minimum fluidization velocity would be by measurement. In practice, however, this is not always possible, especially at different operating conditions, such as at elevated pressure. In the absence of the facility to carry out experiments to determine the minimum fluidization velocity, approximate computation of this is necessary for any design or study of the fluidized bed process and numerous correlations have been proposed in the literature.

In this case the generally accepted approach is to estimate the effect of pressure on minimum fluidization velocity by employing Ergun (1952) equation for pressure loss through a packed bed, which in slightly modified form as Eq.(2.2.1) appears in many books on fluidization; or its numerous simplified variations, such as the most popular Wen and Yu (1966a; 1966b) correlation (Eq.(2.2.2)).

$$\frac{\Delta p}{L} = \frac{150(1-\varepsilon)^2}{\varepsilon^3} \frac{\mu U}{(\phi d_p)^2} + \frac{1.75(1-\varepsilon)}{\varepsilon^3} \frac{\rho_g U^2}{\phi d_p} \quad (2.2.1)$$

Where Δp is the pressure drop, L is the bed height, U is the gas (fluid) superficial velocity, d_p is particle diameter, ϕ is a shape factor, μ is the gas viscosity, ρ_g is the gas density and ε is the voidage of the bed.

$$Re_{mf} = \sqrt{33.7^2 + 0.0408Ga} - 33.7 \quad (2.2.2)$$

Where Re_{mf} is particle Reynolds number at onset of fluidization and Ga is Galileo number³. Particle Reynolds number is defined by the following equation:

³ Galileo number (Ga) and Archimedes number (Ar) are often defined interchangeably in the literature

$$\text{Re} = \frac{d_p U \rho_g}{\mu} \quad (2.2.3)$$

And Galileo or Archimedes number is defined by Eq.(2.2.4)

$$\text{Ga} = \frac{d_p^3 g \rho_g (\rho_p - \rho_g)}{\mu^2} \quad (2.2.4)$$

Where ρ_p is density of bed material.

Equation (2.2.2) is often presented in a generic form as Eq.(2.2.5):

$$\text{Re}_{mf} = \sqrt{C_1^2 + C_2 \text{Ga}} - C_1 \quad (2.2.5)$$

Where C_1 and C_2 are constants with original values 33.7 and 0.0408 respectively.

2.2.1.3 Numerous simplified correlations

Yang (1998) noted that in the design of fluidized bed systems designers encounter two completely different situations: the area of interest has very little information or it has many correlations available and their predictions give sometimes very different results.

There are numerous studies and proposed correlations on the prediction of the minimum fluidization velocity at ambient conditions as well as a number of comprehensive reviews comparing these correlations (Adanez & Abanades, 1991; Couderc, 1985; Grewal & Saxena, 1980; Lippens & Mulder, 1993).

Lippens and Mulder (1993) restricted their analysis to fluidized beds operating at ambient conditions and fluidised with air or nitrogen only and tested statistically 33 equations with 80 measurements reported in the literature on 20 solids. Their conclusion is that the well-known Ergun equation has the smallest standard deviation and is the correct equation to describe the bed pressure drop at minimum fluidization.

The great majority of the proposed in the literature correlations are based on the Ergun equation, modified after an experimental evaluation based on limited numbers of data and materials, and quite often they are purely

empirical. Those empirical correlations have limited value and according to Lippens and Mulder (1993), preference should be given to complete characterization of the fluidized bed including determination of particle shape factor ϕ and voidage at minimum fluidization ϵ_{mf} as described by Geldart (1990). Lippens and Mulder (1993) explain the widely accepted success of the Wen and Yu correlation in engineering practice as a first approximation because it simply offers the correct order of magnitude.

2.2.2 PRESSURE EFFECTS ON MINIMUM FLUIDIZATION VELOCITY

Since the mid-1970s many researchers have studied how increased pressure affects the minimum fluidization velocity. They have experimentally found that the effect of pressure on the minimum fluidization velocity depends on particle size. The results of the experiments show a clear decrease in the minimum fluidization velocity with increasing pressure for particles larger than $100\mu\text{m}$ (Geldart B and D materials); and the pressure influence is more pronounced for the larger particles (e.g. Borodulya et al., 1982; Bouratoua et al., 1993; Chiba et al., 1986; Chitester et al., 1984; Gilbertson et al., 1998; King & Harrison, 1982; Knowlton, 1977; Llop et al., 1995; Marzocchella & Salatino, 2000; Nakamura et al., 1985; Olowson & Almstedt, 1991; Saxena & Vogel, 1977; Sobreiro & Monteiro, 1982; Vogt et al., 2001).

According to Botterill (1975), similar trends with increase in static pressure were reported in Russian by Sechenov and Altshuler as early as 1958, and later by Chekhov et al. in 1961.

Other experiments showed that for fine Geldart A particles less than $100\mu\text{m}$ the minimum fluidization velocity is unaffected by pressure (Chitester et al., 1984; Foscolo et al., 1989; King & Harrison, 1982; Piepers et al., 1984; Rowe et al., 1982; Sobreiro & Monteiro, 1982).

2.2.2.1 Dependence of pressure influence on particle size and density

The experimental findings are explained by Rowe (1984) who rearranged the Ergun equation (2.2.1) to express the minimum fluidization velocity in terms

of operating variables - particle size and density, gas density and viscosity - and graphically showed how pressure *would* be expected to affect the minimum fluidization velocity for a typical granular material with a range of particle sizes from 50 μm to 10mm and a density of 1250kg/m³ fluidised with nitrogen (Figure 2-1). The curve for 50 μm particles runs parallel and very close to the X-axis and is omitted from the figure. The bed voidage at the onset of fluidization ϵ_{mf} was assumed to be constant and equal 0.5 in all cases.

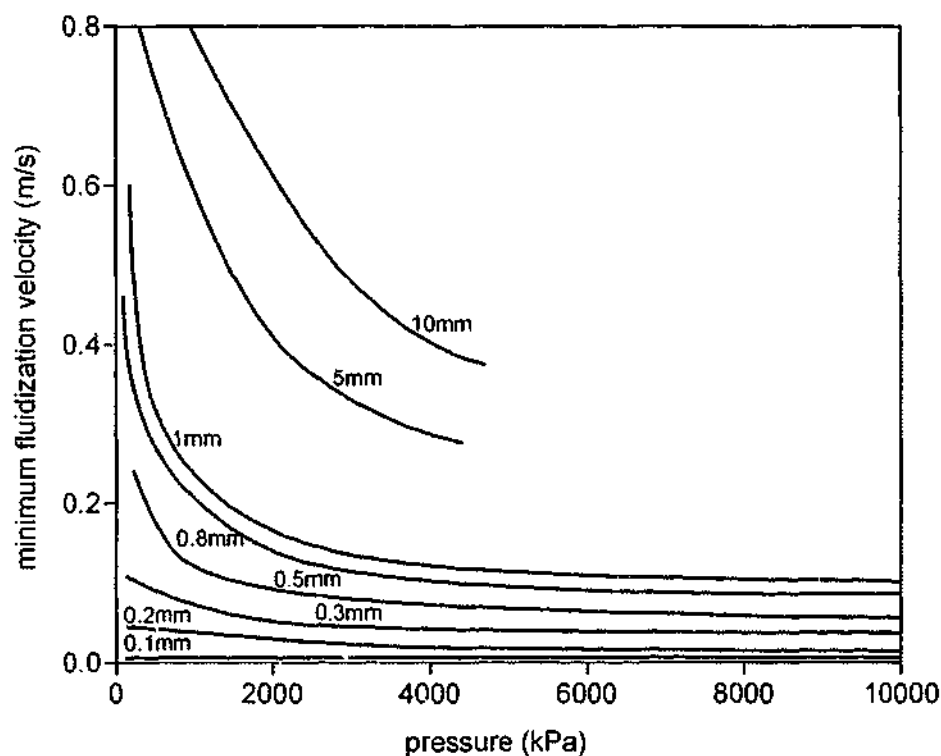


Figure 2-1. Effect of operating pressure on minimum fluidization velocity for spherical particles in a size range from 100 μm to 10mm and density of 1250kg/m³ (from Rowe, 1984)

As the two term structure of the Ergun equation and simplified Wen and Yu correlation suggests, in the laminar flow region for $Re_{mf} < 2$ and small/light particles with $d_p < 100\mu\text{m}$ the viscous loss is dominant compared to the kinetic loss; and the minimum fluidization velocity (U_{mf}) is inversely proportional to the gas viscosity (Hartman & Svoboda, 1986; Hartman & Vesely, 1993):

$$U_{mf} \propto \frac{d_p^2(\rho_p - \rho_g)}{\mu} \quad (2.2.6)$$

Pressure does not influence gas viscosity more than 10% within moderate ranges (Loomis, 1980) and to within an accuracy of 1% viscosity of air or nitrogen can be used at pressures up to 1200kPa at 300K with further reduction in the influence of pressure on viscosity at higher temperatures (UK Department of Trade and Industry, 1972). Since the bed material density is much larger than that of gas, the minimum fluidization velocity is virtually independent of pressure.

For larger/dense particles and turbulent flow ($Re_{mf} > 1000$), where the kinetic loss predominates, the minimum fluidization velocity is inversely proportional to the square root of the gas density or pressure and, therefore decreases with pressure:

$$U_{mf} \propto \sqrt{\frac{d_p(\rho_p - \rho_g)}{\rho_g}} \quad (2.2.7)$$

In the transition region of flow where the particle Reynolds number at the onset of fluidization is in the range from 2 to 1000, the minimum fluidization velocity is proportional to the power of pressure ranging from 0 to -0.5.

2.2.2.2 Testing correlations at high pressure conditions

The trends of varying pressure can be predicted by the Ergun equation (2.2.1) or numerous correlations. However, quite often the absolute values of predictions based on the correlations are significantly in error (Olowson & Alnstedt, 1991). King and Harrison (1982) fluidised ballotini, sand and coarse polymer particles at pressures up to 2500kPa and compared their experimental data with predictions from both Ergun equation and Wen and Yu correlation. They found that the Ergun equation gave a closer fit for spherical particles (ballotini) and the Wen and Yu correlation was in better agreement for irregular solids (sand and polymer).

Knowlton (1977) studied fluidization of coal, lignite, char, coke and siderite at pressures up to 6800kPa and found that agreement between experimental data and values of U_{mf} obtained from the Wen and Yu correlation Eq.(2.2.2)

was poor with predicted values being low for all pressures and materials except for larger anthracite.

Saxena and Vogel (1977) fluidised coarse dolomite particles at pressures from 179 to 834kPa and also found that values obtained from the Wen and Yu correlation were consistently smaller than the experimental values, so a new set of constants was proposed. Nakamura et al. (1985) experimentally measured the minimum fluidization velocity for Geldart B and D spherical uniformly-sized glass beads at 4900kPa and proposed their own set of constants.

Borodulya et al. (1982) performed an experimental study of hydrodynamics and heat transfer in a cylindrical fluidized bed at pressures up to 8000kPa using quartz sand and glass ballotini as bed material and proposed another set of constants.

Chitester et al. (1984) fluidised coal, char and ballotini particles of different sizes at pressures of 2169, 4238 and 6306kPa and noted that the Wen and Yu correlation underpredicts the minimum fluidization velocity values when applied to a bed of fine particles at high pressure and gives an accurate prediction for a bed of large particles, and proposed another set of constants valid for high pressure operation.

Different sets of constants C_1 and C_2 for Wen and Yu type correlations proposed in the literature for fluidization under elevated pressure are shown in Table 1.

Table 1. Comparison of constants C_1 and C_2 in Wen and Yu correlation (Eq.(2.2.5)) with constants proposed for similar correlations for predicting minimum fluidization velocity at elevated pressure

Correlation	Constant C_1	Constant C_2
Wen and Yu (1966a)	33.7	0.0408
Saxena and Vogel (1977)	25.28	0.0571
Chitester et al. (1984)	28.7	0.0494

Correlation	Constant C_1	Constant C_2
Nakamura et al. (1985)	33.95	0.0465
Borodulya et al. (1982)	16	0.0370

Other researchers compared their experimental results with predictions from either Wen and Yu or Chitester et al. correlation and found only a fair agreement (Marzocchella & Salatino, 2000; Olowson & Almstedt, 1991; Sobreiro & Monteiro, 1982; Vogt et al., 2001).

Recently two new equations for predicting the minimum fluidization velocity for round ($\phi > 0.8$) and sharp ($0.5 < \phi \leq 0.8$) particles at vacuum, atmospheric and elevated pressure conditions were proposed in the literature (Llop et al., 1996). However, the authors compared only the equation developed for sharp particles with the experimental results reported in (Llop et al., 1995) when they studied fluidization of various fractions of silica sand with air within the pressure range from 100 to 1200kPa.

2.2.3 PREDICTION OF MINIMUM FLUIDIZATION VELOCITY AT HIGH PRESSURE

Several methods for better prediction of the minimum fluidization velocity at high pressure are suggested in the literature and all of them are based on experimental determination of U_{mf} for a given material at ambient conditions first.

2.2.3.1 Method of Werther (1977)

According to (Vogt et al., 2001) in a paper published in German, Werther (1977) suggested a method to calculate the minimum fluidization velocity of a fluidization process which is not at ambient conditions. Superficial gas velocity and voidage at incipient fluidization should be determined first at ambient conditions, then these parameters can be used to calculate a characteristic particle diameter ϕd_p from the Ergun equation (2.2.1) in the following way:

$$\phi d_p = \frac{1.75 \rho_g U_{mf}^2}{2 \varepsilon_{mf}^3 (\rho_p - \rho_g) g} + \sqrt{\frac{150(1 - \varepsilon_{mf}) \mu U_{mf}}{\varepsilon_{mf}^3 (\rho_p - \rho_g) g} + \left(\frac{1.75 \rho_g U_{mf}^2}{2 \varepsilon_{mf}^3 (\rho_p - \rho_g) g} \right)^2} \quad (2.2.8)$$

Using the calculated value of the characteristic particle diameter ϕd_p and assuming that voidage at minimum fluidization conditions ε_{mf} is independent of gas density ρ_g and viscosity μ the minimum fluidization velocity at conditions different from the ambient can be calculated as follows:

$$U_{mf} = \frac{300(1 - \varepsilon_{mf}) \nu}{7 \phi d_p} \left(\sqrt{1 + \frac{7 \varepsilon_{mf}^3 g (\phi d_p)^3 (\rho_p - \rho_g)}{22500(1 - \varepsilon_{mf})^2 \nu^2 \rho_g}} - 1 \right) \quad (2.2.9)$$

Where gas density and kinematic viscosity (ν) are values at actual operating conditions.

2.2.3.2 Method of Knowlton (1999)

Another technique which can improve the accuracy of prediction of the minimum fluidization velocity using a correlation is suggested by Knowlton (1999). First it is necessary to determine U_{mf} experimentally at ambient conditions, then using this value, back-calculate an effective particle size from the given correlation. And only after that, using this effective particle size, calculate U_{mf} at actual conditions, e.g. high operating pressure.

This technique substitutes shape factor and average particle size but does not account for possible changes in voidage. However, it can predict the minimum fluidization velocity more accurately than by using a correlation on its own.

2.2.3.3 Method of Yang et al. (1985)

Another method for estimating U_{mf} at elevated pressures and temperatures is proposed by Yang et al. (1985) and reinforced again more than ten years later (Yang, 1998).

As previously mentioned, if the correct particle shape factor and the voidage to be used in the Ergun equation are not available, they are

substituted with two constants C_1 and C_2 . Many sets of constants have been proposed in the literature with various degrees of success but the Wen and Yu correlation still seems to be most popular and generic. Yang (1998) plotted eleven correlations and found that for large Galileo numbers, the discrepancy between the correlations is less than 40% but for small Galileo numbers, the difference can be more than twofold.

Based on the methodology originally developed by Barnea and Mizrahi (1973) for establishing pressure drop through fixed beds of spherical particles and extended by Barnea and Mednick (1975) for the case of incipient fluidization, Yang et al. (1985) proposed a generalized methodology which allows accurate prediction of the minimum fluidization velocity at elevated pressure or temperature. For graphical presentation a log-log plot of the dimensionless diameter $\sqrt[3]{(\text{Re}^2 C_D)_{mf}}$ vs. the dimensionless velocity $\sqrt[3]{(\text{Re}/C_D)_{mf}}$ for the known value of the bed voidage at incipient fluidization ϵ_{mf} is generated.

At minimum fluidization condition these two dimensionless groups are expressed as:

$$\sqrt[3]{\left(\frac{\text{Re}_e}{C_{D,e}}\right)_{mf}} = \sqrt[3]{\left(\frac{\text{Re}}{C_D}\right)_{mf}} \left[\frac{\sqrt[3]{(1 + \sqrt[3]{(1 - \epsilon_{mf})})}}{\sqrt[3]{\epsilon_{mf}^4} \exp\left(\frac{5(1 - \epsilon_{mf})}{9\epsilon_{mf}}\right)} \right] \quad (2.2.10)$$

$$\sqrt[3]{(\text{Re}_e^2 C_{D,e})_{mf}} = \sqrt[3]{(\text{Re}^2 C_D)_{mf}} \left[\frac{\sqrt[3]{\epsilon_{mf}}}{\sqrt[3]{(1 + \sqrt[3]{(1 - \epsilon_{mf})})} \exp\left(\frac{10(1 - \epsilon_{mf})}{9\epsilon_{mf}}\right)} \right] \quad (2.2.11)$$

Where $C_{D,e}$ is modified drag coefficient, $C_{D,mf}$ is drag coefficient at minimum fluidization, Re_e is modified Reynolds number and Re_{mf} is Reynolds number based on minimum fluidization velocity. Modified drag coefficient and Reynolds number are defined in the following equations:

$$C_{D,\varepsilon} = C_D \frac{\varepsilon^3}{1 + \sqrt[3]{1 - \varepsilon}} \quad (2.2.12)$$

$$\text{Re}_\varepsilon = \text{Re} \left(\frac{1}{\varepsilon \exp\left(\frac{5(1-\varepsilon)}{3\varepsilon}\right)} \right) \quad (2.2.13)$$

Further, the various standard drag correlations given in (Clift et al., 1978) or (Haider & Levenspiel, 1989) for single spherical particles are used to determine drag coefficient C_D as a function of Reynolds number Re .

Combining these drag correlations with Eqs.(2.2.10) and (2.2.11), a series of curves are obtained by plotting the dimensionless diameter vs. the dimensionless velocity with the voidage as a parameter.

The minimum fluidization velocity of the material of interest is determined at ambient conditions, then this data point is located on the proper curve of constant voidage ε_{mf} on a graph, and once the applicable curve of ε_{mf} is found, the minimum fluidization velocity at any pressure can be calculated from the same curve. It is assumed that the voidage at minimum fluidization does not change with pressure (Section 2.2.7 below) and at the desired operating conditions the dimensionless diameter is calculated from Eq.(2.2.11) where

$$\sqrt[3]{(\text{Re}^2 C_D)_{mf}} = \sqrt[3]{\frac{4Ga}{3}} = \left(\frac{d_p}{\sqrt[3]{\frac{3\mu^2}{4g\rho_g(\rho_p - \rho_g)}}} \right) \quad (2.2.14)$$

The corresponding value of the dimensionless velocity is then taken from the graph and the minimum fluidization velocity is calculated using Eq.(2.2.10) and the following equation:

$$\sqrt[3]{\left(\frac{\text{Re}}{C_D}\right)_{mf}} = \left(\frac{U_{mf}}{\sqrt[3]{\frac{4g\mu(\rho_p - \rho_g)}{3\rho_g^2}}} \right) \quad (2.2.15)$$

According to Yang et al. (1985) this approach is applicable in all systems except those with Geldart A particles where ε_{mf} changes with pressure, and with particles which substantially deviate from the spherical shape.

Later Shrivastava et al. (1986) applied this method to the experimental data of Saxena and Vogel (1977) on non-spherical ($\phi=0.88$ and 0.80) dolomite particles of the size range $88-1410\mu\text{m}$ and pressure range $179-834\text{kPa}$ with the excellent agreement between the predicted and experimental results.

2.2.3.4 Method of Bin (1986)

The last procedure based on the Ergun equation (2.2.1) to predict the minimum fluidization velocity at any pressure and for different fluidising gases, which is applicable for practical purposes, is proposed by Bin (1986; 1992).

Shape and structure of particles, moisture content, electrostatic and wall effects may contribute to the accuracy of the obtained data for different solids, and Geldart A powders in particular. Since in reality shape factor of particles can vary from unity and reported values of the voidage at minimum fluidization ε_{mf} are within the range of $0.36-0.66$, the values of constants C_1 and C_2 in Wen and Yu type equations may vary - C_1 from 5 to 246.5 and C_2 from 0.022 to 0.1 . Obviously, there is no universal pair of values for C_1 and C_2 for all bed materials.

Being concerned with a large number of sets of constants already proposed for Wen and Yu type correlations, Bin (1986) recommends experimental determination of U_{mf} and ε_{mf} for a given bed material at ambient conditions using air or nitrogen. Then the Ergun equation can be used and a value of shape factor ϕ can be calculated as a fitting parameter.

Assuming that ε_{mf} and ϕ remain constant (therefore values of C_1 and C_2 in Wen and Yu type correlations are constant), the values of U_{mf} for that bed material at different conditions can be predicted from the Ergun equation. According to Bin (1992), this procedure is satisfactory for a variety of solids

and experimental conditions with the average error below 10% and is much simpler than the methodology proposed by Yang et al. (1985).

2.2.4 MINIMUM BUBBLING VELOCITY

It is generally accepted that in fluidized beds of Geldart B and D materials the minimum bubbling velocity is the same as the minimum fluidization velocity. Fine Geldart A powders, however, have the ability to be fluidised at velocities beyond the minimum fluidization without bubbling and the difference between the minimum bubbling velocity and the minimum fluidization velocity can be as large as ten times (Jacob & Weimer, 1987; Pell, 1990). The fluidized bed expands smoothly and homogeneously in a manner similar to that of liquid fluidized beds until a velocity is reached at which small bubbles appear at the surface.

2.2.4.1 Experimental determination and calculation

Experimental determination of the minimum bubbling velocity is subject to uncertainty since it is based usually on visual observation of bubbling. In this regard another definition of U_{mb} has been suggested as the velocity at which the maximum bed height is observed (Cheremisinoff & Cheremisinoff, 1984).

Unlike the minimum fluidization velocity, the minimum bubbling velocity was correlated for the first time in the late 1970s and until now the only widely accepted correlation appears to be that of Abrahamsen and Geldart (1980a). They examined the effect of gas and powder properties on homogeneous bed expansion and on the ratio U_{mb}/U_{mf} under ambient conditions.

Twenty three different powders of the following types - alumina, glass ballotini and cracking catalyst - were fluidised with air, helium, argon, carbon dioxide and Freon-12. Mean particle size varied from 20 to 72 μ m and particle densities were in the range 1117 - 4600kg/m³. Abrahamsen and Geldart defined Geldart A particles when $U_{mb}/U_{mf} > 1$ and Geldart B

particles when $U_{mb}/U_{mf}=1$, and developed the following correlation to predict U_{mb}/U_{mf} :

$$\frac{U_{mb}}{U_{mf}} = \frac{2300 \rho_g^{0.126} \mu^{0.523} \exp(0.716F)}{d_p^{0.8} g^{0.934} (\rho_p - \rho_g)^{0.934}} \quad (2.2.16)$$

Where F is the mass fraction of fines less than $45\mu\text{m}$ in the powder.

Equation (2.2.16) implies that the minimum bubbling velocity increases with increase in gas density and that if Geldart B material is near the B/A boundary it can shift to Geldart A behaviour with gas density increase.

2.2.5 PRESSURE EFFECTS ON MINIMUM BUBBLING VELOCITY

Geldart and Abrahamsen (1978) reported the results of their experiments with alumina and ballotini fluidised with nitrogen, helium and carbon dioxide at low pressures ranging from sub-atmospheric 20 to 150kPa. They found that the minimum bubbling velocity decreased as the absolute pressure decreased and as the fluidising gas was changed from carbon dioxide to nitrogen, and then to helium.

Later, Abrahamsen and Geldart (1980a) noted that the original interpretation of the data was incorrect and found that under ideal experimental conditions the minimum bubbling velocity could be accurately described by the Eq.(2.2.17) and should increase with operating pressure according to $p^{0.06}$. This indicates a very weak effect of pressure on the minimum bubbling condition.

$$U_{mb} = 2.07 \exp(0.716F) \frac{d_p \rho_g^{0.06}}{\mu^{0.347}} \quad (2.2.17)$$

The dependence of the minimum bubbling velocity on pressure, temperature and type of gas is still relatively unknown and findings in the literature are somewhat controversial. The pressure effect on the minimum bubbling velocity has been experimentally studied by a number of investigators (e.g. Guedes de Carvalho et al., 1978; Jacob & Weimer, 1987;

King & Harrison, 1982; Piepers et al., 1984; Sciazko & Bandrowski, 1985; Varadi & Gracc, 1978).

2.2.5.1 Experimental findings

Guedes de Carvalho et al. (1978) studied the behaviour of glass ballotini with mean particle diameters of 64 and 211 μm and sand with size of 74 μm fluidised by nitrogen and carbon dioxide at pressures up to 2800kPa; and found that in each case the minimum bubbling velocity was only slightly higher than the minimum fluidization velocity and for finer particles it was independent of pressure.

For 211 μm ballotini, the minimum bubbling velocity was reported to decrease a little with increase in operating pressure. The results of the experiments are contrary to the predictions from the Abrahamsen and Geldart correlation (Eq.(2.2.16)) and to further experimental results of King and Harrison (1982) who found that the minimum bubbling velocity increased with pressure for ballotini and sand smaller than 100 μm .

Sobreiro and Monteiro (1982) investigated the influence of pressure up to 3500kPa on the behaviour of various Geldart B materials (alumina, ballotini and iron sulfide particles) fluidised with nitrogen, and their particular interest was to study the influence of pressure on gas velocity and bed voidage at both the minimum fluidization and minimum bubbling conditions. They found that the influence of pressure on the minimum bubbling velocity could be very different indeed, as can be seen in Figure 2-2 and Figure 2-3 but failed to explain their results.

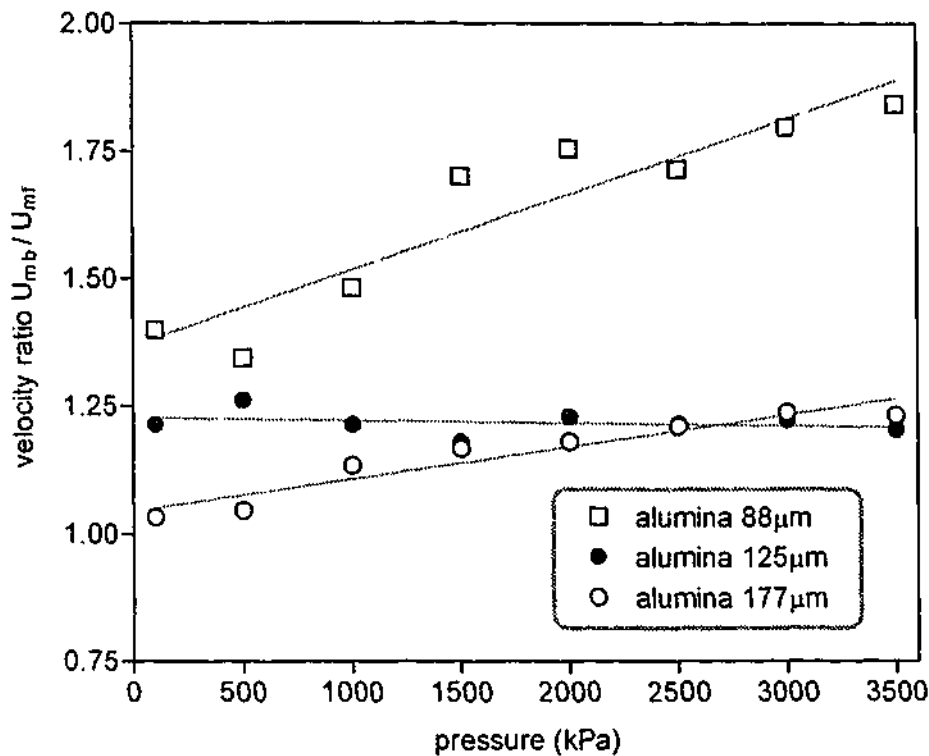


Figure 2-2. Changes in U_{mb}/U_{mf} ratio with pressure for alumina of different sizes according to Sobreiro and Monteiro (1982)

The minimum bubbling velocity of the smallest (88 μm) alumina particles increased from 0.0112 to 0.0164m/s as the pressure was increased to 3500kPa. Sobreiro and Monteiro (1982) found that, although, at ambient conditions this Geldart B material was located very close to the A/B boundary, at elevated pressure its behaviour approached that of a Geldart A powder. This contradicts the lack of influence of pressure on U_{mb} for ballotini and sand particles located on the Geldart A side of the boundary with similar to the alumina diameter and density as reported by Guedes de Carvalho et al. (1978).

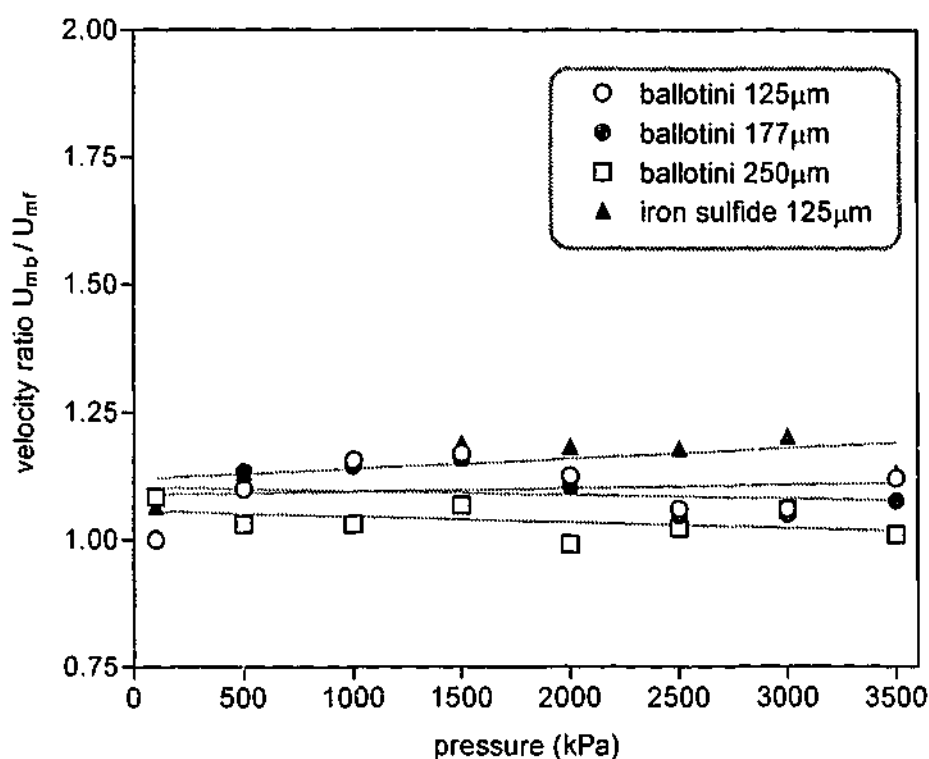


Figure 2-3. Changes in U_{mb}/U_{mf} ratio with pressure for ballotini of different sizes and iron sulfide particles according to Sobreiro and Monteiro (1982)

It would be expected that the minimum bubbling velocity is equal to the minimum fluidization velocity for Geldart B materials. However, Sobreiro and Monteiro (1982) established different, although close, values for both velocities at all experimental conditions for the larger and denser Geldart B particles, and observed the decrease of both minimum fluidization and minimum bubbling velocities with pressure increase.

The same trend was observed by Guedes de Carvalho et al. (1978) and Marzocchella and Salatino (2000), although Varadi and Grace (1978) reported an opposite pressure influence.

In a preliminary study Varadi and Grace (1978) carried out high pressure experiments in a two-dimensional column using sand screened to a size range 250 to 295µm and found that at atmospheric pressure there was no difference between minimum fluidization and minimum bubbling velocities, as expected for a Geldart B material. However, with increasing absolute pressure up to

2170kPa the minimum bubbling velocity steadily increased while the minimum fluidization velocity decreased slightly.

In contrast King and Harrison (1982) did not observe any shift from Geldart B to Geldart A behaviour and found that $U_{mb}/U_{mf} = 1$ for 288 μm sand over the pressure range from 100 to 2500kPa as can be seen in Figure 2-4.

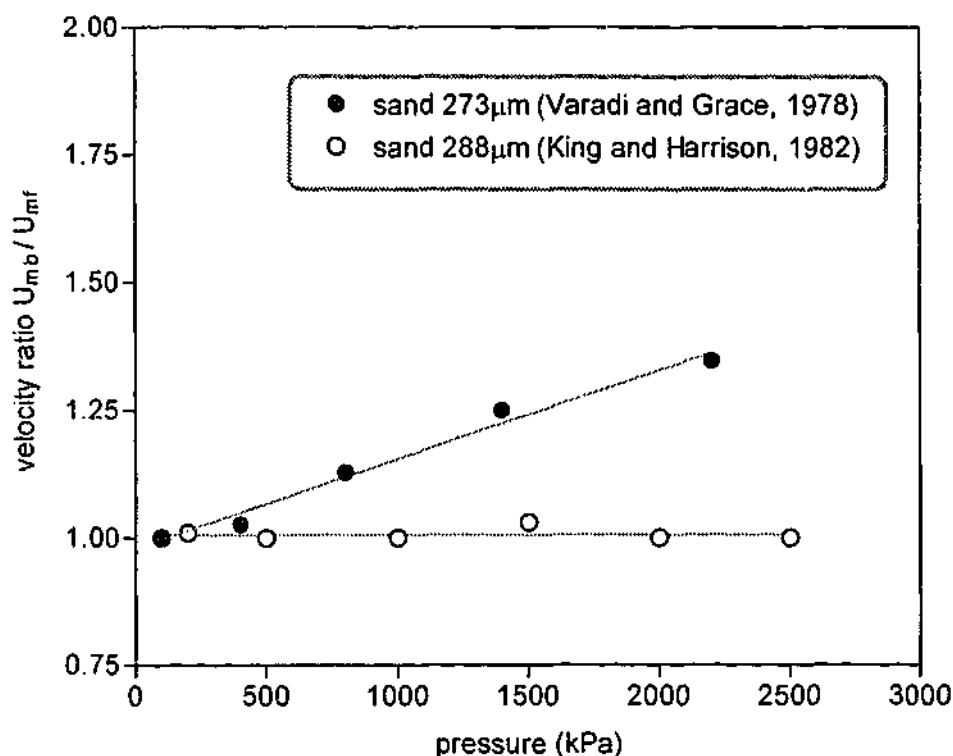


Figure 2-4. Changes in U_{mb}/U_{mf} ratio with pressure for sand of similar sizes according to Varadi and Grace (1978), and King and Harrison (1982)

Rowe et al. (1982) also observed the extension of the range of uniform bed expansion (i.e. an increase in the difference $(U_{mb} - U_{mf})$) with an increase in gas density (pressure), however, the effect was not very great and a five-fold increase in gas density caused approximately 25% increase in the difference $(U_{mb} - U_{mf})$. Later Rowe et al. (1984) observed some uniform expansion before bubbling and, therefore a shift from Geldart B behaviour to that of Geldart A, when they fluidised 450 μm alumina and 262 μm silicon carbide at little more than 200kPa. At atmospheric conditions both materials began to

bubble as soon as they were fluidised. For the alumina the ratio U_{mb}/U_{mf} increased to about 1.25 at 3000kPa and after that did not increase rapidly with pressure.

Piepers et al. (1984) and Rietema and Piepers (1990) carried out experiments with Geldart A 60 μ m cracking catalyst fluidised with helium, methane, neon, nitrogen, argon and hydrogen at pressures up to 1500kPa and confirmed that the bubble point velocity, which essentially is the same as the minimum bubbling velocity, increased with increasing pressure. However, the type of gas has a very strong effect on the variation of the minimum bubbling velocity with pressure. They found a very weak dependence of the minimum bubbling velocity on pressure when fluidising gas was hydrogen, while the variation of the minimum bubbling velocity with pressure was the strongest when using argon.

Sciazko and Bandrowski (Rowe, 1987; Sciazko & Bandrowski, 1985, 1987) carried out some experimental work on the effect of pressure on minimum bubbling velocity of coal mixtures having a wide range of particle sizes and found that in the majority of cases the minimum bubbling velocity increased with increase in pressure. Only in the case of a mixture of the largest typical Geldart B particles did the minimum bubbling velocity diminish with the pressure increase, but to a smaller extent than the minimum fluidization velocity, which at ambient conditions was found to be higher than the minimum bubbling velocity.

Jacob and Weimer (1987) complicated things even further when reporting measurements of the minimum bubbling velocity for Geldart A carbon powders of 44 and 112 μ m size fluidised by synthesis gas in an industrial pilot-scale fluidized bed operating at pressures between 2070 and 12420kPa. For the 112 μ m material the minimum bubbling velocity increases with pressure but the effect of pressure on the minimum bubbling velocity for the 44 μ m powder is somewhat different. The minimum bubbling velocity increases slightly within the pressure range from 2070 to 8280kPa, but then starts decreasing within the pressure range from 8280 to 10350kPa. The authors suggest that this phenomenon needs to be further investigated.

According to Jacob and Weimer (1987) it has generally been found that with increasing pressure for systems of Geldart A powders the minimum bubbling velocity also increases, however, the extent of the pressure effect and the reason for it is uncertain. Two theories have been proposed, one is based on interparticle forces (Piepers et al., 1984), and another is based on hydrodynamic forces (Foscolo & Gibilaro, 1984).

2.2.6 FLUIDIZED BED STABILITY

A fluidized bed is considered to be stable when it uniformly expands in non-bubbling regime and becomes unstable when the first bubbles appear. It is generally accepted that fluidized beds become smoother and the stable region of fluidization is extended to higher velocities when operated at elevated pressure. Theories of fluidized bed stability have been the source of controversy and two separate approaches have been made. One theory is based on the assumption that interparticle forces dominate bed stability and the other assumes that it purely depends on hydrodynamic forces.

2.2.6.1 Interparticle Forces Stability Theory

The Interparticle Forces Stability Theory was proposed by the researchers from Eindhoven University of Technology (Piepers et al., 1984; Piepers & Rietema, 1989; Rietema, 1991; Rietema et al., 1993; Rietema & Piepers, 1990). According to these authors a homogeneous fluidized bed maintains a mechanical structure even when expanded and that the cohesive interparticle forces give the bed certain elasticity characterised by the modulus E . From this theory it follows that for gas-solid fluidization system at the maximum stable bed expansion without bubbling (i.e. minimum bubbling condition) the equation given in (Piepers & Rietema, 1989) holds:

$$\frac{(\rho_p - \rho_g)^2 \rho_p d_p^4 g^2}{\mu^2 E_{mb}} = \left(\frac{150(1 - \epsilon_{mb})}{\epsilon_{mb}^2 (3 - 2\epsilon_{mb})} \right)^2 \quad (2.2.18)$$

Where E_{mb} is elasticity modulus at the minimum bubbling point and can be calculated from the following equation:

$$E_{mb} = \rho_p \left(\frac{U_{mb}(3-2\varepsilon_{mb})}{\varepsilon_{mb}} \right)^2 \quad (2.2.19)$$

If the left-hand side of Eq.(2.2.18) is less than the right-hand side the fluidized bed is stable, if it is greater then the bed is unstable or bubbling.

The reported experimental results (Piepers et al., 1984; Piepers & Rietema, 1989) indicate that the bed voidage and velocity at minimum bubbling point increase with pressure and this is strongly affected by the kind of gas used for fluidization. This is explained to be the result of higher interparticle forces at high pressure due to gas absorption on the particle surfaces.

According to Yates (1996) this theory explains many experimental observations but its weakness is that it is not possible to calculate the elasticity modulus in order to make predictions that can be experimentally tested. The elasticity modulus is a complex function of the material properties of particles, particle size, structure of packing of the particles, and contact and cohesion forces between particles, and not just a property of the solids in the bed.

2.2.6.2 Hydrodynamic Forces Stability Theory

The Hydrodynamic Forces Stability Theory was proposed by Foscolo and Gibilaro (Foscolo et al., 1987; Foscolo et al., 1989; Foscolo & Gibilaro, 1984; Foscolo et al., 1983; Gibilaro, 2001; Gibilaro et al., 1988) and is based on a postulate that fluidized beds are composed of two incompressible and interpenetrating fluids, the gas phase and solids phase which is assumed to behave like a fluid under the influence of drag and buoyancy forces.

The authors presented the bubble point criterion in the form of the following equation:

$$\frac{\sqrt{gd_p}}{U_t} \sqrt{\frac{(\rho_p - \rho_g)}{\rho_p}} = 0.56n \sqrt{(1 - \varepsilon_{mb})} \varepsilon_{mb}^{n-1} \quad (2.2.20)$$

Where U_t is particle terminal fall velocity and n is Richardson and Zaki (1954) parameter. If the left-hand side of Eq.(2.2.20) is less than the right-hand side the fluidized bed is unstable, if it is greater then the bed is stable.

Several researchers put this theory to a test with various degrees of success. While Rowe (1989) gave full support to the theory, Jacob and Weimer (1987) found that the stability criterion equation gives adequate correspondence between estimated and experimental values of ε_{mb} only in some cases.

Some experimental data obtained by Jacob and Weimer (1987), Polotto et al. (1993) and Marzocchella and Salatino (2000) indicated the presence of interparticle forces, so the authors suggested that an appropriate theory might be based on combination of interparticle and hydrodynamic forces.

2.2.7 EFFECT OF PRESSURE ON NON-BUBBLING BED EXPANSION

The bed expansion at different gas velocities is expressed simply as the ratio of bed height (H) to the initial bed height, measured at the minimum fluidization velocity (H_{mf}), although other definitions exist (Section 2.3.2 below).

The bed voidage ε is defined as the fraction of the bed volume occupied by the space between the particles (Howard, 1989) and can be expressed by a simple relationship:

$$\text{voidage} = 1 - \frac{\text{volume of solids}}{\text{volume of bed}}$$

With Geldart A materials, the bed expands uniformly without bubbling as the gas velocity is increased up to the minimum bubbling velocity, when it reaches a maximum height, and gradually collapses to a minimum height with further increase in gas velocity. Then bubbling dominates and the bed expands again with increasing gas velocity.

2.2.7.1 Correlations for bed expansion

The most referenced correlation for bed expansion in non-bubbling fluidization is the Richardson and Zaki (1954) equation which gives a relationship between a superficial gas velocity (U_0) and bed voidage ε :

$$\frac{U_0}{U_t} = \varepsilon^n \quad (2.2.21)$$

Where U_t is superficial gas velocity at a voidage of unity, which is often approximated by the particle terminal fall velocity (U_t); and n is Richardson and Zaki parameter or exponent.

From the results of experiments on 48 gas/solid systems Abrahamsen and Geldart (1980a) correlated the maximum non-bubbling bed expansion ratio H_{mb}/H_{mf} :

$$\frac{H_{mb}}{H_{mf}} = \frac{5.50 \rho_g^{0.028} \mu^{0.115} \exp(0.158F)}{d_p^{0.176} g^{0.205} (\rho_p - \rho_g)^{0.205}} \quad (2.2.22)$$

Where H_{mb} and H_{mf} are bed heights at incipient bubbling and incipient fluidization respectively.

2.2.7.2 Conflicting reports

According to the Abrahamsen and Geldart (1980a) correlation, the maximum bed expansion ratio slightly increases with gas density according to $\rho_g^{0.028}$.

However, the results of experiments presented by Piepers et al. (1984) show that the dependence on pressure given by this correlation is far too low. Their results indicate that the total bed expansion increases substantially with pressure increase from 100 to 1500kPa. Contrary to these results Subzwari et al. (1978) found that raising the gas pressure to 600kPa has relatively little effect on bed expansion, but further increase in pressure to just 700kPa causes significant expansion.

2.2.7.3 Voidage at minimum fluidization conditions

There are also conflicting reports on the effect of increasing pressure on the bed voidage at minimum fluidization (ϵ_{mf}) and minimum bubbling (ϵ_{mb}) conditions.

According to Bin (1986), for industrial design purposes the assumption that ϵ_{mf} does not change with pressure and can be taken as that experimentally determined at atmospheric conditions is justified for the majority of solids. It has been reported by various researchers that the voidage at minimum fluidization ϵ_{mf} is essentially independent of pressure (e.g. King & Harrison, 1982; Sobreiro & Monteiro, 1982; Vogt et al., 2001).

Yang et al. (1985) suggest that the variation of the voidage at incipient fluidization ϵ_{mf} caused by increase in pressure is very small, if at all for Geldart B and D materials. However, for Geldart A powders the voidage at minimum fluidization can change appreciably with pressure. Weimer and Quarderer (1985) carried out their experiments at pressure as high as 6200kPa and observed only very small increase in bed voidage at minimum fluidization for Geldart A materials and no change in voidage for Geldart B solids.

Contrary to that, Olowson and Almstedt (1991) observed slight increase of the voidage at minimum fluidization with pressure for the largest Geldart D particles and did not notice any dependence of the voidage ϵ_{mf} on pressure for the smaller sand particles.

Sobreiro and Monteiro (1982) suggested that the voidage at minimum fluidization is practically independent of pressure but reported that for the lighter and smaller particles the voidage ϵ_{mf} appeared to be consistently lower at ambient pressure than at high pressure. In contrast to that, Llop et al. (1995) reported that with pressure increasing from 100 to 1200kPa the bed voidage at minimum fluidization is practically constant for Geldart D sand particles, decreases slightly for 213 and 450 μ m Geldart B particles, and smoothly increases for 728 μ m Geldart B silica sand.

Saxena and Vogel (1977) reported an increase of up to 10% in the voidage at minimum fluidization value for 700 μm dolomite, fluidised at 800kPa. Similarly, Chitester et al. (1984) reported that the bed voidage at minimum fluidization at high pressure is slightly greater than at atmospheric pressure.

2.2.7.4 Voidage at minimum bubbling conditions

The effect of pressure on the bed voidage at the minimum bubbling conditions is also uncertain. Gibilaro et al. (1988) provided an illustrative example of expected pressure influence on the bubbling point and bed stability based on predictions of a previously developed criterion for the stability of fluidized beds (Foscolo & Gibilaro, 1984), as described by Eq.(2.2.20), for a material with density of 1000kg/m³ fluidised by air at 293K. Figure 2-5 illustrates the strong possible effect of pressure on bed stability for fine powders.

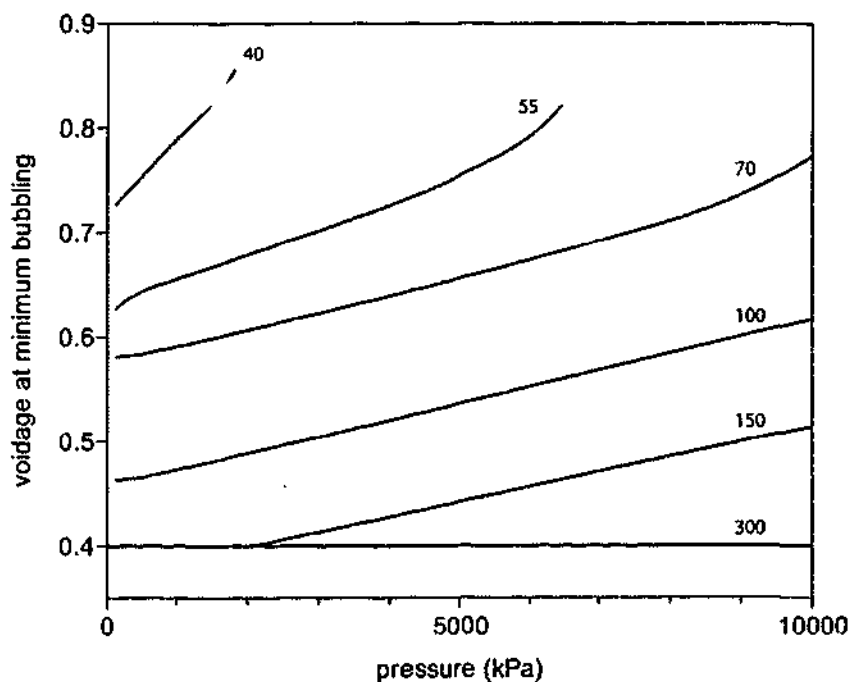


Figure 2-5. Effect of pressure on minimum bubbling voidage for solids with particle size in the range 40 – 300 μm as predicted by the Hydrodynamic Forces Stability Theory (from Gibilaro et al., 1988)

Gibilaro et al. (1988) compared their predictions to the experimental results of Jacob and Weimer (1987) and Crowther and Whitehead (1978),

and later Foscolo et al. (1989) investigated the influence of pressure up to 2900kPa on the expansion of fluidized beds of two FCC catalysts with and without fines in order to test the predictions of their criterion for the stability of fluidized beds. They found that an increase in pressure significantly influences non-bubbling expansion characteristics, which are limited by the minimum bubbling condition. Steady increase in the voidage at minimum bubbling with pressure increase was found but the accuracy in prediction of the minimum bubbling voidage values varied with different materials.

Rowe (1989) analysed the theory of Foscolo and Gibilaro (1984) and presented some of his calculations which give predictions of how the bed voidage at minimum bubbling *would be expected* to vary with pressure. His calculations at pressures in the range 100 to 1000kPa show no measurable change in predicted minimum bubbling voidage. At the same time the particle systems near the Geldart A/B boundary are predicted to be sensitive to pressure when the pressure increase can lead to change from Geldart B to Geldart A behaviour.

2.2.7.5 Experimental observations of voidage at minimum bubbling

The predictions of Rowe (1989) are not in agreement with experimental findings of other researchers (Piepers et al., 1984; Piepers & Rietema, 1989; Rietema & Piepers, 1990) who observed pressure effects on minimum bubbling voidage when fluidising fluid catalytic cracking (FCC) catalyst and polypropylene powder with different gases.

In all cases except one the voidage at minimum bubbling steadily increased with increasing pressure in the range from atmospheric to 1500kPa. In the last case when the catalyst was fluidised with the least dense gas, hydrogen, the minimum bubbling voidage did not change at pressures up to 900kPa and then increased at 1200 and 1500kPa.

Recently Vogt et al. (2002) observed similar increase in minimum bubbling voidage with pressure increase in the range from 8 to 28.4MPa when they

fluidised quartz sand and two sizes of ballotini with supercritical carbon dioxide. At ambient conditions all three materials behaved as Geldart B materials and started to bubble as soon as the gas velocity exceeded the minimum fluidization velocity. A pressure increase resulted in non-bubbling expansion typical for Geldart A behaviour over the whole range of investigated gas velocities.

Sobreiro and Monteiro (1982) reported that the voidage at minimum bubbling condition was essentially independent of pressure for most of the tested powders, although for the Geldart A alumina particles the voidage increased with pressure increase and there was some evidence of the voidage increasing at the higher pressures for the smallest ballotini particles.

The bed voidage was largely underestimated by the Richardson and Zaki (1954) equation when predicted values of the parameter n and superficial gas velocity at a voidage of unity U_i were used. The experimental values of parameter n varied between 8.7 and 12.8 being much higher than predicted values, gas velocity U_i was also much larger than the particle terminal fall velocity. Both parameter n and gas velocity U_i decreased with increasing pressure.

2.2.7.6 Testing of correlations at high pressure conditions

Other researchers also tested the accuracy of the Richardson and Zaki (1954) equation applied to fluidized bed expansion results of high pressure experiments. Crowther and Whitehead (1978), Foscolo et al. (1989) and Jacob and Weimer (1987) also observed general reduction in the values of n and U_i with pressure, with experimental values being higher than predicted.

Marzocchella and Salatino (2000) found that experimental values of gas velocity U_i and parameter n were rather close to theoretical values of particle terminal velocity and the parameter n . Both parameter n and gas velocity U_i decreased with increasing pressure for 88 μm ballotini; but in the case of larger 175 μm ballotini, the gas velocity U_i decreased with increasing pressure

and the parameter n was not affected by pressure in the range 2000 to 8000kPa.

Rowe et al. (1982) found that both parameter n and gas velocity U_i were independent of pressure, but experimental values of the parameter n were markedly higher than the upper value of n observed with liquid fluidized beds at similar Reynolds numbers. The value of gas velocity U_i was, however, less than the calculated particle terminal fall velocity.

2.2.7.7 Other conflicting reports

Another source of controversy came from the same school (Figure 2-6). At first Guedes de Carvalho, King and Harrison (1978) reported virtually no effect of pressure in the range of 100 to 2500kPa on the voidage at minimum bubbling for 64 μ m ballotini and 74 μ m sand. However, later King and Harrison (1982) claimed that the minimum bubbling voidage increased with pressure for similarly sized 61 μ m ballotini and 81 μ m sand.

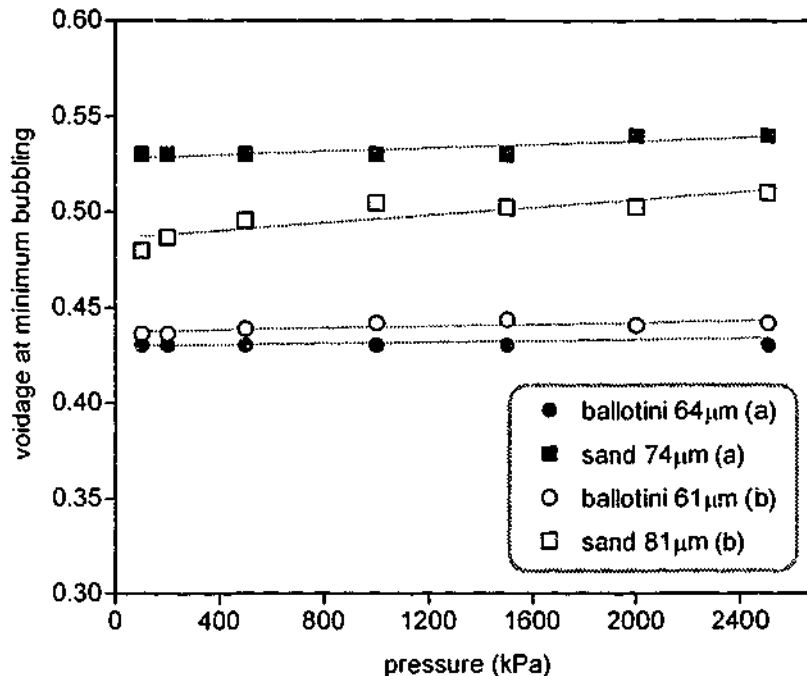


Figure 2-6. Variation of bed voidage at minimum bubbling with pressure as reported by (a) Guedes de Carvalho et al. (1978) and (b) King and Harrison (1982)

After rearranging the Richardson and Zaki (1954) equation for both minimum fluidization and minimum bubbling conditions King and Harrison (1982) stated the following about the minimum bubbling voidage:

$$\epsilon_{mb} = \epsilon_{mf} \sqrt[n]{\left(\frac{U_{mb}}{U_{mf}}\right)} \quad (2.2.23)$$

For fine particles - minimum bubbling voidage increases markedly with pressure since parameter n decreases slightly and U_{mb}/U_{mf} is known to increase.

For larger particles - $\epsilon_{mb} = \epsilon_{mf}$ and is unaffected by pressure since U_{mb}/U_{mf} is constant at unity.

Based on experimental results with three powders fluidised at pressures up to 2500kPa, King and Harrison (1982) claimed that the minimum bubbling voidage for 61 μ m ballotini increased steadily with pressure as predicted by Eq.(2.2.23) while the minimum fluidization voidage was effectively constant and independent of pressure.

A similar trend was claimed for 81 μ m sand. In case of 101 μ m ballotini the difference between ϵ_{mb} and ϵ_{mf} apparently was less and the minimum bubbling voidage increased less rapidly with pressure but still following Eq.(2.2.23).

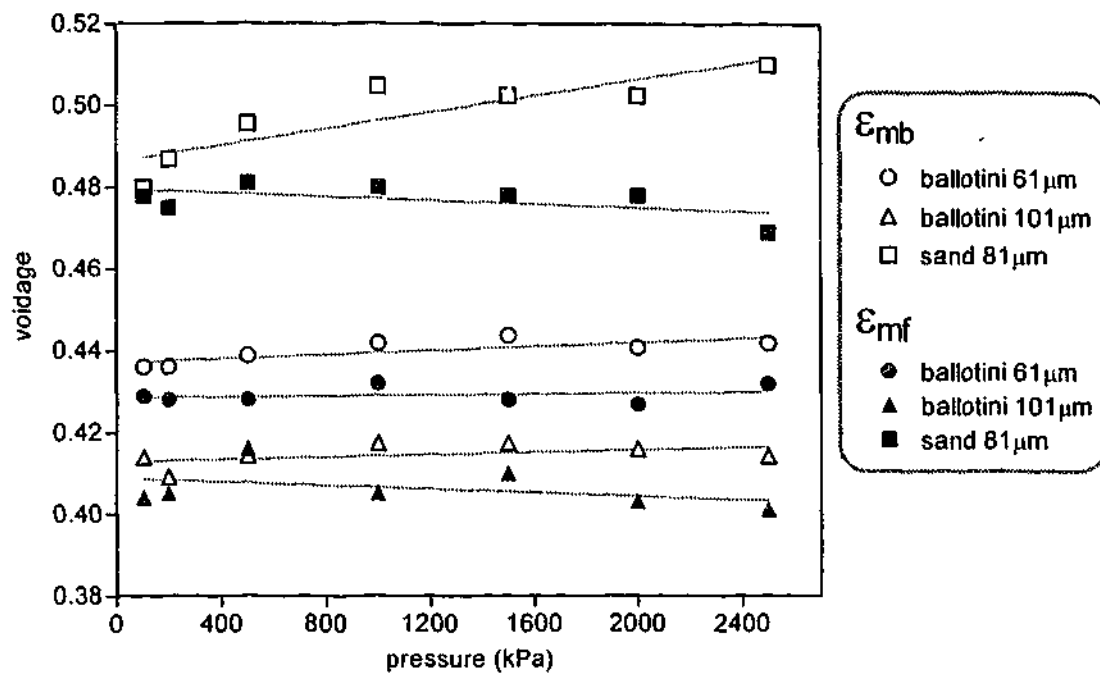


Figure 2-7. Variation of bed voidage at minimum fluidization (ϵ_{mf}) and minimum bubbling (ϵ_{mb}) with pressure as reported by King and Harrison (1982)

However, the value of the increase in minimum bubbling voidage is very small and of the same order as scatter for minimum fluidization voidage which assumed constant. When the data reported by King and Harrison (1982) are plotted at the scale similar to that of other researchers' reports, it is quite difficult to determine the difference between "no pressure effect" and "steady increase" (e.g. 61 μ m ballotini in Figure 2-7).

2.3 BUBBLING FLUIDIZATION AT ELEVATED PRESSURE

The quality of fluidization depends on behaviour and specific characteristics of bubbles, such as bubble shape, size, and velocity of rise of bubbles. Bubble behaviour can be described in terms of frequency, bubble coalescence and break-up. Bubble behaviour and specific parameters have been investigated by means of X-ray (Barreto et al., 1983a, 1983b; Gilbertson et al., 1998; Hoffmann & Yates, 1986; King & Harrison, 1980; Rowe et al., 1984), piezoelectric (Carsky et al., 1990) and capacitance probes (Olowson &

Almstedt, 1990), and by pressure fluctuations (Chan et al., 1987; Weimer & Quarderer, 1985).

2.3.1 DENSE PHASE EXPANSION IN PRESSURISED BUBBLING BEDS

The earliest flow model for bubbling fluidized beds was introduced by Toomey and Johnstone in 1952 (Kunii & Levenspiel, 1991) and is known as the simple two-phase model. This model assumes that all the gas in excess of the minimum fluidization velocity flows through the bed as bubbles and the emulsion remains at minimum fluidising conditions.

The voidage of the dense phase ε_d is assumed to be the same as at the minimum fluidization conditions, i.e. $\varepsilon_d = \varepsilon_{mf}$. However, the validity of this assumption has been questioned and numerous experimental investigations in larger fluidized beds have shown that the dense phase voidage does not stay at ε_{mf} as gas velocity is raised above the minimum fluidization (Kunii & Levenspiel, 1991).

2.3.1.1 Bed collapse experiments with fine materials

The bed collapse technique has been used to evaluate the average dense phase properties in bubbling fluidized beds of fine powders by several researchers (e.g. Abrahamsen & Geldart, 1980b; Barreto et al., 1983b; Formisani et al., 2002; Geldart & Wong, 1985; Lettieri et al., 2000). This technique is quite simple and consists of recording the movement of the bed surface after a sudden termination of the gas supply as described elsewhere (e.g. Abrahamsen & Geldart, 1980b; Rietema, 1991).

Several workers used the bed collapse technique to study the dense phase properties of pressurised bubbling beds of fine powders (e.g. Barreto et al., 1983a; Guedes de Carvalho, 1981; Piepers et al., 1984; Weimer & Quarderer, 1985). There is a general agreement between them that increasing operating pressure causes the dense phase voidage to increase.

Barreto et al. (1983a) observed an increase in apparent dense phase voidage with pressure and noted that the pressure effect was more

pronounced for powders with greater fines content. For a 71 μm zeolite powder with 4% of fines less than 45 μm the dense phase voidage increased only slightly from 0.43 at atmospheric pressure to 0.46 at 2000kPa. For a similar powder but with 50% of fines, however, in the same pressure range the dense phase voidage increased from 0.50 to 0.56.

Weimer and Quarderer (Weimer, 1986; Weimer & Quarderer, 1985) measured dense phase voidage and dense phase superficial gas velocity at pressures up to 8300kPa in a pilot-scale fluidized bed of bubbling Geldart A and Geldart A/B boundary carbon powders. They also found that the magnitude of the pressure effect on the dense phase voidage strongly depended on particle size.

There was a substantial pressure influence on the dense phase voidage for the 66 μm carbon powder (Geldart A material) when the voidage increased from 0.53 at ambient conditions to 0.74 at 6200kPa. For the 108 μm carbon powder (Geldart A side of the A/B boundary) there was only a modest effect of pressure on the dense phase voidage. In this case the voidage increased from 0.44 at atmospheric pressure to 0.51 at 8300kPa. However, for the 171 μm carbon material (Geldart B side of the A/B boundary), Weimer and Quarderer (1985) observed essentially no pressure effect and found the dense phase voidage to be equivalent to the bed voidage at minimum fluidization conditions at all pressures.

The experimental results of Weimer and Quarderer (1985) were later questioned by Rowe (1986) who, based on the theory of Foscolo and Gibilaro (1984), expected to see less change in voidage for the finest powder and more pressure influence on voidage for the coarsest material. However, Piepers et al. (1984) carried the collapse experiments with 59 μm cracking catalyst at pressures up to 1500kPa and found that the dense phase voidage increased from 0.52 at atmospheric pressure to 0.58 at 1500kPa, which is more in line with the observations of Weimer and Quarderer (1985).

Guedes de Carvalho (1981) also observed the same pressure effect on dense phase expansion determined by the similar collapse method. Dense phase

voidage for the bubbling bed of fine silica-alumina particles was always greater than voidage at minimum fluidization and smaller than voidage at minimum bubbling conditions, and increased with pressure from 0.53 at ambient conditions to 0.59 at 1600kPa, and to 0.61 at 2200kPa.

2.3.1.2 Correlations for predicting dense phase voidage

There are a few correlations for predicting dense phase voidage available in the literature; however the accuracy of them has not been widely evaluated at elevated pressure.

Abrahamsen and Geldart (1980b) presented a correlation for predicting dense phase voidage in fluidized beds of fine powders:

$$\frac{H_d}{H_{mf}} = \frac{1 - \varepsilon_{mf}}{1 - \varepsilon_d} = \frac{2.54 \rho_g^{0.016} \mu^{0.066} \exp(0.09F)}{d_p^{0.1} g^{0.118} (\rho_p - \rho_g)^{0.118} H_{mf}^{0.043}} \quad (2.3.1)$$

Where H_d is height of the dense phase and H_{mf} is bed height at minimum fluidization velocity. Equation (2.3.1) includes density effects and clearly shows how the fraction of fines F affects the dense phase properties independently of mean size d_p .

An alternative correlation was proposed by Kmiec (1982) which is presented here as the following equation:

$$\varepsilon_d = \frac{(18\text{Re} + 2.7\text{Re}^{1.687})^{0.209}}{Ga^{0.209}} \quad (2.3.2)$$

Where Ga is Galileo number (Eq.(2.2.4)) and Re is particle Reynolds number defined by Eq.(2.2.3).

2.3.1.3 Experimental testing of correlations

Weimer and Quarderer (1985) used their experimental values of H_{mf} and ε_{mf} in Eq.(2.3.1) to calculate predicted values of ε_d and compared them to those determined experimentally for the 66 and 108 μm solids at all pressures.

Although calculated and experimental values for the coarser material were in reasonably good agreement, Eq.(2.3.1) largely underestimated the effect of pressure on the dense phase voidage for the 66 μ m powder. When the same experimental results were compared to the values predicted by Eq.(2.3.2), an excellent agreement was achieved at all pressures for both powders.

Piepers et al. (1984) also compared their experimental data to the correlation proposed by Abrahamsen and Geldart (1980b). According to Eq.(2.3.1), height of the dense phase should slightly increase with gas density according to $\rho^{0.016}$. Therefore it was expected that a pressure increase from ambient to 1500kPa should cause 4.5% increase in dense phase height. However, the experimental results demonstrated a much higher 21% increase.

2.3.1.4 Dense phase gas velocity

Several workers also determined the superficial dense phase gas velocity U_d as the rate of collapse. The variation of the superficial dense phase gas velocity with pressure is demonstrated in Figure 2-8. In all cases the superficial gas velocity before shutting the gas flow was 0.05m/s.

Again, the pressure influence was greater for smaller particles. Pressure had a substantial effect on dense phase velocity for fine carbon and catalyst particles, and very little effect on dense phase velocity for 108 μ m carbon and 72 μ m catalyst without fines. For the coarsest material, the dense phase velocity was approximately equal to the minimum fluidization velocity and decreased with increased pressure.

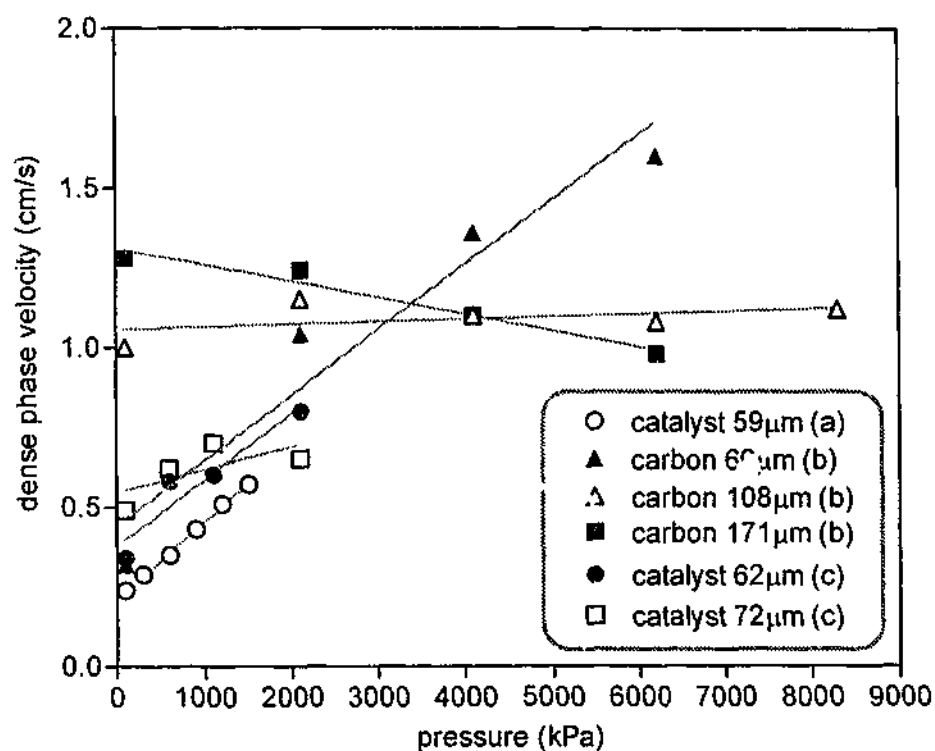


Figure 2-8. Effect of pressure and particle size on superficial dense phase gas velocity as reported by (a) Piepers et al. (1984), (b) Weimer and Quarderer (1985) and (c) Foscolo et al. (1989)

2.3.2 EFFECT OF PRESSURE ON BUBBLING BED EXPANSION

The knowledge of the bed expansion and mean bed voidage is very important for modelling and design of fluidized beds. This information is required for an industrial designer to establish the best possible position for a heat exchanger in fluidized bed reactors and determine the height of freeboard in order to avoid unnecessary loss of solids. This knowledge allows also the bubble fraction in the bed to be determined and the heat transfer coefficient to be calculated.

The bed expansion height varies in a complex manner and is affected by many parameters, such as initial bed height, gas and solids characteristics and gas velocity. Predicting its height is difficult at different conditions and the bubbling behaviour substantially deviates from that predicted by the simple two-phase theory as operating pressure is increased.

2.3.2.1 Experiments with coarse materials

A number of researchers studied how bed expansion is affected by increasing pressure in bubbling fluidized beds with coarse Geldart B (Chiba et al., 1986; Chitester et al., 1984; Llop et al., 1995, 2000) and Geldart D (Denloye, 1982; Miller et al., 1981) particles.

The bed expansion at different gas velocities is expressed simply as the ratio of bed height (H) to the initial bed height, measured at the minimum fluidization velocity (H_{mf}) in some papers (Chiba et al., 1986; Chitester et al., 1984; Miller et al., 1981). Others (Al-Zahrani & Daous, 1996; Llop et al., 1995, 2000) express bed expansion as a parameter δ , described by the following equation:

$$\delta = \frac{H - H_{mf}}{H_{mf}} \quad (2.3.3)$$

The parameter δ sometimes is called bed expansion ratio (Olowson & Almstedt, 1990; Wiman & Almstedt, 1998), bubble fraction (Miller et al., 1981) or bed height fluctuation ratio (Chiba et al., 1986)⁴, and is expressed as:

$$\delta = \frac{H - H_{mf}}{H} \quad (2.3.4)$$

Miller et al. (1981) found that higher operating pressures reduced the bed expansion (H/H_{mf}), but Denloye (1982) and Knowlton (1977) reported that

⁴ This reference is an updated and combined version of two previously published and much referred to papers:

Chiba, S., Kawabata, J., Yumiyama, M., Tazaki, Y., Honma, S., Kitano, K., et al. (1982).

Pressure effects on solid mixing and segregation in gas-fluidized beds of binary solid mixtures. In M. Kwauk & D. Kunii (Eds.), *Fluidization: Science and Technology, Conference Papers China-Japan Symposium* (pp. 69-78). Beijing: Science Press.

Kawabata, J., Yumiyama, M., Tazaki, Y., Honma, S., Chiba, T., Sumiya, T., et al. (1981).

Characteristics of gas-fluidized beds under pressure. *Journal of Chemical Engineering of Japan*, 14(2), 85-89.

the physical properties of the fluidising gas, density and viscosity did not have any significant effect on bed expansion. In contrast, Chiba et al. (1986) and Chitester et al. (1984) observed the increase of bed expansion with pressure.

Chiba et al. (1986) fluidised sand of two sizes, 0.3 and 0.6mm at atmospheric, 400 and 800kPa pressure and noticed that the bed expansion ratio (H/H_{mf}) clearly increased with pressure. The pressure effect was larger for the coarser particles, however at 800kPa the bed expansion ratio became almost the same for both materials.

Chitester et al. (1984) visually studied bed expansion of coal, char and ballotini at atmospheric, 2169, 4238 and 6306kPa. In case of coal (Geldart B material), initial bed expansion occurred with a lower gas velocity at higher pressure and the bed expanded more at high pressures at a given gas velocity. However, for char (Geldart A powder) and ballotini (Geldart A/B boundary material), at a given gas velocity the bed expansion height did not always increase with a pressure increase.

Llop et al. (1995; 2000) determined the bed expansion parameter according to Eq.(2.3.3) for sand at pressures up to 1200kPa and observed unexplained changes in bed expansion at higher pressures. They found that bed expansion increased significantly with pressure but this influence, very strong at low pressures, seemed to reach a maximum at approximately 800kPa and decreased thereafter up to 1200kPa.

Olowson and Almstedt (1990) fluidised silica sand at pressures up to 1600kPa and, although they used the bed expansion parameter according to Eq.(2.3.4), observed similar behaviour. The bed expansion strongly increased up to a maximum at a pressure between 500 and 800kPa and then stayed constant or even slightly decreased with further pressure increase.

2.3.3 BUBBLE CHARACTERISTICS

In many industrial applications the successful performance of fluidized beds largely depends on the bubbling behaviour. However, characteristics such as

bed pressure drop, bed expansion or voidage cannot provide understanding of reaction and heat and mass transfer processes, which depend on the detailed interaction between gas and solids in the bed.

The quality of fluidization depends on behaviour and characteristics of bubbles such as bubble size and shape, velocity of bubble flow, and can be described in terms of frequency and dynamics of bubble splitting and coalescence.

2.3.3.1 Bubble size

Bubbles in bubbling fluidized beds can be irregular in shape and vary in size. Experiments at ambient conditions show that bubble size increases with gas velocity and with height above the distributor, and varies from one system to another (Kunii & Levenspiel, 1991). This makes it difficult to characterise a bubble size, so Kunii and Levenspiel (1991) defined a mean bubble size as a spherical bubble of diameter d_b that represents the bubbles in the bed, usually a mean volumetric size.

In fluidized beds of fine Geldart A particles, bubble size quickly grow to a few centimetres and stays more or less constant due to the equilibrium between bubble coalescence and splitting. Occasionally larger bubbles of a size around 10cm may be observed (Kunii & Levenspiel, 1991). In fluidized beds of coarse Geldart B and D solids, bubble size steadily grows with height in the bed to tens of centimetres.

In general it has been reported that fluidization becomes smoother with high pressure and this behaviour has been attributed to smaller bubbles at increased pressure. Many investigators showed that increasing the operating pressure causes bubble size or volume to decrease in Geldart A materials (Barreto et al., 1983a; Guedes de Carvalho et al., 1978; King & Harrison, 1980; Rowe & MacGillivray, 1980; Subzwari et al., 1978; Weimer & Quarderer, 1985). Weimer and Quarderer (1985) found the decrease in bubble size to be strongly dependent on particle size with greater bubble size decrease for smaller particles.

Chan et al. (1987) used sand, coke and char belonging to Geldart A and B groups in their high pressure experiments and found similar results for all the materials. The average bubble size decreased with pressure more for the Geldart A fine particles (78% reduction) than for the Geldart B coarser particles of the same material (32% reduction) over the same pressure range of 134 to 3100kPa.

Recently Gilbertson et al. (1998) examined size, shape, structure and velocity of bubbles at pressures of up to 2100kPa, when they introduced fixed volumes of nitrogen through a 15mm diameter nozzle into a fluidized bed of Geldart B spherical particles. Although the fixed amounts of gas were injected, no uniform bubbles were formed. Bubbles varied in both size and shape and for the larger gas volume bubble size decreased smoothly with increasing pressure.

However, for Geldart B materials, there have been some conflicting reports in the literature. Schweinzer and Molerus (1988) fluidised Geldart A, B and D materials with Frigen R-115 gas and found that increasing pressure up to 2500kPa caused smaller bubble size and that this was more evident for coarse particles.

King and Harrison (1980) found that in a well-fluidized bed the bubble phase is only affected when fine Geldart A powders are fluidised at high pressure, and reported that for Geldart B materials the bubbles are of the same size and as stable at 2500kPa as at ambient pressure.

Chiba et al. (1986) filmed and inspected more than 100 bubbles, and observed that under pressure up to 800kPa bubbles became flatter, with vertical bubble diameter remaining virtually unchanged with pressure and horizontal diameter increasing, especially in the pressure range of 100 - 400kPa. However, experimental results of Carsky et al. (1990) with Geldart B and D materials indicated that bubble size decreased with increasing pressure within the same range of 100 - 400kPa as the result of bubble interaction and splitting, and remained constant thereafter up to 1300kPa.

Carsky et al. (1990) suggested that the bubble size is a complex, non-monotonic function of pressure.

In contrast to that, other researchers observed an initial increase in bubble size or volume in the lower pressure range up to 1000kPa (Rowe et al., 1984) and 1600kPa (Hoffmann & Yates, 1986) and decrease thereafter up to 8100kPa. This is more or less consistent with the results of Olowson and Almstedt (1990) who observed the similar effect of pressure on the mean pierced length of bubbles for coarse sand, which at atmospheric pressure is close to Geldart B/D boundary. However, their pressure range was between atmospheric and 1600kPa and the mean pierced length of bubbles reached a maximum at around 400kPa.

In a later paper (1992), Olowson and Almstedt stated that an increase in pressure may either cause an increase or a decrease in bubble size, depending on the location in the bed, gas velocity and the pressure level; and the bubble size is determined by a complex balance between coalescence and splitting.

In 1994 a comprehensive summary and analysis of previous research on bubble size under pressurised conditions, as applicable for Pressurised Fluidized Bed Combustion (PFBC), was published (Cai et al. 1994). This work started by determining the general diagram for bubble size variation with both pressure and gas velocity. Cai et al. (1994) arranged the results of previous experiments with coarse materials according to the flow regime and reached the following conclusion:

At constant pressure, with increasing gas velocity, the bubble size increases under the bubbling regime and decreases under the turbulent regime.

At constant gas velocity, the bubble size decreases with increasing pressure except when gas velocity is very low. In this case, there is a dual effect of pressure on bubble size, i.e. there is a small initial increase in bubble size in the lower pressure range

less than 1000kPa and then a decrease with a further increase in pressure.

Based on the data given in the literature (Chan et al., 1987; Chiba et al., 1986; Hoffmann & Yates, 1986; Olowson & Almstedt, 1990; Rowe et al., 1984; Weimer & Quarderer, 1985), Cai et al. (1994) developed the following generalised bubble size correlation for PFBC systems:

$$d_b = 0.2H_f^{0.8} p^{0.06} (U - U_{mf})^{0.42} \exp[-0.00014p^2 - 0.25(U - U_{mf})^2 - 0.1p(U - U_{mf})] \quad (2.3.5)$$

Where d_b is equivalent bubble diameter in the whole bed, H_f is expanded height of the bed and p is pressure given in bar (1bar=100kPa).

This correlation is expected to be applicable for Geldart B particles fluidised in a 1.56m high bed without internals in both bubbling and turbulent regime at pressures up to 7000kPa.

2.3.3.2 Bubble frequency

At first, it seems there is better agreement between researchers on observation that bubble frequency increases with pressure, although Chiba et al. (1986) did not see any significant effect of pressure during their experiments with Geldart B materials.

Chan et al. (1987) observed a linear increase in bubble frequency with pressure. As with bubble size, they found that the change in bubble frequency with pressure was greater for smaller particles. Barreto et al. (1983a) also observed the increase of bubble frequency with pressure at constant volumetric gas flow rate for fine powders. Results of Olowson and Almstedt (1990) also show a clear increase in the bubble activity with increasing pressure, although the effect of pressure is more pronounced at pressures below 1000kPa.

Rowe et al. (1984) simply reported that bubble frequency increased after an initial small decrease, however the plot of variation of bubble frequency with pressure in their paper gives a slightly different picture. The claim is

valid for experiments at a lower gas velocity, however at a higher gas velocity the trend is different – bubble frequency decreases first, then increases up to a maximum at a pressure of approximately 3000kPa, and then decreases again.

2.3.3.3 Bubble rise velocity

Based on simple two-phase theory, the following equations for bubble rise velocity were proposed (Kunii & Levenspiel, 1991):

$$U_{br} = 0.711\sqrt{gd_b} \quad (2.3.6)$$

$$U_b = U_0 - U_{mf} + U_{br} \quad (2.3.7)$$

Where U_{br} is bubble rise velocity for single bubbles, d_b is bubble size, U_b is bubble rise velocity for bubbles in bubbling fluidized bed and U_0 is superficial gas velocity.

Other equations in similar form have been proposed in order to account for the size of fluidized beds and variety of particle sizes (Kunii & Levenspiel, 1991).

Since the bubble rise velocity is proportional to a bubble size according to Eq.(2.3.6), it is expected that the pressure influence on it would be similar to effect of pressure on bubble size. Once again, there are contradictory reports published. According to Chiba et al. (1986) and Gilbertson et al. (1998) the bubble-rise velocity decreases with high pressure. Olowson and Almstedt (1990) observed the opposite trend when the mean bubble rise velocity slightly increased at lower operating pressure up to a constant value at higher pressure.

However, Rowe et al. (1984) and Hoffmann and Yates (1986) observed small initial decrease in bubble rise velocity between 100 and 2000kPa (Hoffmann & Yates, 1986) and up to 1000kPa (Rowe et al., 1984) and then substantial increase. Earlier Rowe and MacGillivray (1980) fluidised Geldart A silicon carbide particles at ambient conditions and pressure of 400kPa and reported an increase in the average bubble velocity, contrary to what would

be expected as a consequence of the reduced bubble size observed in that study, and contrary to the results of experiments with coarse alumina (Rowe et al., 1984).

2.4 OTHER STUDIES OF PRESSURISED FLUIDIZED BEDS

2.4.1 BED-TO-SURFACE HEAT TRANSFER

Since the 1970s a considerable attention has been given to research in the field of fluidized bed combustion and gasification of solid fuels at elevated pressure. The operating conditions of combustion boilers and reaction chambers of gasifiers involve high bed temperatures (1023 – 1173K) and increased fluidising gas pressures (up to 2MPa). Under these conditions, heat transfer between a surface and a fluidized bed has a rather complex conductive – convective – radiative character (Borodulya et al., 1991).

According to Botterill (1975), in bubbling fluidized beds the bed-to-surface heat transfer coefficient h can be presented as a sum of three components:

$$h = h_{pc} + h_{gc} + h_r \quad (2.4.1)$$

Where h_{pc} is particle convective component, h_{gc} is interphase gas convective component and h_r is radiative component of heat transfer. These components can be regarded as independent of each other, and their relative importance varies.

The radiative component becomes important only at high operating temperatures above 873K.

The particle convective component depends on heat transfer through particle exchange between the bulk of the bed material and immediate bed region adjacent to the heat transfer surface. Therefore, it is largely affected by the bubbling behaviour that generates the circulation of the solids in the bed. The particle convective component dominates for small particles, where the effective contact area between particles and surface is large.

With increase of particle size the particle convective component decreases and at the same time the gas convective component increases. The gas convective component also is expected to increase with increasing pressure, because of the increase in gas density.

According to Borodulya et al. (1991), one of the most well-known empirical correlations for calculating the maximum bed-to-surface heat transfer coefficient h has been proposed by Baskakov and Panov (1973), and predicts a strong dependence of the conductive component on pressure. However, this fact was not confirmed by extensive experimental studies carried out at Luikov Heat and Mass Transfer Institute in Minsk during the 1960s and 1970s (Borodulya et al., 1982).

Pressure effect on the particle convective component is considered to be negligible (Botterill, 1989) or very weak (Borodulya et al., 1991). However, the particle convective component could be affected through possible pressure influence on solids circulation in the bed.

Several researchers studied the influence of pressure on convective heat transfer between fluidized beds and surfaces (e.g. Barreto et al., 1986; Botterill & Desai, 1972; Canada & McLaughlin, 1978; Denloye & Botterill, 1978; Molerus & Wirth, 1997a; Olsson & Almstedt, 1995; Xavier et al., 1980; Xianglin et al., 1991).

Convective heat transfer in fluidized beds of fine particles is not expected to change much with pressure and that was observed by Xavier et al. (1980) and Barreto et al. (1986).

The convective heat transfer can be characterised by a dimensionless parameter, the Nusselt number, which is defined as:

$$Nu = \frac{h_{\max} d_p}{\lambda_g} \quad (2.4.2)$$

Where h_{\max} is the maximum heat transfer coefficient and λ_g is gas thermal conductivity.

In order to describe heat transfer experiments under different conditions, Borodulya et al. (1991) analysed the results available in the literature and proposed a relation which combines the Nusselt number at maximum conductive - convective heat transfer ($h_{pc} + h_{gc}$), the Galileo number Ga and the Prandtl number Pr :

$$Nu_{\max} = 0.4Ga^{0.16} \left(\frac{\rho_p}{\rho_g} \right)^{0.14} \left(\frac{c_p}{c_g} \right)^{0.3} + 0.0013Ga^{0.63} Pr \quad (2.4.3)$$

Where c_p and c_g are specific heat capacity of particles and gas, respectively. The Prandtl number is defined as follows:

$$Pr = \frac{\mu c_g}{\lambda_g} \quad (2.4.4)$$

According to Borodulya et al. (1991), Eq.(2.4.3) is valid for particles in the size range from 100 μ m to 4mm, and the operating pressure range from atmospheric to 10MPa. The exponents of the Galileo number and the density ratio in Eq.(2.4.3) are almost equal, and the dependence of the particle convective heat transfer coefficient on pressure is very weak.

Since the gas convective heat transfer coefficient is proportional to the square root of gas density, fluidization at elevated pressures is expected to enhance this component. Experimental confirmation of higher heat transfer coefficients in pressurised fluidized beds of coarse particles can indeed be found in the literature (e.g. Borodulya et al., 1980; Canada & McLaughlin, 1978; Denloye & Botterill, 1978; Xavier et al., 1980).

The experimental data presented by Borodulya et al. (1980) show that the effect of pressure increases with particle size. A pressure increase from 1100 to 8100kPa resulted in 29% increase in a maximum heat transfer coefficient for the 126 μ m sand particles, 110% increase for 1.22mm sand particles, and 140% increase for the 3.1mm glass ballotini.

2.4.2 BED PENETRATION BY GAS JETS

When gas is blown upwards from an orifice into a fluidized bed, either a permanent jet or discrete bubbles form at the orifice. If a jet forms, it may penetrate the bed right to the surface as in the spouted bed or it may decay at some height into a stream of bubbles. Knowing which behaviour will occur is of considerable importance for industrial design of fluidized beds especially in the distributor region.

Knowlton and Hirsan (1980) undertook an investigation to determine the effect of pressure on jet penetration. Their study was conducted in a 0.3m semicircular apparatus fitted with 25.4mm diameter nozzle over a pressure range of 345 – 517kPa using three materials of widely different densities.

They found that jet penetration increased sharply with pressure increase at low range and then increases at a slower rate as system pressure is increased further. They also compared their experimental data with five available in the literature correlations predicting jet penetration at low pressure and found that all of them underestimated the effect of pressure.

Using the experimental data of Knowlton and Hirsan (1980), Yang (1981) modified his original equation for high pressure and developed a new correlation for the maximum penetration length L_{max} in the following form:

$$\frac{L_{max}}{d_0} = 7.65 \left[\frac{1}{R_{cf}} \frac{\rho_g}{(\rho_p - \rho_g)} \frac{U_0^2}{gd_0} \right]^{0.472} \quad (2.4.5)$$

Where d_0 is jet nozzle diameter, U_0 is average jet nozzle velocity and R_{cf} is ratio of complete fluidization velocity at pressure p over that at atmospheric pressure.

However, this correlation can be applied only to bed materials fluidised with gas velocity equal to the complete fluidization velocity as established by Knowlton (1977).

Yates et al. (1986) investigated the effect of pressure on the depth of jet penetration and found also that the existing correlations, developed for ambient conditions, show poor agreement with experimental data at elevated

pressures. They measured jet penetrations in cylindrical bed of two coarse materials at pressures up to 2000kPa and separately at temperatures up to 1073K. Their results at high pressure gave a correlation similar to that of Yang (1981) but high temperature results were a little different so, according to (Yates, 1996), the following correlation appears to be the only correlation available for both elevated pressure and temperature:

$$\frac{L_{\max}}{d_0} = 9.77 \left[\frac{1}{R_{cf}} \frac{\rho_g}{(\rho_p - \rho_g)} \frac{U_0^2}{gd_0} \right]^{0.38} \quad (2.4.6)$$

2.4.3 SOLIDS MIXING

The work of Chiba et al. (1986) describes the experimental data of the minimum fluidization velocity and solids mixing for binary mixtures of silica sand and coal char in a fluidized bed under pressures up to 800kPa. The results of their experiments in a three-dimensional bed indicated that the minimum fluidization velocity of binary mixtures decreased but its variation with the extent of mixing could not be evaluated.

In fluidized beds of multi-component solid mixtures both mixing and segregation occur simultaneously, and are caused by bubbles. The authors observed behaviour of the bubbles in a two-dimensional bed and confirmed qualitatively but not quantitatively that solids mixing had been promoted by pressurisation.

2.4.4 PARTICLE ENTRAINMENT

Ejection of particles from the surface of a bubbling bed and their removal from the bed in the gas stream is known as entrainment or carryover. For industrial design purposes it is desirable to know the rate of entrainment, size distribution of entrained particles in relation to the size distribution in the bed, and variation of those parameters with gas and solids properties.

Although there have been a large number of experimental studies of entrainment, very few separate studies of pressure effects on entrainment are reported in the literature.

From early research published in Russian in late 1950s and early 1960s, it was found that entrainment of catalyst particles by the gas stream reduced with increase in operating pressure in the range up to 2000kPa (Fridland, 1963). Contrary to this, Chan and Knowlton (1984a) carried out an investigation to determine the pressure effect on entrainment of solids from fluidized beds and found that the total entrainment rate increased sharply with increasing pressure and gas velocity.

At pressure up to 2070kPa, they found that the specific entrainment rate constant was linearly proportional to gas density. At higher pressure (up to 3100kPa), the entrainment rate constant increased more rapidly and the relationship was no longer linear.

Pemberton and Davidson (1984) also studied entrainment of polymer particles from bubbling fluidized beds at pressures up to 2000kPa and found a similar increasing trend in the entrainment rate constant.

Chan and Knowlton (1984b) also conducted an investigation to determine the effect of system pressure on the transport disengaging height above which the entrainment is constant, and found that it increased linearly with both pressure and gas velocity over the pressure range up to 3100kPa.

2.4.5 TRANSITION FROM BUBBLING TO TURBULENT FLUIDIZATION

Turbulent fluidization is often regarded as the transition regime from bubbling fluidization to fast or lean-phase fluidization. In bubbling fluidization, bubble motion becomes more and more vigorous with the increase in gas velocity.

Usually this is reflected in the increase of the amplitude of the pressure fluctuations; however with further increase in gas velocity the fluctuations will reach a maximum and then decrease gradually to a certain level. The

variation in fluctuations defines the transition from bubbling to turbulent fluidization.

As the minimum bubbling velocity defines the end of non-bubbling fluidization and the beginning of bubbling fluidization, the gas velocity corresponding to the peak of pressure fluctuations in the bed U_c defines the onset of the transition to the turbulent regime.

A few workers carried out experiments to investigate the effects of operating pressure on the transition from bubbling to turbulent fluidization. Cai et al. (1989) conducted a study on pressure influence using eight kinds of Geldart A and B solids. Varying the operating pressure of their experiments between atmospheric and 800kPa, they found that the maximum point velocity U_c was lowered with the increase of pressure and, therefore, the transition occurred in advance. They also found that the influence of pressure was more significant for large and heavy particles.

On the basis of the experimental data, the following correlation was recommended by Cai et al. (1989) for prediction of the transition velocity U_c :

$$\frac{U_c}{\sqrt{gd_p}} = \left(\frac{\mu_{(ref)}}{\mu} \right)^{0.2} \left[k \left(\frac{\rho_{g(ref)}}{\rho_g} \right) \left(\frac{\rho_p - \rho_g}{\rho_g} \right) \left(\frac{D}{d_p} \right) \right]^{0.27} \quad (2.4.7)$$

Where for a three-dimensional bed without internals, D is the diameter of a fluidized bed, $\mu_{(ref)}$ and $\rho_{g(ref)}$ are gas viscosity and density respectively at atmospheric pressure and temperature of 293K, and k is constant defined as:

$$k = 0.27 \sqrt{\left(\frac{0.211}{D^{0.27}} + \frac{0.00242}{D^{1.27}} \right)} \quad (2.4.8)$$

It is commonly accepted that the transition to turbulent flow is marked by improved quality or "smoothness" of fluidization characterised by the absence of large discrete bubbles and increased bed voidage.

Using a rapid response nuclear density gauge, Weimer and Jacob (1986) measured the bed density fluctuations in a smaller fluidized bed of fine carbon powders at operating pressure of 2070, 4140 and 6210kPa and

observed that the "quality" of fluidization improved at high pressures. The pressure effect was substantial for the 108 μm material and modest for the 66 μm powder.

They observed the higher bed voidage for the 66 μm powder than those indicative of turbulent fluidization for fine powders fluidised at atmospheric conditions. The fact that higher voidage was achieved at lower gas velocity U_c as pressure increased indicated that turbulent fluidization was achievable at lower gas velocities relative to operation at ambient conditions.

However, Weimer and Jacob (1986) did not observe a sudden decrease in the pressure fluctuations as the indicator of transition to turbulent fluidization and reported that at all gas velocities the 66 μm powder was fluidised turbulently at high pressures.

Chitester et al. (1984) also confirmed "smoother" fluidization at high pressures. They observed that the turbulent regime was reached at lower gas velocities as the operational pressure was increased. At the highest pressure of their experimental programme (6485kPa), the bed appeared to be uniform with the voids of dense phase and the emulsion phase becoming indistinguishable.

Tsukada et al. (1993) determined velocity U_c , which they called the offset velocity of bubbling fluidization, in a laboratory-scale circulating fluidized bed under different operating pressures up to 700kPa and found also that the velocity decreased with pressure increase and was proportional to $p^{-0.3}$.

Recently a computational study involving the discrete particle simulation approach has been carried out to assess the influence of operating pressure on the flow behaviour of fluidized beds (Li & Kuipers, 2001). The results of this study show that high operating pressure reduces the minimum fluidization velocity, widens the uniform non-bubbling regime and leads to a quick transition to the turbulent regime. In comparable flow regimes, elevated pressure enhances gas-solid interaction, suppresses particle-particle interactions and formation of large bubbles.

2.5 CONCLUSIONS

Although many experiments have been done on fluidization under pressure in the past 50 years, as seen by the large volume of publications in this area, no consistent conclusions have been drawn in many cases. Apart from common agreement on the influence of pressure on minimum fluidization velocity, the effects of pressure on all other parameters are associated with some degree of controversy.

Often it is difficult to derive consistent results from the reported experimental data on the pressure effects on fluidized bed behaviour due to different conditions and experimental techniques, and considerable scatter of the experimental data. Some results from different researchers under similar conditions or with similar materials are controversial, and some interpretations of the experimental results are questionable.

It is clear, however, that there are significant differences in fluidized bed behaviour under elevated pressure between different bed materials. Some of the differences cannot be accounted for simply on the basis of change in gas density with pressure.

Chapter 3

EXPERIMENTAL

This chapter describes the experimental high-pressure facility and provides detailed information about equipment, instruments and materials used in the present work.

3.1 EXPERIMENTAL FACILITY

Experiments were conducted to investigate fluidization fundamentals of Geldart A and B solids at operating pressures up to 2500 kPa in a high-pressure fluidization cold model facility built for this study (Figure 3-1).

The pressure vessel, capable of operating at pressures up to 2600 kPa, was 2.38m-high and was equipped with 5 glass observation ports. A 15cm-diameter plastic fluidized bed model was inserted into the pressure vessel and used to study physical behaviour of gas-fluidized beds.

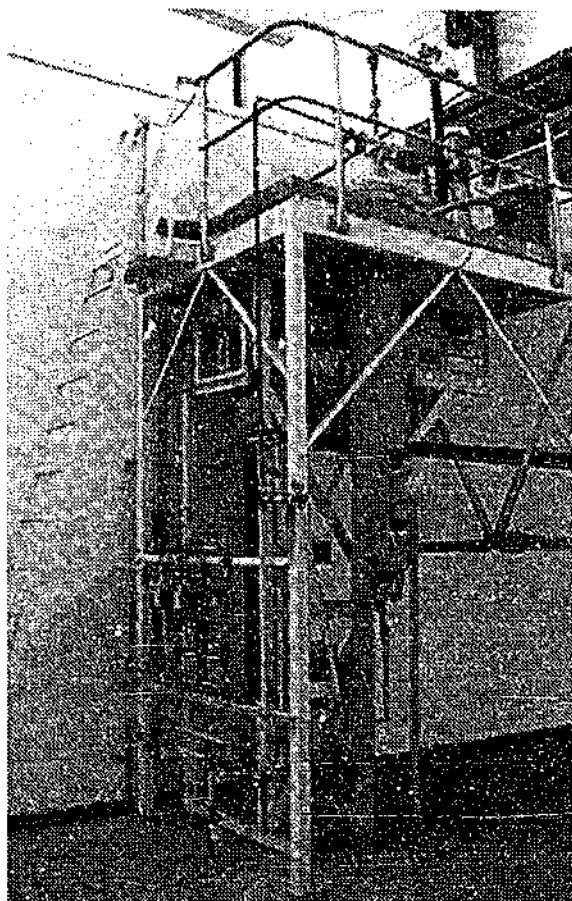


Figure 3-1. General view of the high-pressure cold fluidized bed facility built for this work

3.2 FLUIDIZED BED APPARATUS

The fluidized bed used in this study was a flanged column made of clear acrylic plastic with the following dimensions - 146mm internal diameter, 152mm external diameter, and 1250mm height. A transparent metric scale was adhered to the column in order to measure the bed height during the experiments. The bottom flange of the column was bolted to a carbon steel plenum chamber and distributor assembly, and the top flange was bolted to an expanded top freeboard for solids disengagement.

The expanded conical top was made of carbon steel and had a top diameter of 250mm. Four 25mm-diameter tubes were inserted through the expanded section and welded vertically in order to equalise pressure on inside and outside of the plastic column.

A carbon steel plenum chamber and distributor assembly (Figure 3-2) was designed and manufactured according to recommendations given by Svarovsky (1987).

Two types of distributor plates were specially made for the study. The first distributor was intended for experiments with coarse materials and made from a sintered bronze plate with nominal pore size of $12\mu\text{m}$. The plate manufacturer estimated pressure drop through the plate to be 4.9kPa at a superficial gas velocity of 0.5m/s .

The second distributor was designed for experiments with fine bed materials so that the pressure drop was approximately 6.5kPa at a superficial gas velocity of 0.01m/s in accordance with recommendations by Svarovsky (1987). In order to achieve this it was made from seven layers of filter paper (Whatman No. 5) with glued edges and supported between two perforated 2mm -thick steel plates. The perforated plates had a large number of 3mm -diameter holes arranged in triangular pitch of 5mm .

Results of the measurement of pressure drop through the distributor plates are presented in Figure 3-3 and Figure 3-4.

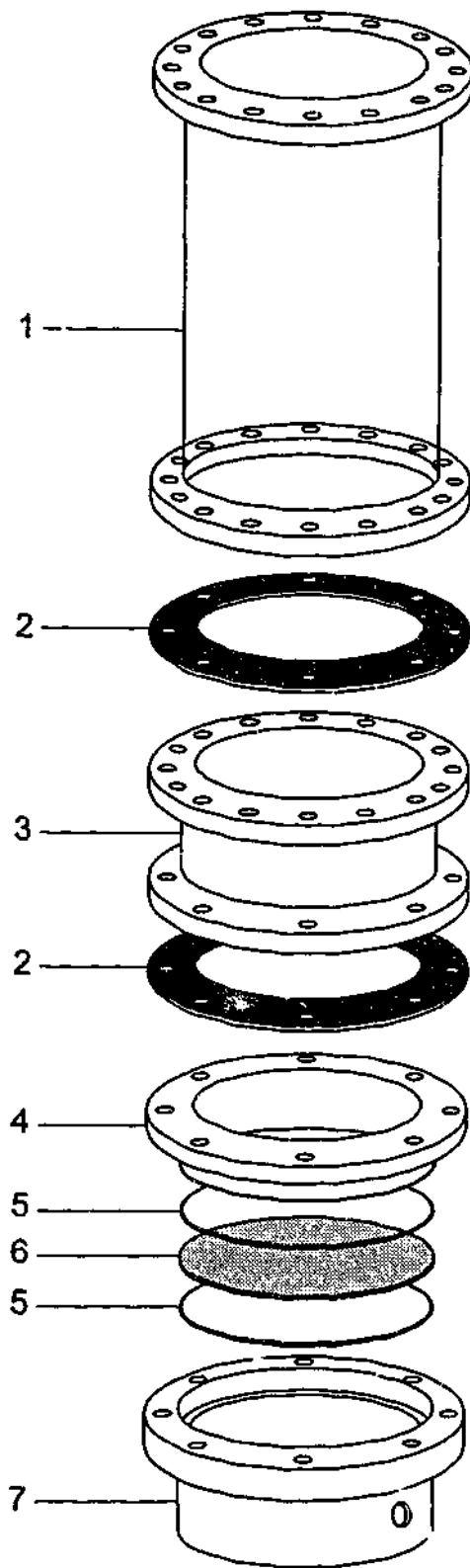


Figure 3-2. Expanded view of the plenum chamber and distributor assembly, where 1 - clear plastic fluidized bed, 2 - rubber gaskets, 3 - intermediate steel collar, 4 - steel collar for sealing the distributor, 5 - rubber O-rings, 6 - distributor plate, and 7 - steel plenum chamber

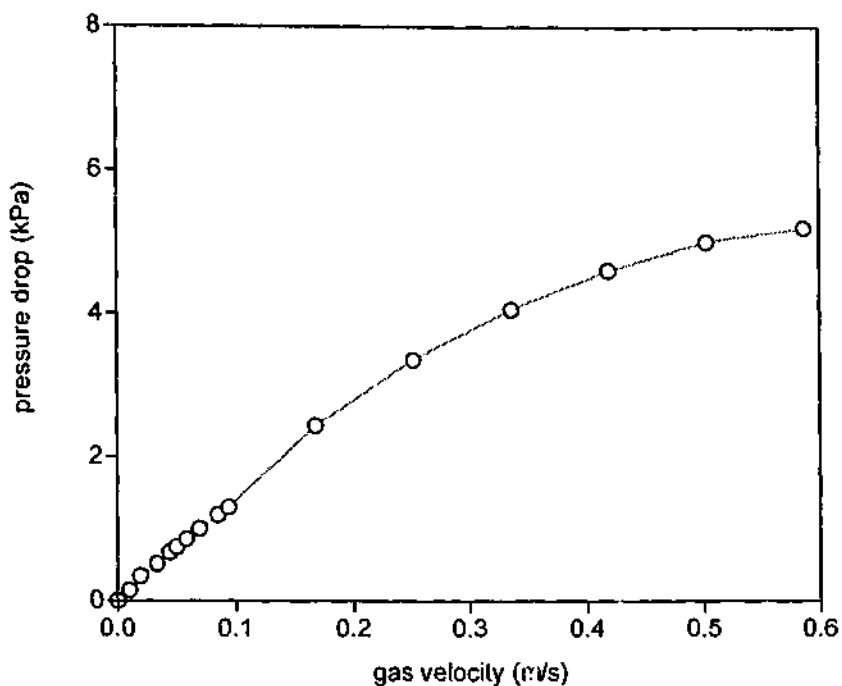


Figure 3-3. Pressure drop versus superficial gas velocity for sintered bronze distributor

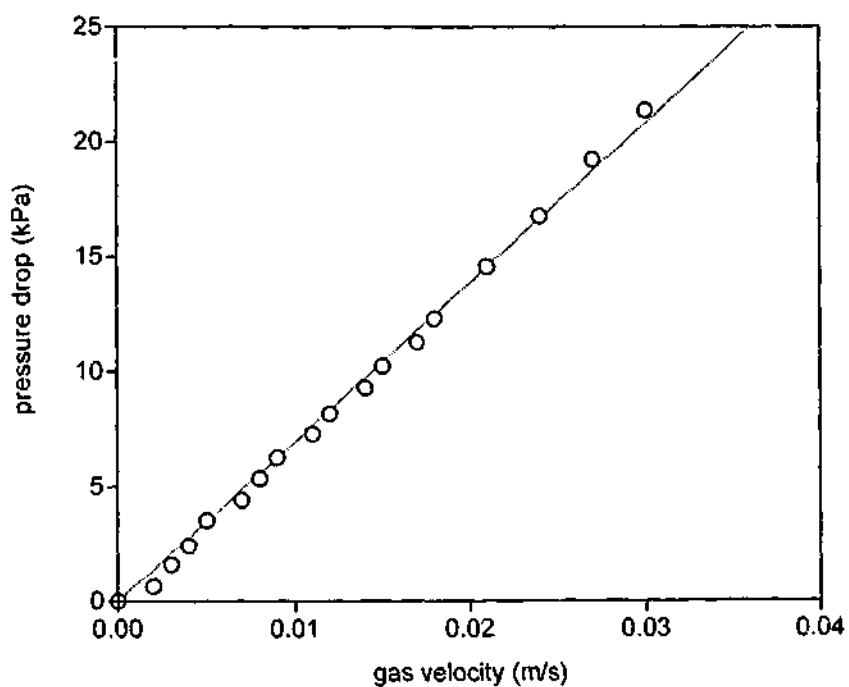


Figure 3-4. Pressure drop versus superficial gas velocity for paper based distributor

The assembled fluidized bed column was inserted into the pressure vessel and positioned vertically. For stabilisation of the fluidized bed column inside

of the pressure vessel, the expanded top section of the bed was bolted to the pressure vessel and a bolt was welded to the bottom of the plenum chamber assembly and tightened to the bottom blind flange of the pressure vessel through a separate support plate.

A pressure rated rubber hose was used for the gas supply inside of the pressure vessel and was connected via 19mm brass plumbing compression couplings to the plenum chamber and to a drilled and threaded opening in a side blind flange of the pressure vessel. Another rubber hose similarly attached to outside of the flange was connected to the permanent gas supply piping.

Before the experimental programme was started the assembled fluidized bed vessel was tested for leaks as described by Svarovsky (1987).

Provisions were made in the design of the lid of the pressure vessel for charging/discharging of solids and inserting bed differential pressure probe and an additional probe. After disconnecting the piping, the lid could be removed for access to the fluidized bed assembly.

Removal of the fluidized bed vessel from the pressure vessel involved major disassembly of the vessel proper and disconnecting incoming and outgoing gas and instrumentation piping. In order to keep this labour- and time-consuming task to a minimum, a simpler method for charging and removal of solids was used.

A copper pipe could be inserted freely through an open M54 port in the lid of the pressure vessel so it would reach the distributor plate. The required amount of bed material was loaded through the pipe and a metal funnel. Metal was preferred to plastic in order to eliminate the possibility of electrical charging of solids by friction while passing through the funnel and pipe. When required, the solids were removed from the bed with an industrial vacuum cleaner connected to the copper pipe.

3.3 PROCESS AND INSTRUMENTATION

The process and instrumentation diagram of the pressurised fluidized bed used in this study of pressure effects on fluidization is shown in Figure 3-5. Equipment parts list is presented in Table 2.

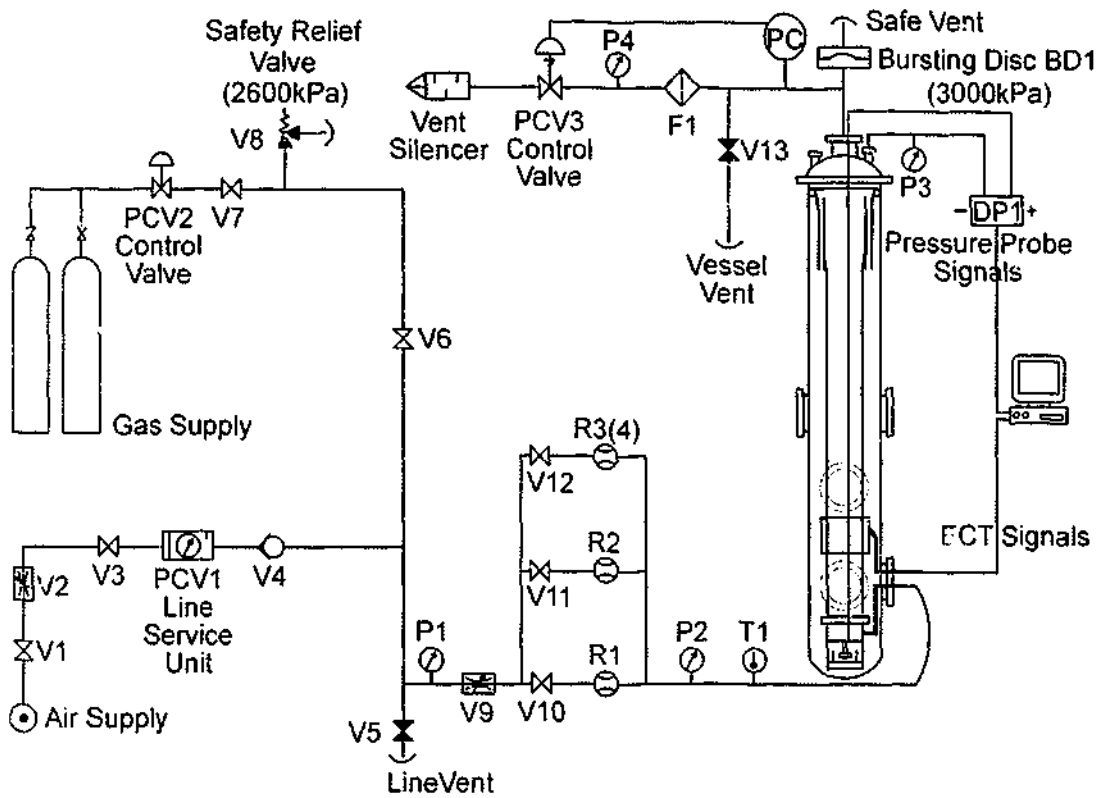


Figure 3-5. Process and instrumentation diagram of the pressurised fluidized bed apparatus used in this study

Table 2. List of equipment and instruments used in experimental set-up

Symbol	Description
V1, V3, V5 - V7, V10 - V13	Isolation valves
V2, V9	Flow control valves
V4	Non-return valve
V8	Safety relief valve
P1 - P4	Pressure gauges
T1	Temperature indicator

Symbol	Description
F1	Line filter
PCV1	Line service unit consisting of pressure regulator, air filter and moisture trap
R1 - R3	Rotameters Krohne H250
R4	Rotameter with flow controller Krohne DK32
PCV2	Manifold pressure regulator
PCV3	Backpressure control valve Samson 3510 with integral positioner
BD1	Safety bursting disc
DP1	Bed differential pressure transmitter Honeywell STD-924
PC	Universal digital controller Honeywell UDC300

3.4 MEASURING GAS FLOW

Fluidising gas for experiments was supplied either from a centralised building compressed air supply or from dedicated gas cylinders.

In experimental work at ambient conditions, it is customary to provide information about the calibration of flow meters in appendices. Since the operating pressure directly affects the gas density and, therefore, the gas flow rates determined by rotameters, it has been decided to provide more information about the gas flow measurement in this chapter.

Originally three variable area flow meters (rotameters R1 - R3) were installed in parallel for measuring the volumetric flow rate of the fluidising gas. They were of H250 RR M9 type supplied by Krohne Messtechnik and operated on the float principle. The flow meters were designed for operating at elevated pressure and calibrated by the manufacturer for air at temperature of 298K and gauge pressure of 2500kPa(g). Under those

conditions the flow meters measured the volumetric flow rate of air in the following ranges:

- R1 0.07 – 0.7m³/h
- R2 0.4 – 4m³/h
- R3 2 – 20m³/h

Later it became clear that the range of the flow meters was excessive for experiments with fine Geldart A materials. The fourth miniature variable area flow meter R4 with flow regulator was selected and it could be installed in line instead of the largest flow meter R3. The flow meter was of DK32 type, also supplied by Krohne Messtechnik. It was calibrated by the manufacturer for air at temperature of 298K and absolute pressure of 2500kPa for the following flow range:

- R4 0.02 – 0.11m³/h

The flow meters were selected in such way that it would be slight overlap in the readings between the consecutive rotameters, and only one rotameter would be in operation at any particular time.

Rotameters calibrated at certain pressure would not read correctly at either higher or lower pressure, unless properly compensated for difference in gas properties at different operating pressures and temperatures. The actual fluidising gas flow rates during each experiment were determined using Krohne variable area flow meter calculation software program⁵.

The manufacturer in accordance with the German standard VDI/VDE 3513 Part 2, defined accuracy of the flow meters using the following relationship:

⁵ KroVaCal. (Version 3.1.4) [computer software]. Duisburg: Krohne Messtechnik (www.krohne.com).

$$E_a = \frac{AC(25+0.75)}{F} \quad (3.4.1)$$

Where E_a is actual error in %, AC is accuracy class of flow meters and F is percentage of the full-scale flow. Accuracy class AC was 1.6 for the rotameters R1 – R3, and 4 for the rotameter R4.

Placing a calibrated rotameter in series with the system flow meters, and comparing readings of a system flow meter under various operating pressure conditions with those of the calibrated rotameter accomplished independent verification of factory calibration of the flow meters.

Gas Technology Services, a testing laboratory accredited by the National Association of Testing Authorities, Australia (NATA), provided two calibrated reference Fischer & Porter tube type variable area flow meters especially for the verification. The actual reference gas flow rates during each test were determined using Gas Technology Services flow meter calculation software program⁶.

Calibration verification for rotameters R1, R2 and R4 was performed at different operating pressures. In all cases the agreement between the flow meters was very good as can be seen in Figure 3-6 – Figure 3-8.

⁶ Performance Calculator. (Version 2.0) [computer software]. Highett: Gas Technology Services
(www.gastechnology.com.au).

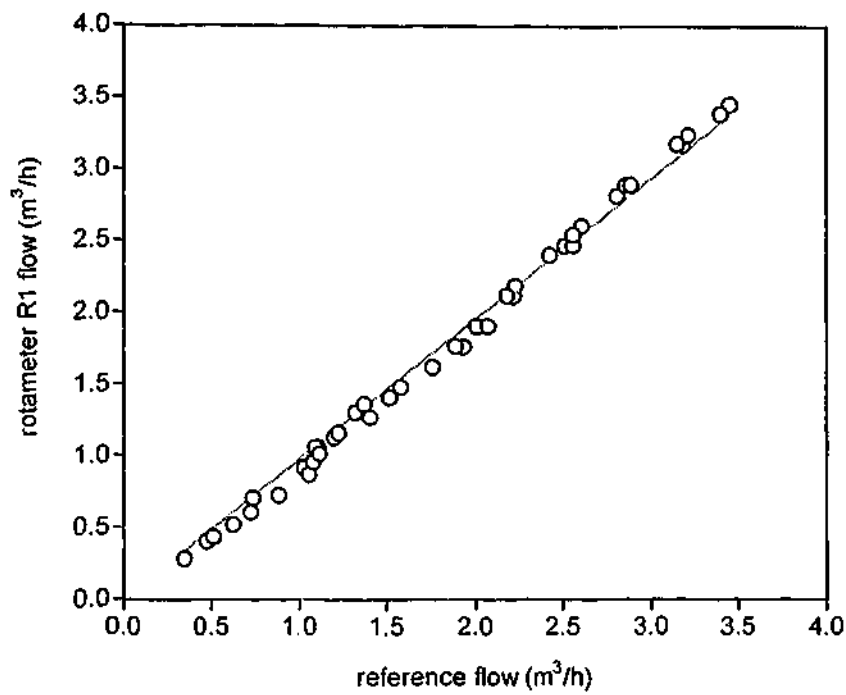


Figure 3-6. Verification of rotameter R1 calibration at atmospheric and 600kPa operating pressures

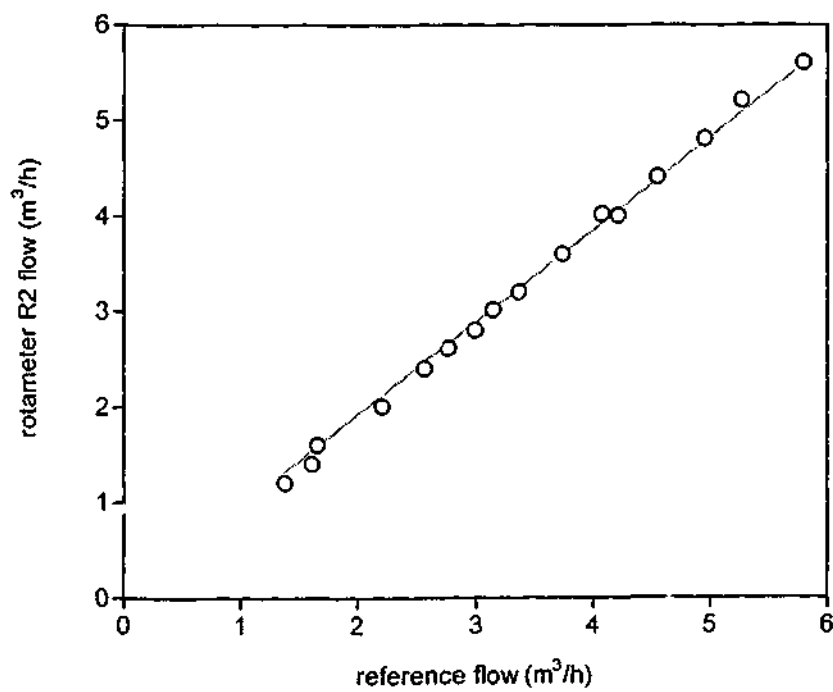


Figure 3-7. Verification of rotameter R2 calibration at atmospheric and 400kPa operating pressures

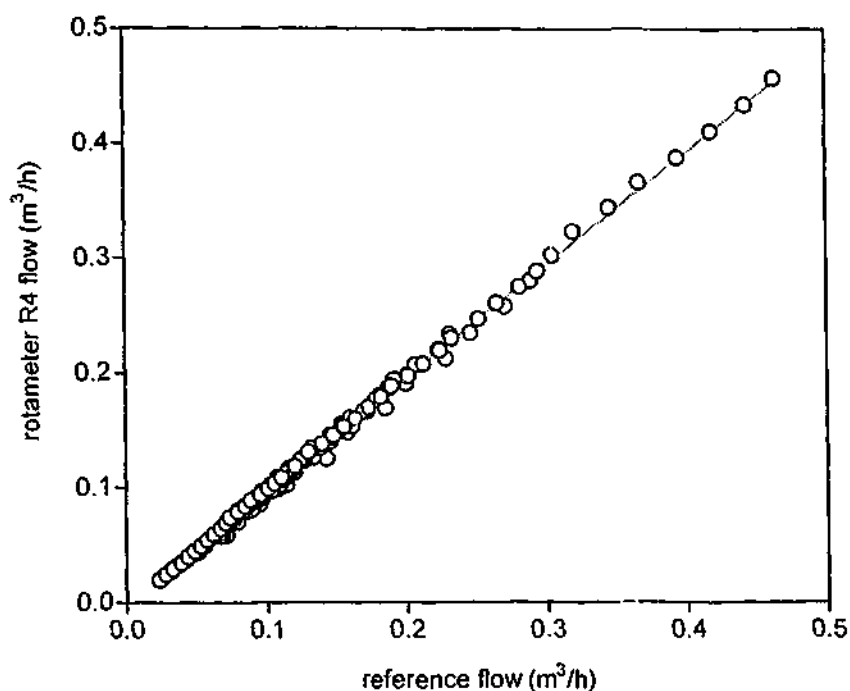


Figure 3-8. Verification of rotameter R4 calibration at various operating pressures (100, 300, 500, 700, 1100, 2100 and 2500kPa)

3.5 CONTROL OF OPERATING PRESSURE

Supply gas pressure was regulated to that required for each experiment at the source. When compressed air from the centralised supply was used both flow rate and pressure were set to a maximum possible by fully opening valve V2 and line service unit PCV1. Supply pressure varied on day-by-day basis depending on the air compressor load but usually was in the range 600 – 750kPa. When gas cylinders were used for high-pressure experiments, supply pressure was regulated by valve PCV2 to the required level below a maximum safe value of 2650kPa.

However, the proper operating pressure in the fluidized bed was set with a backpressure control valve with integral positioner PCV3 manufactured by Samson AG. For regulating pressure and activating the valve PCV3, a microprocessor-based universal digital controller UDC3000 by Honeywell Inc. was used. A typical accuracy of the controller PC was $\pm 0.20\%$ of its span.

The experimental facility was of an open circuit type so the same gas was used for pressurising the system and as an actual fluidising gas. Therefore, the system was pressurised first to a desired operating pressure with the aid of the digital controller PC and control valve PCV3, and only then could the fluidising gas flow rate be adjusted to a desired value. When the system reached a steady state as observed on the screen of the digital controller, the experiment could start.

Excess gas was discharged to atmosphere through an expanded vent and silencer outside of the building.

3.6 ENSURING SAFE OPERATION

Before commissioning the experimental facility Hazard and Operability Study (HAZOP) and Risk Assessment were completed. Safe operating procedures are included in Appendix A.

The effects of a sudden release of high pressure are similar to an explosion. Some typical incidents leading to sudden pressure release could be breaking of a valve on a gas cylinder, breaking of a high-pressure line, using high-pressure equipment above its safe working pressure or sudden pressurising of a vessel by the quick opening of a supply valve.

In order to eliminate hazards of high pressure the following preventative measures were taken:

- The pressure vessel was designed and constructed according to AS1210-1989 Class 3 in March 1997. Design pressure and temperature were 2750kPa and 333K respectively.
- Five observation windows were made of 15mm thick borosilicate glass and supplied as part of the certified pressure vessel.
- Fluidising gas supply lines were made of copper piping of Type B with nominal size DN25 as per AS1432-1990 and rated for safe working

pressure 3700kPa at 323K. Connection of the supply lines and instrumentation was made via pressure-rated brass bulkhead fittings.

- The flow meters R1, R2, R3 and R4 were armoured and rated for working pressure 2600kPa.
- Air filter regulator PCV1 was rated for 1000kPa and used only for building compressed air supply, normally not exceeding 800kPa. When the bottled compressed gas was used, the building compressed air supply line including the regulator was protected from high pressure by non-return valve V4.
- All pressure gauges were rated and graduated for pressure of 4000kPa.
- A mechanical backpressure regulator PCV3 and digital controller PC, rated for 20000kPa, controlled the operating pressure. The regulator was protected by a filter F1 rated for 2500kPa and capable of removing 99.99% of 0.3 μ m particles. The need for change of the filter element could be determined by the difference between the pressure readings on controller PC and pressure gauge P4 exceeding 40kPa.
- The simple plastic fluidized bed vessel was installed within the pressure vessel; however, pressure equalisation ports in the expanded top section ensured that the pressure difference across the plastic wall of the fluidized bed vessel was no more than would be experienced by an atmospheric fluidized bed apparatus. The pressure equalisation ports were fitted with fabric filters to prevent fine dust falling into space between the vessels and fouling observation windows. The plenum chamber assembly of the fluidized bed apparatus was subjected to a higher pressure difference across its walls but was made of steel.
- Gas supply line was fitted with a relief valve V8, set at 2700kPa, as a primary means of avoiding overpressure of the system. The gas exit line

after the pressure vessel was equipped with a conventional metal bursting disc assembly with burst pressure 3100kPa at 298K, as a final emergency measure to prevent over pressurising of the vessel. The bursting disc was tested for rupture twice by the supplier with the result of 3070kPa.

- All connections, threaded joints and flanges were tested for gas leaks before starting the experimental programme and after every disassembly or opening of the pressure vessel, and rotameter replacement.

3.7 BED PRESSURE DROP MEASUREMENT

Fluidized bed pressure drop was taken as a difference between pressures immediately above the distributor plate and in the freeboard of the bed.

A simple pressure probe consisted of 3m long steel tube with outside diameter of 10mm, which was inserted vertically all the way down to the distributor plate. The bottom end of the tube had a 3mm high recess cut from two sides for allowing the gas to enter the tube. A small sintered bronze disc was inserted into the bottom end of the tube for preventing the solids from entering the probe.

As the second part of the differential bed pressure probe, another tube of the same diameter was inserted into the top section of the fluidized bed vessel. A Honeywell ST 3000 Smart Transmitter model STD 924 was set up to measure the differential pressure between the measuring points. The upper range limit of the transmitter DP1 was 100kPa and the minimum span was 2.5kPa. Accuracy including combined effects of linearity, hysteresis and repeatability was $\pm 0.10\%$ of the calibrated span.

An output signal proportional to the measured pressure difference was transmitted in an analogue 4 to 20mA format to a microprocessor based data acquisition unit Datataker DT100. From there the signal in a digital format was transferred to a simple PC286 computer, used exclusively for the task of

measuring pressure difference. The laboratory data logger Datalogger was operated with its proprietary software program⁷.

Although the differential pressure transmitter was factory calibrated for the range 0 - 25kPa, it was calibrated again in situ using a mercury manometer. A pipette bulb was connected simultaneously via a T-branch to the inlet port of a mercury manometer and the inlet pressure sensing port of the pressure transmitter DP1 while both outlets were open to atmosphere. When pressure was applied with the pipette bulb, the differential pressure across the manometer was measured in millimetres of mercury, and the output of the transmitter was also recorded every second for periods of 180 seconds. The obtained calibration line is shown in Figure 3-9.

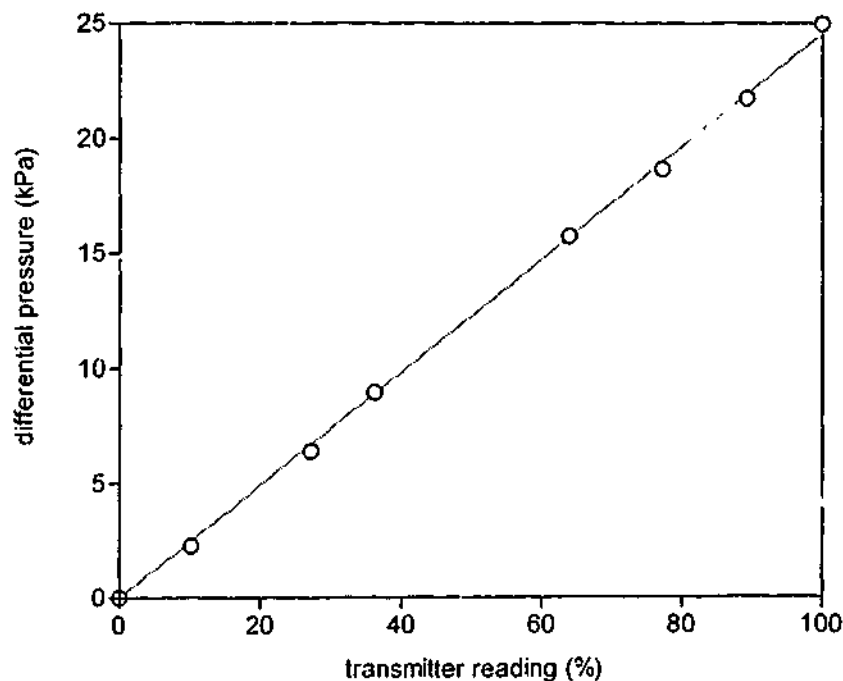


Figure 3-9. Calibration curve for the differential pressure transmitter DP1

⁷ DeTerminal. (Version 2.02) [computer software]. Boronia: Data Electronics (Aust)
(<http://datataker.com>).

3.8 ELECTRICAL CAPACITANCE TOMOGRAPHY

3.8.1 ELECTRICAL CAPACITANCE TOMOGRAPHY SYSTEM

The electrical capacitance tomography (ECT) system used in this work was a single plane system with driven guard drive circuitry of PTL300 type manufactured by Process Tomography Ltd. Typical ECT system, which is based on design developed at University of Manchester, Institute of Science and Technology (UMIST), consists of a capacitance sensor, a capacitance-measuring unit and a control computer.

The PTL300 system used in this work consisted of a Pentium 133MHz computer containing a custom built ECT circuit board, and a data acquisition module type DAM200, and was controlled by proprietary software*.

3.8.2 CAPACITANCE SENSOR DESIGN

The design of the capacitance sensor is important for success and normally is unique for each application. In general, capacitance sensors can contain sets of 6, 8 or 12 measurement electrodes together with axial guard electrodes, and can be mounted either inside or outside the vessel. If the vessel is made of electrically non-conducting material, the sensor is usually mounted on the outside surface, and the measurement is non-invasive. An earthed shield usually surrounds the sensor and minimises the external influence.

The size and number of electrodes depends on the application. A larger number of electrodes give an image of higher resolution but with low measurement sensitivity. The measurement sensitivity can be increased by using longer electrodes but the axial resolution will be lower. For higher axial resolution a number of short electrodes can be used together with axial guard electrodes which are excited separately.

* PCECT Capacitance Tomography System. (Version 2.1) [computer software]. Wilmslow: Process Tomography (www.tomography.com).

The required electrode pattern for this work was designed using CAD software in accordance with PTL application note AN3 (*Engineering design rules for ECT sensors*, 2001). The maximum number of measurement electrodes (12) was used together with driven guard electrodes. The size of each electrode was 35 by 50mm. The sensor was fabricated using standard printed circuit board design techniques from flexible copper-coated plastic laminate that was etched with the electrode pattern and wrapped tightly around the fluidized bed plastic vessel (Figure 3-10).

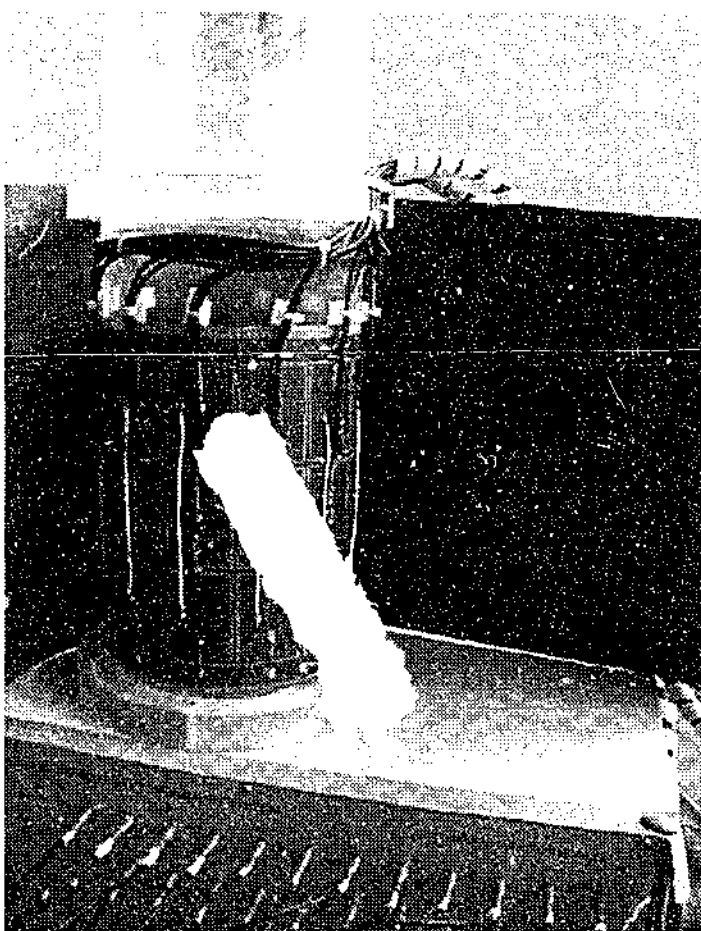


Figure 3-10. Capacitance sensor with the earth screen open, fitted to the fluidized bed vessel and connected to the DAM209 data acquisition unit

3.8.3 CONNECTING LEADS

The measurement and guard electrodes must be connected to the data acquisition module by screened coaxial cables of RG174 type, terminated in miniature coaxial connectors. The maximum cable length should be less than 1.5m.

The capacitance sensor had to be positioned inside the pressure vessel and, since the data acquisition module was not designed for operation at elevated pressure, it was located outside of the pressure vessel. Therefore, it became necessary to direct 24 coaxial cables and an earth wire out of the pressure vessel without gas leaks and pressure loss.

Two possible ways were considered - drilling 25 holes in the side blind flange of the pressure vessel and pressure tight sealing of individual cables as they pass through the openings; or trying to seal the bundle of all the cables and thus drilling only one larger opening in the flange.

Drilling a large number of holes in the pressure vessel was not a very appealing option from a viewpoint of safety regulations at high pressure, and a search for available pressure tight cable glands resulted only in glands designed for underwater applications with insufficient pressure rating of 1000kPa. Therefore, the second option became a preferred one.

At first all the cables were fitted through a 75mm-long piece of copper tube of 19mm diameter, then the tube was positioned approximately in the midpoint of the cables length and packed tightly with epoxy resin. When the resin hardened, the cables became sealed inside of the tube, which could be passed through the flange in a fashion similar to the gas supply arrangement. A hole was drilled in the side flange, and a plumbing compression coupling was threaded into the opening from the internal side of the flange. In this way the copper tube and the bundle of cables were successfully sealed and could withstand the high operating pressure.

However, the gas could escape from the pressure vessel through individual coaxial cables between the central conductors and the shields. To eliminate the possibility of gas leaking inside of the cables, all the soldered connections

between the leads and the electrodes, which can be seen in Figure 3-10, were completely covered with non-conductive epoxy resin.

Later it was found that in another application of electrical tomography at elevated pressure and temperature, 16 cables were individually sealed in a more complicated manner through the wall of a polymerisation autoclave (Dyakowski, 2002).

3.9 EQUIPMENT USED FOR STUDYING PARTICLE MOTION

A conventional thyristor photoflash (Sunpak model 2000BZ) was used as a light impulse source for experimental study of the influence of pressure on the motion particles near the fluidized bed wall surface.

A pulse (1/5000s) of bright light was transmitted from outside of the pressure vessel via fibre optics and illuminated a 7mm-diameter region of the luminescent bed material adjacent to a transparent vessel wall. After illumination these particles showed an afterglow for up to three minutes, which was recorded on Hi8 videotape using a conventional digital video camera (Sony model DCR-TRV 120E).

For transmitting a light pulse inside of the dark pressure vessel a 3mm-diameter fibre optic light guide was fabricated. It had standard crimped termination at each end, which was filled with epoxy resin and polished. In the middle of a 2m-long guide a few centimetres of the sheath were removed; this part was inserted into a 12mm-diameter stainless steel tube and filled with epoxy resin. After removal of the ECT sensor and leads the opening in the pressure vessel flange was used for passing the light guide assembly. Using compression couplings and reducing fittings, the tube with light guide inside was sealed through the flange in similar way to the ECT cables.

In order to transmit the full energy of the flash through the fibre optic, a simple cardboard adapter was used. A photoflash-sized cardboard box was made and painted black inside. A 4mm-diameter hole was made in the bottom of the box and one of the crimped ends of the fibre optic was

inserted through this opening and positioned in front of the photoflash, which was covered with the box and sealed with adhesive tape.

Another end of the fibre optic was supported with a simple wire and Blu-Tack[®] arrangement inside the pressure vessel and positioned next to the transparent fluidized bed wall in such way, that it was at approximately mid-height of the bed level and could be clearly seen through one of the observation windows (Figure 3-11).

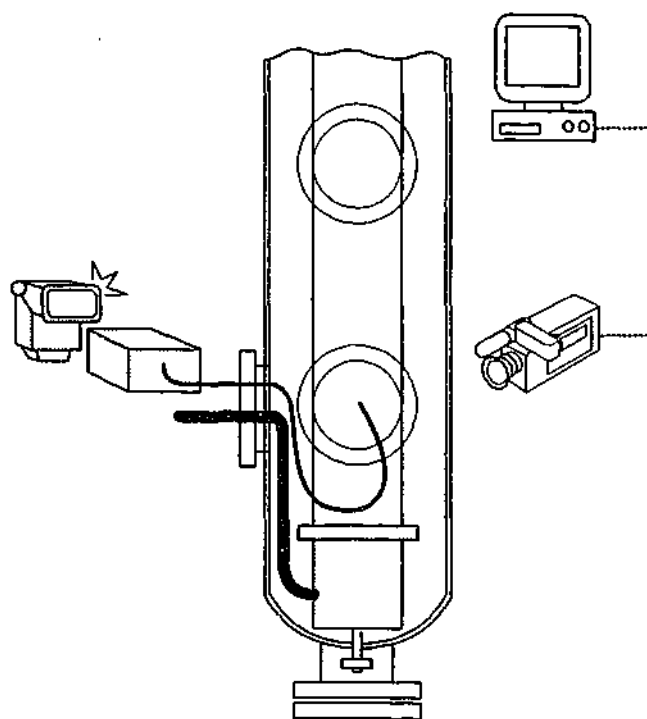


Figure 3-11. Experimental setup for studying particle motion along the wall

3.10 FLUIDISING GASES AND BED MATERIALS

Compressed air from a centralised building supply was usually used for experiments when operating pressure did not exceed 600kPa. For experiments that were run at higher operating pressure, industrial grade nitrogen supplied from a bank of 12 gas cylinders was used. Only on a few occasions was nitrogen used in experiments at pressures below 600kPa.

The following solids were used in experiments - silica sand, FCC catalyst, luminescent pigment Lumilux[®] of two sizes as main materials, and

vermiculite as an additional material. Location of the bed materials on Geldart (1973) classification diagram at ambient conditions is shown in Figure 3-12.

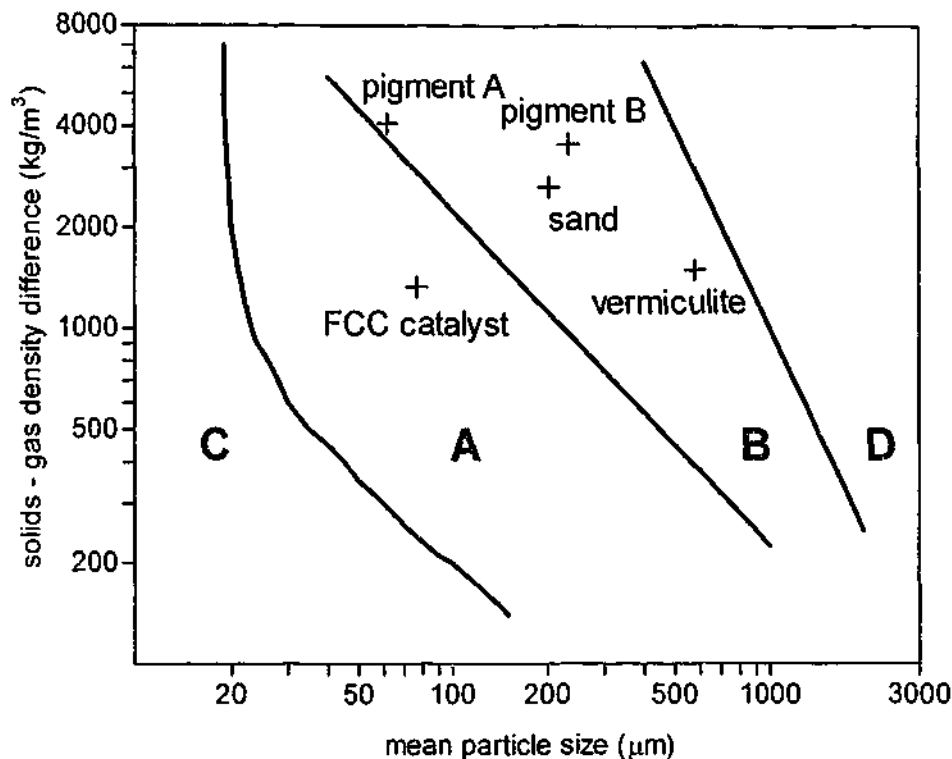


Figure 3-12. Location of solids used in experiments on powder classification diagram by Geldart (1973)

Size and shape of particles can be visually estimated from Figure 3-13 for catalyst, Figure 3-14 for sand, Figure 3-15 for pigment A, Figure 3-16 for pigment B and Figure 3-17 for vermiculite. Information on mean particle diameter, particle density and amount of fines below 45μm is summarised in Table 3.

In order to determine particle physical properties small representative samples were obtained by riffling actual bed solids. Sauter (surface-volume) mean diameter, particle size distribution and fines content were determined using a light scattering technique on Malvern Instruments Mastersizer. Particle density was determined by using a mercury intrusion analysis on the representative dried samples.

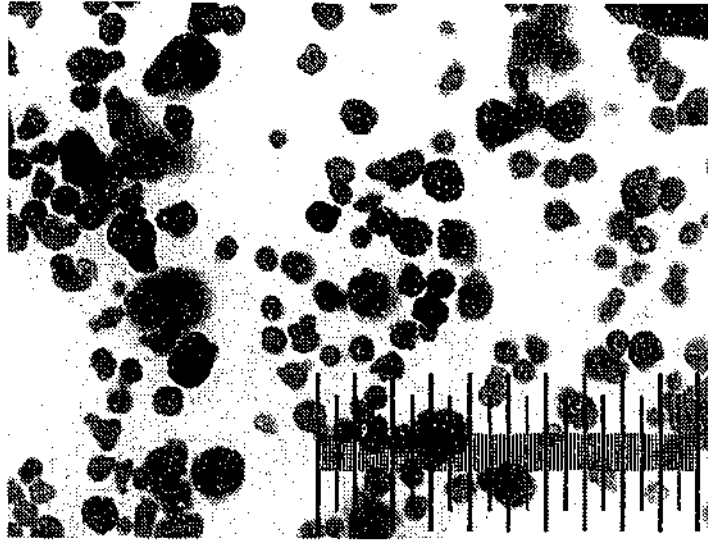


Figure 3-13. Particles of FCC catalyst under 10x magnification (full scale is 1mm)

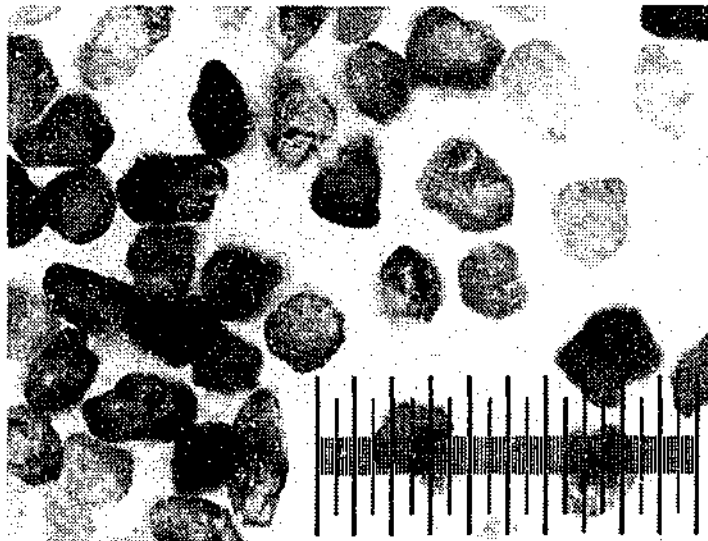


Figure 3-14. Particles of silica sand under 10x magnification (full scale is 1mm)

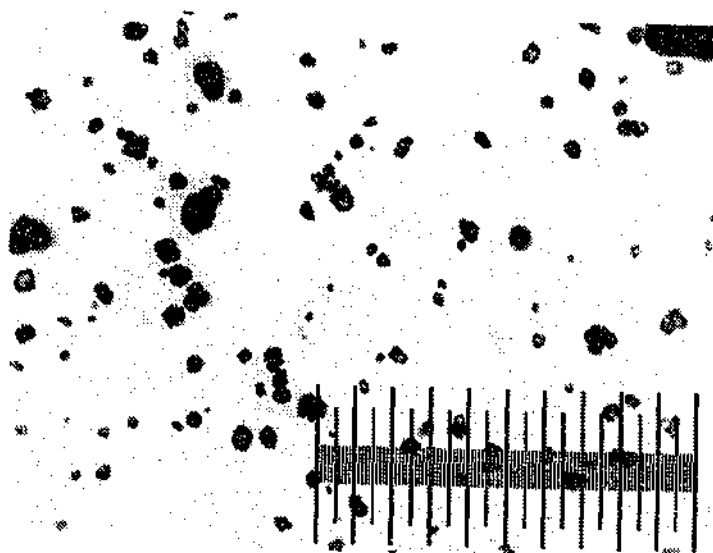


Figure 3-15. Particles of luminescent pigment A under 10x magnification (full scale is 1mm)

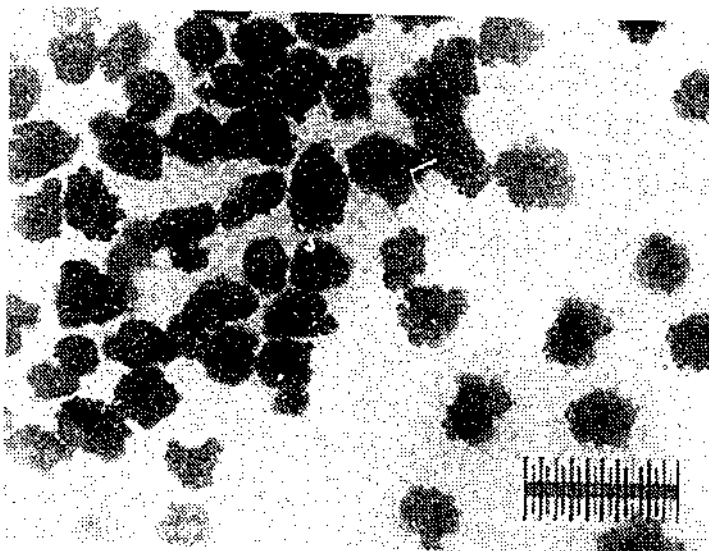


Figure 3-16. Particles of agglomerated in V-blender luminescent pigment B under 5x magnification (full scale is 1mm)

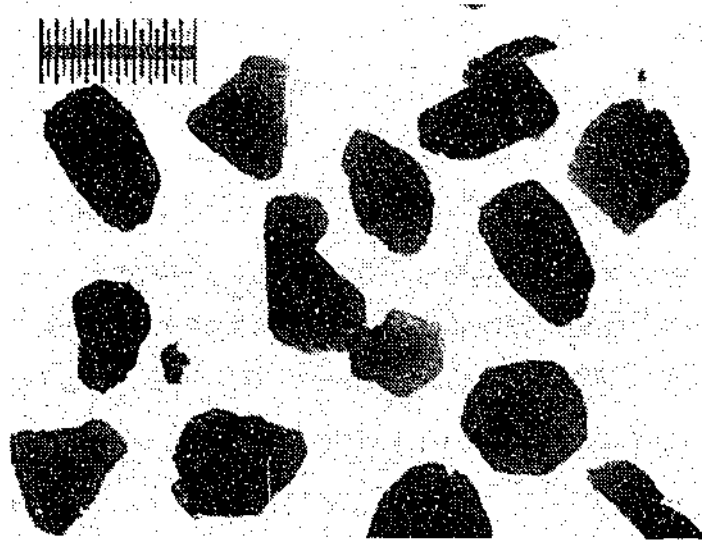


Figure 3-17. Particles of vermiculite under 5x magnification (full scale is 1mm)

Table 3. Typical characteristics of bed materials used in experiments

Material	Sauter mean diameter d_p (μm)	Particle density ρ_p (kg/m^3)	Content of fines below $45\mu\text{m}$ F (%)
FCC Catalyst	77	1330	10.1
Silica sand	203	2650	0
Pigment A	62	4090	19.6
Pigment B	234	3550	0
Vermiculite	581	1510	0

In order to test the possibility of Geldart B behaviour changing to that of Geldart A at elevated pressures, an attempt was made to select a relatively light Geldart B material, positioned close to the A/B boundary. Various plastics and cork were rejected because of expected problems caused by static electricity. A natural mineral, vermiculite, was eventually found; however its position on the Geldart powder classification diagram (Figure 3-12) showed that its expected behaviour was close to that of Geldart B/D solids.

Luminescent pigment selected for filming particles motion near to the wall of the fluidized bed (pigment A) was inorganic luminescent pigment for

visual effects Lumilux® Effect green N-E product No. 50915 with chemical composition of ZnS:Cu, manufactured by Honeywell Specialty Chemicals Seelze GmbH.

Pigment B was prepared by agglomerating the original pigment A. It was important to have the final product strong enough to successfully withstand the process of fluidization without breaking down. Three binding agents were considered - water based satin varnish (Cabot's "Clear Floor"), polyvinyl acetate (PVA) emulsion and 3% solution of sodium carboxymethyl cellulose (SMC) in water.

Nine (three for each binding agent) test bodies (compacts) were prepared for testing the bond strength of the material in the following way. Three quantities of original pigment were mixed together with the binding agents in proportion 9:1. Approximately 15g of prepared test materials were required for each compact. That quantity was placed into a mould of 25mm internal diameter and the whole mould and die assembly was placed in the press, where the sample was compacted to the pressure of 10MPa. After that all the compacts were left for 24 hours curing time.

Measurement of the compressive force required to break the compact across its diameter and calculation of the bond tensile strength were carried out as recommended by Mellor and Hawkes (1971). Average tensile strength of compacts was as follows:

- $1148 \pm 22\text{kPa}$ with "Clear Floor" varnish
- $705 \pm 89\text{kPa}$ with PVA emulsion
- $76 \pm 2\text{kPa}$ with SMC solution

Based on these results the water based clear varnish was selected as a binding agent.

Two batches of 8kg of the original luminescent pigment Lumilux® (pigment A) and the binder were mixed for ten minutes in a liquid-solids blender LB-

9274 by Patterson-Kelley Co. The binder addition level was 15% of solids. After mixing the material was cured in a warm oven for 24 hours. The dry material was sieved in a Tyler RoTap[®] Testing Sieve Shaker with the stack of the following sieves - 850, 600, 425, 300, 212 μ m, and a pan.

Since the amount of pigment in each size fraction was not sufficient for loading the fluidized bed column to a desired level, a mixture of two fractions 212-300 and 300-425 μ m was used for experiments as pigment B.

The strength of the prepared material and its ability to withstand the friction between the particles were assessed during the fluidization test. A small sample (about 100g) of the material was analysed for size distribution and then fluidised in a vigorously bubbling bed for at least 30 minutes. The test was successful and the size analysis, performed after the fluidization, proved that the material agglomerates were not broken.

Chapter 4

MINIMUM FLUIDIZATION AND MINIMUM BUBBLING CONDITIONS

This chapter focuses on basic fluidization parameters such as minimum fluidization and minimum bubbling velocities. These velocities as well as bed voidage at minimum fluidization and bubbling conditions, determined experimentally at elevated pressures, are presented here and compared to the existing correlations.

4.1 EXPERIMENTAL DETERMINATION OF THE MINIMUM FLUIDIZATION VELOCITY

4.1.1 OVERVIEW

It is generally accepted that the best method to determine the minimum fluidization velocity is by measurement. As mentioned in Section 2.2.1, a standard method of determination of minimum fluidization velocity by experiment is by measuring the dependence of bed pressure drop on gas velocity. At the minimum fluidization velocity the bed weight is fully supported by the gas flow and the pressure drop becomes constant.

Although the minimum fluidization velocity is the basic information required for the design and development of fluidized bed processes, in industry fluidized bed reactors are mostly operated at superficial gas velocities well above the minimum fluidization velocities. Therefore, the minimum fluidization velocity is not a quantity with a precise significance for industrial applications and large inaccuracies in the prediction of the minimum fluidization velocity values are more or less acceptable.

In science, however, discussion on accurate prediction of the minimum fluidization velocity still seems to remain of much interest. At the same time

the experimental technique for measuring the minimum fluidization velocity varies and can be prone to some inaccuracies.

The minimum fluidization velocity is taken as the velocity at the intersection point of the line corresponding to the constant bed pressure drop in the fluidised state and the extrapolated straight line of the packed bed region. Many researchers observed two different bed pressure drop versus superficial gas velocity curves while increasing and decreasing the gas flow.

There is no agreed procedure for determining the precise point of the minimum fluidization velocity and, usually, the two straight lines are obtained as the gas flow rate is gradually reduced in increments from a vigorously bubbling state. In this case, a slightly larger value of the minimum fluidization velocity is obtained. That makes sense for industrial applications as it provides a maximum experimental value for the minimum fluidization velocity and, therefore, the lowest limit for potential defluidization of a process.

According to Svarovsky (1987) better reproduction of results can be obtained by allowing the bed to mix first by bubbling freely before turning the gas flow rate down to zero and then taking pressure drop measurements, while increasing gradually the gas flow rate. However, various researchers have described three different points representing the minimum fluidization velocity on the increasing gas velocity curve for Geldart A materials, as reviewed by Fletcher et al. (1993).

Although not proven for ordinary fluidized beds, it was found that in a magnetic fluidized bed the minimum fluidization velocity is the point of intersection of the constant pressure drop line with the packed bed line representing the bed pressure drop for *increasing* gas velocity points only (Rhodes et al., 2001; Saxena & Shrivastava, 1990). When the gas flow is decreased the intersection point gives not the minimum fluidization but the minimum bubbling velocity.

It appears that depending on the direction of gas velocity change, a number of experimental points describing the minimum fluidization velocity can be obtained.

4.1.2 EXPERIMENTAL METHOD

The same experiments were carried out in order to determine the minimum bubbling velocity, bed expansion and voidage; and the details of the experimental procedure are given here.

A well-known method of measuring the dependence of the bed pressure drop on the superficial gas velocity was used for establishing the experimental values of the minimum fluidization velocity. Pressure drop measurements were obtained for both increasing and decreasing gas velocities.

Different bed materials were investigated at pressures between atmospheric and 2100kPa. The mass of bed solids used in the experiments, static bed height at ambient conditions, and the pressure range are given in Table 4. The amount of bed solids was selected so that the top surface of the bed would be clearly visible through one of the pressure vessel's observation windows. The experimental set-up and bed materials are more thoroughly described in Chapter 3.

Table 4. The mass of bed solids, static bed height and the experimental pressure range for different materials used in the experiments to establish the minimum fluidization and minimum bubbling velocities and bed expansion

Material	Mass of bed material (kg)	Static bed height (m)	Absolute operating pressure (kPa)
FCC Catalyst	7.60	0.535	101, 300, 400, 500, 700, 900, 1000, 1100, 1700, 1900, 2100

Material	Mass of bed material (kg)	Static bed height (m)	Absolute operating pressure (kPa)
Silica sand	9.00	0.400	101, 200, 300, 400, 500, 600, 1600
Pigment A	6.00	0.173	101, 400, 600, 1100, 1900
Pigment B	3.78	0.205	101, 500, 1300
Vermiculite	1.50	0.420	101

A certain procedure was followed for preparing the bed for the experiments. Prior to each experiment at ambient conditions, the pressure vessel was open and the air supply pressure was set to the gauge pressure of 10 kPa. The bed was fluidised at superficial gas velocities well above the onset of fluidization for at least 15 minutes, allowing bed solids to fully mix. The air supply was then slowly turned off by closing the flow control valve. That ensured an initial packed bed of similar structure in each experiment.

In high-pressure experiments the same gas was used for pressurising the system and then for fluidising the bed material. Therefore, prior to each experiment, the backpressure controller was set to a pre-determined operating pressure and the system was pressurised to that level first.

At the same time the gas passed through the fluidized bed, which was properly fluidised for much longer than at the ambient conditions. Then the gas supply was slowly turned off, allowing the bed to settle in the pressurised environment.

In actual experiments, measurements of the pressure drop were taken for both increasing and decreasing gas velocities. After each gas velocity change, the pressure in the system was allowed to stabilise for at least ten minutes. When both pressure and gas flow became stable, results of the pressure drop measurements were recorded at a frequency of 1 Hz for at least three minutes.

At the same time, the bed height and the general behaviour of fluidization were visually observed and recorded in a logbook.

4.1.3 EXPERIMENTAL RESULTS

For each experiment a straight line was drawn from the origin through the series of bed pressure drop points until it crossed the horizontal line representing the maximum value of the bed pressure drop Δp_{max} , computed from the following relation:

$$\Delta p_{max} = \frac{mg}{A} \quad (4.1.1)$$

Where mg is the weight of the solids in the bed and A is the effective cross-sectional area of the fluidized bed. The horizontal line, computed from this relation, generally fitted the experimental points for the bubbling bed well.

Where measurements showed a hysteresis effect between increasing and decreasing gas velocities, both intersection points were established as lower and upper values of the minimum fluidization velocity at a given experimental condition. For comparison between experiments at different operating pressures the average of those two points was taken as the minimum fluidization velocity.

Typical graphs of the results obtained at ambient conditions are presented in Figure 4-1 -- Figure 4-5.

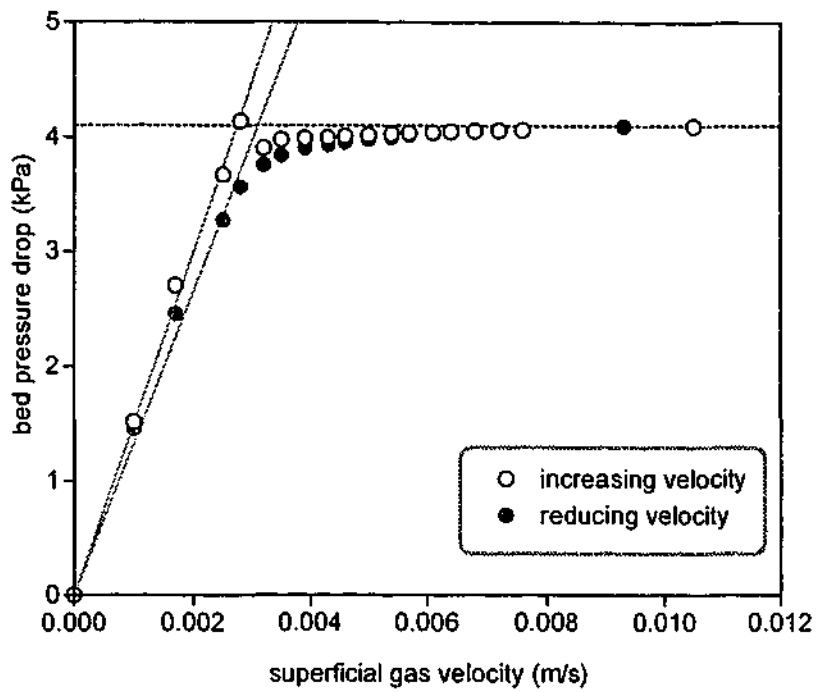


Figure 4-1. Bed pressure drop as a function of increasing and decreasing superficial gas velocity for FCC catalyst at atmospheric pressure

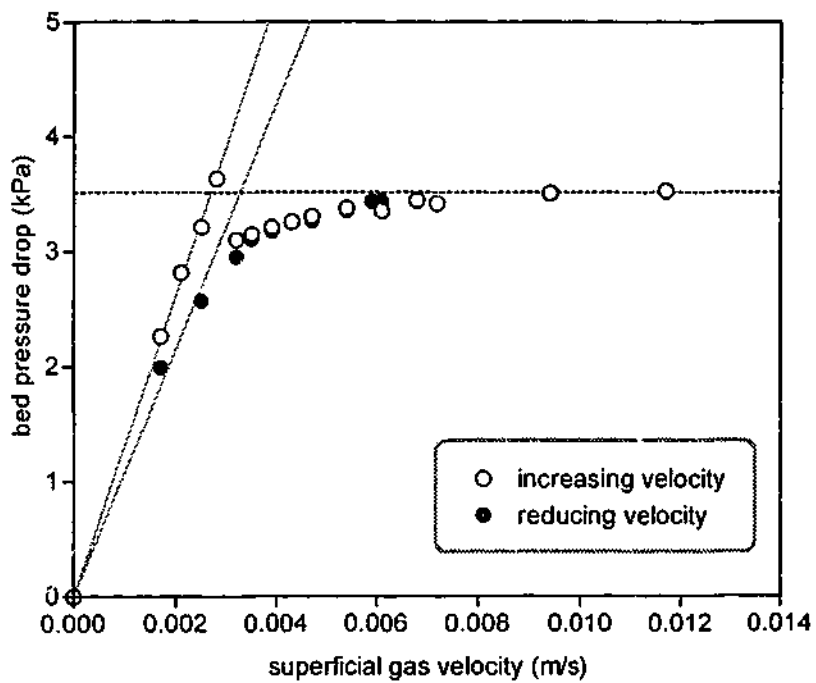


Figure 4-2. Bed pressure drop as a function of increasing and decreasing superficial gas velocity for pigment A at atmospheric pressure

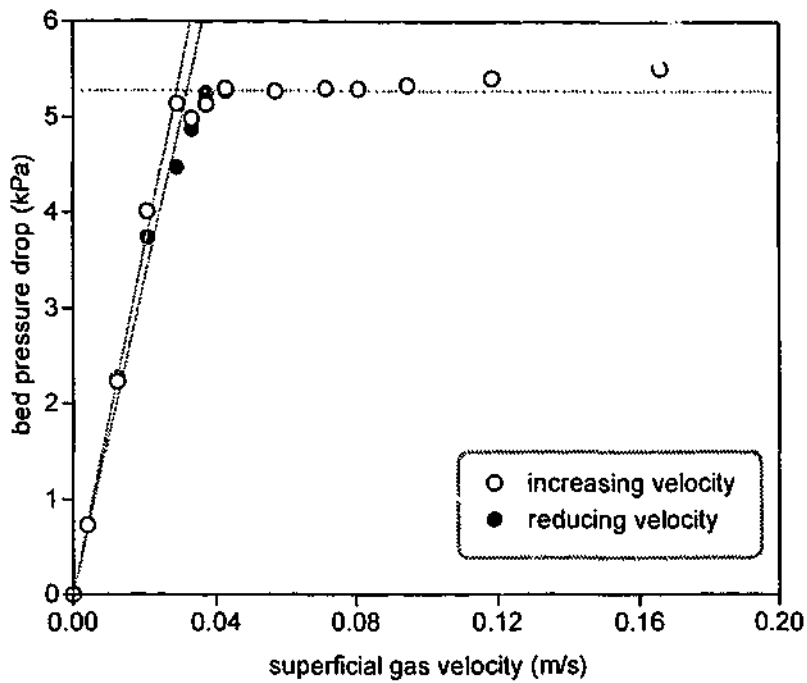


Figure 4-3. Bed pressure drop as a function of increasing and decreasing superficial gas velocity for silica sand at atmospheric pressure

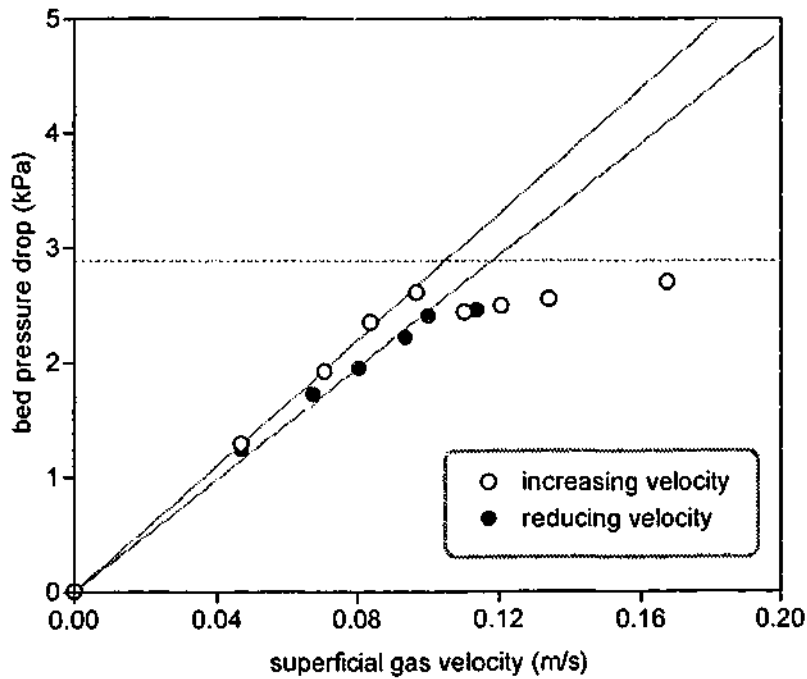


Figure 4-4. Bed pressure drop as a function of increasing and decreasing superficial gas velocity for pigment B at atmospheric pressure

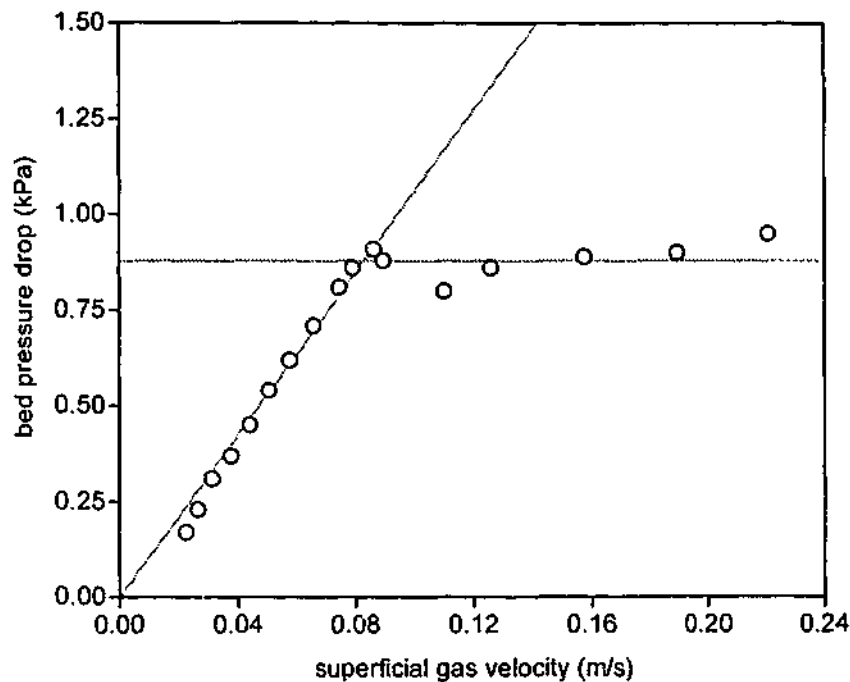


Figure 4-5. Bed pressure drop as a function of increasing superficial gas velocity for vermiculite at atmospheric pressure

Vermiculite was found to be a difficult material for fluidization under available laboratory conditions, especially for the experiments described in the next chapter. Therefore, the experimental programme with vermiculite consisted of only a limited number of experiments. At ambient conditions, the minimum fluidization velocity was established only as a reference in the direction of increasing gas velocity (Figure 4-5). No experiments were carried out to determine the minimum fluidization velocity at elevated pressure.

4.2 INFLUENCE OF PRESSURE ON MINIMUM FLUIDIZATION

4.2.1 INFLUENCE OF PRESSURE ON THE MINIMUM FLUIDIZATION VELOCITY

Many researchers have previously studied the pressure effect on the minimum fluidization velocity and found that the minimum fluidization velocity is not affected by pressure for fine Geldart A powders and decreases with pressure increase for coarse materials. More details on previous studies are given in Chapter 2.

Because of the large number of independent studies available, no attempt was made to cover this subject in depth again. Only two Geldart A and B materials (FCC catalyst and silica sand respectively) were studied at a wide range of pressures between 101 and 2100kPa, some other materials were tested at as little as three pressure settings.

As previously described in Section 2.2.1, numerous correlations for predicting the minimum fluidization velocity have been suggested. Probably the most widely used correlation is one proposed by Wen and Yu (1966a):

$$\text{Re}_{mf} = \sqrt{33.7^2 + 0.0408Ga} - 33.7 \quad (4.2.1)$$

However, this popular correlation was based only on data obtained at atmospheric pressure. A less well-known correlation, also based on data at ambient conditions, was proposed in a paper published in French (Thonglimp et al., 1984) and, according to Couderc (1985), gave the best results with low mean deviations when compared to numerous other correlations:

$$\text{Re}_{mf} = \sqrt{31.6^2 + 0.0425Ga} - 31.6 \quad (4.2.2)$$

Four similar correlations based on experiments carried out at elevated pressures have also been proposed in the literature. These are:

Saxena and Vogel (1977) correlation:

$$\text{Re}_{mf} = \sqrt{25.28^2 + 0.0571Ga} - 25.28 \quad (4.2.3)$$

Borodulya et al. (1982) correlation:

$$\text{Re}_{mf} = \sqrt{16^2 + 0.0370Ga} - 16 \quad (4.2.4)$$

Chitester et al. (1984) correlation:

$$\text{Re}_{mf} = \sqrt{28.7^2 + 0.0494Ga} - 28.7 \quad (4.2.5)$$

Nakamura et al. (1985) correlation:

$$\text{Re}_{mf} = \sqrt{33.95^2 + 0.0465Ga} - 33.95 \quad (4.2.6)$$

All the correlations are based on the Ergun (1952) equation, and are simplified by assuming constant values for the relations between the bed voidage at the minimum fluidization conditions and the particle shape factor.

The Ergun (1952) equation at the minimum fluidization conditions can be written as:

$$(1 - \varepsilon_{mf})(\rho_p - \rho_g)g = 150 \frac{(1 - \varepsilon_{mf})^2}{\varepsilon_{mf}^3} \frac{\mu U_{mf}}{(\phi d_p)^2} + 1.75 \frac{(1 - \varepsilon_{mf})}{\varepsilon_{mf}^3} \frac{\rho_g U_{mf}^2}{\phi d_p} \quad (4.2.7)$$

In order to calculate the minimum fluidization velocity from Eq.(4.2.7), it is necessary to determine values of the bed voidage at the minimum fluidization and the particle shape factor. Knowing the mass of the bed solids m , the bed voidage ε can be determined by measuring the bed height H and applying the following relation:

$$\varepsilon = 1 - \frac{m}{\rho_p HA} \quad (4.2.8)$$

One of the methods for prediction of the minimum fluidization velocity, based on using Eq.(4.2.7), was suggested by Werther (1977) and has been used in the present work. Values of the minimum fluidization velocity experimentally determined at ambient conditions and the voidage at minimum fluidization, obtained from Eq.(4.2.8), were used to calculate a characteristic particle diameter ϕd_p from the Ergun (1952) equation. Following this method, which is described in Section 2.2.3, the minimum fluidization velocity values at various operating pressures were calculated.

Previously it was quite often found that the absolute values of predictions based on the correlations, available in the literature, were significantly in error (e.g. Knowlton, 1977; Marzocchella & Salatino, 2000; Olowson & Almstedt, 1991). A comparison between the experimentally measured values of the minimum fluidization velocity and the calculated values from the Ergun (1952) equation in accordance with the method of Werther (1977), and the values, calculated from Eqs.(4.2.1) – (4.2.6), is shown in Figure 4-6 – Figure 4-9.

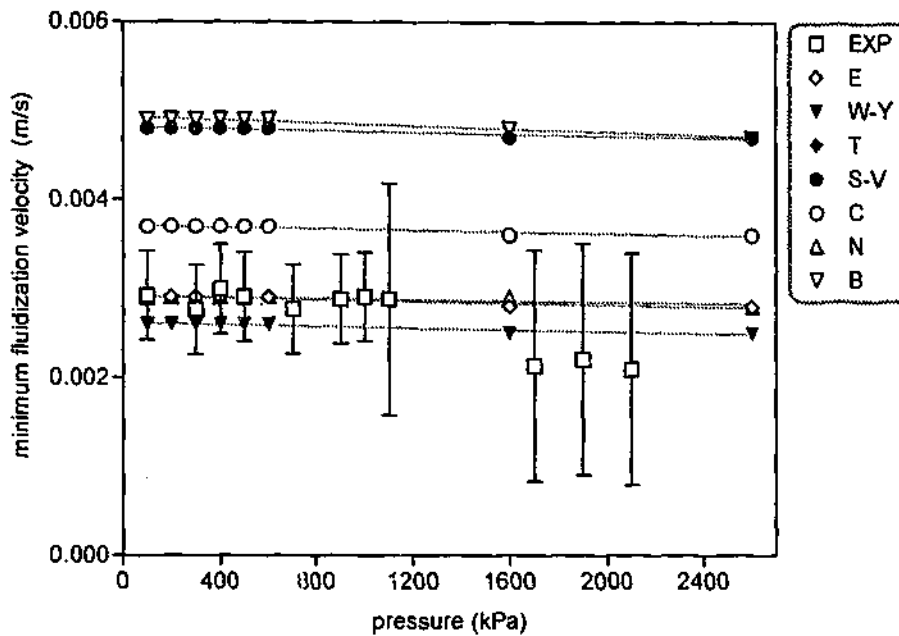


Figure 4-6. Variation of the minimum fluidization velocity with pressure for FCC catalyst (EXP - experimental values, E - (Ergun, 1952; Werther, 1977), W-Y - (Wen & Yu, 1966a), T - (Thonglimp et al., 1984), S-V - (Saxena & Vogel, 1977), C - (Chitester et al., 1984), N - (Nakamura et al., 1985), and B - (Borodulya et al., 1982))

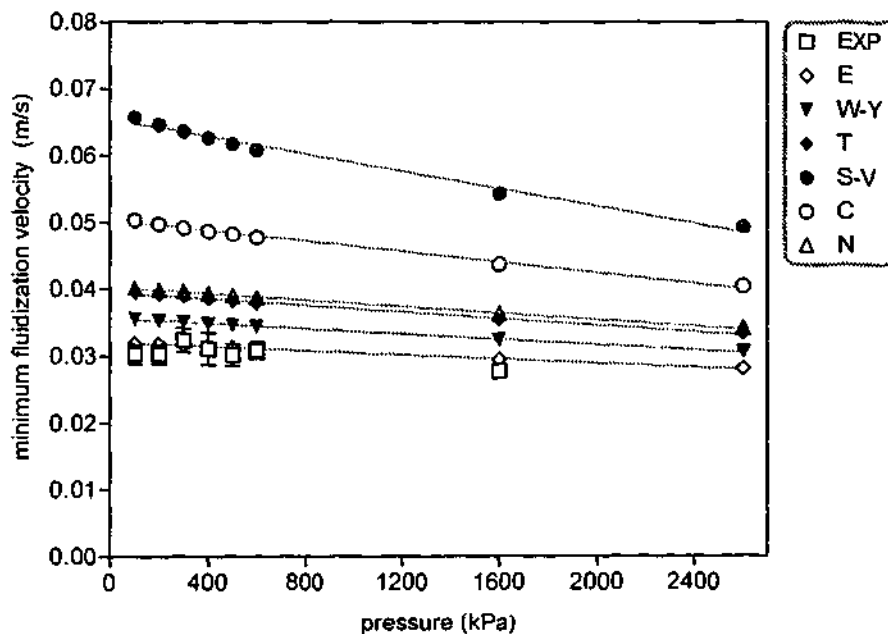


Figure 4-7. Variation of the minimum fluidization velocity with pressure for silica sand (EXP - experimental values, E - (Ergun, 1952; Werther, 1977), W-Y - (Wen & Yu, 1966a), T - (Thonglimp et al., 1984), S-V - (Saxena & Vogel, 1977), C - (Chitester et al., 1984), N - (Nakamura et al., 1985), and B - (Borodulya et al., 1982))

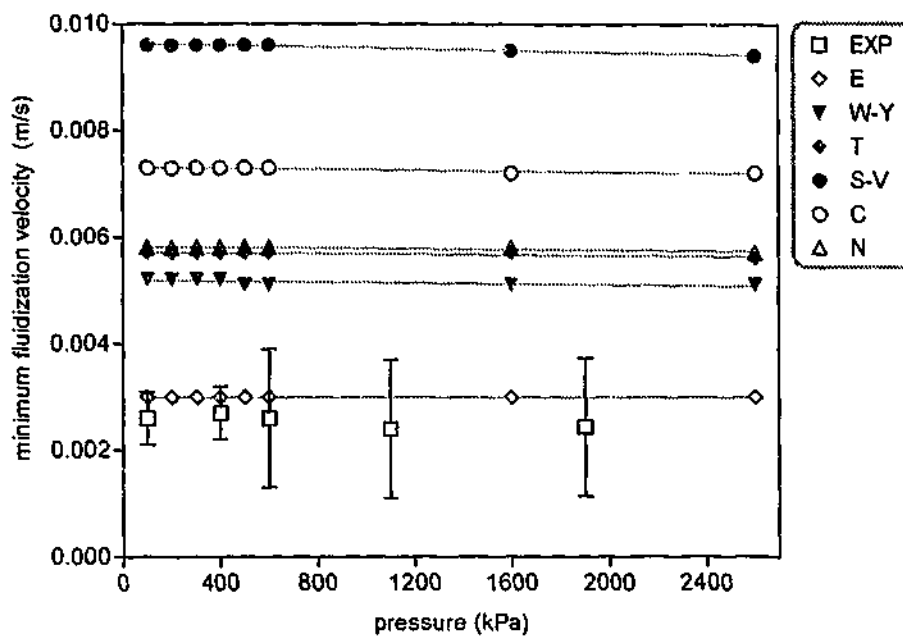


Figure 4-8. Variation of the minimum fluidization velocity with pressure for pigment A (EXP - experimental values, E - (Ergun, 1952; Werther, 1977), W-Y - (Wen & Yu, 1966a), T - (Thonglimp et al., 1984), S-V - (Saxena & Vogel, 1977), C - (Chitester et al., 1984), N - (Nakamura et al., 1985), and B - (Borodulya et al., 1982))

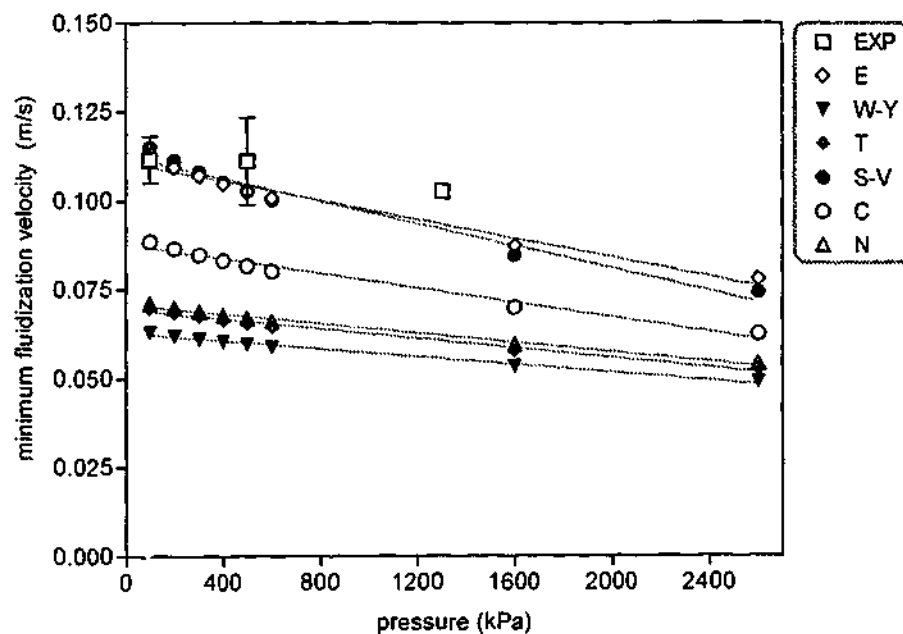


Figure 4-9. Variation of the minimum fluidization velocity with pressure for pigment B (EXP - experimental values, E - (Ergun, 1952; Werther, 1977), W-Y - (Wen & Yu, 1966a), T - (Thonglimp et al., 1984), S-V - (Saxena & Vogel, 1977), C - (Chitester et al., 1984), N - (Nakamura et al., 1985), and B - (Borodulya et al., 1982))

The plots (Figure 4-7 and Figure 4-9) show a very slight decrease in the minimum fluidization velocity values with increasing pressure for Geldart B solids. Large number of workers (e.g. Borodulya et al., 1982; Bouratoua et al., 1993; Chiba et al., 1986; Chitester et al., 1984; Gilbertson et al., 1998; King & Harrison, 1982; Knowlton, 1977; Llop et al., 1995; Marzocchella & Salatino, 2000; Nakamura et al., 1985; Olowson & Almstedt, 1991; Saxena & Vogel, 1977; Sobreiro & Monteiro, 1982; Vogt et al., 2001) have observed the decrease in the minimum fluidization velocity with increasing pressure for Geldart B materials.

The plots also show that the pressure effect on the minimum fluidization velocity is more pronounced for the coarser and denser particles. The minimum fluidization velocity of silica sand decreased from 3.1cm/s at ambient conditions to 2.8cm/s at 1600kPa, and the minimum fluidization velocity of pigment B decreased from 11.2cm/s at atmospheric pressure to 10.3cm/s at 1300kPa.

For Geldart A materials, Figure 4-6 and Figure 4-8 show some decrease of the minimum fluidization velocity with pressure. For both materials the minimum fluidization velocity was approximately 0.3cm/s at ambient conditions. Although it was found to decrease a little at pressures above 1700kPa, the actual decrease was less than 0.5mm/s and was attributed rather to a possible experimental error than to the influence of pressure.

At lower operating pressures, the whole experimental range of gas velocities was covered by the smallest rotameter R4, with the minimum fluidization velocity being measured in the upper range of the scale. In the pressure range 1200 - 1600kPa, the minimum fluidization velocity could not be adequately measured, since the onset of fluidization coincided with the moment of switching the gas flow from the rotameter R4 to a larger rotameter R1. At higher operating pressures, the minimum fluidization velocity could be measured only in the lower (10 - 16%) range of the rotameter R1, where the instrument error was the highest.

Other workers observed that for fine Geldart A particles the minimum fluidization velocity was unaffected by pressure (e.g. Chitester et al., 1984; Foscolo et al., 1989; King & Harrison, 1982; Piepers et al., 1984; Rowe et al., 1982; Sobreiro & Monteiro, 1982).

Depending on the physical properties of particles, the correlations agree with the experimental results with variable success. For the FCC catalyst, Figure 4-6 shows that the Ergun (1952) equation and the correlations of Wen and Yu (1966a), Thonglimp et al. (1984) and Nakamura et al. (1985) predict the minimum fluidization velocity values very well. However, the correlations of Chitester et al. (1984), and to larger extent of Saxena and Vogel (1977) and Borodulya et al. (1982) overestimate the minimum fluidization velocity values.

For the pigment A, which is also a Geldart A material but much denser than the catalyst, only the Ergun (1952) equation predicts the minimum fluidization velocity well. None of the correlations agree with the experimental results as can be seen in Figure 4-8. Moreover, the correlations of Saxena and Vogel (1977) and Borodulya et al. (1982) overestimate the experimental values of the minimum fluidization velocity by more than three times.

Similar results can be observed for the silica sand Geldart B material in Figure 4-7, where only the Ergun (1952) equation agrees well with the experimental results and all the correlations more or less overestimate the minimum fluidization velocity values.

The minimum fluidization velocity for the agglomerated pigment B was experimentally determined only at ambient conditions and at two elevated operating pressures (500 and 1300kPa). The Ergun (1952) equation again provides the closest fit, although not perfect, and this time all the correlations underestimate the limited number of the experimental values (cf. Figure 4-9). It was experimentally found that the voidage at incipient fluidization increased with a pressure increase for this material (Section 4.2.2 below). When the experimental values of ε_{mf} were used in the Ergun (1952)

equation, it fitted perfectly the three experimental values of the minimum fluidization velocity.

Lippens and Mulder (1993) tested statistically 33 equations and correlations for predicting the minimum fluidization velocity at ambient conditions and concluded that the original Ergun (1952) equation was the best equation to describe the bed pressure drop at incipient fluidization. The majority of the empirical correlations, available in scientific literature, are based on the Ergun (1952) equation, simplified after an experimental evaluation based on limited numbers of data and materials. The popularity of the correlation of Wen and Yu (1966a) is attributed to a fact that it is quite simple and offers the correct order of magnitude in industrial practice.

According to Lippens and Mulder (1993), the empirical correlations may be applicable in the industry but have limited value in science, and the preference should be given to a full characterization of the fluidized bed. This should include the determination of particle shape and the voidage at minimum fluidization as described by Geldart (1990).

The analysis of the experimental results at elevated pressure, obtained in the present study, supports this view. None of the correlations consistently gave satisfactory results when applied to all the materials at various operating conditions. At the same time, the Ergun (1952) equation provided the best fit to experimental values on every occasion.

As discussed in Section 2.2.3, several methods for prediction of the minimum fluidization velocity at elevated pressure were found in the literature with all of them based on experimental determination of the minimum fluidization velocity at ambient conditions first. A method to calculate the minimum fluidization velocity of a process, which is not at ambient conditions, originally proposed by Werther (1977) and based on the Ergun (1952) equation, was used in this study with a very good result.

4.2.2 BED VOIDAGE AT MINIMUM FLUIDIZATION AT ELEVATED PRESSURE

The experimental values of the voidage at minimum fluidization ϵ_{mf} were determined from Eq.(4.2.8), using measured bed height values corresponding to the minimum fluidization velocity at both increasing and decreasing gas velocity. The average of the two values was used as a parameter for comparison at various operating pressures.

It was experimentally found that the voidage at minimum fluidization was essentially independent of pressure for:

- FCC catalyst ($\epsilon_{mf}=0.42$) in a pressure range 101-2100kPa
- Silica sand ($\epsilon_{mf}=0.50$) in a pressure range 101-1600kPa
- Pigment A ($\epsilon_{mf}=0.50$) in a pressure range 101-1900kPa

Other workers (e.g. King & Harrison, 1982; Sobreiro & Monteiro, 1982; Vogt et al., 2001) also observed the independence of the voidage at minimum fluidization on pressure.

However, for the dense and agglomerated pigment B, the voidage at minimum fluidization increased from 0.69 at atmospheric pressure to 0.71 at 500kPa and to 0.72 at 1300kPa. This observation is based on a limited number of experimental points but agrees with findings of Olowson and Almstedt (1991), who observed slight increase of ϵ_{mf} with increasing pressure for large sand particles and did not notice any pressure effect on ϵ_{mf} for smaller sand particles. Llop et al. (1995) also observed an increase of ϵ_{mf} with increasing pressure for large sand particles but reported a slight decrease of ϵ_{mf} for smaller sand particles. Saxena and Vogel (1977) also reported an increase in ϵ_{mf} for coarse dolomite.

Yang et al. (1985) suggested, however, that the variation of the voidage at minimum fluidization caused by a pressure increase would be very small, if at all, for coarse materials (Geldart B and D) and substantial for Geldart A powders. That was not observed in the present study. Weimer and Quarderer

(1985) carried out their experiments at much higher pressures and did not observe any voidage change for a Geldart B material and noticed only very small increase in the voidage at minimum fluidization for Geldart A materials.

4.3 EXPERIMENTAL DETERMINATION OF THE MINIMUM BUBBLING VELOCITY

4.3.1 OVERVIEW

Fine powders show an ability to be fluidised at velocities above the minimum fluidization velocity without the formation of bubbles. The bed of those particles smoothly expands until a certain minimum bubbling velocity is reached at which small bubbles appear on the surface.

Visual observation of the fluidized bed behaviour provides a common and simple but subjective way of determining the minimum bubbling velocity. When the gas flow is gradually increased, the gas velocity at which the first distinct bubbles appear on the bed surface should be recorded. Alternatively, the gas velocity is noted at which bubbling stops when the gas flow is decreased. According to Geldart (1986) and Svarovsky (1987), the average of the two values provides the minimum bubbling velocity, or more appropriate values can be taken during decreasing gas flow.

The first bubbles must not be confused with the small channels, which often appear and resemble small volcanoes. Genuine bubbles usually appear in several places on the bed surface and are about 10mm in diameter; and the channels are smaller in diameter and usually stay in one place.

The determination of the minimum bubbling velocity based on visual observation is subject to uncertainty. Due to wall effects or non-uniformity of distributors some bubbles may be observed while the bed is still expanding homogeneously.

The minimum bubbling velocity can be determined less subjectively as the velocity at which the maximum bed height is observed (Harriott & Simone, 1983). However, according to Geldart (in Svarovsky, 1987), the method of

plotting bed height as function of gas velocity gives the minimum bubbling velocity reproducibly and coincides with visual observation only when using bed depths greater than about 0.6m. At lower bed heights, the minimum bubbling velocity values determined visually are smaller than those found from the bed height plot.

4.3.2 EXPERIMENTAL METHOD

Detailed information was given in Section 4.1.2. At each gas velocity the bed height was recorded and, based on visual observation, general behaviour of the bed was noted.

For visual observation of the bed surface through the pressure vessel's glass window the static bed heights had to be below 0.6m for all the materials. Therefore, it was expected that the minimum bubbling velocity values determined visually would be less than those found from the bed height graph.

4.4 INFLUENCE OF PRESSURE ON MINIMUM BUBBLING

4.4.1 PRESSURE EFFECT ON THE MINIMUM BUBBLING VELOCITY

It was expected that at ambient conditions, silica sand, pigment B and vermiculite would behave as Geldart B materials, and FCC catalyst and pigment A would show a non-bubbling expansion as Geldart A materials. A series of experiments at ambient conditions proved this to be correct for all the materials.

For sand, pigment B and vermiculite, non-bubbling fluidization was not observed, and visually determined values of the minimum bubbling velocity coincided with the experimental values of the minimum fluidization velocity at atmospheric pressure. Further experiments at pressures up to 2100kPa resulted in the beginning of bubbling as soon as the minimum fluidization velocity had been reached.

These results are contradictory to findings of Sobreiro and Monteiro (1982) and Sciazko and Bandrowski (1985; 1987), who were able to establish separate values for the minimum bubbling and minimum fluidization velocities for Geldart B materials, where by definition of Abrahamsen and Geldart (1980a) $U_{mb}/U_{mf} = 1$.

Similar to findings of King and Harrison (1982) and contrary to Varadi and Grace (1978), no shift from Geldart B to Geldart A behaviour was observed in this study over the pressure range 101 to 2100kPa.

Pigment A and FCC catalyst showed a typical Geldart A behaviour, both expanding without bubbling within a certain gas velocity range at ambient conditions. At all the experimental conditions the height of the homogeneously expanded bed of the FCC catalyst was at least 0.6m. In all cases the minimum bubbling velocity values, determined visually, were equal to values, obtained from the maximum bed height. Much denser pigment A could be fluidized satisfactorily only at much lower bed heights, and in all cases visually determined minimum bubbling velocity was slightly lower than that found from the bed height graph.

Since it is much more difficult to establish accurately the minimum bubbling velocity than the minimum fluidization velocity, only one correlation for determining the minimum bubbling velocity under ideal experimental conditions has been proposed (Abrahamsen & Geldart, 1980a). This equation indicates a very weak effect of pressure on the minimum bubbling velocity via the gas density, ρ_g :

$$U_{mb} = 2.07 \exp(0.716F) \frac{d_p \rho_g^{0.06}}{\mu^{0.347}} \quad (4.4.1)$$

A comparison between the experimentally measured values of the minimum bubbling velocity and the predicted values from Eq.(4.4.1) is shown in Figure 4-10 and Figure 4-11.

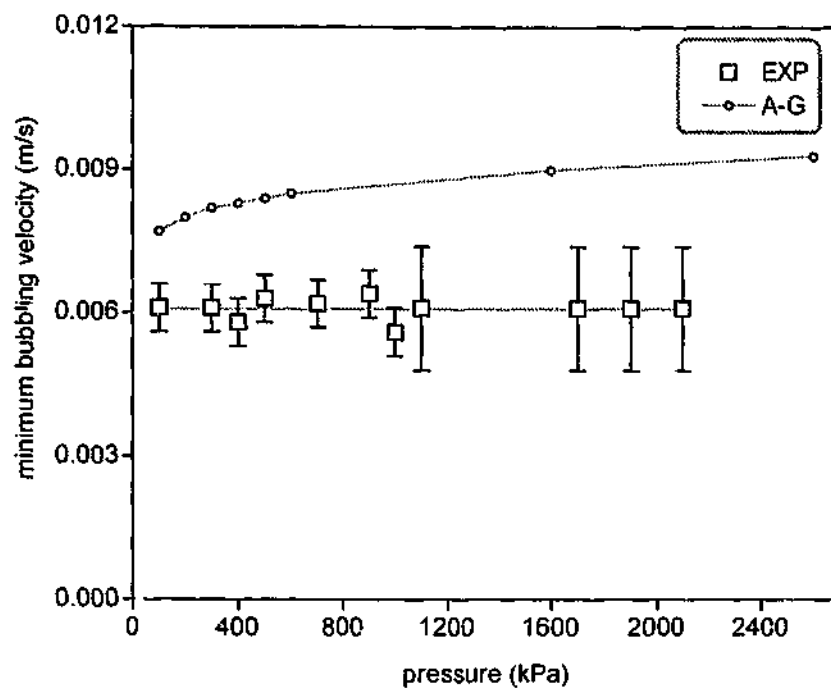


Figure 4-10. Variation of the minimum bubbling velocity with pressure for FCC catalyst (EXP - experimental values and A-G - (Abrahamsen & Geldart, 1980a))

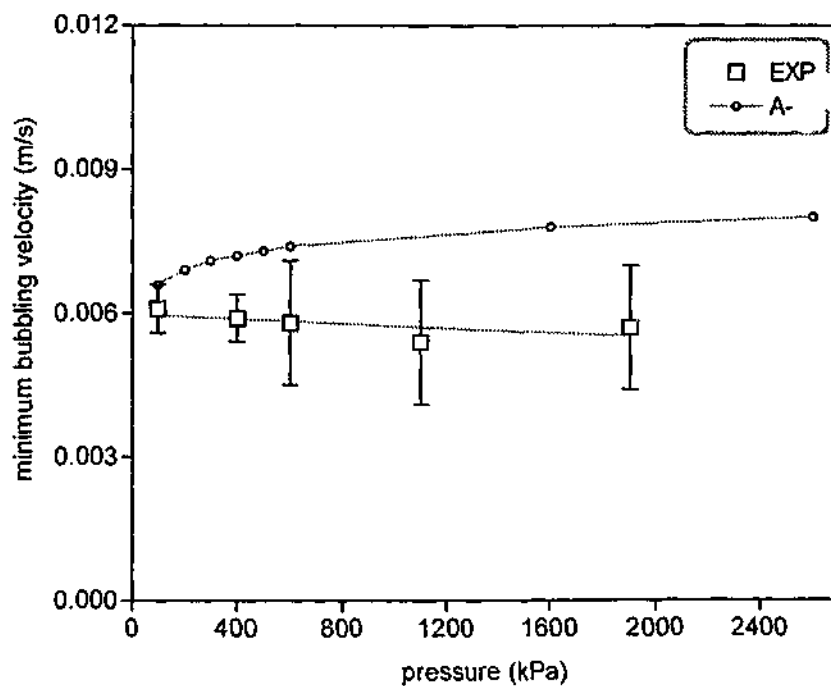


Figure 4-11. Variation of the minimum bubbling velocity with pressure for pigment A (EXP - experimental values and A-G - (Abrahamsen & Geldart, 1980a))

Both Figure 4-10 and Figure 4-11 show that the minimum bubbling velocity was found to be relatively unaffected by pressure increase in the range up to 2100kPa for both catalyst and pigment A. Similar pressure effect was reported by Guedes de Carvalho et al. (1978). However, other workers found that the minimum bubbling velocity for FCC catalyst, fluidised with gases different to air, increased to a different degree, with increasing pressure up to 1500kPa (Piepers et al., 1984; Rietema & Piepers, 1990). Jacob and Weimer (1987) found slight increase in the minimum bubbling velocity at first, then a decrease, but their experiments were carried out within a much higher pressure range.

Equation (4.4.1) is not commonly used on its own. Abrahamsen and Geldart (1980a) combined it with yet another correlation for the minimum fluidization velocity (Baeyens & Geldart, 1974) and proposed a more popular relation:

$$\frac{U_{mb}}{U_{mf}} = \frac{2300 \rho_g^{0.126} \mu^{0.523} \exp(0.716F)}{d_p^{0.8} g^{0.934} (\rho_p - \rho_g)^{0.934}} \quad (4.4.2)$$

Thus, Geldart A behaviour corresponds to the velocity ratio being more than unity. The minimum bubbling to minimum fluidization velocity ratios calculated from the experimental values of the minimum bubbling and minimum fluidization velocities and compared to the predictions of Eq.(4.4.2) are presented in Figure 4-12 and Figure 4-13.

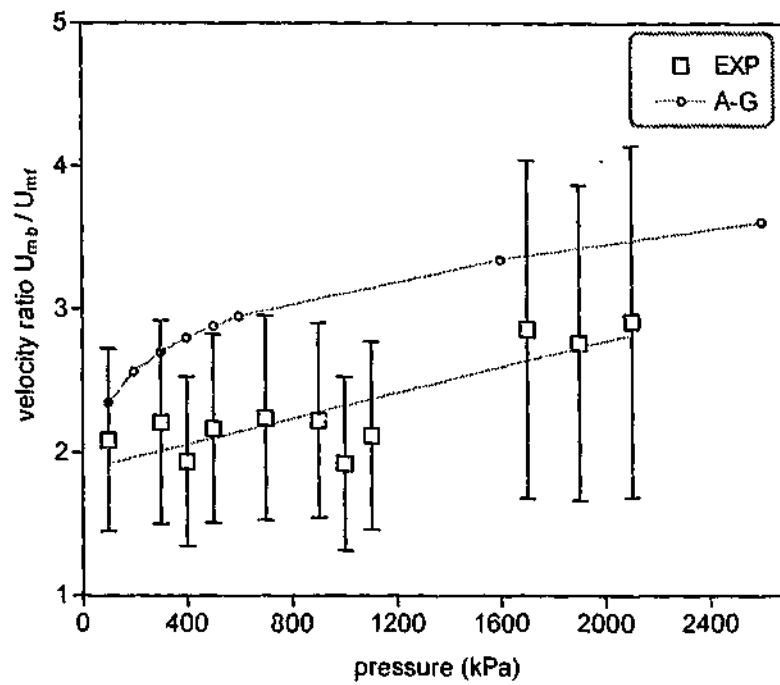


Figure 4-12. Variation of the minimum bubbling to minimum fluidization velocity ratio with pressure for FCC catalyst (EXP - experimental values and A-G - (Abrahamsen & Geldart, 1980a))

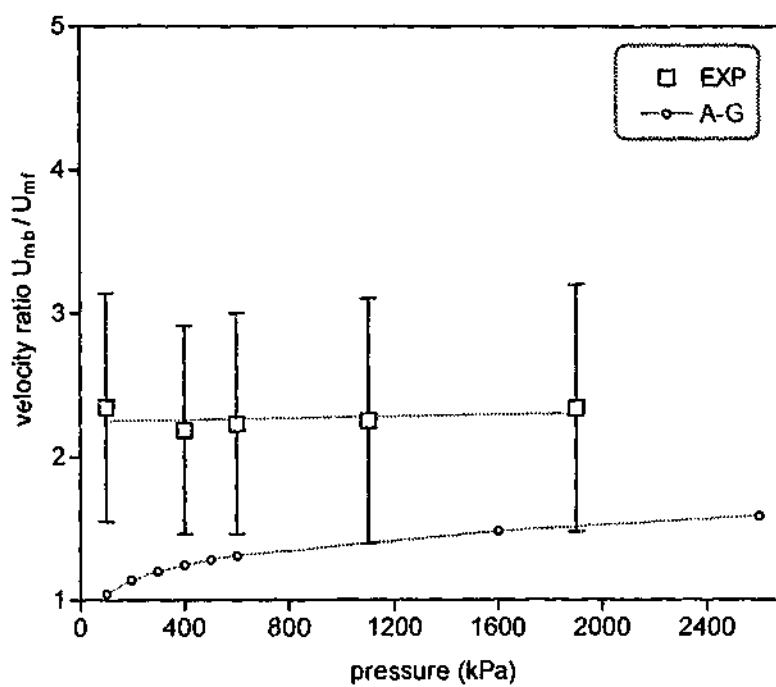


Figure 4-13. Variation of the minimum bubbling to minimum fluidization velocity ratio with pressure for pigment A (EXP - experimental values and A-G - (Abrahamsen & Geldart, 1980a))

As can be seen in Figure 4-12 and Figure 4-13, both experimentally determined and predicted velocity ratio values increase with increasing pressure. However, the slight increase in experimental values is caused mainly by a negligible decrease in the minimum fluidization velocity (Section 4.2.1 above), which in turn could have been caused by an experimental error. Since both the minimum fluidization and minimum bubbling velocities are very low, a small variation of just 0.5mm/s in either of them could position the velocity ratio anywhere in the range between two and three.

Equation (4.4.2) predicts an increase in the velocity ratio with increasing pressure but the accuracy of prediction is quite low. It overestimates the experimental values for the FCC catalyst and underestimates the experimental values for much heavier pigment A.

4.4.2 BED EXPANSION AND VOIDAGE AT MINIMUM BUBBLING AT ELEVATED PRESSURE

With Geldart A materials, the fluidized bed expands uniformly without bubbling as the gas velocity is increased up to the minimum bubbling velocity, when it reaches a maximum height. Thus, the maximum bed expansion ratio is expressed as the ratio of the bed height at the minimum bubbling velocity to the initial bed height, measured at the minimum fluidization velocity.

Abrahamsen and Geldart (1980a) correlated the maximum non-bubbling bed expansion ratio in the following way:

$$\frac{H_{mb}}{H_{mf}} = \frac{5.50 \rho_g^{0.028} \mu^{0.115} \exp(0.158F)}{d_p^{0.176} g^{0.205} (\rho_p - \rho_g)^{0.205}} \quad (4.4.3)$$

According to this correlation the maximum bed expansion ratio should slightly increase with pressure. A comparison between the maximum bed expansion ratio determined experimentally at various operating pressures and that predicted from Eq.(4.4.3) is shown in Figure 4-14 and Figure 4-15.

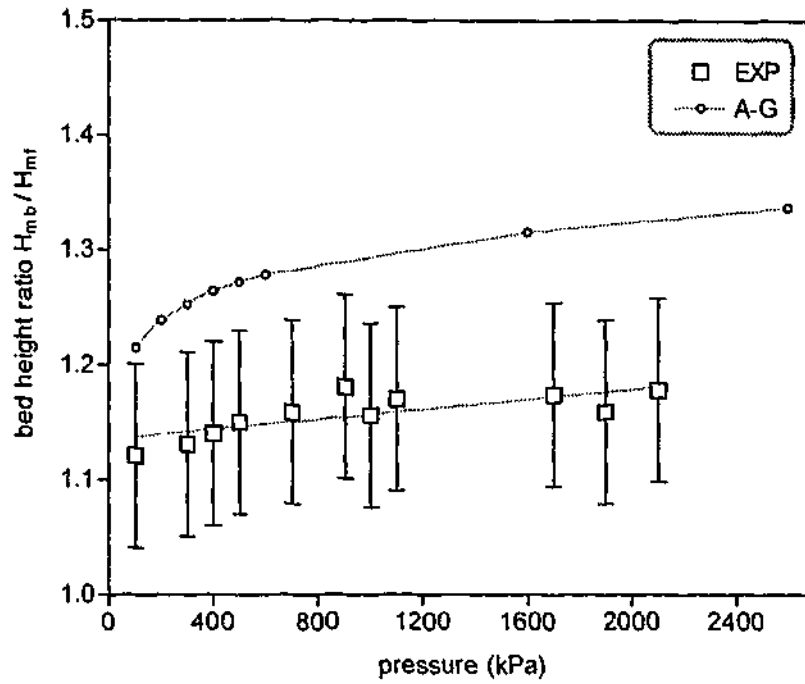


Figure 4-14. Variation of the maximum bed expansion ratio with pressure for FCC catalyst (EXP - experimental values and A-G - (Abrahamsen & Geldart, 1980a))

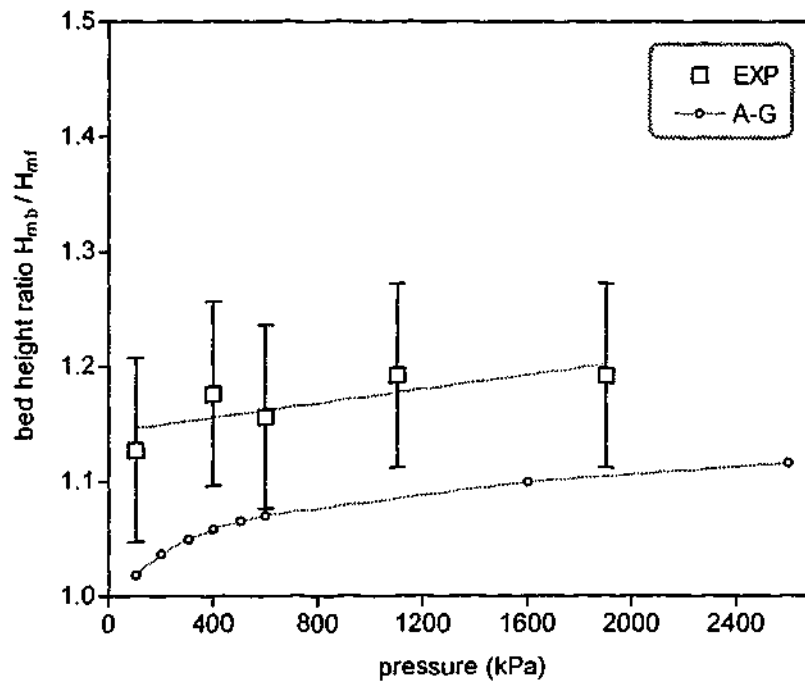


Figure 4-15. Variation of the maximum bed expansion ratio with pressure for pigment A (EXP - experimental values and A-G - (Abrahamsen & Geldart, 1980a))

As can be seen in Figure 4-14 and Figure 4-15, the effect of pressure on the maximum bed expansion within the pressure range 101 - 2100kPa was found to be negligible for both Geldart A materials used in this work. Compared to Eq.(4.4.2), the accuracy of Eq.(4.4.3) is better, however it again overestimates the experimental values for the FCC catalyst and underestimates the experimental values for much heavier pigment A.

The experimental results and predictions from Eq.(4.4.3), however, contradict the experimental results presented by Piepers et al. (1984) who reported a substantial increase in the total bed expansion with pressure increase up to 1500kPa.

The experimental values of the voidage at minimum bubbling ϵ_{mb} were determined from Eq.(4.2.8), using measured bed height values corresponding to the minimum bubbling velocity. The bed voidage at minimum bubbling is presented together with the voidage at minimum fluidization in Figure 4-16 and Figure 4-17.

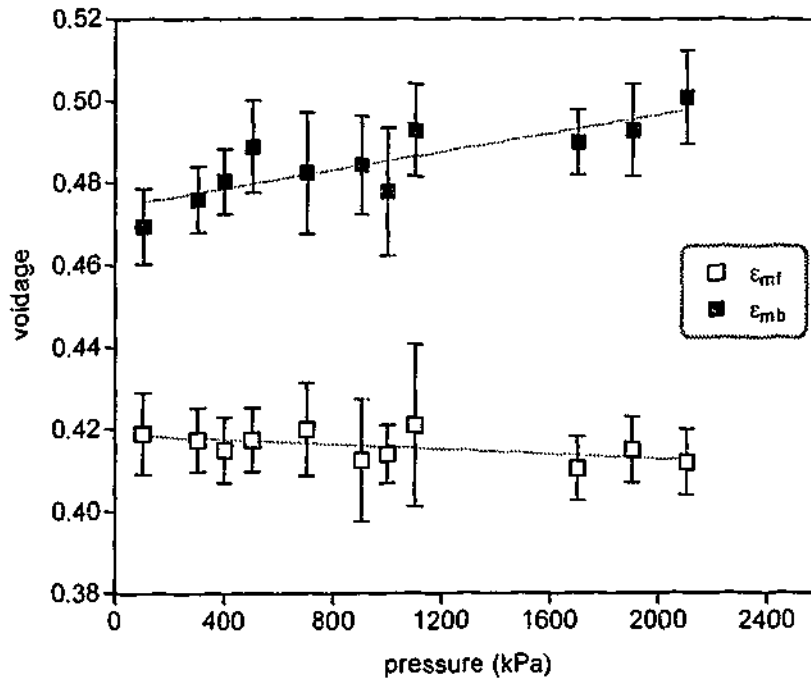


Figure 4-16. Variation of bed voidage at minimum fluidization (ϵ_{mf}) and minimum bubbling (ϵ_{mb}) with pressure for FCC catalyst

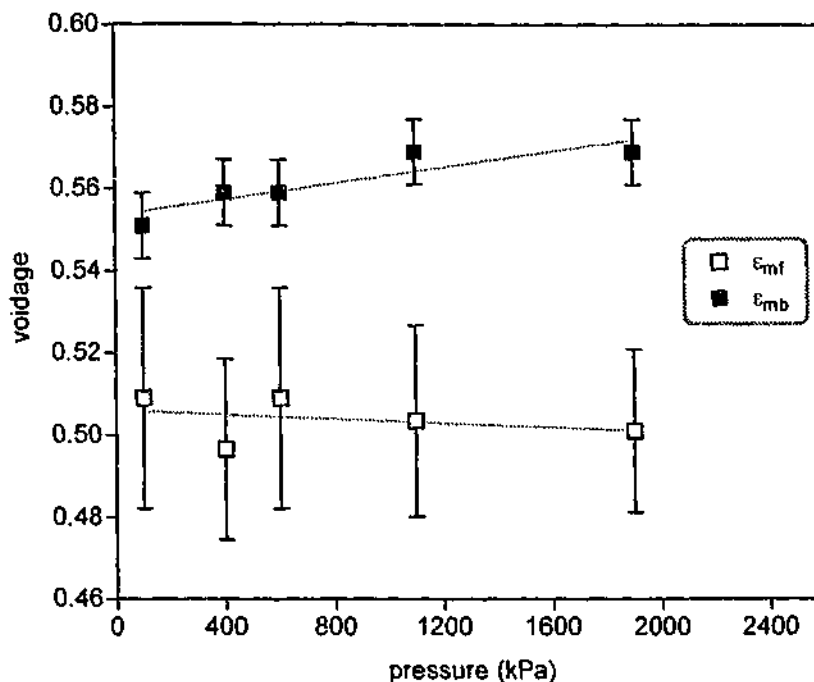


Figure 4-17. Variation of bed voidage at minimum fluidization (ϵ_{mf}) and minimum bubbling (ϵ_{mb}) with pressure for pigment A

Based on the Hydrodynamic Forces Stability Theory (Section 2.2.6), Rowe (1989) theoretically predicted no measurable change in minimum bubbling voidage at pressures up to 1000kPa. However, in this study the bed voidage at minimum bubbling for FCC catalyst was found to increase from 0.47 at ambient conditions to 0.49 at 1000kPa, and to 0.50 at 2100kPa. For pigment A, the bed voidage at minimum bubbling increased from 0.55 at atmospheric pressure to 0.57 at 1900kPa.

Similar slight increase caused by pressure was noticed for some Geldart A materials by other workers (Foscolo et al., 1989; Godard & Richardson, 1968; Guedes de Carvalho, 1981; Guedes de Carvalho et al., 1978; King & Harrison, 1982; Sobreiro & Monteiro, 1982). Piepers et al. (1984) observed slightly greater increase in the minimum bubbling voidage for 59 μ m-sized catalyst within the similar pressure range (from 0.58 at atmospheric pressure to 0.63 at 1500kPa).

4.5 SUMMARY

It is widely accepted that the minimum fluidization velocity decreases with increasing pressure, however, this decrease becomes negligible for fluidized beds of fine Geldart A particles, and only becomes significant for larger particles. Experimental results of the present study support this view.

Although the best method to determine the minimum fluidization velocity is by experiment, another satisfactory approach is to fully characterize the bed solids and to estimate the minimum fluidization velocity by using the Ergun equation. Numerous simplified correlations for prediction of the minimum fluidization velocity are available; however, the correlations used in this study did not predict the experimental values with sufficient accuracy.

The bed voidage at minimum fluidization was found to be practically independent of pressure in the pressure range studied for FCC catalyst, sand and pigment A. However, it was found to increase with pressure increase for coarse and dense pigment B.

It is generally accepted that the minimum bubbling velocity has the same value as the minimum fluidization velocity for Geldart B and D materials but Geldart A powders have the ability to expand without bubbling at much higher velocities than the minimum fluidization velocity. For sand, pigment B and vermiculite non-bubbling fluidization was not observed, and visually determined values of the minimum bubbling velocity for these materials coincided with the experimental values of the minimum fluidization velocity. No shift from Geldart B to Geldart A behaviour was observed in this study over the pressure range 101 to 2100kPa.

Both the minimum bubbling velocity and the maximum bed expansion ratio were found to be practically unaffected by pressure increase in the range up to 2100kPa for both catalyst and pigment A. Existing correlations for predicting the minimum bubbling velocity and the maximum bed expansion ratio did not fit the experimental values very well. In this study for both Geldart A materials, the bed voidage at minimum bubbling was found to increase slightly within the studied pressure range.

Chapter 5

EXPERIMENTAL OBSERVATION OF VOIDAGE IN A PRESSURISED BUBBLING FLUIDIZED BED

Results of the experimental observation of fluidized bed voidage at elevated pressure, using a novel non-invasive technique of the electrical capacitance tomography, are presented in this chapter. These results are complemented by the results of the bed collapse experiments carried out with a Geldart A material at various operating pressures.

5.1 EXPERIMENTAL DETERMINATION OF THE BED VOIDAGE

5.1.1 MEASURING DENSE PHASE VOIDAGE

When fluidized beds operate in the bubbling regime, they consist of the dense (emulsion) phase and bubbles. The dense phase voidage is an important parameter in determining the fluidized bed performance because it is widely believed that it has a direct influence on chemical reactions in the fluidized bed. It affects the degree of gas-solid contact and heat and mass transfer. It is also believed that in Geldart A powders the equilibrium size of the bubbles may be controlled by the dense phase voidage (Geldart, 1986).

The dense phase voidage is generally taken as being equal to its value at the minimum fluidization point for Geldart B and D materials, but can be higher for Geldart A powders (Geldart, 1986; Yates, 1997).

A few methods have been used to measure the dense phase voidage in bubbling fluidized beds. For Geldart A bed materials the voidage can be measured by means of the bed collapse technique. This method has a few variations but generally it involves abruptly stopping the gas flow to a vigorously bubbling fluidized bed and measuring the rate of collapse of the bed surface (e.g. Geldart & Xie, 1995; Grace, 1992; Rietema, 1991).

Other techniques for measuring voidage in fluidized beds involve the use of capacitance probes, optical fibres, X-ray or γ -ray attenuation and capacitance tomographic imaging (Louge, 1997; Yates, 1997). According to Yates and Simons (1994), using various probes immersed in the bed is more suitable for examining the flow of bubbles than dense phase voidage. Thus, Almstedt and Olsson (1982; 1985) used a double needle-type capacitance probe and measured bubble rise velocities in a pilot-scale pressurised bubbling bed combustor. However, both capacitance instruments and optical fibre sensors have been extensively used, although with some difficulties, for determining solids volume fraction in atmospheric circulating fluidized beds (Louge, 1997).

5.1.2 NON-INVASIVE TECHNIQUES

Non-invasive technique based on the use of γ -radiation was applied to an industrial pilot-scale pressurised reactor by Weimer and Quarderer (1985) in order to investigate the dense phase properties of fine materials. To estimate the dense phase voidage they combined the γ -ray attenuation direct measurements of solids densities with the bed collapse method.

Since the 1960s, investigations of the behaviour of gas bubbles in both atmospheric and pressurised fluidized beds using X-ray attenuation have been extensively conducted by several researchers at University College London. Application of this technique to measurements of dense phase voidage in fluidized beds is described by Yates (1997).

Another non-invasive technique for fast measurement of solids volume fraction in bubbling fluidized beds was pioneered at Morgantown Energy Technology Centre (METC) in the US and at the University of Manchester, Institute of Science and Technology (UMIST) in the UK. By the early 1990s both development groups had successfully demonstrated the technique, which became known as the electrical capacitance tomography (ECT).

The principle of the technique is to reconstruct the two-dimensional distribution of the dielectric properties of an object from the measurement of

electrical capacitance taken between pairs of electrodes. Brief comparison of the METC system and the UMIST system is given by Louge (1997). Some theory and principles of capacitance tomography applied to both systems, and especially to the METC system, can be found in (Halow, 1997). Dyakowski et al. (2000) and Byars (2001) provide more detailed information on applications and development of the electrical capacitance tomography based on the UMIST system.

Since the early 1990s both ECT systems have been used for research in the area of fluidization (e.g. Halow & Nicoletti, 1992; Makkawi & Wright, 2001; Wang et al., 1995), however the previous use of capacitance tomography was limited to the atmospheric fluidized beds. However, this promising non-invasive technique is still under development and, apart from the present work, it seems that no other fluidization study has been carried out using the tomographic imaging in a pressurised environment.

5.2 ELECTRICAL CAPACITANCE TOMOGRAPHY

5.2.1 PTL300 ECT SYSTEM

As described in Section 3.8, the ECT system used in this work was based on the UMIST design and was a PTL300 single plane system with driven guard electrodes.

The PTL300 ECT system was developed primarily for use with mixtures of two materials having different dielectric constants. For these two-phase mixtures, the ECT system could provide information about the relative proportions of the two materials inside the sensor and display their approximate radial distribution across the ECT sensor plane. Successful applications of the PTL300 system include imaging liquid-gas mixtures in oil pipelines and gas-solids mixtures in fluidized beds and pneumatic conveying systems.

In fluidization research, ECT systems measure the inter-electrode capacitances of an external or internal ECT sensor and from these

measurements produce cross-sectional images of material inside the fluidized bed. The advantage of tomographic imaging is that it is non-invasive technique that can give measurement of overall voidage fluctuations over the entire cross-section of a vessel. Although, the ECT systems produce relatively low-resolution images, they can do this at high speed (up to 200 frames per second).

The PTL300 ECT system can be used in different modes:

- it can display on-line images and record the inter-electrode capacitance measurements while images are displayed;
- images can be displayed and captured at selected data rates, and can be replayed at the same or different rates;
- the normalised permittivity of individual pixels in the image and the values of the normalised inter-electrode capacitances can be displayed in either on-line or replay modes.

5.2.2 PRINCIPLE OF OPERATION

Comprehensive application notes provided by Process Tomography Ltd (*Engineering design rules for ECT sensors*, 2001; *Generation of ECT images from capacitance measurements*, 2001) explain how the design of a capacitance sensor influences the performance of the ECT system and describe how the permittivity distribution of the material inside the sensor is obtained from measurements of the capacitances between pairs of electrodes.

Another note (*Calculation of volume ratio for ECT sensors*, 1999) thoroughly explains how the overall voidage (volume ratio or concentration) of a mixture of two dielectric materials inside the sensor, and also the distribution of this voidage across the sensor, is calculated.

Briefly, the principle of operation of the PTL300 ECT system is as follows:

- Initially the sensor properties are measured or calculated and the sensitivity map is produced. This map is a numerical matrix whose elements correspond to the 1024 individual pixels in a square 32 by 32 grid, which is superimposed on the sensor cross-section. The sensitivity map describes how the measured capacitance between any combination of electrodes changes when a change is made to a single pixel's dielectric constant. For a 12-electrode sensor, there are 66 independent electrode-pair capacitance measurements.
- Capacitance change measured between any two electrodes caused by an object with a given dielectric constant varies with the location of the object. For a circular sensor, the ECT system is least sensitive at the centre of the vessel, and from knowledge of the sensitivity variation with position for each pixel allowance for this effect is made and stored in the sensitivity map file.
- The sensor is calibrated at each end of the permittivity range by filling the sensor with the lower permittivity material (air) and measuring all of the individual inter-electrode capacitances. Then this operation is repeated using the higher permittivity material (fluidized bed solids). These data is used to set up the measurement parameters and is stored in a calibration data file.
- Once calibrated, the capacitances between all pairs of sensor electrodes are measured continuously at high speed, giving 66 measurements per image frame. An image reconstruction algorithm is used to compute the cross sectional distribution of the permittivity of the material inside the sensor. A fast but approximate linear back-projection algorithm is supplied as standard with the PTL300 system but other alternative algorithms can be used in off-line mode only to produce more accurate images.

5.2.3 EXPERIMENTAL METHOD

Experiments using the ECT equipment were carried out at operating pressures ranging from 300 to 1900kPa, using Geldart A FCC catalyst as bed material, and ultra-pure nitrogen and compressed air as fluidising gases. Another series of experiments was conducted at operating pressures ranging from ambient to 1700kPa, using Geldart B silica sand as bed material, and industrial nitrogen and compressed air as fluidising gases.

5.2.3.1 Calibration

All voidage values obtained from the ECT measurements are relative and based on the assumption that the solids volume fraction is 100% when the sensor is filled with the higher permittivity material and is zero when the sensor is filled with the lower permittivity material. In the fluidization research, the lower permittivity material is a fluidising gas, usually air with a relative permittivity of 1. Since the second reference material of higher permittivity is in powder form, the upper calibration point is formed by a mixture of the granular bed material and the fluidising gas.

Before commencing experiments, the ECT system was calibrated by filling the sensor with the two reference materials in turn and by measuring the inter-electrode capacitances at the two extreme values of relative permittivity.

As the first calibration step, the fluidized bed vessel was emptied using an industrial vacuum cleaner, and the inter-electrode capacitances were measured for all possible combinations of electrodes while the bed contained only air as the lower permittivity material. The fluidized bed vessel was then filled with either 5kg of FCC catalyst to a static bed height of 44cm or 10kg of sand to the bed height of 42cm for Geldart A and Geldart B series of experiments respectively.

Secondly, in order to complete the calibration for experiments at ambient conditions when the pressure vessel was open, the air supply pressure was set to the gauge pressure of 100kPa and the bed was vigorously fluidised for

approximately 20 minutes, in order to stabilise the possible static electricity charge in the system and to fully mix bed solids. The air supply was then slowly turned off by closing the flow control valve, and the bed was allowed to settle for approximately 15 minutes, and only then were the inter-electrode capacitances measured again. That ensured an initial packed bed of similar structure in each experiment and provided capacitance measurements corresponding to a packed bed at the experimental conditions.

In high-pressure experiments the same gas was used for pressurising the system and then for fluidising the bed material. Therefore, prior to completing step 2 of the calibration process, the pressure vessel was sealed and the backpressure controller was set to a pre-determined operating pressure and the system was pressurised to that level first.

At the same time the gas passed through the fluidized bed, which was properly fluidised even longer than at the ambient conditions. Then the gas supply was slowly turned off, allowing the bed to settle for approximately 15 minutes in the pressurised environment, and only then were the inter-electrode capacitances measured again and the settled bed height recorded. That again ensured an initial packed bed of similar structure in each experiment and provided capacitance measurements corresponding to a packed bed at actual experimental conditions.

Following the usual practice for electrical capacitance tomography (*Calculation of volume ratio for ECT sensors*, 1999), a linear relationship between capacitance and solids volume fraction was assumed between the two calibration points. In terms of the absolute bed voidage, as used in the fluidization research, the lower calibration point (ECT reading 0) corresponded to gas only and voidage $\varepsilon=1$, and the upper calibration point (ECT reading 100) corresponded to a packed bed with voidage, determined from Eq.(5.2.1):

$$\varepsilon_0 = 1 - \frac{m}{\rho_p A H_0} \quad (5.2.1)$$

Where m and ρ_p are mass and density of bed material respectively, A is bed area, and H_0 is packed bed height.

Since some drift in the very sensitive electronic capacitance measuring circuitry was observed after a few hours of fluidization, it became necessary to carry out such a calibration twice a day and check its accuracy before and after each experiment. It was accepted that the upper calibration ECT reading of 100% could drift by no more than 5% after completing each experiment.

5.2.3.2 Experiments

In actual experiments at pre-determined operating pressure, the gas velocity was an experimental variable. After each gas velocity change, the pressure in the system was allowed to stabilise for at least ten minutes. When both pressure and gas flow became stable, the tomographic data were logged on an ECT dedicated computer. The ECT system generated a cross-sectional image of the bed and showed the solids volume fraction (the ratio of solids to gas) at sensor level.

The ECT sensor consisted of 12 rectangular electrodes, 35mm wide and 50mm high, positioned around the fluidized bed. The centres of the electrodes were located at the height of 250mm above the distributor plate, or approximately at a half of the static bed height for both studied materials.

The output was in the form of 32x32 pixels matrix which was averaged to provide the average solids volume fraction as a single value between 0 (gas) and 100 (packed bed). For each operating condition, 16000 frames of data were logged and each frame was recorded by the ECT system at a frequency of approximately 81 Hz.

Under each set of operating conditions, the behaviour of the bed was also characterised by visual inspection and recording of bed height versus gas velocity.

5.2.4 EXPERIMENTAL RESULTS

Results of the experiments with FCC catalyst and silica sand were produced by the ECT system in two types of data:

- time series image frames of the local solids volume fraction distribution at a given horizontal level in the form of a 32x32 pixels matrix;
- time series data points of the average solids volume fraction representing the whole bed at a given horizontal level.

It is accepted that the tomographic images obtained from the capacitance measurements are usually of relatively low resolution (e.g. Byars, 2001; Dyakowski et al., 2000; Makkawi & Wright, 2002). A linear back-projection algorithm, supplied as standard with the PTL300 system, is mathematically simple and fast because the image reconstruction process is reduced to matrix-vector multiplication. However, the images are only approximate and suffer from blurring.

Image resolution and accuracy can be improved by employing an iterative linear back-projection algorithm. However, this is very time consuming, especially for large files. This and other reconstruction algorithms for capacitance tomographic imaging are still under development with some encouraging results (Dyakowski, 2002; Dyakowski et al., 2000; Isaksen, 1996; Isaksen & Nordtvedt, 1993).

According to the Process Tomography Ltd Application Note AN1 (*Generation of ECT images from capacitance measurements*, 2001), the linear back-projection algorithm will always underestimate areas of high permittivity and overestimate areas of low permittivity. The images produced by this method will always be approximate, since the method spreads the true image over the whole sensor area. Because the image has been spread out over the whole area, the magnitude of the image pixels will be less than the true values. However, the sum of all of the pixels will

approximate to the true value, and the linear back-projection algorithm is therefore useful for calculating the average voidages.

Visual analysis of a number of image frames, based on the linear back-projection algorithm, was carried out in this work. It confirmed the findings of other researchers that the ECT images were very blurred and not very accurate. Apart from a possible large single bubble no other individual bubbles could be identified in the process of fluidization.

Image improvement based on the iterative linear back-projection algorithm, and further frame-by-frame image analysis were considered to be very tedious and prohibitive because of the time consuming nature, large number of image files (16000 per gas velocity) and computer power requirements. Therefore, no further visualisation and image analysis were carried out in this work.

Some experiments were unsuccessful, and their results were excluded from further data analysis. For example, in the middle of some of the earlier experiments it was found that switching the lights in the laboratory or occasional presence of mobile (cellular) phones and pagers within short distance from the ECT equipment, considerably affected and even froze the system.

This was a major nuisance because of the lost gas and time, depressurising and pressurising equipment and repeated calibration process. However, by learning from these early experiments and taking appropriate precautions, we were able to generate a reliable set of data covering a range of operating conditions.

For other experiments, coarse vermiculite was selected for investigation of possibility of shift of this Geldart B material at ambient conditions to a typical Geldart A behaviour at elevated pressure. However, the tomographic imaging experiments using this material were found to be excessively problematic, and the results of the experiments were at any rate inconclusive.

Images generated by the ECT system always suggested a non-bubbling expansion, with hardly any change due to increase in gas velocity. However, that differed completely from the visual observation of the bed bubbling

behaviour. After completing the experiments with vermiculite, the upper calibration point for a packed bed was as low as 56%, compared to the original value of 100%. In this case, static electricity was suspected to have affected the results, but apparently could not be stabilised even after prolonged vigorous fluidization.

This unacceptable drift in the calibration of the ECT equipment was observed after carrying out each of the repeated experiments. The experimental programme with vermiculite was aborted and the ECT development group at UMIST was informed about the problems with this particular material (Dyakowski, 2002).

Although when using the FCC catalyst and silica sand, the unacceptably large drift in the calibration of the ECT was not observed, the ECT reading corresponding to the packed bed was always checked before and after each experiment and the calibration was frequently performed.

5.2.5 QUANTITATIVE ANALYSIS

5.2.5.1 Time series analysis

Some quantitative description of the bubbling bed dynamics can be obtained from time series analysis of fluctuations of the average solids volume fraction. Time series of the cross-sectional average solids volume fraction fluctuations representing the whole bed at a given horizontal level were processed by using the PTL proprietary software based on the linear back-projection algorithm⁹, Microsoft Excel and software developed at Delft University of Technology to specifically analyse experimental time series fluctuations in fluidized beds¹⁰.

At each given gas velocity, 16000 frames of data were logged over more than three minutes of dynamic operation and recorded by the ECT system at

⁹ Ibid.

¹⁰ RRChaos. (Version 2.26) [computer software]. Delft: Chemical Process Technology Department, Delft University of Technology (www.reactorresearch.nl).

the rate of approximately 81 frames per second. The PCECT software averaged the output, which was in the form of 32x32 pixels matrix and provided for each frame the average volume fraction as a single value between 0 (gas) and 100 (packed bed). From 16000 values of the relative voidage and the sample frequency the RRChaos software calculated the relevant time series statistics.

All analysis was made on time series with data points X_i , where $i=1,2,3,\dots,n$, measured at equal time intervals Δt , and therefore, with a sampling frequency of $f=1/\Delta t$. Parameter X is the cross-section average solids volume fraction (relative voidage) and n is the total number of samples, equal to 16000. As previously mentioned, the sampling frequency f varied slightly around 81Hz.

The following parameters were calculated by the software – average, minimum and 1% minimum, maximum and 99% maximum values in time series; peak-peak and normalised peak-peak distances, and 1% – 99% peak-peak and normalised peak-peak distances; average absolute deviation and relative average absolute deviation; number of cycles and average number of points per cycle; average, minimum and maximum cycle frequencies and cycle frequency absolute deviation; as well as average, minimum and maximum cycle times and cycle time absolute deviation.

Three parameters were selected out of this extensive list for further analysis – average, average absolute deviation and average cycle frequency. The average of the time series data points of the average solids volume fraction representing the whole bed at a given horizontal level was defined as:

$$\bar{X} = \frac{1}{n} \sum_{i=1}^n X_i \quad (5.2.2)$$

Time series analysis of the measured fluctuating signals operates in time domain, frequency domain or in state space domain used in non-linear analysis. Although some analysis techniques were originally proposed for pressure fluctuations time series, in this work they have been applied to the analysis of the voidage fluctuations resulting from the ECT measurements.

Schouten and van den Bleek (1998) proposed a test method for monitoring the quality of fluidization using the short-term predictability of pressure fluctuations which combines features of three types of time series analysis: statistical, spectral and chaos analysis.

First, in the test method the average absolute deviation is chosen as a statistical measure of the width of the probability distribution function of the measured fluctuations. Second, the length of the reconstructed points in state-space is based on the average cycle time, which is of course directly related to the average cycle frequency. And third, the comparison of the distributions of state-space distances through the degrees of predictability is a part of chaos analysis.

In time domain the most common method is to study the amplitude of signals, expressed as standard deviation or variance. According to Schouten et al. (1994a), the average absolute deviation ΔX of the data points from the solids volume fraction average value is a robust estimator of the width of time series around the mean and is defined as:

$$\Delta X = \frac{1}{n} \sum_{i=1}^n |X_i - \bar{X}| \quad (5.2.3)$$

According to Zijerveld et al. (1998), the average absolute deviation is comparable with the standard deviation and shows similar dependence on operating conditions.

The average cycle frequency f_c is the reciprocal of the average cycle time, which is defined as the average time to complete a full cycle after the first passage through the time series average.

Those parameters should make possible to compare results between measurements at various gas velocities and different operating pressures since their values are unambiguous and can be readily calculated. In the time series the average absolute deviation and the average cycle time are measures of the characteristic length and time scale, respectively, and used in the reconstruction of an attractor from which the Kolmogorov entropy is estimated for the chaos analysis.

In frequency domain, power spectral analysis has been generally used as a qualitative analysis with the interpretation of power spectra being subjective. Validating the hydrodynamic scaling relationships is one of the important applications of frequency domain analysis of pressure fluctuations (Johnsson et al., 2000).

5.2.5.2 Deterministic chaos

Recently it has been suggested that the irregular behaviour of the fluidized bed dynamics is due to the fact that the fluidized bed is a chaotic non-linear system. Several workers (Daw & Halow, 1993; Johnsson et al., 2000; Schouten & van den Bleek, 1991; van den Bleek et al., 2002; van der Stappen et al., 1993a) found that time series from pressure and voidage measurements show the characteristics of deterministic chaos.

However, non-linear state-space analysis methods are still a subject of research. Chemical Process Technology Department at Delft University of Technology, where the RRChaos software was developed, has been one of the major centres of research in this area since 1990 (Schouten et al., 1996).

According to some researchers in this area (Johnsson et al., 2000; Zijerveld et al., 1998), chaotic systems are governed by non-linear interactions between the system variables and all methods of non-linear chaos analysis are based on the construction of an attractor of the system in state-space. The attractor forms a fingerprint of the system and reflects its hydrodynamic state. The most common method to characterise the attractor is the evaluation of the correlation dimension and the Kolmogorov entropy, where the correlation dimension expresses the number of degrees of freedom of the system and the Kolmogorov entropy is a measure of the predictability of the system and the sensitivity to the initial state.

The Kolmogorov entropy, K , is a number expressed in bits/s and can be calculated from a time series of only one characteristic variable of the system, solids volume fraction in this case. In bubbling fluidized beds, the Kolmogorov entropy calculated from these experimental data could be

related to the gas velocity U , fluidized bed diameter D and bed height H_0 according to Eq.(5.2.4) (Kuehn et al., 1996). It ranges from zero for periodic systems to infinity for completely random systems. Generally, the Kolmogorov entropy is small in cases of more or less regular behaviour, and large for very irregular dynamic behaviour such as fluctuations in turbulent flow.

$$K = 10.7 \left(\frac{U - U_{mf}}{U_{mf}} \right)^{0.4} \frac{D^{1.2}}{H_0^{1.6}} \quad (5.2.4)$$

Van den Bleek et al. (2002) developed a model to explain this correlation. The basis for the model is that the Kolmogorov entropy characterises the information loss of the system per unit of time and is proportional to the number of bubbles, erupting at the bed surface per unit of time, and the bubble impact which is given by the ratio of bubble size to bed diameter. Practical methods and the RRChaos software have been developed at Delft University of Technology to estimate the Kolmogorov entropy from measured time series (Schouten et al., 1994b).

In this work, by using the RRChaos software, the following non-linear parameters were calculated: Kolmogorov entropy in bits/s, in bits/cycle, relative standard error of the Kolmogorov entropy and the maximum possible Kolmogorov entropy in bits/s.

5.3 INFLUENCE OF PRESSURE ON VOIDAGE FLUCTUATIONS

5.3.1 EXPERIMENTAL RESULTS AT ELEVATED PRESSURE

Electrical capacitance tomography was used to observe the bubbling behaviour of fluidized beds containing either 5kg of FCC catalyst or 10kg of silica sand. Experiments with Geldart A catalyst were carried out at ambient temperature and at elevated pressures of 300, 500, 700, 900, 1100, 1300, 1500, 1700, 1900 and 2100kPa. Experiments with Geldart B silica sand were carried out at ambient temperature and at atmospheric pressure as well as elevated pressures of 200, 300, 400, 500, 600, 1100, 1300, 1700 and 2100kPa.

At each pressure, measurements of relative solids volume fraction were taken at a number of superficial gas velocities above the minimum fluidization velocity. At each velocity, 16000 values of the cross-section average solids volume fraction were logged and recorded by the ECT system. That corresponded to approximately 190 seconds of dynamic operation.

The experimental data was processed by using the RRChaos software, and for each set of 16000 original measurements, the following data was selected for further analysis: average relative solids volume fraction and its average absolute deviation in %, average cycle frequency with its absolute deviation in Hz, and Kolmogorov entropy in bits/s.

5.3.2 BED VOIDAGE AT ELEVATED PRESSURE

The experimental values of the average relative solids volume fraction were expressed in percentage points, and under the existing operating conditions usually fluctuated somewhere between 100% in a non-fluidized state and 55% in a bubbling regime. The value of 100% was established during the calibration procedure and corresponded to a packed bed with a known bed height.

Based on the packed bed height and previously determined values of the mass and density of the bed material, and the cross-section area of the bed, the packed bed voidage was calculated from Eq.(5.2.1). For the FCC catalyst, the packed bed voidage ε_p was equal to 0.476, and for the silica sand this value was 0.463. For both materials, calibration procedures were completed at various operating pressures and the packed bed height, and therefore voidage, did not vary with pressure.

The experimental results presenting average bed voidage, average absolute deviation of the bed voidage and average cycle frequency for Geldart A FCC catalyst are shown in Figure 5-1, Figure 5-3 and Figure 5-5, and those for Geldart B silica sand are presented in Figure 5-2, Figure 5-4 and Figure 5-6. To reduce cluttering, the results at some intermediate operating pressures

were omitted from the plots, if they were too close to the neighbouring constant-pressure lines and followed similar trends.

5.3.2.1 Average total bed voidage

Typically with Geldart A materials, the fluidized bed expands uniformly without bubbling as the superficial gas velocity is increased up to the minimum bubbling velocity, when it reaches the maximum height, and gradually collapses to a minimum height with further increase in gas velocity.

Other researchers (Abrahamsen & Geldart, 1980b; Geldart et al., 1984; Geldart & Radtke, 1986; Geldart & Wong, 1985) carried out a large number of experiments with various Geldart A powders at ambient conditions and found that up to the superficial gas velocities of about 0.03m/s the total bed height, and therefore voidage, decrease as the velocity is increased. It was also observed that further increase in gas velocity then increased the total bed height.

Similar results were obtained at various operating pressures in this study. As can be seen in Figure 5-1, the average total bed voidage reduces with increasing gas velocity above the minimum bubbling velocity of 0.006m/s and up to about 0.03m/s, and generally increases thereafter.

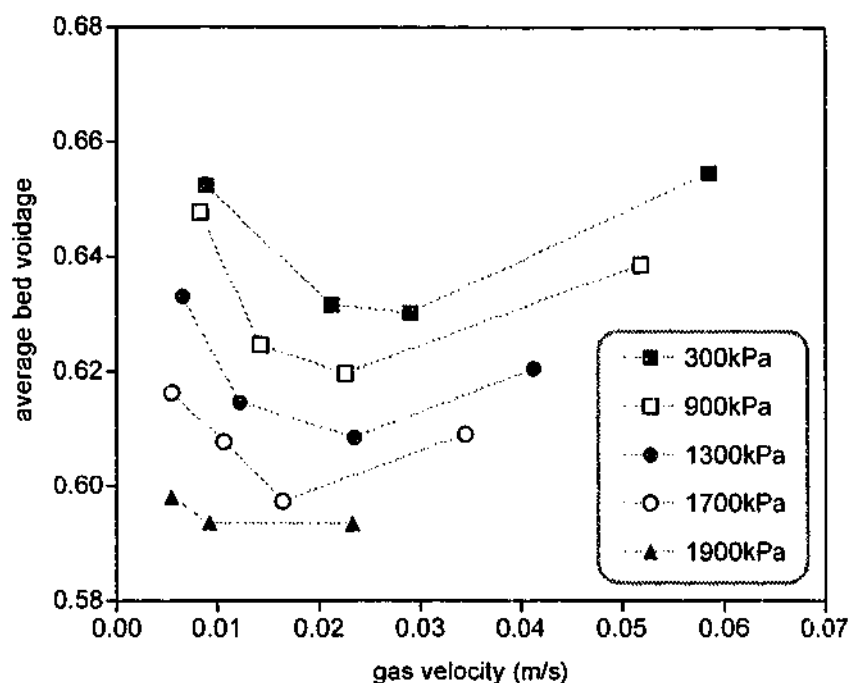


Figure 5-1. Variation in average bed voidage with gas velocity for FCC catalyst over a range of operating pressures from 300 to 1900kPa (lines are used to guide the eye)

It might be expected that the total bed expansion would increase if more gas is put into the fluidized bed as bubbles. However, according to Geldart et al. (1984), the reduction in the bed expansion just above the minimum bubbling velocity in Geldart A powders occurs because the dense phase volume in the bubbling bed is reduced more rapidly than the bubble hold-up increases. The cause of this reduction in dense phase voidage is due to small interparticle forces which make the powder slightly cohesive and are continually disrupted by the bubbles passage and increase in powder circulation (Geldart & Radtke, 1986).

The effect of operating pressure on the cross-section averaged total bed voidage for the Geldart A FCC catalyst can be clearly seen in Figure 5-1. This diagram shows that any pressure increase is accompanied by the reduction of the average bed voidage.

The ECT system used in this work can only provide information about the total bed voidage, consisting of the dense phase voidage and bubbles volume held up within the bed and averaged across one cross-sectional plane.

Therefore, based on these results alone, we cannot determine whether the decrease in the bed voidage with the increase in operating pressure, seen in Figure 5-1, is caused by a reduction in dense phase voidage or volume of bubbles in the bed, or both.

Later, from the bed collapse experiments with the FCC catalyst it was found that the dense phase voidage *increased* with the increase in pressure (Section 5.4.4 below). The decrease in the bubbling bed voidage or expansion with increase in pressure, found in this work from the ECT dynamic measurements, can therefore be explained by the reduction in volume of bubbles held up within the bed at higher operating pressures.

This might be in line with the observations of other researchers (Barreto et al., 1983a; Chan et al., 1987; Guedes de Carvalho et al., 1978; King & Harrison, 1980; Rowe & MacGillivray, 1980; Subzwari et al., 1978; Weimer & Quardern, 1985), who reported that fluidization became smoother at higher pressures and attributed that to smaller bubbles in Geldart A powders at increased pressure. However, in the present work, because of the ECT limitations in image generating, no conclusion on the volume or size of individual bubbles could be reached.

The results of the ECT experiments with the Geldart B silica sand are different from those for the FCC catalyst. As can be seen in Figure 5-2, a considerable increase in the bed voidage with increasing gas velocity takes place at each operating pressure. This is expected as more gas is put into the fluidized bed as bubbles. In comparison to Geldart A powders, the interparticle forces in Geldart B materials are negligible compared with the hydrodynamic forces acting in the fluidized bed.

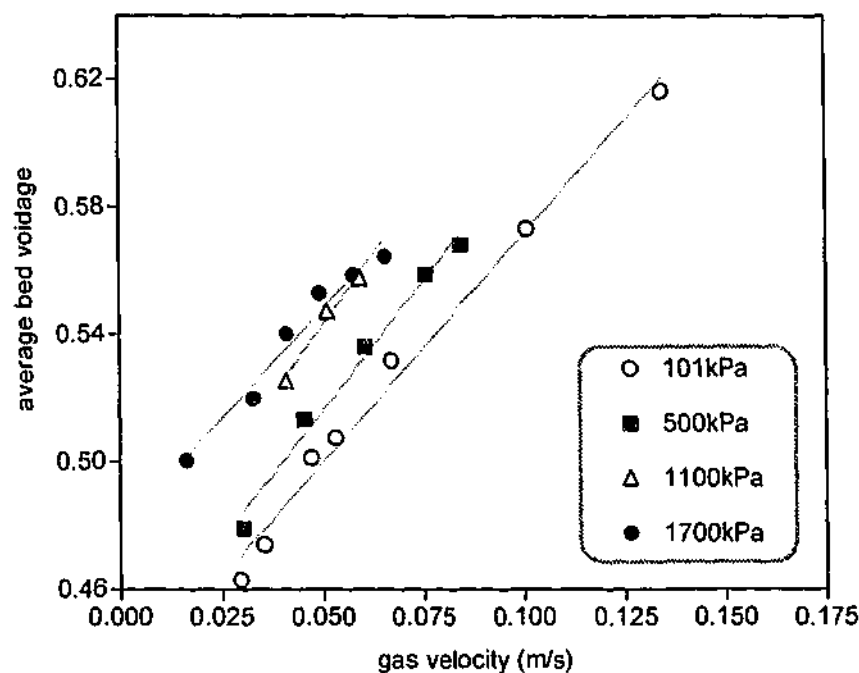


Figure 5-2. Variation in average bed voidage with gas velocity for silica sand over a range of operating pressures from atmospheric to 1700kPa

The effect of operating pressure on the cross-section averaged total bed voidage for the Geldart B silica sand can also be seen in Figure 5-2. This diagram shows that any pressure increase is accompanied by the apparent increase in the average bed voidage. An increase in bed expansion with pressure in bubbling beds, consisting of Geldart B silica sand and coal, was also observed by other researchers (Chiba et al., 1986; Chitester et al., 1984). This information is important for practical application of the gasification of coal in a pressurised fluidized bed.

However, some unexplained changes in bed expansion at higher pressures were observed by Olowson and Almstedt (1990) and Llop et al. (1995; 2000), who fluidised silica sand and found that the bed expansion strongly increased with pressure up to a maximum at approximately 800kPa and then stayed constant or even slightly decreased thereafter at pressures up to 1600kPa.

Although in the present work, no obvious decrease in total bed voidage was observed at higher operating pressures, it was also found that the pressure influence was stronger at lower pressures. Under operating conditions

considered in this study, as can be seen in Figure 5-2, an increase in bed voidage in the pressure range 1100 - 1700kPa is quite small and becomes almost non-existent at higher gas velocities.

Olowson and Almstedt (1992) found in their fluidization work with Geldart B sand that the bubble size is determined by a complex balance between splitting and coalescence, and an increase in pressure may cause either increase or decrease in bubble size, depending on the location in the bed, gas velocity and the pressure level.

In a comprehensive summary and analysis of previous research on bubble size under pressurised conditions, applicable for the pressurised fluidized bed combustion, Cai et al. (1994) reached the conclusion that in fluidized beds of coarse materials the bubble size decreases with increasing pressure except when gas velocity is low. At low gas velocities, there is a dual effect of pressure on bubble size, i.e. there is an initial increase in bubble size in the pressure range less than 1000kPa and then a size decrease with further increase in pressure.

Because of the limitations of visual image analysis using ECT data explained in Section 5.2.4 above, no conclusions could be reached about the characteristics of the individual bubbles in this study. However, the bed voidage results, obtained from the dynamic ECT data under the range of operating conditions in this study and presented in Figure 5-2, are in accordance with the views of Olowson and Almstedt (1992) and Cai et al. (1994).

5.3.2.2 Characteristic length in the time series

In bubbling fluidized beds the main source of signal (pressure or voidage) fluctuations originates from the formation of bubbles. The intensity of the signal can be measured and compared in a statistical manner by using the average absolute deviation.

Therefore it was expected that the average absolute deviation in the bed voidage would steadily increase with increasing gas velocity when more and

more gas is put into the bed as bubbles. This was indeed the case for both Geldart A and Geldart B materials, as can be seen in Figure 5-3 and Figure 5-4.

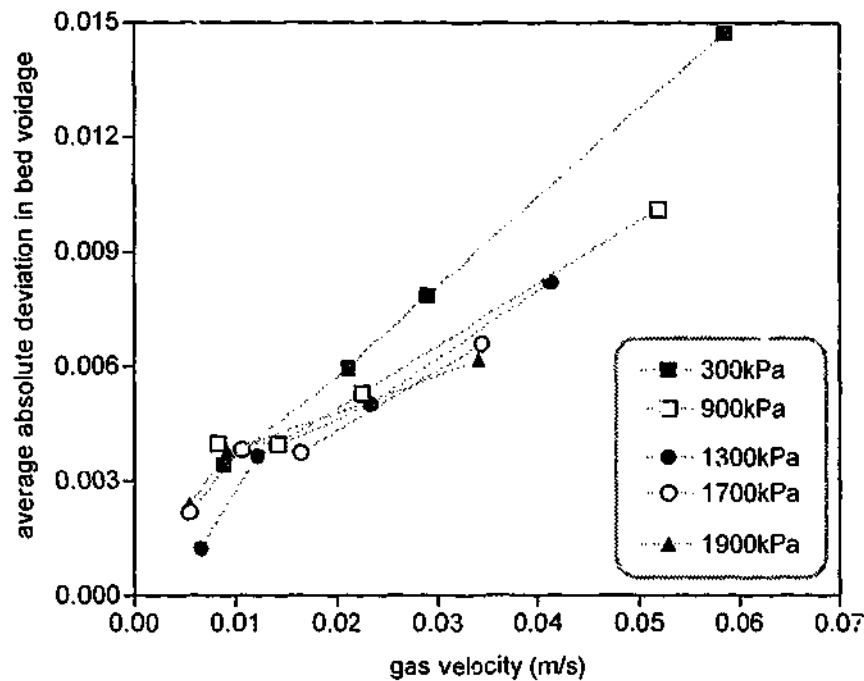


Figure 5-3. Variation in average absolute deviation in bed voidage with gas velocity for FCC catalyst over a range of operating pressures from 300 to 1900kPa (lines are used to guide the eye)

However, the effect of operating pressure on the amplitude of the voidage fluctuations is again different for the Geldart A and Geldart B materials used in this work. Comparison between the average absolute deviations of bed voidage fluctuation measured at different operating pressures for the Geldart A FCC catalyst is shown in Figure 5-3. There is a continuous increase in the average absolute deviation curves with gas velocity which means that the fluidized bed remains in the bubbling state. The pressure effect is indicated by the decrease of the average absolute deviation with increasing pressure which means more uniform bubbling in the fluidized bed at elevated pressure.

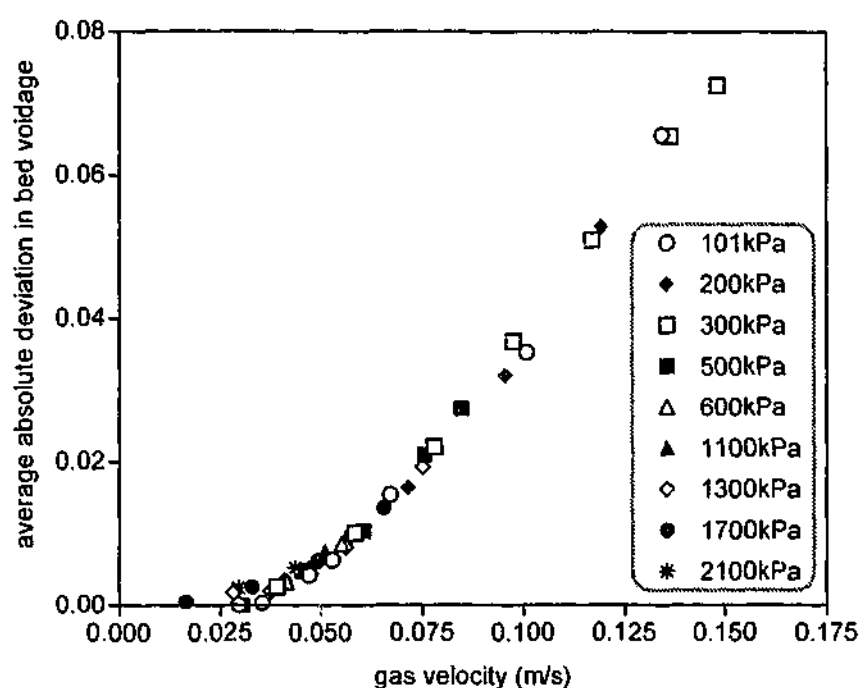


Figure 5-4. Variation in average absolute deviation in bed voidage with gas velocity for silica sand over a range of operating pressures from atmospheric to 2100kPa

For the Geldart B silica sand, as can be seen in Figure 5-4, increasing operating pressure from ambient to 2100kPa has practically no effect on the average absolute deviation in bed voidage and bubbling behaviour of the bed. Once again, the fluidized bed remains in the bubbling state within the range of gas velocities studied, as can be seen from the increase in the average absolute deviation with increasing gas velocity.

5.3.2.3 Time scale in the time series

In bubbling fluidized beds, it is widely believed that the bubble cycle frequency is in the range of 2 - 5Hz (Makkawi & Wright, 2002). In this work the dependency of the average cycle frequency on gas velocity and operating pressure for the Geldart A FCC catalyst and the Geldart B silica sand is shown in Figure 5-5 and Figure 5-6, respectively.

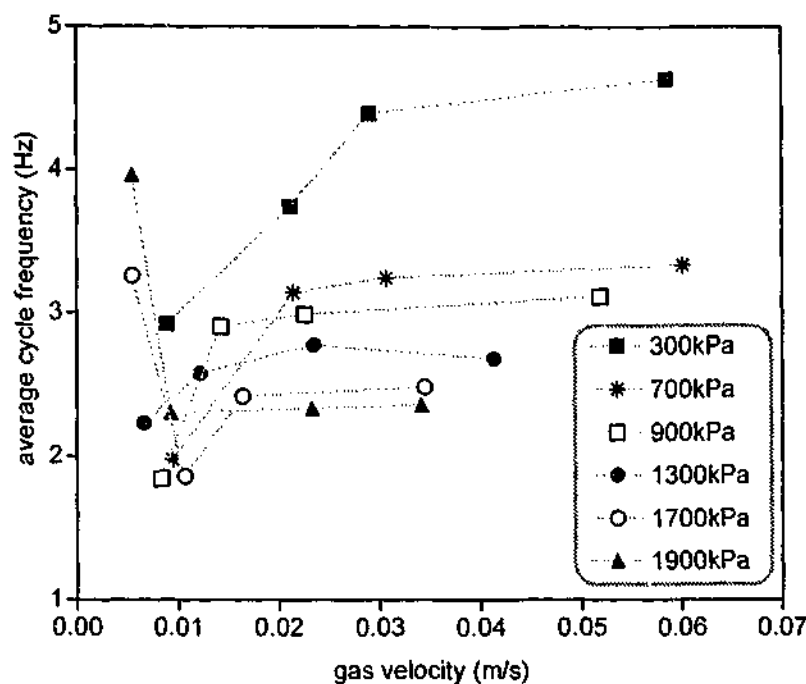


Figure 5-5. Variation in average cycle frequency with gas velocity for FCC catalyst over a range of operating pressures from 300 to 1900kPa (lines are used to guide the eye)

In the low velocity range, as can be seen in Figure 5-5, the average cycle frequency for the Geldart A FCC catalyst changes quite noticeably, usually decreasing first and then increasing with increasing gas velocity. In the intermediate regime around the minimum fluidization and minimum bubbling conditions, the average cycle frequency was found to be very sensitive to small disturbances, apparently caused by experimental noise.

Similar large differences between different pressure fluctuations measurements in the intermediate regime were observed at ambient conditions by van der Stappen et al. (1993a) and Daw and Halow (1993).

However, in the bubbling state, the average cycle frequency is a robust and reproducible measure for the time scale of the time series of voidage (or pressure) fluctuations. When the bed reaches a steady bubbling state the average cycle frequency appears to level off and becomes practically independent of further gas velocity increase within the studied range.

The effect of operating pressure on the average cycle frequency in the bubbling regime can be seen in Figure 5-5. It shows that the average cycle frequency is considerably lower at higher operating pressures.

According to Bai et al. (1999), experimental results presented by van der Stappen et al. (1993b) suggest that higher cycle frequencies correspond to more complex dynamic systems. Therefore, the ECT experimental results, presented in Figure 5-5, show that increasing the operating pressure leads to a less dynamic fluidized bed system in line with other researchers' observations of smoother fluidization for Geldart A materials at high pressure.

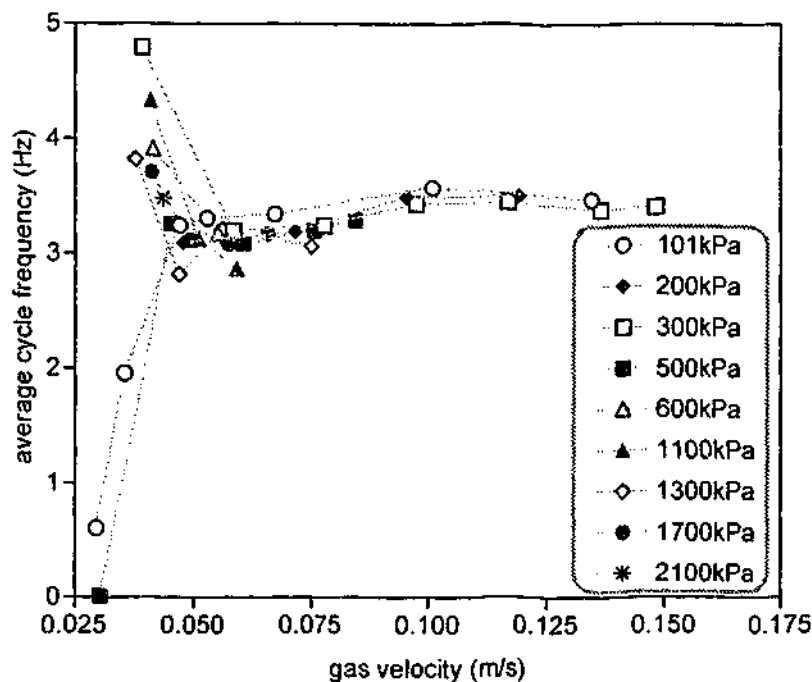


Figure 5-6. Variation in average cycle frequency with gas velocity for silica sand over a range of operating pressures from atmospheric to 2100kPa (lines are used to guide the eye)

For the Geldart B silica sand, in the intermediate regime near the minimum fluidization and at gas velocities below approximately 0.04m/s, the average cycle frequency is very sensitive and the differences between different measurements are quite large, as shown in Figure 5-6.

When the bubbling bed is developed, the average cycle frequency of voidage fluctuations is about constant at a value of about 3.2Hz at all the operating pressures tested in the range from atmospheric to 2160 Pa. Similarly, the constant value of the average cycle frequency of pressure fluctuations of about 3.3Hz in a bubbling bed was reported by van der Stappen et al. (1993a) who fluidised Geldart B polystyrene particles at ambient conditions. From Figure 5-6, it can be observed that in the fully developed bubbling regime the average cycle frequency is practically independent of pressure.

5.3.2.4 Chaos analysis

Based on extensive experience of Daw and Halow in the area of evaluation of fluidization quality through chaotic time series analysis, the Kolmogorov entropy for pressure drop measurements made in fluidized beds at conditions above the minimum fluidization typically ranges from about 0.5 to 30 bits per second (Daw & Halow, 1993).

As previously mentioned, the average absolute deviation is a measure of the characteristic length and the average cycle frequency is a measure of the time scale in the time series. As such, both invariants were used in the reconstruction of the attractor, from which the Kolmogorov entropy was calculated by using the RRChaos software.

Since for the Geldart B material studied, both invariants were found to be practically independent of pressure, it is expected that the Kolmogorov entropy for this material would be also more or less unaffected by pressure.

Other researchers (e.g. Daw & Halow, 1993; van der Stappen et al., 1993a) found at ambient conditions that in the intermediate gas velocity regime the Kolmogorov entropy varies considerably tending to be much higher than in the freely bubbling bed. According to van der Stappen et al. (1993a), in the freely bubbling state, the Kolmogorov entropy settles at a value of about 17 bits per second in the fluidized bed of a Geldart B material.

In order to observe the dynamic processes in fluidized beds and be able to apply fully a chaotic time series analysis, Daw and Halow (1993) recommend acquiring time series fluidized bed pressure drop or voidage measurements at an optimum sampling rate of 200Hz.

Schouten and van den Bleek (1998) have found that in order to sufficiently accommodate the chaos analysis attractor in its state space, the required sampling frequency should be at approximately 100 times the average cycle frequency. Based on the average cycle frequency of 3.2Hz for the bubbling bed of the Geldart B sand, the required sampling frequency should be more than 300Hz.

However, the ECT system used in this work was not capable of sampling frequency above 90Hz. Taking into consideration this limitation of the equipment, it was accepted that the chaos analysis of the experimental data might not be complete.

According to Kuehn et al. (1996), a number of points per cycle in the voidage time series from the ECT measurements is rather low which may lead to an over-estimation of the Kolmogorov entropy. The Kolmogorov entropy calculated from the results of the ECT experiments with the Geldart A material is presented in Figure 5-7.

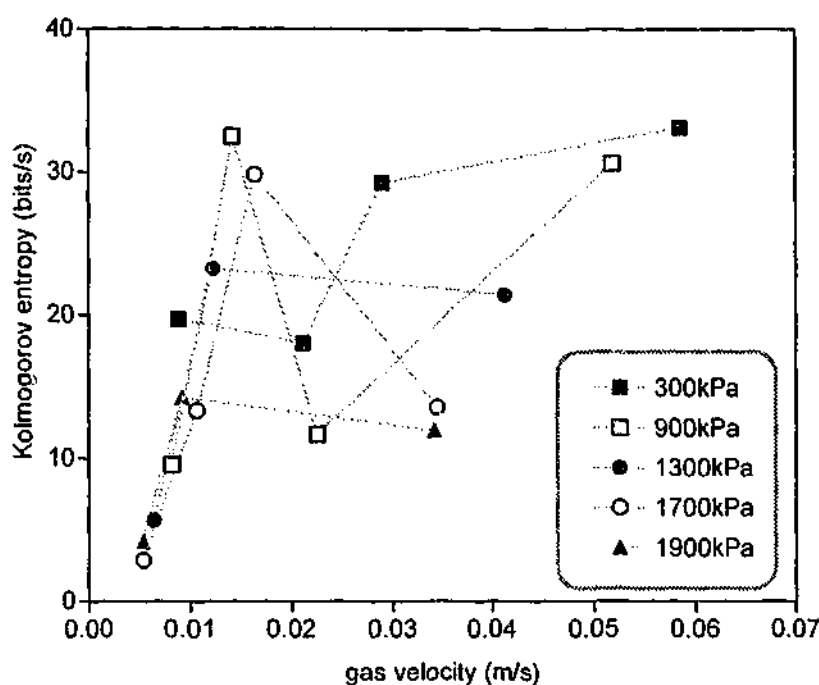


Figure 5-7. Kolmogorov entropy as a function of gas velocity for FCC catalyst over a range of operating pressures from 300 to 1900kPa (lines are used to guide the eye)

As can be seen in Figure 5-7, at minimum bubbling ($U_{mb} \cong 0.006\text{m/s}$), the Kolmogorov entropy seems to have a minimum, generally less than 5 bits per second, which is lower than in the freely bubbling state. This is in good agreement with results of van der Stappen et al. (1993a), who qualitatively explained this in the following way – at gas velocities where the first bubbles appear, the bubbles are independent of each other and rise through the bed with no or minor interaction. This behaviour is relatively simpler and more periodic compared to the developed bubbling state, where bubbles are influencing each other in a more complex way.

In the freely bubbling state, the Kolmogorov entropy is expected to settle at a certain value, which could be as high as 32 at the operating pressure of 300kPa or as low as 12 at 1900kPa. However, because of the equipment limitations previously explained, Figure 5-7 shows possibly not the absolute values but merely trends. Like the average cycle frequency in Figure 5-5, the Kolmogorov entropy results do not settle until the gas velocity is beyond 0.03m/s.

Using this basis for comparison, the final data points in Figure 5-7 are more representative of the Kolmogorov entropy in the bubbling bed. The observed trend in the bubbling bed is that with increasing pressure the Kolmogorov entropy decreases.

When the Kolmogorov entropy decreases, the fluidized bed hydrodynamics become more predictable. Zijerveld et al. (1998) explain it by an increase in bubble size at the bed surface. This is in agreement with Schouten et al. (1996), who related the Kolmogorov entropy K to the bubble size d_b as follows:

$$K = \frac{1.5(U - U_{mf})D}{d_b^2} \quad (5.3.1)$$

According to this equation, the Kolmogorov entropy decreases with an increase in bubble size. Based on this and the trends presented for the Geldart A material in Figure 5-7, it appears that the bubble size increases with increasing pressure. However, this is contradictory to the previous research and the results of this study presented in Figure 5-1.

As previously mentioned, generally it has been reported that fluidization becomes smoother with high pressure, which has been attributed to smaller bubbles at increased pressure. Many workers found that increasing the operating pressure causes bubble size to decrease in Geldart A materials (Barreto et al., 1983a; Chan et al., 1987; Guedes de Carvalho et al., 1978; King & Harrison, 1980; Rowe & MacGillivray, 1980; Subzwari et al., 1978; Weimer & Quarderer, 1985).

A possible explanation might be that Eq.(5.3.1) was developed based on the pressure fluctuations obtained during the experiments with coarse Geldart B polyethylene particles (0.56mm) and silica sand (0.4mm) carried out at ambient conditions. As previously mentioned, it was found that bubbling behaviour in fluidized beds of coarse Geldart B materials differs noticeably from that in fluidized beds of Geldart A powders even at ambient conditions.

Even with the Geldart B materials, there are some apparently conflicting reports coming from the same school. For example, Zijerveld et al. (1998) found that in the bubbling bed the Kolmogorov entropy decreases with superficial gas velocity and decreases with an increase in bubble size. Earlier van der Stappen et al. (1993a) found that in a freely bubbling bed the Kolmogorov entropy settles at a value of about 17 bits per second.

In another related study (Kuehn et al., 1996), a strong dependency of the Kolmogorov entropy on fluidization velocity was found. Higher gas velocity and more turbulent hydrodynamics cause an increase of the Kolmogorov entropy. At the same time, experiments at ambient conditions show that bubble size increases with gas velocity (Kunii & Levenspiel, 1991).

Obviously, deterministic chaos theory can provide numerical and graphical tools that can quantify and visualise the fluidized bed hydrodynamics, however it is still in its early days and much more work has to be done. It is necessary to verify further the correlations and incorporate other particle systems. So far, it seems that the chaos analysis method has been mainly applied to scale-up of the dynamic behaviour of the fluidized bubbling reactors and fluidization regime transitions in the circulating fluidized beds (Schouten et al., 1996; Zijerveld et al., 1998).

5.4 BED COLLAPSE EXPERIMENTS

5.4.1 COLLAPSE TEST TECHNIQUE

The voidage and gas velocity in the dense phase are usually determined by the bed collapse technique, developed by Rietema (1967), who questioned the validity of the simple two-phase theory and suggested that for fine powders the dense phase during bubbling has a higher voidage than that at the minimum fluidization velocity.

Since their introduction in the 1960s, bed collapse experiments have been used by a number of research workers to characterise dense phase properties of bubbling fluidized beds of Geldart A powders (e.g. Abrahamsen &

Geldart, 1980b; Barreto et al., 1988; Barreto et al., 1983a; Formisani et al., 2002; Foscolo et al., 1989; Geldart et al., 1984; Geldart & Wong, 1985; Geldart & Xie, 1995; Guedes de Carvalho, 1981; Lettieri et al., 2000; Piepers et al., 1984; Wang et al., 2001; Weimer & Quarderer, 1985).

The general approach in a bed collapse experiment is to fluidise the bed material at some gas velocity exceeding the minimum fluidization, record the average bed height, and then suddenly shut off the supply of gas. The descent of the bed surface is then recorded as a function of time to give a collapse rate curve. According to Abrahamsen & Geldart (1980b), collapse tests should be carried out at superficial gas velocities exceeding 0.04m/s in order to determine the dense phase properties in vigorously bubbling fluidized beds of fine powders.

The bed collapse is considered to consist of several successive stages:

- an initial stage of rapid collapse, as a result of bubbles escaping from the bed;
- an intermediate stage of slower bed surface fall at a constant rate of collapse velocity U_c , until the bed height approaches a certain critical height H_c ;
- a final stage, where the bed settles further between the critical height and the settled bed height H_s , by solid consolidation.

More details about this technique and the differences between the collapse curves for Geldart A and cohesive Geldart C powders are given by Geldart and Wong (1985). Geldart and Wong (1985), as well as other researchers (e.g. Guedes de Carvalho, 1981; Piepers et al., 1984), simply cut off the gas supply and allowed all the gas in excess of that when atmospheric pressure is reached to escape by flowing upwards through the bed. The discharged gas includes not only that contained between the particles, but also the gas found in the plenum chamber below the distributor and in the piping downstream of the isolation valve. Therefore, the collapse test results

obtained in different columns could have been different even if all other conditions were identical.

In order to eliminate this factor, other researchers (e.g. Formisani et al., 2002; Foscolo et al., 1989; Lettieri et al., 2000) have installed a second valve to simultaneously vent the plenum chamber. However, this method does not ensure the lack of reverse flow.

An excellent review comparing different bed collapse methods has been presented by Grace (1992), who examined the collapse behaviour of different materials, with different venting modes, different plenum chamber volumes, different gas velocities and different distributors. Grace (1992) concluded that, during the collapse process, the plenum chamber should be vented in a controlled manner to maintain zero distributor pressure drop. It was found that over-venting of the plenum chamber could be clearly worse than not venting at all.

Grace (1992) recommended that if simple single venting through the bed was used, the volume of the plenum chamber and the distributor pressure drop should be as small as possible. Alternatively, an analytical method for correction for excess gas in the plenum chamber and pipework is available (Geldart & Wong, 1985).

5.4.2 EXPERIMENTAL METHOD

Bed collapse experiments were carried out at room temperature and the operating pressures ranging from atmospheric to 1600kPa, using 6.56kg of Geldart A FCC catalyst as bed material, and industrial nitrogen as fluidising gas. The experimental programme was based on a "single-vented" technique given by Geldart and Wong (1985).

At atmospheric pressure, an experiment was carried out as follows: the gas flow rate was set at a predetermined level so that the bed was bubbling, and the average bed height was recorded. When the gas supply was suddenly turned off with the isolation valve V10 (Figure 3-5), the bed began to

collapse and the height was recorded on a video camera as a function of time at a rate of 25 frames per second.

Bed height after the test at ambient conditions was about 0.497m. The plenum chamber was not vented simultaneously and the combined internal volume of the chamber and the pipework downstream of the isolation valve was estimated to be equal to 0.00115m³.

Since the bed height fluctuated due to bubbling, five repeat tests were made and an average bed height was taken. Similar tests were also carried out at different predetermined gas flow rates.

The same procedure was followed at elevated pressures, however the vessel was pressurised first to a pre-determined operating pressure level in a similar way as was described in previous chapters. Sudden shutting of the gas supply put a certain stress on the pressurised supply pipework and the gas source; therefore some additional safety measures were taken. No experiments above approximately 1700kPa could be safely carried out without triggering the pressure relief valve and so were not attempted.

Geldart recommends starting the collapse tests from a bed fluidised with a superficial gas velocity above 0.04m/s (Abrahamsen & Geldart, 1980b) and carried out some experiments at an initial velocity of 0.08m/s (Geldart & Wong, 1985), and even 0.1m/s (Geldart & Xie, 1995). However, because of the open circuit design limitations and safety restrictions at elevated pressure, it was not always possible in this work. At each experiment the highest possible initial gas velocity was attempted and varied from 0.054m/s at atmospheric pressure to 0.008m/s at 1600kPa, compared to the minimum bubbling velocity value of 0.006m/s.

Abrahamsen and Geldart (1980b) observed that up to about 0.03m/s the total bed height and the dense phase height decreased as the velocity was increased. With further increase in gas velocity, the total bed height increased, but the dense phase height levelled off. In other work with FCC catalysts, Lettieri et al. (2000) were aware of that observation but chose to

use fluidization gas velocity prior to the collapse tests as low as 0.013m/s in order to minimise clutriation of fines from the bed.

In this work, a number of collapse tests were carried out at ambient conditions with starting gas velocities of 0.018, 0.030, 0.042 and 0.054m/s. In all cases, the bed collapse curves clearly coincided. This is in agreement with findings of Weiner and Quarderer (1985) who repeated their bed collapse experiments at various initial values of the gas velocity for all pressures and materials and found that the dense phase voidage was independent of the starting gas velocity.

However, Piepers et al. (1984) repeated their experiments at 0.02, 0.03, 0.04 and 0.05m/s at various pressures and observed a decrease in the dense phase voidage with increasing starting velocity at the low operating pressures only (200 and 400kPa). Within the pressure range 700 – 1600kPa, they found the dense phase voidage to be practically independent of the gas velocity immediately before the bed collapse.

5.4.3 EXPERIMENTAL RESULTS AT VARIOUS OPERATING PRESSURES

Bed collapse experimental results had been obtained in a form of video recording, from which the plots of bed height decrease with time were constructed. The results of the second intermediate stage when the bed surface falls at a constant rate of collapse velocity U_c , until the bed height approaches a certain critical height H_c , are plotted in Figure 5-8. It should be noted that the error bars for the curve at atmospheric pressure are based on the total of 20 experiments, five for each of four initial fluidization gas velocities.

Similar collapse curves for a FCC catalyst at various operating pressures were observed by Foscolo et al. (1989).

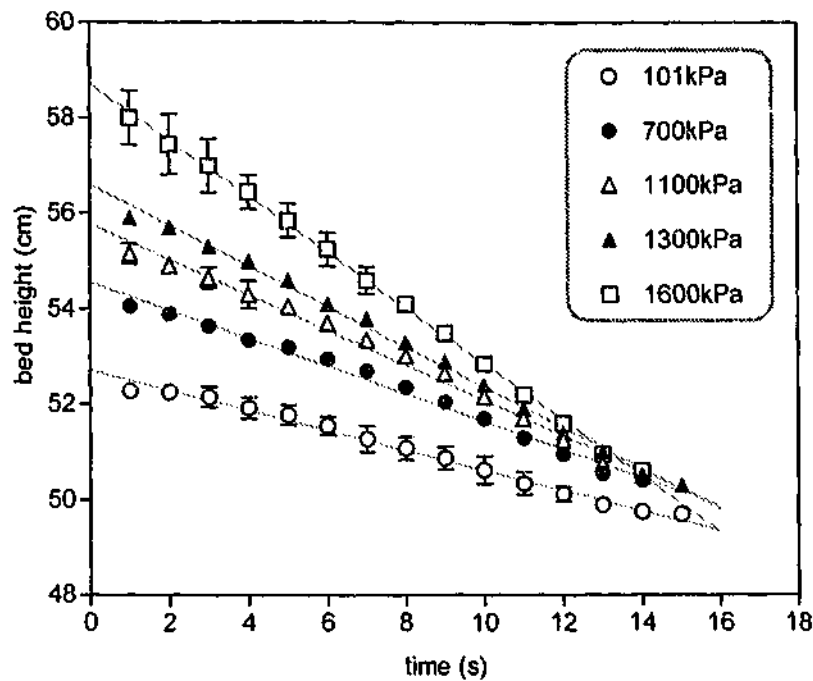


Figure 5-8. Bed surface collapse curves for FCC catalyst at various operating pressures

The straight line portions of the bed collapse curves were extrapolated back to time zero and it was assumed that the intercept with the bed height axis gives the height which the dense phase would occupy in the bubbling bed.

Abrahamsen and Geldart (1980b) correlated the dense phase expansion (Eq.(2.3.1)) which includes the gas density effect. According to this correlation the dense phase expansion should slightly increase with increasing the operating pressure. A comparison between the dense phase expansion determined experimentally from the bed collapse tests at various operating pressures and that predicted from the correlation by Abrahamsen and Geldart (1980b) is presented in Figure 5-9. For comparison with the maximum non-bubbling bed expansion for this material shown in Figure 4-14, the scale of both graphs is the same.

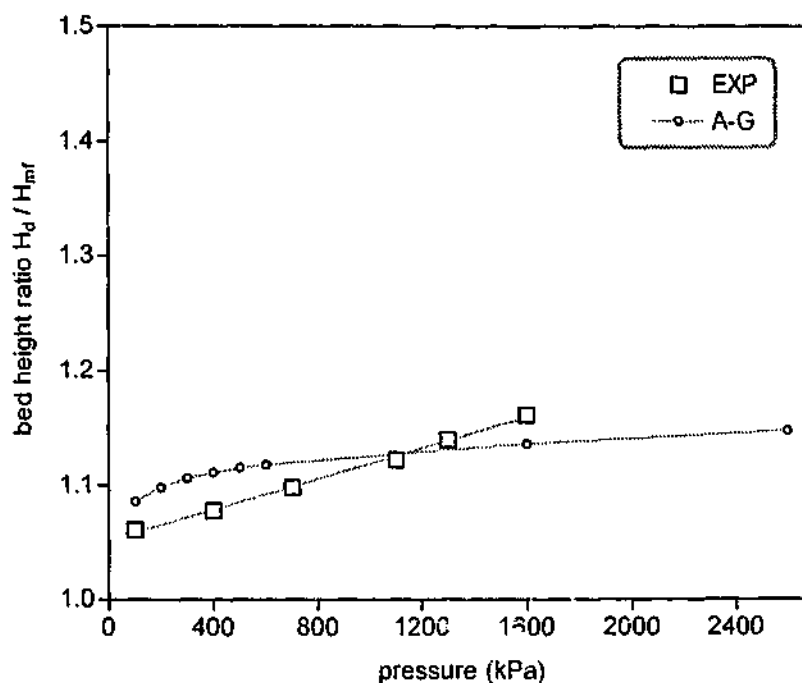


Figure 5-9. Variation of the dense phase expansion with pressure for FCC catalyst (EXP - experimental values and A-G - (Abrahamsen & Geldart, 1980a))

As can be seen in Figure 5-9, the dense phase expansion linearly increases with increasing pressure within the studied range 101 - 1600kPa. Compared to the predictions of the correlation by Abrahamsen and Geldart (1980b), the experimental results show much higher rate of increase, and therefore, a much stronger influence of operating pressure than the factor $\rho_g^{0.016}$ included in the correlation.

Similar results were observed in the previous work (Piepers et al., 1984; Weimer & Quarderer, 1985). As noted by Barreto et al. (1988), the extensive experiments of Abrahamsen and Geldart were carried out with air at atmospheric pressure and the effect of gas density arose as a consequence of the correlation method.

According to the correlation, it was expected that a pressure increase from atmospheric to 1500kPa should cause only 4.5% increase in the dense phase height for a FCC catalyst fluidised with nitrogen (Piepers et al., 1984). However, their experimental results demonstrated a much higher 21% increase. Weimer and Quarderer (1985) also found that the correlation

proposed by Abrahamsen and Geldart (1980b) largely underestimated the effect of pressure on the dense phase voidage for a Geldart A powder.

5.4.4 INFLUENCE OF PRESSURE ON THE DENSE PHASE VOIDAGE

Bed collapse experiments are primarily intended to obtain a direct value of the dense phase voidage. Once the initial heights of the dense phase of the bed had been determined from the collapse curves obtained at various operating pressures (Figure 5-9), the experimental values of the dense phase voidage were calculated by employing the usual relationship:

$$\varepsilon_d = 1 - \frac{m}{\rho_p H_d A} \quad (5.4.1)$$

For the Geldart A FCC catalyst studied in this work, the dependence of the bed voidage at minimum bubbling on pressure was previously presented together with the influence of pressure on voidage at minimum fluidization in Figure 4-16. Now, the experimental values of all the voidages - dense phase voidage, settled bed voidage, minimum bubbling voidage and minimum fluidization voidage - are presented together for comparison in Figure 5-10.

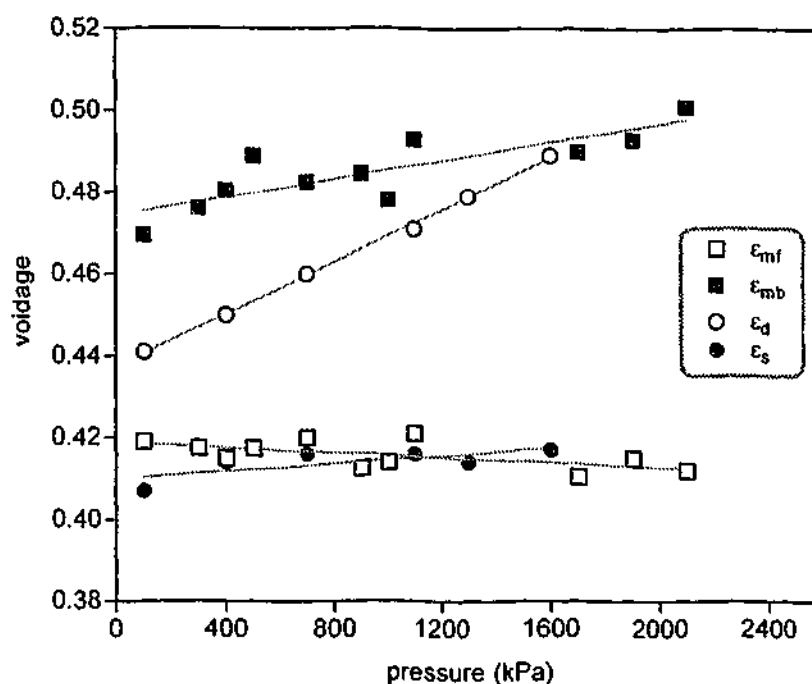


Figure 5-10. Variation with pressure of dense phase voidage (ϵ_d), settled bed voidage (ϵ_s), minimum fluidization voidage (ϵ_{mf}) and minimum bubbling voidage (ϵ_{mb}) for FCC catalyst

As can be seen in Figure 5-10, within the studied pressure range, the dense phase voidage was found to be higher than the voidage at minimum fluidization and to increase steadily with increasing pressure for a Geldart A powder. This is in line with the observations of other researchers (Barreto et al., 1983a; Foscolo et al., 1989; Guedes de Carvalho, 1981; Piepers et al., 1984; Weimer & Quarderer, 1985).

5.5 SUMMARY

It is widely believed that the voidage of the dense phase in the bubbling fluidized bed is important parameter in determining the bed performance because it has a direct influence on chemical reactions in the fluidized bed. It affects the degree of gas-solid contact and heat and mass transfer.

A few methods have been used to measure the dense phase voidage in bubbling fluidized beds. For Geldart A bed materials the dense phase voidage is usually measured by means of the bed collapse technique.

The bed collapse tests were carried out with the FCC catalyst with the results of the experiments similar to those of other researchers. Within the studied pressure range 101 – 1600kPa, the dense phase voidage was found to be higher than the voidage at minimum fluidization and increased steadily with increasing pressure.

Since the early 1990s the electrical capacitance tomography systems have been used for research in the area of fluidization, however until now the use of capacitance tomography was limited to the atmospheric fluidized beds. This promising non-invasive technique is still under development and, apart from the present work; it appears that no other study of fluidization in a pressurised environment has been carried out using the electrical capacitance tomography.

The tomographic images obtained from the capacitance measurements were of relatively low resolution and suffered from blurring; and no image analysis was carried out in this work. Results of the experiments were produced by the ECT system in time series data points of the average solids volume fraction representing the whole bed at a given horizontal level.

It was found that the pressure increase was accompanied by the reduction of the cross-section averaged total bed voidage for the Geldart A catalyst. The results of the ECT experiments with the Geldart B silica sand were different from those for the FCC catalyst. It was observed that any pressure increase was accompanied by the increase in the average bed voidage.

The intensity of the voidage fluctuations was measured and compared by using the average absolute deviation. For the FCC catalyst, the pressure effect was indicated by the decrease of the average absolute deviation with increasing pressure. For the silica sand, increasing operating pressure up to 2100kPa had practically no effect on the average absolute deviation in bed voidage and bubbling behaviour of the bed.

The average cycle frequency is considered to be a robust and reproducible measure for the time scale of the time series of voidage fluctuations. When the bed reached a steady bubbling state the average cycle frequency

appeared to level off and became practically independent of further gas velocity increase within the studied range.

Effect of operating pressure on the average cycle frequency in the bubbling regime for the catalyst was such, that the average cycle frequency was considerably lower at higher operating pressures.

In the freely bubbling state, the average cycle frequency of voidage fluctuations for the silica sand was practically independent of pressure and became constant at a value of about 3.2Hz at all the operating pressures tested in the range from atmospheric to 2100kPa.

Chapter 6

EXPERIMENTAL OBSERVATION OF THE MOTION OF PARTICLES NEAR THE WALL SURFACE IN A PRESSURISED BUBBLING FLUIDIZED BED

This chapter presents the experimental findings of influence of operating pressure on the motion of Geldart A and B luminescent particles near the fluidized bed wall surface. Understanding of the effect of pressure on the motion of particles at the wall should permit better understanding of the effect of pressure on wall-to-bed heat transfer.

6.1 OVERVIEW

In bubbling fluidized beds the total bed-to-surface heat transfer coefficient is presented as a sum of three independent components - particle convective, gas convective and radiative (Botterill, 1975). The main factors in the heat transfer between a surface and a fluidized bed are movement of particles close to the surface and their residence time at the surface.

According to Botterill (1975), the good heat transfer properties of fluidized beds are the result of the high heat capacity of bed particles and their mobility. At temperatures below 873K, when the radiative heat transfer component is negligible, the particles in the bulk of the fluidized bed exchange heat by the gas phase conduction and stay in the bulk of the bed long enough to reach the same temperature as their neighbouring particles.

When some of the particles are swept into close proximity with the heat transfer surface, there is a high local temperature gradient between the surface and the particles. The longer the particles stay at the surface, the more their temperature approaches the surface temperature which leads to reduction in the local temperature gradient and the effective rate of heat transfer. Highest rates of heat transfer between a surface and a fluidized bed

are obtained therefore, when there is rapid exchange of material between the adjacent to the heat transfer region and the bulk of the bed, i.e. when particle residence times at the surface are very short.

However, it is common for vertical surfaces to become covered by the downward return flow of solids. In 1953 Toomey and Johnstone (in Botterill, 1975) described the now well-known appearance of particle motion close to the wall, in which there is upward flow of particles through the centre of the column induced by bubbles, and comparatively slow downward flow at the wall. In general, material adjacent to the wall is only occasionally disturbed by rising bubbles and slugs which penetrate to the wall.

For particles less than 500 μm , pressure effect on the bed-to-surface heat transfer is considered to be negligible (Botterill, 1975, 1989). However, according to Molerus and Wirth (1997a), the heat transfer clearly depends on pressure within the range of particle sizes from 50 μm to 1mm and the influence of particle motion on the heat transfer should manifest itself in a similar pressure dependence.

6.2 MOTION OF PARTICLES

6.2.1 EXPERIMENTAL METHOD

With transparent side walls of the fluidized bed column direct observation of the motion of particles along the wall was possible through one of the pressure vessel's observation windows. Experimental observation of the motion of particles near the wall surface was based on the pulsed light method described by Molerus and Wirth (1997a).

The motion of particles at the wall surface was visualised by using particles of a luminescent pigment as bed solids (Section 3.10). Six kilograms of the original pigment (pigment A) were used for charging the fluidized bed in the series of experiments with a Geldart A material. In order to study the particle motion in a bed filled with a Geldart B material, six kilograms of the

mixture of two fractions, 212 - 300 and 300 - 425 μm , of the agglomerated luminescent pigment (pigment B) were used as bed solids.

A pulse of bright light from a conventional photoflash with an adaptor was transmitted from outside of the pressure vessel via a specially made fibre optic light guide as described in Section 3.9. The flash illuminated a 7mm-diameter spot of the luminescent bed material adjacent to a transparent fluidized bed vessel wall inside of the pressure vessel. After illumination, the spot consisting of a cluster of particles, showed an afterglow for several seconds. The fibre optic light guide was positioned in such way, that the illuminated spot was at approximately mid-height of the bed level and could be clearly seen through one of the observation windows (Figure 6-1).

A digital video camera was mounted in front of the window and covered with some lightproof fabric. All the remaining observation windows were blocked so that it was completely dark inside and only the illuminated spot on the black background was visible through the camera viewfinder.

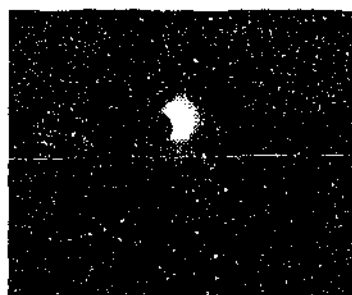


Figure 6-1. An example of the illuminated cluster of particles as seen on a video camera (actual size)

Under fixed bed conditions the illuminated spot was still visible after three minutes. When the bed was fluidised the illuminated spot shifted along the wall surface while its shape deformed and its luminosity decreased. However, the illuminated particles stayed in close proximity as a cluster, and the spot remained a single identifiable object until it disappeared. When an image disappeared from view, it could be assumed that, depending on gas velocity, the image either moved out of the camera view or its brightness diminished.

Experiments were carried out at different gas velocities up to fifteen times the minimum fluidization velocity under various pressure conditions. The pressure range was from atmospheric to 2100kPa for experiments with pigment A, and up to 1600kPa for experiments with the agglomerated pigment B. However, because of the relatively high material density and the gas supply limitations, it was not possible to fluidise the pigment B well above the minimum fluidization velocity at operating pressures higher than 800kPa.

Pressurisation of the vessel and setting the operating pressure and gas velocities were carried out in the same way as was described above (Section 4.1.2). At predetermined operating pressure and gas velocity, an experiment proper consisted of illuminating a small cluster of particles with the flash and filming the spot until it disappeared. At each gas velocity, at least ten and, sometimes up to 14 separate flashes were recorded. The fate of each independent light pulse was analysed separately using image analysis software.

6.2.2 DATA ANALYSIS

The images of the illuminated spot were captured in a black-and-white mode by a digital video camera at a rate 25 frames per second. Digital videos were downloaded on a dedicated computer equipped with a special card and software¹¹, and edited using Adobe Premiere 5.1 video processing software. Image analysis was then carried out in order to quantify the statistics of particle movement near to the wall surface.

Videos were first processed with free image processing software¹² where all the frames were extracted. Separate frames were then organised in stacks for each light pulse. For each experimental condition up to 14 stacks of frames

¹¹ miroVIDEO DVTools. (Version 1.6) [computer software]: Pinnacle Systems
(www.pinnaclesys.com).

¹² IrfanView. (Version 3.61) [computer software]. Vienna: Skiljan, Irfan (www.irfanview.com).

were analysed with free image analysis software¹³. Each pixel of the image was characterised by its X and Y coordinates and luminosity, expressed in dimensionless form on a greyscale, where 0 is black and 255 is white. From filming a reference ruler in daylight it was determined that on linear scale each pixel was equal to 0.25mm.

At the packed bed conditions, it was observed that the cluster of illuminated particles remained visible as a still spot decreasing in intensity with time. The initial step in digital data analysis involved discrimination of illuminated spots from the rest of the bed material. In general, the procedure for this image identification involves examination of the greyscale values histogram for a normal image consisting of both illuminated spot and dark background.

Since the lighting conditions were uniform and image contrast was quite high, the accurate detection of the image boundary was possible using the global thresholding method (Agarwal et al., 1997). As a result, it was found that applying a greyscale threshold ($L_{threshold}$) of 60 accurately characterised illuminated spots while they were visible.

On each frame, the following data for the illuminated spot was obtained – image area in mm²; mean, maximum and minimum luminosity within the image threshold on a greyscale; and X–Y coordinates of the centre of gravity of the image. More than 160 thousand files were processed and the results were organised for separate light pulses at each gas velocity. Further statistical analysis was performed using special software¹⁴, where for each gas velocity data from 10 – 14 flashes were averaged, plotted and nonlinear regression was applied.

Since the detection of clusters depended on their visibility, it could be possible that the disappearance of images resulted from loss of material

¹³ ImageJ. (Version 1.27) [computer software]. Bethesda: Rasband, Wayne
(<http://rsb.info.nih.gov/ij/>).

¹⁴ Prism. (Version 3.02) [computer software]. San Diego: GraphPad Software
(www.graphpad.com).

luminosity with time or possibly from clusters mixing. A simple analysis showed that the light source had enough power to sufficiently illuminate a spot and the material had enough luminosity such that the illuminated object could still be observed by the end of each test.

The effect of particle motion in a fluidized bed on cluster maximum luminosity compared to that of packed bed is illustrated in Figure 6-2. In both cases the luminosity decay was found to be exponential in time, however, the rate of decay was much higher in the fluidized bed.

The packed bed results in Figure 6-2 illustrate the natural decay of the material luminosity with time. It was found that the motionless illuminated spot was clearly visible for at least 100 seconds (2500 frames), and some afterglow could be distinguished on the dark background even after three minutes.

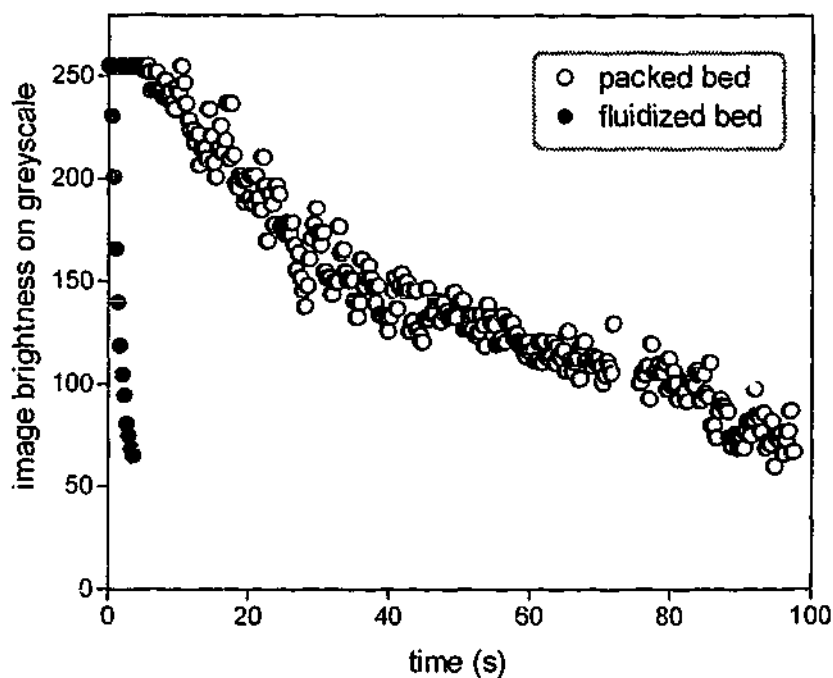


Figure 6-2. Decay of maximum image luminosity on a greyscale in packed bed of pigment A compared to fluidized bed at atmospheric pressure (fluidization gas velocity $U = 0.012\text{m/s}$)

In comparison, the experiments showed that in a fluidized bed the illuminated spot always became invisible in less than four seconds (100

frames). Based on such large difference between the natural material luminosity decay and the luminosity loss during fluidization, it was assumed that under the experimental conditions the former had no effect on the latter. Therefore, it was assumed that the luminosity decay during fluidization is only caused by the fact that the illuminated cluster particles move away from the wall and are replaced by dark particles.

Although for agglomerated pigment B the natural material luminosity decay with time was less than for the original pigment, it was still much larger than the image luminosity decay during the fluidization experiments.

6.3 PARTICLE MOTION OBSERVATION AT SIMILAR FLUIDIZATION VELOCITIES

Some influence of operating pressure on particle motion near the fluidized bed wall can be illustrated through results of experiments carried out using Pigment A at different pressures but at similar fluidization velocities at approximately five times the minimum fluidization velocity.

As can be seen in Figure 6-3 - Figure 6-7, the illuminated spot shifts down along the wall surface while its shape deforms and luminosity decreases.

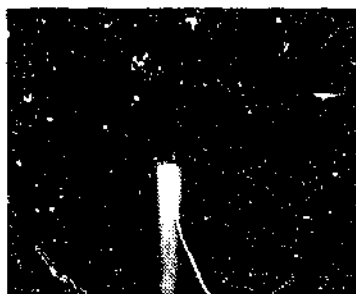


Figure 6-3. Image trajectory for pigment A at atmospheric pressure and gas velocity of 0.012m/s (actual size)



Figure 6-4. Image trajectory for pigment A at 500kPa and gas velocity of 0.011m/s (actual size)



Figure 6-5. Image trajectory for pigment A at 1100kPa and gas velocity of 0.011m/s (actual size)



Figure 6-6. Image trajectory for pigment A at 1500kPa and gas velocity of 0.011m/s (actual size)



Figure 6-7. Image trajectory for pigment A at 2000kPa and gas velocity of 0.011m/s (actual size)

These pictures (Figure 6-3 - Figure 6-7) are produced by superimposing all the separate frames during the image lifetime and show the motion of the illuminated clusters of particles along the wall surface. These images are typical and similar observations were made under different operating conditions. Some qualitative conclusions can emerge from the visual analysis of these results. For example, in these videos, the direction of the motion of the illuminated clusters of particles was observed to be downward as expected.

As can be seen in Figure 6-3, at ambient conditions the illuminated cluster travels down along the wall and disappears from the camera view. Its brightness decreases slightly but the image is expected to be visible at the wall for some time after it disappears below the camera view. It seems that, under given experimental conditions, the majority of cluster particles move downward in close proximity to the wall and only a small number of particles is replaced by the particles coming from within the bed.

At higher operating pressures, the motion behaviour appears to change. Although the clusters also move downward, they do not disappear below the camera view. Brightness of the clusters decreases much faster and it appears that the lateral mixing becomes predominant and the illuminated particles move inside of the bed. With increasing pressure this behaviour becomes stronger (Figure 6-4 - Figure 6-7).

In an attempt to quantify these observations, the decay of mean luminosity of the illuminated clusters at different pressures and similar gas velocities for Pigment A is presented in Figure 6-8.

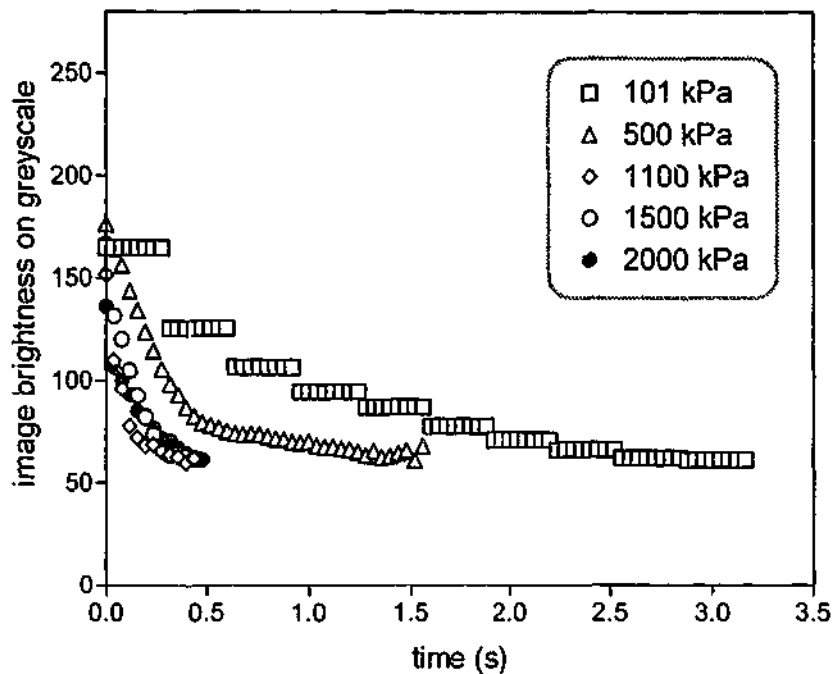


Figure 6-8. Difference between mean image luminosities on a greyscale for pigment A at different operating pressures and similar fluidization velocities

In all cases the luminosity decay was found to be exponential in time. A number of linear and nonlinear regression models was tested and it was found that a one phase exponential decay model (Draper & Smith, 1981; Motulsky, 1996) predicted the experimental data very well. The following equation was used for the decay model:

$$L - L_{threshold} = (L_0 - L_{threshold}) \exp(-kt) \quad (6.3.1)$$

Where the function of luminosity on a greyscale (L) starts at an initial level of span ($L_0 - L_{threshold}$) above constant plateau ($L_{threshold}$) and decays with time (t) to the plateau ($L_{threshold}$) at a rate constant (k). The value of the plateau ($L_{threshold}$) was determined by the threshold applied to the images during the processing.

One of the characteristic parameters of an exponential decay model is the half-life which is the time it takes for the parameter (L), or image luminosity, to drop by half. In the case presented in Figure 6-8, the half-life time decreased from 0.62 seconds at atmospheric pressure to 0.11 seconds at

2000kPa. For comparison, the half-life time of the natural luminosity decay of pigment A established in the fixed bed was 41.84 seconds.

6.4 PARTICLE MOTION OBSERVATION AT VARIOUS PRESSURES

6.4.1 DECAY OF MEAN LUMINOSITY

The previous section describes only a part of the study of the effect of pressure on the particle motion at the wall for pigments A and B.

6.4.1.1 Pigment A

For pigment A, variation of the rate constant k with superficial gas velocity at different operating pressures is presented in Figure 6-9.

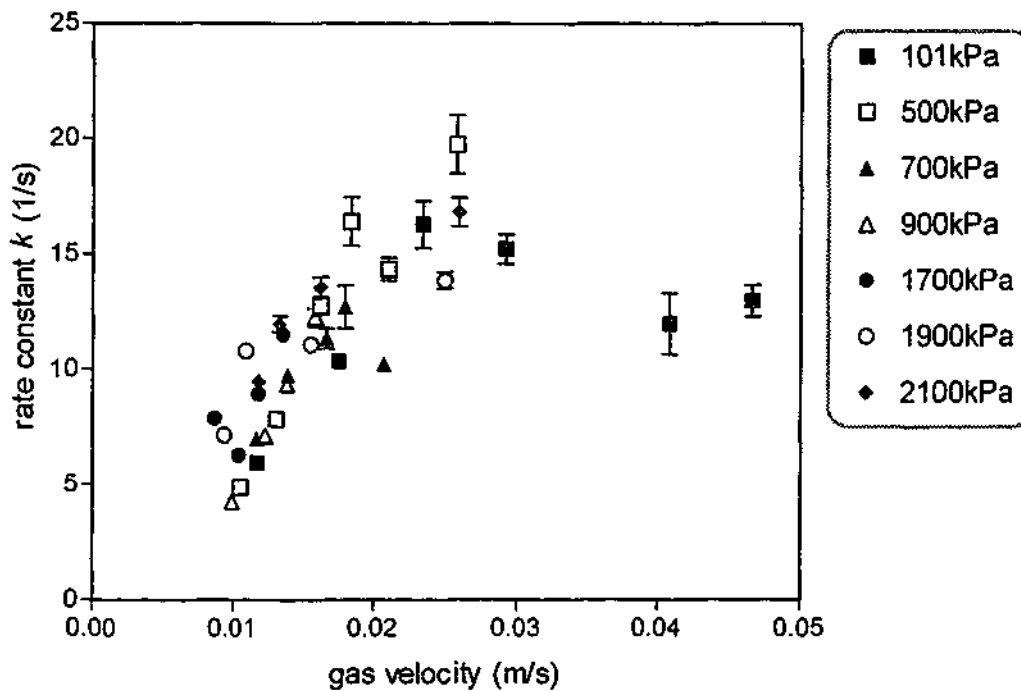


Figure 6-9. Variation in exponential luminosity decay constant k for pigment A with superficial gas velocity in the pressure range 101 – 2100kPa

Figure 6-9 demonstrates that at atmospheric pressure the rate of the luminosity decay and therefore the exchange rate of particles increases with

increasing gas velocity and reaches a maximum at around ten times U_{mf} . Further increasing gas velocity results in decreasing and levelling off of the rate constant.

Similar behaviour can be observed at the operating pressure of 700kPa; although at much lower values of the rate constant k . Due to the limitations of the experimental setup it was not possible to obtain further experimental data at high gas velocities and at high pressures, therefore it is not possible to confirm similar behaviour at other operating conditions. Within the investigated range of gas velocities up to 0.025m/s, no significant pressure effect on the rate of the luminosity decay can be observed in Figure 6-9.

In order to illustrate the last four data points at ambient conditions presented in Figure 6-9, the summation of separate frames during the image lifetime, which show the motion of the illuminated clusters of Geldart A particles along the wall surface at respective gas velocities are presented below. On each picture (Figure 6-10 – Figure 6-13), separate image trajectories resulting from ten independent light impulses are added together.



Figure 6-10. Image trajectory for pigment A at atmospheric pressure and gas velocity of 0.023m/s

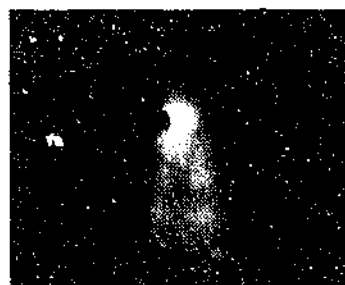


Figure 6-11. Image trajectory for pigment A at atmospheric pressure and gas velocity of 0.029m/s

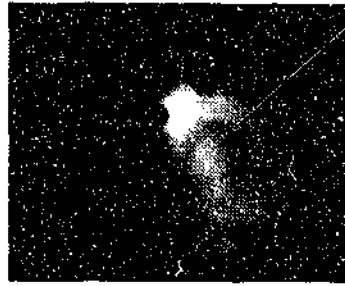


Figure 6-12. Image trajectory for pigment A at atmospheric pressure and gas velocity of 0.041m/s

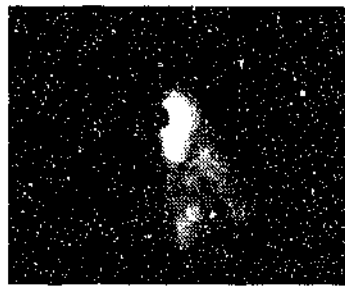


Figure 6-13. Image trajectory for pigment A at atmospheric pressure and gas velocity of 0.046m/s

6.4.1.2 Pigment B

For agglomerated pigment B, the variation of the rate constant k at different operating pressures is shown in Figure 6-14.

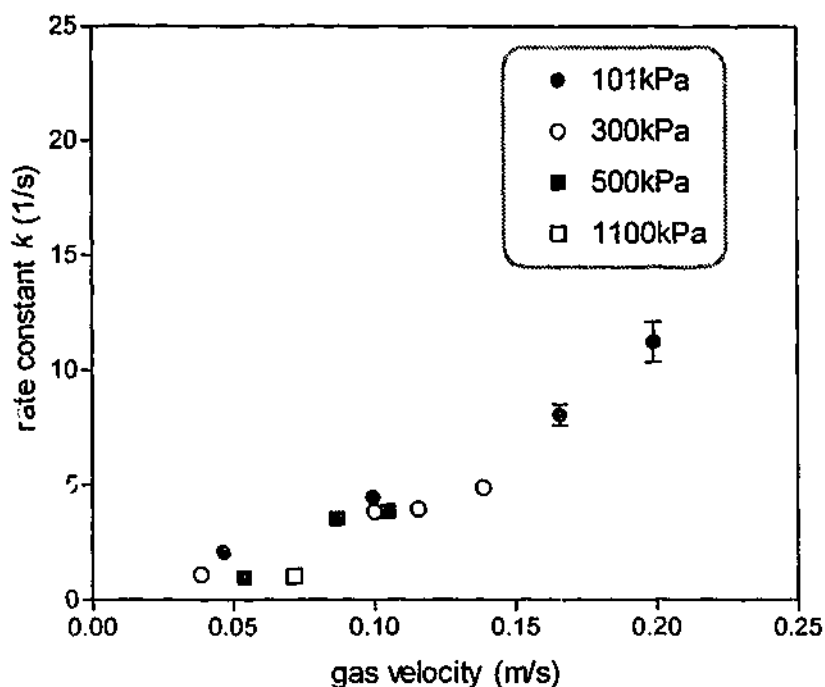


Figure 6-14. Variation in exponential luminosity decay constant k for pigment B with superficial gas velocity in the pressure range 101 - 1100kPa

As can be seen in Figure 6-14, in the fixed bed the rate constant k is generally constant at approximately two within the operating pressure range of 101 - 1100kPa and increases to almost five at the minimum fluidization conditions. Further increasing superficial gas velocity (up to two times the minimum fluidization velocity) results in an increase of the rate constant k . However, no significant pressure effect on the rate constant can be observed in the somewhat limited range of experimental pressures and velocities.

6.4.2 ANALYSIS OF THE EXPERIMENTAL DATA

As illustrated above (Figure 6-2), the increased rate of decay in luminosity in a fluidized bed, compared to that in a fixed bed, is attributed to the fact that the originally illuminated particles move away from the wall during the fluidization process and are replaced by particles coming from the rest of the bed.

Based on the rules for conditional probability, Molerus and Wirth (1997a) deduced an equation for the exchange frequency of particles f perpendicular to a solid surface. It was postulated that the probability $W(t)$ that a particle in contact with the wall at time $t = 0$, moves inside of the fluidized bed, is proportional to the time interval Δt , i.e. equivalent to $f\Delta t$. Using the initial condition when $W(0) = 1$, Molerus and Wirth (1997a) obtained the following equation:

$$W(t) = \exp(-ft) \quad (6.4.1)$$

This equation indicates that the luminosity decay L , related to initial brightness L_0 , directly corresponds to the constant slope of the fluidized bed curve and the parameter f can be determined by plotting $\ln(L/L_0)$ versus time:

$$\ln\left(\frac{L}{L_0}\right) = -ft \quad (6.4.2)$$

Based on the area of the original illuminated spot and the particle size, the initial number of the illuminated particles n_{p0} next to the bed wall can be estimated from the following relationship:

$$n_{p0} \frac{\pi d_p^2}{4} = (1 - \varepsilon) \frac{\pi D_0^2}{4} \quad (6.4.3)$$

Where d_p is the mean particle diameter, D_0 is the diameter of the illuminated spot and ε is bed voidage.

According to Molerus and Wirth (1997a), the illuminated spot diameter D_0 is equivalent to the fibre optic diameter, which is true only if the fibre-optic is positioned perpendicular to the wall surface right against it. However, positioned like this, the fibre optic would completely block the original illuminated spot so that filming and further image analysis of the original spot would not be possible. For clear view in this study, the 3mm-diameter fibre optic did not touch the wall surface and was positioned at a slight angle in such way that in a fixed bed the diameter of the initial illuminated spot was 7mm.

Using Eq.(6.4.3) and experimentally obtained values of bed voidage at the initial conditions, the original number of illuminated particles for pigment A was estimated to be around 6375, and around 260 for pigment B.

Since the luminosity decay in a fluidized bed is caused by the motion of particles, Molerus and Wirth (1997a) estimated the number of particles in an image with luminosity L from $L/n_p = L_0/n_{p0}$ as follows:

$$n_p = (1 - \varepsilon) \left(\frac{D_0}{d_p} \right)^2 \left(\frac{L}{L_0} \right) \quad (6.4.4)$$

In this study, based on the image threshold value of 60 and Eq.(6.4.4), the final number of particles left at the wall can be estimated at 21 for pigment A and just one for pigment B.

Comparing Eq.(6.3.1) to Eq.(6.4.2) shows that the rate constant k determined earlier corresponds to the particle exchange frequency f defined by Molerus and Wirth (1997a).

6.4.3 MEAN RESIDENCE TIMES AT THE WALL

The mean residence time of illuminated particles near to the wall was deduced by Molerus and Wirth (1997a) as a reciprocal of the particle exchange frequency f . The mean residence time τ , established in this work as a reciprocal of rate constant k presented in Figure 6-9 and Figure 6-14, is shown in Figure 6-15 for pigment A and Figure 6-16 for pigment B.

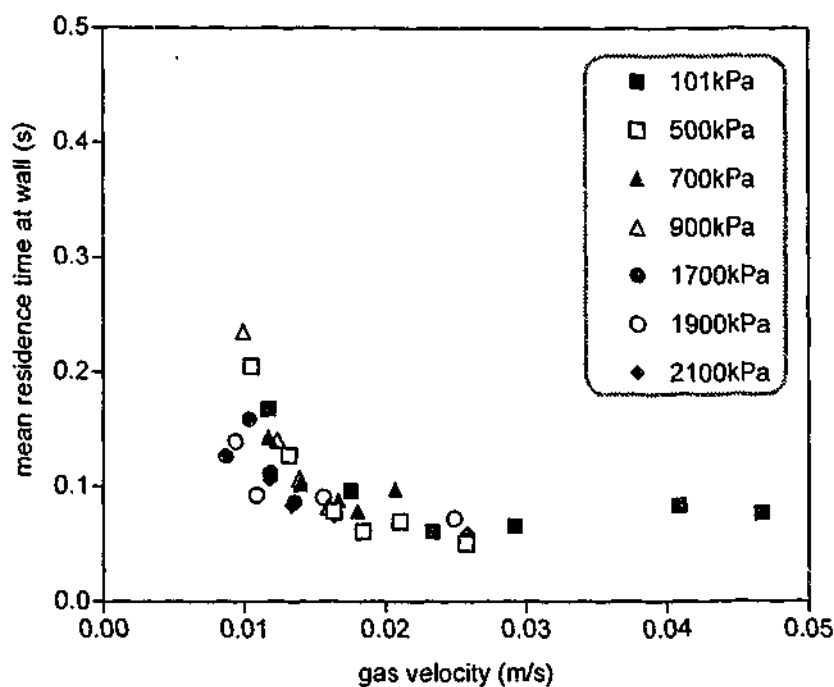


Figure 6-15. Mean time between pigment A particle illumination and departure from the wall versus gas velocity at various operating pressures

For pigment A, as can be seen in Figure 6-15, mean residence times measured close to the wall decrease with increasing gas velocity in the range three to ten times U_{mf} and become practically independent of gas velocity in vigorously bubbling fluidized bed.

The values of the mean residence times settle at below 0.1s, which means that during the experiments the illuminated images disappeared within only three frames on video and could not be measured with higher accuracy. Considering the experimental error of $\pm 0.04s$, it is not possible to establish any significant pressure effect on particle residence times at the wall.

As previously mentioned, the highest rates of heat transfer between a surface and a fluidized bed are obtained when particle residence times at the surface are very short. Therefore, from Figure 6-15 it can be estimated that the typical mean residence times measured close to the wall at maximum heat transfer are practically independent of pressure and approximately equal to 0.1s.

This, however, does not agree well with the experimental data presented by Molerus and Wirth (1997a), who observed the following mean residence times of illuminated particles with the size of $50\mu\text{m}$ at vertical solid surfaces in a fluidized bed at maximum heat transfer - 1.28s at 100kPa, 0.35s at 500kPa, 0.52s at 1000kPa and 0.45s at 2000kPa. Contrary to their claim that the heat transfer clearly depends on pressure and expectations of a similar pressure dependence on particle motion, there is no particular trend in their data, but the magnitude is considerably higher than the values measured in the present work.

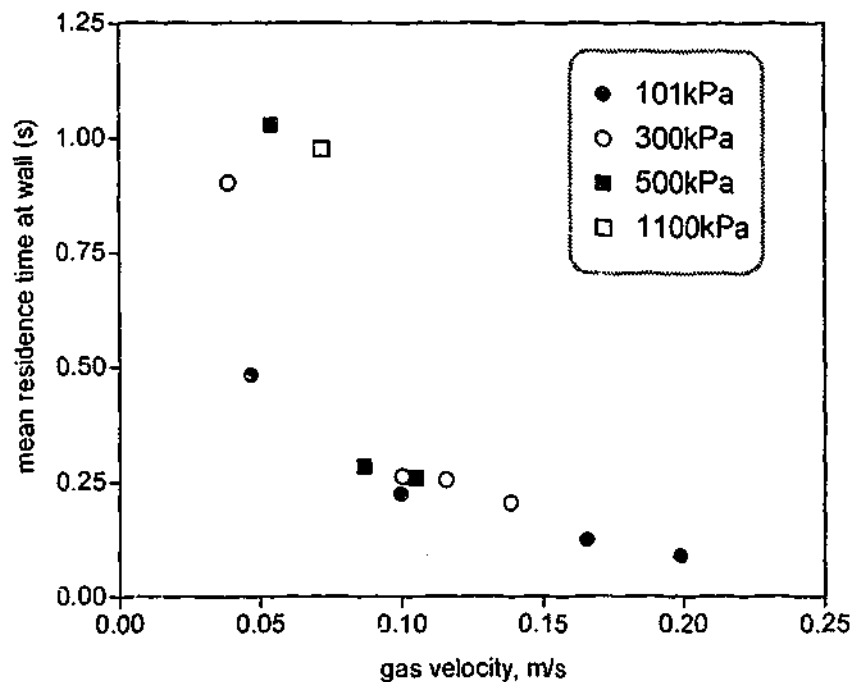


Figure 6-16. Mean time between pigment B particle illumination and departure from the wall versus gas velocity at various operating pressures

For pigment B, the investigated range of superficial gas velocities was much narrower and did not exceed two times U_{mf} at atmospheric pressure. As was found with pigment A, mean residence times measured close to the wall for pigment B were found to decrease with increasing gas velocity (Figure 6-16).

Again, no significant pressure effect on the particle residence times at the wall can be observed in the somewhat limited range of experimental pressures and velocities. However, absolute residence time values again are lower than observed by Molerus and Wirth (1997a) on a similarly sized material.

In their work it is not clear how the illuminated image was distinguished from the background; therefore, applying linear regression to the luminosity decay curve, plotted in semi-log coordinates for the whole image greyscale (0 - 255), as opposed to the non-linear regression for only the visible image threshold, could possibly produce different results.

6.4.4 RELATING WALL CONTACT TIME TO HEAT TRANSFER

In practice, it is common for fluidized beds to contain fixed surfaces to extract heat. For fluidized bed combustion, the important heat transfer surfaces are vertical and horizontal heat transfer tubes immersed in the bed. By using the internal cooling tubes, a large total heat transfer surface can be obtained. The effect of pressure on bed-to-immersed horizontal tube heat transfer has been investigated by Olsson and Almstedt (1995) who found a significant increase in the heat transfer coefficient with increasing the operating pressure.

It should be noted that in this study, both the experimental setup and method did not permit studying heat transfer or particle motion inside the fluidized bed. Instead, the particle motion near to the external fluidized bed wall was studied, which might be more practical for heat transfer in the circulating fluidized beds.

One way of evaluating the impact of the observed mean particle residence times at the wall is to use them in conjunction with the cluster renewal model, developed for bubbling fluidized beds by Mickley and Fairbanks (1955).

Based on this model, it was found that for the particle convective heat transfer component h_{pc} the following equation holds (Zevenhoven et al., 1999):

$$\frac{1}{h_{pc}} = \frac{\delta}{\lambda_g} + \sqrt{\frac{\pi\tau}{\lambda_p \rho_p c_p}} \quad (6.4.5)$$

Where δ equals the distance between illuminated particles and the wall, λ_g is the gas thermal conductivity of this gap, τ is the time during which particles are moving in contact with the wall before moving into the bulk of the bed, and λ_p , ρ_p , c_p are thermal conductivity, density and specific heat capacity of the particles, respectively.

The only gas related parameter in Eq.(6.4.5), gas thermal conductivity λ_g , is independent of pressure for the ideal (perfect) gas. For real gases, however, the gas thermal conductivity is a rather complex function of pressure and temperature, and usually increases with increase in either pressure or temperature (Prokhorov, 1983).

If the illuminated particles stay in contact with the wall for a period of time equal to the mean residence time, it can be assumed that the gap δ is zero. In this case, the particle convective heat transfer component h_{pc} is proportional to $\tau^{0.5}$.

For Geldart A solids, Figure 6-15 shows that at superficial gas velocities below 0.015m/s, the mean residence times slightly decrease with pressure, and therefore, the particle convective heat transfer component is expected to increase slightly with elevated pressure. However, with further increase in gas velocity the mean residence times reach a minimum value and are not influenced by pressure. Thus, the particle convective heat transfer coefficient does reach a maximum in a bubbling bed, which must be dependent only on particle physical properties and not on operating pressure or superficial gas velocity despite the fact that this maximum occurs at a certain gas velocity.

This observation of the pressure effect is in line with findings of other workers (Barreto et al., 1986; Botterill, 1975; Xavier & Davidson, 1985;

Xavier et al., 1980) who did not observe much variation in the particle convective heat transfer for small particles at pressures above atmospheric. According to Borodulya et al. (1991), the weak dependence of the conductive - convective heat transfer coefficient on pressure in fluidized beds of small (less than 1mm) particles is a well-known experimental fact. Although, some researchers would probably disagree (Molerus & Wirth, 1997a).

6.5 PARTICLE MOTION VELOCITY

6.5.1 OBSERVATION OF PARTICLE MOTION PARALLEL TO THE WALL

Solids motion in bubbling fluidized beds is driven by bubbles, which carry particles upward in their drifts and wakes. This upward flow of solids is balanced by a downward solids flow, which occurs in regions where there are no bubbles.

Earlier presented pictures (Figure 6-3 - Figure 6-7) represent the summation of separate frames during the image lifetime and show typical trajectories of the illuminated clusters of particles along the wall surface. Similar observations were made under different operating conditions. As expected, the predominant direction of movement of the illuminated image along the wall was downward.

On each frame, the X-Y coordinates of the centre of gravity of the illuminated image were also obtained. For each image the variation of the centre of gravity in vertical and horizontal direction with time was plotted and analysed. Visual analysis of all the plots representing image motion in vertical direction (downward) and in horizontal direction (sideways) at various operating conditions proved that axial movement was always linear.

Initial X_0 - Y_0 coordinates corresponded to the centre of gravity of the original image at the time of light impulse $t = 0$, and the final X_n - Y_n coordinates described the centre of gravity of the disappearing image at the time equal to the mean residence time $t = \tau$. The distance travelled by the

image during the mean residence time was established as $(X_n - X_0)$ in horizontal direction and as $(Y_n - Y_0)$ in vertical direction.

Axial particle motion velocities were obtained for each light impulse at various operating conditions by dividing these distances by the corresponding mean residence time. Resulting velocities were then averaged according to the operating conditions and plotted.

6.5.2 AXIAL PARTICLE MOTION VELOCITY AT ELEVATED PRESSURES

6.5.2.1 Vertical velocity

The main direction of the illuminated spot movement was downward and the vertical image velocity is plotted in Figure 6-17 for pigment A and in Figure 6-18 for pigment B.

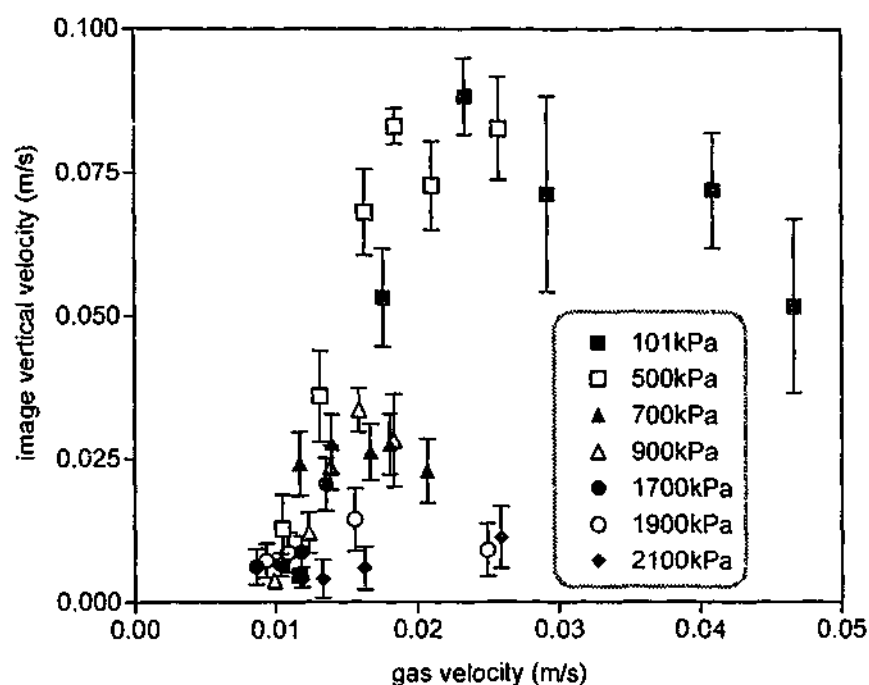


Figure 6-17. Particle motion velocity in vertical direction versus superficial gas velocity at various operating pressures for pigment A

For pigment A, the particle migration velocities U_y along the wall in vertical direction were oriented downward and reached a maximum value of

about 0.08m/s at atmospheric pressure. Similar to results presented in Figure 6-9, after reaching a maximum the vertical velocity at ambient conditions decreases with further increase in superficial gas velocity.

At operating pressures above 500kPa, the particle migration velocities U_y along the wall in vertical direction are much lower than at ambient conditions. Some trend for the vertical motion velocity to decrease with increasing the operating pressure can be observed in Figure 6-17. Similar result can also be qualitatively estimated from the image trajectories presented in Figure 6-3 - Figure 6-7.

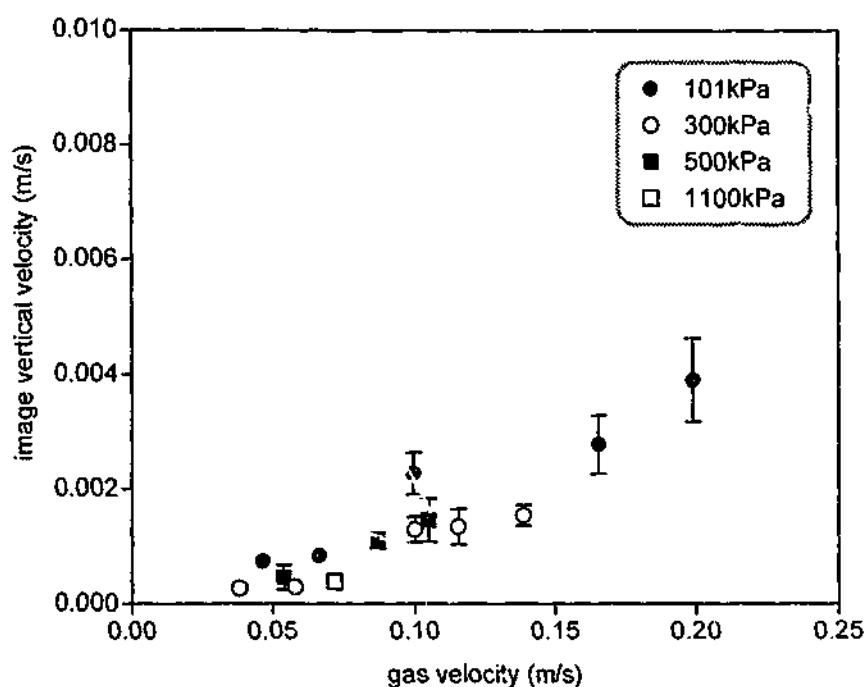


Figure 6-18. Particle motion velocity in vertical direction versus superficial gas velocity at various operating pressures for pigment B

For pigment B, the particle motion velocities U_y along the wall in vertical direction were also oriented downward and reached a maximum value of only about 0.004m/s at atmospheric pressure. Within the studied range, no pressure effect on the vertical particle motion velocity could be established (Figure 6-18).

6.5.2.2 Horizontal velocity

Since the predominant movement of the illuminated image was downward, the particle motion velocity in horizontal direction was much smaller for pigment A (Figure 6-19) and practically nonexistent for pigment B.

This observation is in line with the experimental results of Bellgardt and Werther (1986) who found at ambient conditions in a large fluidized bed that vertical solids mixing was at least one order of magnitude higher than lateral mixing.

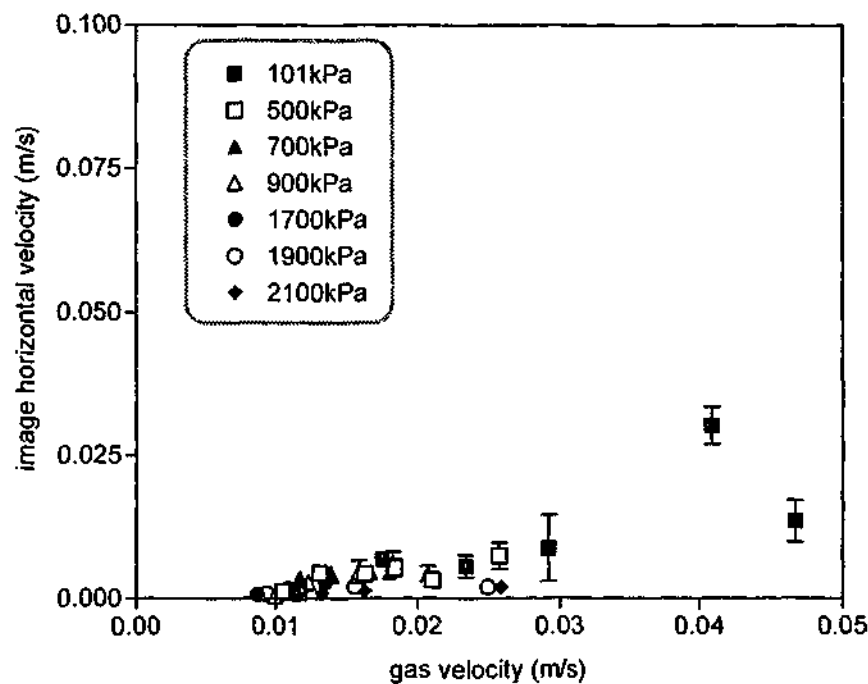


Figure 6-19. Particle motion velocity in horizontal direction versus superficial gas velocity at various operating pressures for pigment A

In bubbling fluidized bed with pigment A as bed material, some apparently random horizontal deviation off the vertical axis was observed while the illuminated image shifted downward. As shown in Figure 6-19, in general lateral particle migration velocities U_x lower than 0.01m/s were measured. Although small by itself, the horizontal movement of the illuminated cluster at operating pressures above 700kPa was less obvious than at ambient conditions.

6.6 SUMMARY

Main factors in the heat transfer between a wall and a fluidized bed are movement of particles close to the wall and their residence time at the wall. Experimental measurement of particle motion in a bubbling fluidized bed can provide a better understanding of wall-to-bed heat transfer. Although of less practical importance for pressurised fluidized bed combustors where the heat transfer takes place inside the bed, this experimental method could be successfully applied to studying bed-to-wall heat transfer in circulating fluidized beds.

The influence of operating pressure, up to 2100kPa, on the motion of Geldart A and B particles near the fluidized bed wall surface was studied using luminescent pigment as bed solids. Digital image analysis was applied to the experimental data with the aim of quantifying the statistics of particle motion near to the wall. Image analysis of the movement of the illuminated cluster of particles gave its statistically determined axial velocities along the surface; and the decay in luminosity defined the particle exchange frequency in the direction perpendicular to the wall surface.

For both Geldart A and B solids, no significant pressure effect on particle residence times at the wall within the vigorously bubbling fluidized bed was established. This observation is in line with findings of other researchers who did not observe much variation in the particle convective heat transfer for small particles at pressures above atmospheric.

Chapter 7

CONCLUSIONS AND RECOMMENDATIONS

Research in the field of fluidization under pressurised operating conditions has been carried out since the 1950s. However, until the energy crisis in the 1970s, apart from a few papers and a book published in Russian, there was very little published information dealing with the influence of pressure on the operation of fluidized bed processes. Since then several industrial processes based on fluidized bed technology and operating at elevated pressure, usually in the range up to 2500kPa, have been developed with various commercial success, so that more feed could be processed without a corresponding increase in the bed size.

With the development of pressurised fluidized bed coal combustion and gasification processes the need for more experimental investigations of fluidization at elevated pressure became clear. Although many academic and industrial researchers have studied the effect of pressure on fluidized bed behaviour, as seen by the large volume of publications in this area since the 1970s, quite often consistent conclusions have not been drawn.

Despite the numerous studies of the pressure effects on fluidization, less than one page of text in total was dedicated to this topic in a well-known textbook on fluidization (Kunii & Levenspiel, 1991). Although some data on the influence of pressure on the hydrodynamic behaviour of fluidized beds have been obtained, the effect of pressure on most fluidization parameters is associated with some degree of controversy.

Yang (1998) noted that in the area of fluidization two completely different situations are present – the area of interest has very little information or it has many studies available with sometimes very different results. In starting the present study both situations were encountered. One of the original objectives was to extend the very brief summary given by Kunii and

Levenspiel (1991) and provide a current overall picture of research in the influence of pressure on fluidized bed behaviour. This objective was addressed in Chapter 2.

Another objective of the project was to experimentally study the influence of elevated operating pressure on fluidization phenomena, such as minimum fluidization and minimum bubbling velocities, bed expansion and voidage, and particle motion near to the fluidized bed wall. Series of experiments were conducted in a bubbling fluidized bed at operating pressures up to 2500kPa with several Geldart A and B bed materials.

Chapter 4 covered the experimental findings of the current study on the influence of pressure on characteristic gas velocity, bed expansion and voidage at both minimum fluidization and minimum bubbling conditions.

It is commonly accepted that the minimum fluidization velocity decreases with increasing pressure and this decrease only becomes significant for larger particles and is generally negligible in fluidized beds of fine Geldart A powders. This view is supported by the experimental results presented in Chapter 4. It is also generally accepted that although the best method to determine the minimum fluidization velocity at different conditions is experimental, another satisfactory approach is to fully characterise the bed solids and to estimate the minimum fluidization velocity by using the Ergun equation.

In order to simplify this task several correlations have been proposed in the literature. Many researchers found these correlations to provide only approximate estimates of the minimum fluidization velocity, suitable for industrial estimation only, since the industrial fluidized bed processes usually operate at velocities well above the minimum fluidization. However, these copious simplified correlations keep appearing in scientific literature where more precise information is required.

Several correlations were used in this study and in general did not predict the experimental values with sufficient accuracy. Instead, it is recommended that better prediction of the minimum fluidization velocity at high pressure

can be achieved by using the Ergun equation and employing a method proposed by Werther (Vogt et al., 2001; Werther, 1977), and based on experimental determination of the minimum fluidization velocity for a given bed material at ambient conditions first.

In the pressure range studied in this work, bed voidage at minimum fluidization was found to be practically independent of pressure for the Geldart A materials and Geldart B sand. However, it was found to increase with increasing pressure for coarse and dense Geldart B pigment B.

By definition the minimum bubbling velocity has the same value as the minimum fluidization velocity for Geldart B and D solids but Geldart A powders have the ability to expand without bubbling at much higher velocities than the minimum fluidization velocity.

It has been implied that with pressure increase Geldart B solids could demonstrate Geldart A type behaviour. In this work, for Geldart B materials non-bubbling fluidization was not observed, and no shift from Geldart B to Geldart A expansion behaviour was observed over the pressure range from atmospheric pressure to 2100kPa. However, for Geldart A powders, the minimum bubbling velocity was experimentally determined.

For both Geldart A materials used the minimum bubbling velocity and the maximum bed expansion ratio were found to be practically unaffected by increasing pressure up to 2100kPa. Existing correlations for predicting the minimum bubbling velocity and the maximum bed expansion ratio did not fit the experimental values very well. In line with observations of other researchers, bed voidage at minimum bubbling was found to increase slightly within the studied pressure range for both powders.

Chapter 5 described the series of experiments carried out in a pressurised bubbling bed in order to measure the mean bed voidage and the dense phase voidage which are important parameters in determining the bed performance. The relatively new non-invasive technique, electrical capacitance tomography (ECT), was used for the first time to study bubbling fluidized bed behaviour at elevated pressures.

Experiments using the ECT equipment were carried out at operating pressures up to 1900kPa with Geldart A FCC catalyst as bed solids. Another series of experiments was conducted at operating pressures up to 2100kPa with Geldart B sand.

Results of the experiments were produced by the ECT system in two types of data, as time series image frames of the local solids volume fraction distribution or time series data points of the average solids volume fraction representing the whole cross-section of the fluidized bed.

Tomographic images obtained from the capacitance measurements are usually of relatively low resolution. Visual analysis of several image frames, based on simple and fast linear back-projection algorithm, was carried out in this work. It confirmed the observations of other researchers that the ECT images were very blurred and only approximate.

Previously many researchers commented on the improvement of fluidization at elevated pressures and on the smoothness of fluidization compared with atmospheric pressure. The usual explanation is that increase in pressure causes the reduction in bubble size. However, evidence of this is conflicting for operation of fluidized beds of coarse particles, appropriate for the pressurised fluidized bed combustors. Regretfully, in the process of fluidization, no individual bubbles could be identified and measured using the existing ECT setup.

Image resolution and accuracy can be improved by using an iterative linear back-projection algorithm, however this process is very time consuming, especially for large files. In this work, no further visualisation and image analysis were carried out because image improvement based on the iterative linear back-projection algorithm, and further frame-by-frame image analysis were considered to be very tedious and technologically prohibitive.

However, the iterative linear back-projection algorithm and other reconstruction algorithms for capacitance tomographic imaging are under development with some encouraging results. This together with constant improvement and cost reduction of computers will most certainly allow in the

nearest future to use the ECT systems for analysis of individual bubbles at various conditions including high pressure.

In this work, some quantitative description of the bubbling bed dynamics at various operating pressures was obtained from time series analysis of fluctuations of the average solids volume fraction. For Geldart A catalyst, it was found that any pressure increase was accompanied by the reduction of the mean bed voidage.

For Geldart B sand, however, the trend was opposite and the pressure increase was accompanied by the increase in the average bed voidage. An increase in bed expansion with pressure in bubbling beds, consisting of Geldart B sand and coal, was also observed by other researchers.

In bubbling beds the main source of voidage fluctuations originates from the formation of bubbles. The intensity of the voidage fluctuations was measured and compared by using the average absolute deviation. The pressure influence on the amplitude of the voidage fluctuations was again different for Geldart A and B materials used in this work.

For Geldart A material, the pressure effect was indicated by the decrease of the average absolute deviation with increasing pressure which meant more uniform bubbling at elevated pressure. For Geldart B material, increasing pressure up to 2100kPa had no effect on the average absolute deviation in voidage fluctuations.

In the bubbling state, the average cycle frequency is considered to be a measure for the time scale of the voidage fluctuations time series. For Geldart A material, the average cycle frequency decreased with increasing operating pressure. This suggested that increasing the operating pressure lead to a less dynamic fluidized bed system in line with other researchers' observations of smoother fluidization for Geldart A materials at high pressure. For Geldart B solids, the average cycle frequency was found to be independent of pressure.

Recently it has been suggested that the irregular behaviour of the fluidized bed dynamics is due to the fact that the fluidized bed is a chaotic non-linear

system, and the deterministic chaos theory could provide numerical and graphical tools to quantify and visualise the fluidized bed hydrodynamics. However, it is still in the development stage and much more work has to be done.

In order to observe the dynamic processes in fluidized beds and be able to apply fully a chaotic time series analysis, it was recommended to acquire time series fluidized bed voidage measurements at an optimum sampling rate of 200 - 300Hz. However, the ECT system used in this work was not capable of a sampling frequency above 90Hz. Taking into consideration this limitation of the equipment, it was accepted that the chaos analysis of the experimental data in this work was not complete.

Apart from the ECT measurements, bed collapse tests were carried out at various pressures up to 1600kPa, using Geldart A FCC catalyst as bed solids. Results of the experiments, presented in Chapter 5, were similar to those of other researchers. The dense phase voidage was found to be higher than the voidage at minimum fluidization and increased steadily with increasing pressure.

A series of extensive studies of the bed-to-immersed surface heat transfer in a pressurised fluidized bed combustor were carried out at Chalmers University of Technology in Sweden in the 1990s. In this work, the influence of operating pressure on the motion of Geldart A and B particles near to the fluidized bed wall, which permits better understanding of the effect of pressure on wall-to-bed heat transfer, was studied using luminescent pigment as bed solids. The experimental results of this study were discussed in Chapter 6.

Highest rates of wall-to-bed heat transfer are obtained when there is rapid exchange of material between the adjacent to the heat transfer region and the bulk of the bed, i.e. when particle residence times at the surface are very short. For Geldart A solids mean residence times measured close to the wall decreased with increasing gas velocity and became practically independent of gas velocity in vigorously bubbling fluidized bed.

The values of the mean residence times settled at below 0.1s, which meant that during the experiments the illuminated images disappeared within only three frames on video and could not be measured with higher accuracy. For Geldart A solids, it was not possible to establish any significant pressure effect on particle residence times at the wall within the vigorously bubbling fluidized bed. This observation is in line with findings of other researchers who did not observe much variation in the particle convective heat transfer for small particles at pressures above atmospheric.

This, however, did not agree well with the experimental data presented by Molerus and Wirth (1997a), whose publication was a basis for the present study. The magnitude of their residence time results was considerably higher than the values measured in the present work. However, contrary to their own claim that the heat transfer clearly depends on pressure and expectations of a similar pressure dependence on particle motion, there was no particular trend in their data.

For dense Geldart B pigment, the investigated range of superficial gas velocities was, unfortunately, much narrower and did not exceed two times minimum fluidization velocity at atmospheric pressure. Again, no significant pressure effect on the particle residence times at the wall could be observed in the somewhat limited range of experimental pressures and velocities. However, absolute residence time values again were much lower than observed by Molerus and Wirth (1997a) on a similarly sized material.

Solids motion in bubbling fluidized beds is driven by bubbles, which carry particles upward in their drifts and wakes. This upward flow of solids is balanced by a downward solids flow, which occurs in regions where there are no bubbles, usually along the bed walls. As expected, the predominant direction of movement of the cluster of illuminated particles along the wall was downward.

For Geldart A pigment, the particle migration velocity along the wall in vertical direction was oriented downward and reached a maximum value of about 0.08m/s at atmospheric pressure, and after reaching the maximum

decreased with further increase in superficial gas velocity. At operating pressures above 500kPa, the particle migration velocities along the wall in vertical direction were observed to be much lower than at ambient conditions.

For Geldart B pigment, the particle motion velocity along the wall in the vertical direction was also oriented downward and reached a maximum value of only about 0.004m/s at atmospheric pressure. Within the limited studied range, no pressure effect on the vertical particle motion velocity could be established.

It is expected that commercial lignite gasification will be carried out in a bubbling fluidized bed with bed solids in a wide range of sizes from 20 μ m to 6mm. In this study, it was found that pressure practically had no effect on bubbling behaviour for Geldart B solids and caused more uniform bubbling for Geldart A solids. The average bed voidage increased with increasing pressure for Geldart B solids and decreased for Geldart A solids. For fine solids, the voidages of dense phase and at minimum bubbling increased with increasing pressure; while the minimum fluidization voidage was found to be independent of pressure. For coarse particles, however, the minimum fluidization voidage was found to increase with increasing pressure.

In conclusion, pressure affects the operation of fluidized beds because, according to the perfect gas law, it directly affects gas density in a system. However, using both well-established and novel techniques in this study, it was confirmed that the influence of pressure on fluidized bed systems cannot be considered independently of particles physical characteristics.

The effects of pressure have been more thoroughly investigated in bubbling fluidized beds with Geldart A and B materials. Because of the gas supply limitations of the experimental setup, it was not possible to study the behaviour of fluidized beds consisting of Geldart D solids. The literature review proved that relatively little attention has been paid to these coarse materials, which is probably because of the higher cost of the larger equipment suitable for such work.

It appears that the future technologies for fluidized bed combustion and gasification of solid fuels are more and more inclined towards the circulating fluidized beds; this is another area that should be addressed in future work on fluidization at elevated pressure.

Appendix A

Operating procedures

(a) Start-up procedure

The primary aim of the start-up procedure is to establish the experimental conditions at elevated pressure safely.

1. Initially, drain valves V5 and V13 are open, all other valves are closed. All pressure gauges show atmospheric pressure. Line filter F1 is clean. Line service unit PCV1 and regulator PCV2 are closed.
2. Switch on power and instrument compressed air supply for digital pressure controller PC and ensure that the controller is set to atmospheric pressure.
3. Close drain valves V5 and V13 and open isolation valves V1 and V2.
4. Slowly open line service unit PCV1 and increase pressure up to operating pressure with a maximum of 600kPa. Check pressure gauges P1, P2 and P4.
5. Set the gas flow path either through flow meter R1 or R2, or R3(4) as appropriate according to flow rates expected during each experiment; and carefully open corresponding flow meter's isolation valve (V10, V11 or V12). Ensure that the relevant flow meter shows no flow.

6. Carefully vary the flow rate with the aid of flow adjusting control valve V9, preventing the float from accelerating up to the upper limit and possibly damaging the measuring section.
7. Using digital back pressure controller PC set required pressure.
8. Observing the controller PC adjust the flow rate as per step 6. After setting the required gas flow rate check pressure gauges P1 and P2 for correct operating pressure.

For experiments carried out at pressures not exceeding 600kPa the start-up procedure is complete at this point. For experiments carried out at higher pressure or when using different from compressed air gas, continue the start-up procedure as follows:

9. Check that gas cylinders are securely clamped in upright position and properly connected.
10. In order to save bottled gas pressurise the system to a maximum pressure (approximately 600kPa) as per steps 1 to 8.
11. Repeat step 7 to set a higher pressure.
12. Reduce flow to zero by adjusting flow control valve V9 and close the relevant flow meter's isolation valve (V10, V11 or V12). Shut down the building compressed air supply by closing valve V2.
13. Check that pressure regulator PCV2 next to the gas cylinder(s) is fully closed.
14. Carefully open cylinder valve until the high pressure gauge of the regulator PCV2 indicates the pressure of the gas in the cylinder, ensuring that the valve is not opened more than necessary. Check joints for leaks using soapy water.

15. Carefully open pressure regulator PCV2 and increase pressure slowly up to required operating pressure, ensuring that it does not exceed 2500kPa.
16. Open isolation valves V6 and V7 and check pressure gauges P1, P2 and P4.
17. Repeat steps 5, 6 and 8.

(b) End of experiment shut-down procedure

1. Close valve V2 if using building compressed air or cylinder(s) valve.
2. Reduce gas flow with flow control valve V9.
3. Using pressure controller PCV3 gradually decrease back pressure in steps of 200kPa to zero.
4. After gas is drained completely through the outlet vent outside, carefully open drain valves V5 and V13 to drain all the inlet and outlet lines.
5. Close all the isolation valves, flow control valve V9, pressure regulator PCV2 and line service unit PCV1.
6. Check that difference in pressure readings between pressure controller PCV3 and pressure gauge P4 is less than 40kPa. If larger, disassembly the filter F1, inspect and clean the element.
7. Switch off the pressure controller PCV3.

(c) Emergency shut-down considerations

Overpressure in the lines may occur due to human error – manual setting of pressure regulator PCV2 to a higher than 2500kPa pressure, or blockage of the gas exit line.

A pressure relief valve V8 is installed outside close to the pressure regulator PCV2 and set at 2600kPa as a primary means of avoiding overpressure of the pressure vessel. Gas exit line is 100mm in diameter, large enough to prevent blockage.

A pressure relief bursting disc is set at 3000kPa and installed on the pressure vessel gas outlet in anticipation of a worst case scenario. A rupture disc is used since under adverse conditions the escaping gas would carry solids, which may foul a conventional relief valve. In emergency situation disconnect gas supply under pressure by closing cylinder valve.

(d) Solids discharge

When required solids are removed from the fluidized bed without disassembly of the pressure vessel using a large industrial vacuum cleaner in the following way:

1. Open the largest port on the top flange of the pressure vessel using a special spanner.
2. Clean internally the vacuum cleaner barrel to prevent contamination.
3. Using 2.5m long copper pipe of 30mm diameter and a vacuum cleaner hose remove solids out of the bed.

Appendix B Curriculum Vitae

EDUCATION

- [1998 - 2003] Monash University Australia
PhD in Chemical Engineering
- [1995 - 1996] Monash University Australia
Graduate Diploma in Engineering Maintenance Management
- [1980 - 1985] Ural State Technical University Russia
1st Class Honours Degree in Mechanical Engineering

PROFESSIONAL EXPERIENCE

- [1997 -1998] Sancell Pty Ltd Springvale, Australia
Project engineer
- [1994 -1996] BHP Steel Pty Ltd Western Port, Australia
Development engineer
- [1992 -1993] Hyatt Continental Montreux, Switzerland
Technician
- [1986 -1991] Combined cement works Sukhoy Log, Russia
Senior mechanical engineer
- [1985 -1986] Combined cement works Sukhoy Log, Russia
Maintenancce engineer

ADDITIONAL PROFESSIONAL ACTIVITIES

Organised the 4th Australian Student Conference on Particle Technology

Attended and presented papers at the 6th World Congress of Chemical Engineering and the World Congress on Particle Technology 4

Laboratory demonstrator and tutor in Thermodynamics at Monash University

Attended courses on Particle Technology, Bulk Materials Handling, Power Generation from Coal, Safety, Project Management, Quality Control and Computer Skills for Engineers and Scientists

Attended seminars and workshops on Pneumatics, Power Transmission, Equipment Alignment and Compressed Air Handling and Filtration

PUBLICATIONS

Sidorenko, I. (1999). *Pressure effects on fluidized bed behaviour* (Literature Review and Progress Report 99026). Mulgrave: CRC for Clean Power from Lignite.

Sidorenko, I., & Rhodes, M. J. (1999). *Pressure effects on fluidized bed behaviour*. Paper presented at the 4th Australian Particle Technology Student Conference, Monash University.

Sidorenko, I., & Rhodes, M. J. (2000). *Pressure effects on fluidized bed behaviour*. Paper presented at the 7th Annual Conference of CRC for Clean Power from Lignite, University of Adelaide.

Sidorenko, I., & Rhodes, M. J. (2001a). *The use of Electrical Capacitance Tomography to study the influence of pressure on fluidized bed behaviour*. Paper presented at the 6th World Congress of Chemical Engineering, Melbourne.

Sidorenko, I., & Rhodes, M. J. (2001b). *The use of tomography to study fluidization under high pressure*. Paper presented at the 8th Annual Conference of CRC for Clean Power from Lignite, Monash University.

Sidorenko, I., & Rhodes, M. J. (2002a). *The influence of pressure on fluidized bed behaviour*. Paper presented at the World Congress on Particle Technology 4, Sydney.

Sidorenko, I., & Rhodes, M. J. (2002b). *Observation of the influence of pressure on particle motion near to the wall of a fluidized bed*. Paper presented at the 9th Annual Conference of CRC for Clean Power from Lignite, Monash University.

PROFESSIONAL MEMBERSHIPS

The Institution of Engineers, Australia

American Society of Mechanical Engineers

References

- Abrahamsen, A. R., & Geldart, D. (1980a). Behavior of gas-fluidized beds of fine powders. Part I. Homogeneous expansion. *Powder Technology*, 26, 35-46.
- Abrahamsen, A. R., & Geldart, D. (1980b). Behavior of gas-fluidized beds of fine powders. Part II. Voidage of the dense phase in bubbling beds. *Powder Technology*, 26, 47-55.
- Adanez, J., & Abanades, J. C. (1991). Minimum fluidization velocities of fluidized-bed coal-combustion solids. *Powder Technology*, 67, 113-119.
- Adlhoeh, W., Sato, H., Wolff, J., & Radtke, K. (2000). *High-temperature Winkler gasification of municipal solid waste*. Paper presented at the Gasification Technologies Conference, San Francisco.
- Agarwal, P. K., Hull, A. S., & Lim, K. S. (1997). Digital image analysis techniques for the study of bubbling fluidized beds. In J. Chaouki, F. Larachi & M. P. Duducovic (Eds.), *Non-Invasive Monitoring of Multiphase Flows* (pp. 407-454). Amsterdam: Elsevier Science.
- Almstedt, A. E., & Olsson, S. E. (1982). *Measurements of bubble behaviour in a pressurized fluidized bed burning coal, using capacitance probes*. Paper presented at the 7th International Conference on Fluidized Bed Combustion, Philadelphia.
- Almstedt, A. E., & Olsson, S. E. (1985). *Measurements of bubble behaviour in a pressurized fluidized bed burning coal, using capacitance probes - Part II*. Paper presented at the 8th International Conference on Fluidized Bed Combustion, Houston.
- Altshuler, V. S., & Sechenov, G. P. (1963). *Processy v kipjashchem sloe pod davleniem (in Russian)*. Moscow: Izdatelstvo Akademii Nauk SSSR.
- Al-Zahrani, A. A., & Daous, M. A. (1985). Bed expansion and average bubble rise velocity in a gas-solid fluidized bed. *Powder Technology*, 87, 255-257.
- Baeyens, J., & Geldart, D. (1974). Predictive calculations of flow parameters in gas fluidized beds and fluidization behavior of various powders. In H. Angelino, J. P. Coudere, H. Gibert & C. Laguerie (Eds.), *Fluidization and its Application* (pp. 263-273). Toulouse: Societe de Chimie Industrielle.
- Bai, D., Issangya, A. S., & Grace, J. R. (1999). Characteristics of gas-fluidized beds in different flow regimes. *Industrial & Engineering Chemistry Research*, 38(3), 803-811.
- Barnea, E., & Mednick, R. L. (1975). Correlation for minimum fluidisation velocity. *Transactions of the Institution of Chemical Engineers*, 53, 278-281.
- Barnea, E., & Mizrahi, J. (1973). Generalized approach to the fluid dynamics of particulate systems. 1. General correlation for fluidization and sedimentation in solid multiparticle systems. *Chemical Engineering Journal*, 5(2), 171-189.

- Barreto, G. F., Lancia, A., & Volpicelli, G. (1986). Heat transfer and fluid dynamic characteristics of gas-fluidized beds under pressure. *Powder Technology*, 46, 155-166.
- Barreto, G. F., Mazza, G. D., & Yates, J. G. (1988). The significance of bed collapse experiments in the characterization of fluidized beds of fine powders. *Chemical Engineering Science*, 43(11), 3037-3047.
- Barreto, G. F., Yates, J. G., & Rowe, P. N. (1983a). The effect of pressure on the flow of gas in fluidized beds of fine particles. *Chemical Engineering Science*, 38(12), 1935-1945.
- Barreto, G. F., Yates, J. G., & Rowe, P. N. (1983b). The measurement of emulsion phase voidage in gas fluidized beds of fine powders. *Chemical Engineering Science*, 38(3), 345-350.
- Baskakov, A. P., & Panov, O. M. (1973). Comparison of maximum coefficients of heat transfer to a surface submerged in a fluidized bed with an estimate obtained from an empirical formula. *Journal of Engineering Physics*, 45(6), 896-901.
- Bellgardt, D., & Werther, J. (1986). A novel method for the investigation of particle mixing in gas-solid systems. *Powder Technology*, 48, 173-180.
- Bin, A. K. (1986). Minimum fluidization velocity at elevated temperatures and pressures. *Canadian Journal of Chemical Engineering*, 64(5), 854-857.
- Bin, A. K. (1992). Minimum fluidization velocity at different conditioning. Comments. *Powder Technology*, 71, 111-111.
- Borodulya, V. A., Ganzha, V. G., & Podbereskii, A. I. (1980). Heat transfer in a fluidized bed at high pressure. In J. R. Grace & J. M. Matsen (Eds.), *Fluidization* (pp. 201-207). New York: Plenum Press.
- Borodulya, V. A., Ganzha, V. L., & Kovensky, V. I. (1982). *Gidrodynamika i teploobmen v psevdoozhizhenom sloye pod davleniem (in Russian)*. Minsk: Nauka i Technika.
- Borodulya, V. A., Teplitsky, Y. S., Markevich, I. I., Hassan, A. F., & Yeryomenko, T. P. (1991). Heat transfer between a surface and a fluidized bed : consideration of pressure and temperature effects. *International Journal of Heat and Mass Transfer*, 34(1), 47-53.
- Botterill, J. S. M. (1975). *Fluid-bed Heat Transfer*. London: Academic Press.
- Botterill, J. S. M. (1989). Fluidized bed behaviour at high temperatures and pressures. In L. K. Doraiswamy & A. S. Mujumdar (Eds.), *Transport in Fluidized Particle Systems* (pp. 33-70). Amsterdam: Elsevier Science.
- Botterill, J. S. M., & Desai, M. (1972). Limiting factors in gas fluidized bed heat transfer. *Powder Technology*, 6, 231.
- Bouratoua, R., Molodtsov, Y., & Koniuta, A. (1993). *Hydrodynamic characteristics of a pressurized fluidized bed*. Paper presented at the 12th International Conference on Fluidized Bed Combustion, La Jolla.
- BP makes leap to VAM fluidised bed process. (1998). *European Chemical News*, November 23-29, 37.

- Brockmeier, N. F. (1987). Gas phase polymerization. In J. I. Kroschwitz (Ed.), *Encyclopedia of Polymer Science and Engineering* (2nd ed., Vol. 7, pp. 480-488). New York: John Wiley & Sons.
- Byars, M. (2001). *Developments in Electrical Capacitance Tomography*. Paper presented at the 2nd World Congress on Industrial Process Tomography, Hannover.
- Cai, P., Chen, S. P., Jin, Y., Yu, Z. Q., & Wang, Z. W. (1989). Effect of operating temperature and pressure on the transition from bubbling to turbulent fluidization. *AIChE Symposium Series*, 85(270), 37-43.
- Cai, P., Schiavetti, M., De Michele, G., Grazzini, G. C., & Miccio, M. (1994). Quantitative estimation of bubble size in PFBC. *Powder Technology*, 80, 99-109.
- Calculation of volume ratio for ECT sensors*. (PTL application note No. AN2)(1999). Wilmslow: Process Tomography Ltd.
- Canada, G. S., & McLaughlin, M. H. (1978). Large particle fluidization and heat transfer at high pressures. *AIChE Symposium Series*, 74(176), 27-37.
- Carsky, M., Hartman, M., Il'enko, B. K., & Makhorin, K. E. (1990). The bubble frequency in a fluidized bed at elevated pressure. *Powder Technology*, 61, 251-254.
- Chan, I. H., & Knowlton, T. M. (1984a). The effect of pressure on entrainment from bubbling gas-fluidized beds. In D. Kunii & R. Toei (Eds.), *Fluidization IV* (pp. 283-290). New York: Engineering Foundation.
- Chan, I. H., & Knowlton, T. M. (1984b). The effect of system pressure on the transport disengaging height (TDH) above bubbling gas-fluidized beds. *AIChE Symposium Series*, 80(241), 24-33.
- Chan, I. H., Sishla, C., & Knowlton, T. M. (1987). The effect of pressure on bubble parameters in gas-fluidized beds. *Powder Technology*, 53, 217-235.
- Cheremisinoff, N. P., & Cheremisinoff, P. N. (1984). Hydrodynamics of fluidization. In *Hydrodynamics of Gas-Solids Fluidization* (pp. 137-206). Houston: Gulf Publishing.
- Chiba, S., Kawabata, J., & Chiba, T. (1986). Characteristics of pressurized gas-fluidized beds. In N. P. Cheremisinoff (Ed.), *Encyclopedia of Fluid Mechanics* (Vol. 4, pp. 929-945). Houston: Gulf Publishing.
- Chitester, D. C., Kornosky, R. M., Fan, L. S., & Danko, J. P. (1984). Characteristics of fluidization at high pressure. *Chemical Engineering Science*, 39(2), 253-261.
- Clift, R., Grace, J. R., & Weber, M. E. (1978). *Bubbles, Drops and Particles*. New York: Academic Press.
- Coudere, J. P. (1985). Incipient fluidization and particulate systems. In J. F. Davidson, R. Clift & D. Harrison (Eds.), *Fluidization* (2nd ed., pp. 1-46). London: Academic Press.
- Creasy, D. E. (1971). Gas fluidisation at pressures and temperatures above ambient. *British Chemical Engineering*, 16(7), 605-610.

- Crowther, M. E., & Whitehead, J. C. (1978). Fluidization of fine particles at elevated pressure. In J. F. Davidson & D. L. Keairns (Eds.), *Fluidization* (pp. 65-70). Cambridge: Cambridge University Press.
- Daw, C. S., & Halow, J. S. (1993). Evaluation and control of fluidization quality through chaotic time series analysis of pressure-drop measurements. *AIChE Symposium Series*, 89(296), 103-122.
- Denloye, A. O. (1982). Bed expansion in a fluidized bed of large particles. *Journal of Powder and Bulk Solids Technology*, 6(3), 11-16.
- Denloye, A. O., & Botterill, J. S. M. (1978). Bed to surface heat transfer in a fluidized bed of large particles. *Powder Technology*, 19, 197-203.
- Draper, N. R., & Smith, H. (1981). *Applied Regression Analysis*. New York: John Wiley & Sons.
- Dyakowski, T. (2002, August 3). [personal communication]. Clayton
- Dyakowski, T., Jeanmeure, L. F. C., & Jaworski, A. J. (2000). Applications of electrical tomography for gas-solids and liquid-solids flows - a review. *Powder Technology*, 112, 174-192.
- Engineering design rules for ECT sensors*. (PTL application note No. AN3)(2001). Wilmslow: Process Tomography Ltd.
- Ergun, S. (1952). Fluid flow through packed columns. *Chemical Engineering Progress*, 48, 89-94.
- Fletcher, J. V., Deo, M. D., & Hanson, F. V. (1993). Fluidization of a multi-sized Group B sand at reduced pressure. *Powder Technology*, 76, 141-147.
- Formisani, B., Girimonte, R., & Pataro, G. (2002). The influence of operating temperature on the dense phase properties of bubbling fluidized beds of solids. *Powder Technology*, 125, 28-38.
- Foscolo, P. U., Di Felice, R., & Gibilaro, L. G. (1987). An experimental study of the expansion characteristics of gas fluidized beds of fine catalysts. *Chemical Engineering and Processing*, 22(2), 69-78.
- Foscolo, P. U., Germana, A., Di Felice, R., De Luca, L., & Gibilaro, L. G. (1989). An experimental study of the expansion characteristics of fluidized beds of fine catalysts under pressure. In J. R. Grace, L. W. Shemilt & M. A. Bergougnou (Eds.), *Fluidization VI* (pp. 187-194). New York: Engineering Foundation.
- Foscolo, P. U., & Gibilaro, L. G. (1984). A fully predictive criterion for the transition between particulate and aggregate fluidization. *Chemical Engineering Science*, 39(12), 1667-1675.
- Foscolo, P. U., Gibilaro, L. G., & Waldram, S. P. (1983). A unified model for particulate expansion of fluidized beds and flow in fixed porous media. *Chemical Engineering Science*, 38(8), 1251-1260.

- Fridland, M. I. (1963). The effect of pressure on productivity and on entrainment of particles in fluidized bed equipment. *International Chemical Engineering*, 3(4), 519-522.
- Geldart, D. (1973). Types of gas fluidization. *Powder Technology*, 7, 285-292.
- Geldart, D. (1986). Single particles, fixed and quiescent beds. In D. Geldart (Ed.), *Gas Fluidization Technology* (pp. 11-32). Chichester: John Wiley & Sons.
- Geldart, D. (1990). Estimation of basic particle properties for use in fluid-particle process calculations. *Powder Technology*, 60, 1-13.
- Geldart, D., & Abrahamsen, A. R. (1978). Homogeneous fluidization of fine powders using various gases and pressures. *Powder Technology*, 19, 133-136.
- Geldart, D., Harnby, N., & Wong, A. C.-Y. (1984). Fluidization of cohesive powders. *Powder Technology*, 37, 25-37.
- Geldart, D., & Radtke, A. L. (1986). The effect of particle properties on the behavior of equilibrium cracking catalysts in standpipe flow. *Powder Technology*, 47, 157-165.
- Geldart, D., & Wong, A. C.-Y. (1985). Fluidization of powders showing degrees of cohesiveness - II. Experiments on rates of de-aeration. *Chemical Engineering Science*, 40(4), 653-661.
- Geldart, D., & Xie, H. Y. (1995). The collapse test as a means for characterizing Group A powders. In J.-F. Large & C. Laguerie (Eds.), *Fluidization VIII (preprints)* (Vol. 1, pp. 263-270). Tours: Engineering Foundation.
- Generation of ECT images from capacitance measurements. (PTL application note No. AN1)(2001). Wilmslow: Process Tomography Ltd.
- Gibilaro, L. G. (2001). *Fluidization-Dynamics*. Oxford: Butterworth-Heinemann.
- Gibilaro, L. G., Di Felice, R., & Foscolo, P. U. (1988). On the minimum bubbling voidage and the Geldart classification for gas-fluidized beds. *Powder Technology*, 56, 21-29.
- Gilbertson, M. A., Cheesman, D. J., & Yates, J. G. (1998). Observations and measurements of isolated bubbles in a pressurized gas-fluidized bed. In L. S. Fan & T. M. Knowlton (Eds.), *Fluidization IX* (pp. 61-68). New York: Engineering Foundation.
- Godard, K., & Richardson, J. F. (1968). The behaviour of bubble-free fluidised beds. *ICHEME Symposium Series*(30), 126-135.
- Gogolek, P. E. G., & Grace, J. R. (1995). Fundamental hydrodynamics related to pressurized fluidized bed combustion. *Progress in Energy and Combustion Science*, 21(5), 419-451.
- Grace, J. R. (1992). Agricola aground: characterization and interpretation of fluidization phenomena. *AIChE Symposium Series*, 88(289), 1-16.
- Grewal, N. S., & Saxena, S. C. (1980). Comparison of commonly used correlations for minimum fluidization velocity of small solid particles. *Powder Technology*, 26, 229-234.

- Guedes de Carvalho, J. R. F. (1981). Dense phase expansion in fluidized beds of fine particles. The effect of pressure on bubble stability. *Chemical Engineering Science*, 36(2), 413-416.
- Guedes de Carvalho, J. R. F., King, D. F., & Harrison, D. (1978). Fluidization of fine particles under pressure. In J. F. Davidson & D. L. Keairns (Eds.), *Fluidization* (pp. 59-64). Cambridge: Cambridge University Press.
- Haider, A., & Levenspiel, O. (1989). Drag coefficient and terminal velocity of spherical and nonspherical particles. *Powder Technology*, 58, 63.
- Halow, J. S. (1997). Electrical capacitance imaging of fluidized beds. In J. Chaouki, F. Larachi & M. P. Duducovic (Eds.), *Non-Invasive Monitoring of Multiphase Flows* (pp. 263-307). Amsterdam: Elsevier Science.
- Halow, J. S., & Nicoletti, P. (1992). Observations of fluidized bed coalescence using capacitance imaging. *Powder Technology*, 69, 255-277.
- Harriott, P., & Simone, S. (1983). Fluidizing fine powders. In N. P. Cheremisinoff & R. Gupta (Eds.), *Handbook of Fluids in Motion* (pp. 653-663). Ann Arbor: Science.
- Hartman, M., & Svoboda, K. (1986). Predicting minimum fluidization velocities for fluidized beds. In N. P. Cheremisinoff (Ed.), *Encyclopedia of Fluid Mechanics* (Vol. 4, pp. 757-780). Houston: Gulf Publishing.
- Hartman, M., & Vesely, V. (1993). Incipient fluidization at different conditions and free-fall velocities of particles. In N. P. Cheremisinoff (Ed.), *Encyclopedia of Fluid Mechanics* (Vol. Suppl. 2, pp. 137-167). Houston: Gulf Publishing.
- Hoffmann, A. C., & Yates, J. G. (1986). Experimental observations of fluidized beds at elevated pressures. *Chemical Engineering Communications*, 41(1-6), 133-149.
- Howard, J. R. (1989). Particles and fluidization. In *Fluidized Bed Technology: Principles and Applications* (pp. 15-69). Bristol: Adam Hilger.
- Isaksen, O. (1996). A review of reconstruction techniques for capacitance tomography. *Measurement Science and Technology*, 7(3), 325-337.
- Isaksen, O., & Nordtvedt, J. E. (1993). A new reconstruction algorithm for process tomography. *Measurement Science and Technology*, 4(3), 1464-1475.
- Jacob, K. V., & Weimer, A. W. (1987). High-pressure particulate expansion and minimum bubbling of fine carbon powders. *AIChE Journal*, 33(10), 1698-1706.
- Johnsson, F., Zijerveld, R. C., Schouten, J. C., van den Bleek, C. M., & Leckner, B. (2000). Characterization of fluidization regimes by time-series analysis of pressure fluctuations. *International Journal of Multiphase Flow*, 26(4), 663-715.
- King, D. F., & Harrison, D. (1980). The bubble phase in high-pressure fluidized beds. In J. R. Grace & J. M. Matsen (Eds.), *Fluidization* (pp. 101-108). New York: Plenum Press.
- King, D. F., & Harrison, D. (1982). The dense phase of a fluidized bed at elevated pressures. *Transactions of the Institution of Chemical Engineers*, 60(1), 26-30.

- Kmiec, A. (1982). Equilibrium of forces in a fluidized bed - experimental verification. *Chemical Engineering Journal*, 23, 133.
- Knowlton, T. M. (1977). High-pressure fluidization characteristics of several particulate solids, primarily coal and coal-derived materials. *AIChE Symposium Series*, 73(161), 22-28.
- Knowlton, T. M. (1999). Pressure and temperature effects in fluid-particle systems. In W. C. Yang (Ed.), *Fluidization Solids Handling and Processing: Industrial Applications* (pp. 111-152). Westwood: Noyes Publications.
- Knowlton, T. M., & Hirsan, I. (1980). The effect of pressure on jet penetration in semicylindrical gas-fluidized beds. In J. R. Grace & J. M. Matsen (Eds.), *Fluidization* (pp. 315-324). New York: Plenum Press.
- Komatsu, H., Maeda, M., & Muramatsu, M. (2001). A large capacity pressurized fluidized bed combustion boiler combined cycle power plant. *Hitachi Review*, 50, 105-109.
- Kuehn, F. T., Schouten, J. C., Mudde, R. F., van den Bleek, C. M., & Scarlett, B. (1996). Analysis of chaos in fluidization using electrical capacitance tomography. *Measurement Science and Technology*, 7(3).
- Kunii, D., & Levenspiel, O. (1991). *Fluidization Engineering* (2nd ed.). Boston: Butterworth-Heinemann.
- Kurkela, E. (2001). *Review of Finnish biomass gasification technologies* (OPET Report No. 4). Espoo: VTT Energy.
- Lettieri, P., Yates, J. G., & Newton, D. (2000). The influence of interparticle forces on the fluidization behavior of some industrial materials at high temperature. *Powder Technology*, 110, 117-127.
- Li, J., & Kuipers, J. A. M. (2001). Effect of pressure on flow behaviors in dense gas-fluidized beds: a discrete particle simulation study. In M. Kwauk, J. Li & W. C. Yang (Eds.), *Fluidization X* (pp. 389-396). New York: United Engineering Foundation.
- Lippens, B. C., & Mulder, J. (1993). Prediction of the minimum fluidization velocity. *Powder Technology*, 75, 67-78.
- Llop, M. F., Casal, J., & Arnaldos, J. (1995). Incipient fluidization and expansion in fluidized beds operated at high pressure and temperature. In J.-F. Large & C. Laguerie (Eds.), *Fluidization VIII* (Vol. 1, pp. 131-138). New York: Engineering Foundation.
- Llop, M. F., Casal, J., & Arnaldos, J. (2000). Expansion of gas-solid fluidized beds at pressure and high temperature. *Powder Technology*, 107, 212-225.
- Llop, M. F., Madrid, F., Arnaldos, J., & Casal, J. (1996). Fluidization at vacuum conditions. A generalized equation for the prediction of minimum fluidization velocity. *Chemical Engineering Science*, 51(23), 5149-5157.
- Loomis, A. W. (Ed.). (1980). *Compressed Air and Gas Data* (3rd ed.). New Jersey: Ingersoll-Rand.

- Louge, M. (1997). Experimental techniques. In J. R. Grace, A. A. Avidan & T. M. Knowlton (Eds.), *Circulating Fluidized Beds* (pp. 312-368). London: Blackie.
- Makkawi, Y. T., & Wright, P. C. (2001). *Application of process tomography as a tool for better understanding of fluidization quality in a conventional fluidized bed*. Paper presented at the 2nd World Congress on Industrial Process Tomography, Hannover.
- Makkawi, Y. T., & Wright, P. C. (2002). Optimization of experiment span and data acquisition rate for reliable electrical capacitance tomography measurement in fluidization studies - a case study. *Measurement Science and Technology*, 13(in press), 1-11.
- Marzocchella, A., & Salatino, P. (2000). Fluidization of solids with CO₂ at pressures from ambient to supercritical. *AIChE Journal*, 46(5), 901-910.
- May, W. G., & Russell, F. R. (1953). *High-pressure fluidization*. Paper presented at the New Jersey Section of the American Chemical Society Meeting-in-Miniature.
- Mellor, M., & Hawkes, I. (1971). Measurement of tensile strength by diametral compression of discs and annuli. *Engineering Geology*, 5, 173-225.
- Mickley, H. S., & Fairbanks, D. F. (1955). Mechanism of heat transfer to fluidized beds. *AIChE Journal*, 1(3), 374-384.
- Miller, G., Kolar, A., Zakkay, V., & Hakim, S. (1981). Bed expansion studies and slugging characteristics in a pressurized fluidized bed of large particles. *AIChE Symposium Series*, 77(205), 166-173.
- Molerus, O., & Wirth, K.-E. (1997a). Particle migration at solid surfaces and heat transfer in bubbling fluidized beds. In *Heat Transfer in Fluidized Beds* (pp. 5-17). London: Chapman & Hall.
- Molerus, O., & Wirth, K.-E. (1997b). Prediction of minimum fluidization velocity. In *Heat Transfer in Fluidized Beds* (pp. 48-50). London: Chapman & Hall.
- Motulsky, H. J. (1996). *Intuitive Biostatistics*. Oxford: University Press.
- Nakamura, M., Hamada, Y., Toyama, S., Fouda, A. E., & Capes, C. E. (1985). An experimental investigation of minimum fluidization velocity at elevated temperatures and pressures. *Canadian Journal of Chemical Engineering*, 63(1), 8-13.
- Olowson, P. A., & Almstedt, A. E. (1990). Influence of pressure and fluidization velocity on the bubble behavior and gas flow distribution in a fluidized bed. *Chemical Engineering Science*, 45(7), 1733-1741.
- Olowson, P. A., & Almstedt, A. E. (1991). Influence of pressure on the minimum fluidization velocity. *Chemical Engineering Science*, 46(2), 637-640.
- Olowson, P. A., & Almstedt, A. E. (1992). Hydrodynamics of a bubbling fluidized bed: influence of pressure and fluidization velocity in terms of drag force. *Chemical Engineering Science*, 47(2), 357-366.
- Olsson, S. E., & Almstedt, A. E. (1995). Local instantaneous and time-averaged heat transfer in a pressurized fluidized bed with horizontal tubes: influence of pressure,

- fluidization velocity and tube-bank geometry. *Chemical Engineering Science*, 50(20), 3231-3245.
- Pai, D. H. (1995). Advanced pressurized fluidized-bed combustion: Basic concept, repowering potential and applicability to the China market. *Heat Engineering, Winter*, 2-15.
- Pell, M. (1990). *Gas Fluidization*. Amsterdam: Elsevier Science.
- Pemberton, S. T., & Davidson, J. F. (1984). Elutriation of fine particles from bubbling fluidized beds. In D. Kunii & R. Toei (Eds.), *Fluidization IV* (pp. 275-282). New York: Engineering Foundation.
- Piepers, H. W., Cottaar, E. J. E., Verkooijen, A. H. M., & Rietema, K. (1984). Effects of pressure and type of gas on particle-particle interaction and the consequences for gas-solid fluidization behavior. *Powder Technology*, 37, 55-70.
- Piepers, H. W., & Rietema, K. (1989). Effects of pressure and type of gas on gas-solid fluidization behaviour. In J. R. Grace, L. W. Shemilt & M. A. Bergougnou (Eds.), *Fluidization VI* (pp. 203-210). New York: Engineering Foundation.
- Poletto, M., Salatino, P., & Massimilla, L. (1993). Fluidization of solids with carbon dioxide at pressures and temperatures ranging from ambient to nearly critical conditions. *Chemical Engineering Science*, 48(3), 617-621.
- Frokhov, A. M. (Ed.). (1983). *Fizicheskii Encyclopedicheskii Slovar (in Russian)*. Moscow: Sovetskaya Encyclopaedia.
- Rhodes, M. J. (1998). Fluidization. In *Introduction to Particle Technology* (pp. 97-138). Chichester: John Wiley & Sons.
- Rhodes, M. J., Wang, X. S., Forsyth, A. J., Gan, K. S., & Phadtajaphan, S. (2001). Use of a magnetic fluidized bed in studying Geldart Group B to A transition. *Chemical Engineering Science*, 56, 5429-5436.
- Richardson, J. F., & Zaki, W. T. (1954). Sedimentation and fluidisation. Part 1. *Transactions of the Institution of Chemical Engineers*, 32, 35.
- Rietema, K. (1967). Application of mechanical stress theory to fluidization. In A. A. H. Drinkenburg (Ed.), *Proceedings of the International Symposium on Fluidization* (pp. 154). Amsterdam: Netherlands University Press.
- Rietema, K. (1991). *The Dynamics of Fine Powders*. London: Elsevier Applied Science.
- Rietema, K., Cottaar, E. J. E., & Piepers, H. W. (1993). The effect of interparticle forces on the stability of gas-fluidized beds. II. Theoretical derivation of bed elasticity on the basis of van der Waals forces between powder particles. *Chemical Engineering Science*, 48(9), 1687-1697.
- Rietema, K., & Piepers, H. W. (1990). The effect of interparticle forces on the stability of gas-fluidized beds - I. Experimental evidence. *Chemical Engineering Science*, 45(6), 1627-1639.

- Roberts, A. G., Pillai, K. K., & Stantan, J. E. (1983). Pressurized fluidized combustion. In J. R. Howard (Ed.), *Fluidized Beds: Combustion and Applications* (pp. 171-197). London: Applied Science.
- Rowe, P. N. (1984). The effect of pressure on minimum fluidization velocity. *Chemical Engineering Science*, 39(1), 173-174.
- Rowe, P. N. (1986). Letters to the editor. *AIChE Journal*, 32(5), 877.
- Rowe, P. N. (1987). Effect of pressure on the minimum bubbling velocity of polydisperse materials. Comments. *Chemical Engineering Science*, 42(2), 387-388.
- Rowe, P. N. (1989). The dense phase voidage of fine powders fluidised by gas and its variation with temperature, pressure and particle size. In J. R. Grace, L. W. Shemilt & M. A. Bergougnou (Eds.), *Fluidization VI* (pp. 195-202). New York: Engineering Foundation.
- Rowe, P. N., Foscolo, P. U., Hoffmann, A. C., & Yates, J. G. (1982). Fine powders fluidized at low velocity at pressures up to 20 bar with gases of different viscosity. *Chemical Engineering Science*, 37(7), 1115-1117.
- Rowe, P. N., Foscolo, P. U., Hoffmann, A. C., & Yates, J. G. (1984). X-ray observation of gas fluidized beds under pressure. In D. Kunii & R. Toei (Eds.), *Fluidization IV* (pp. 53-60). New York: Engineering Foundation.
- Rowe, P. N., & MacGillivray, H. J. (1980). A preliminary X-ray study of the effect of pressure on a bubbling gas fluidised bed. In *Fluidised Combustion: Systems and Applications* (Vol. 3, pp. IV-1 (1-9)). London: Institute of Energy.
- Saxena, S. C., & Shrivastava, S. (1990). The influence of an external magnetic field on an air-fluidized bed of ferromagnetic particles. *Chemical Engineering Science*, 45(4), 1125-1130.
- Saxena, S. C., & Vogel, G. J. (1977). The measurement of incipient fluidization velocities in a bed of coarse dolomite at temperature and pressure. *Transactions of the Institution of Chemical Engineers*, 55(3), 184-189.
- Schouten, J. C., Takens, F., & van den Bleek, C. M. (1994a). Estimation of the dimension of a noisy attractor. *Physical Review E*, 50(3), 1851-1861.
- Schouten, J. C., Takens, F., & van den Bleek, C. M. (1994b). Maximum-likelihood estimation of the entropy of an attractor. *Physical Review E*, 49(1), 126-129.
- Schouten, J. C., & van den Bleek, C. M. (1991). Chaotic behavior in a hydrodynamic model of a fluidized bed reactor. *Proc. Int. Conf. Fluid. Bed Combust.*, 11th(Vol. 1), 459-466.
- Schouten, J. C., & van den Bleek, C. M. (1998). Monitoring the quality of fluidization using the short-term predictability of pressure fluctuations. *AIChE Journal*, 44(1), 48-60.
- Schouten, J. C., van der Stappen, M. L. M., & van den Bleek, C. M. (1996). Scale-up of chaotic fluidized bed hydrodynamics. *Chemical Engineering Science*, 51(10), 1991-2000.

- Schweitzer, J., & Molerus, O. (1988). Bubble flow in pressurized gas/solid fluidized beds. *Particulate Science and Technology*, 6(3), 285-304.
- Sciazko, M., & Bandrowski, J. (1985). Effect of pressure on the minimum bubbling velocity of polydisperse materials. *Chemical Engineering Science*, 40(10), 1861-1869.
- Sciazko, M., & Bandrowski, J. (1987). Effect of pressure on the minimum bubbling velocity of polydisperse materials. Reply to comments. *Chemical Engineering Science*, 42(2), 388.
- Scott, D., & Carpenter, A. M. (1996). *Advanced power systems and coal quality* (Report No. IEACR/87). London: IEA Coal Research.
- Shrivastava, S., Mathur, A., & Saxena, S. C. (1986). On the determination of minimum fluidization velocity by the method of Yang et al. *AIChE Journal*, 32(7), 1227-1229.
- Sobreiro, L. E. L., & Monteiro, J. L. F. (1982). The effect of pressure on fluidized bed behavior. *Powder Technology*, 33, 95-100.
- Steiner, C., Kameda, O., Oshita, T., & Sato, T. (2002). *EBARA's fluidized bed gasification: atmospheric 2x225 t/d for shredding residues recycling and two-stage pressurized 30 t/d for ammonia synthesis from waste plastics*. Paper presented at the 2nd International Symposium on Feedstock Recycling of Plastics, Oostende
- Subzwari, M. P., Clift, R., & Pyle, D. L. (1978). Bubbling behavior of fluidized beds at elevated pressures. In J. F. Davidson & D. L. Keairns (Eds.), *Fluidization* (pp. 50-54). Cambridge: Cambridge University Press.
- Svarovsky, L. (1987). *Powder Testing Guide: Methods of Measuring the Physical Properties of Bulk Powders*. London: Elsevier Applied Science.
- Table 2-229 Thermophysical properties of compressed air. (1997). In D. W. Green (Ed.), *Perry's Chemical Engineers' Handbook* (7th ed., pp. 2-208). Sydney: McGraw-Hill.
- Thonglimp, V., Hiquily, N., & Laguerie, C. (1984). Vitesse minimale de fluidisation et expansion des couches fluidisees par un gaz (in French). *Powder Technology*, 38, 233-253.
- Tsukada, M., Nakanishi, D., & Horio, M. (1993). The effect of pressure on the phase transition from bubbling to turbulent fluidization. *International Journal of Multiphase Flow*, 19(1), 27-34.
- UK Department of Trade and Industry. (1972). *Viscosity of Gases in Metric Units*. Edinburgh: Her Majesty's Stationery Office.
- UK Department of Trade and Industry. (1998). *Gasification of solid and liquid fuels for power generation* (Technology Status Report No. TSR 008). London.
- UK Department of Trade and Industry. (1999). *Cleaner coal technologies: Options*. London.
- UK Department of Trade and Industry. (2000). *Fluidised Bed Combustion systems for power generation and other industrial applications* (Technology Status Report No. TSR 011). London.

- US Department of Energy. (1996). *Clean Coal Technology: The Pinon Pine Power Project* (Topical Report No. 8). Washington DC.
- US Department of Energy. (1999). *Market-based Advanced Coal Power Systems* (Final Report No. DOE/FE-0400). Washington DC.
- van den Bleek, C. M., Coppens, M.-O., & Schouten, J. C. (2002). Application of chaos analysis to multiphase reactors. *Chemical Engineering Science*, 57, 4763-4778.
- van der Stappen, M. L. M., Schouten, J. C., & van den Bleek, C. M. (1993a). Application of deterministic chaos theory in understanding the fluid dynamic behavior of gas-solids fluidization. *AIChE Symposium Series*, 89(296), 91-102.
- van der Stappen, M. L. M., Schouten, J. C., & van den Bleek, C. M. (1993b). *Deterministic chaos analysis of the dynamical behaviour of slugging and bubbling fluidized beds*. Paper presented at the 12th International Conference on Fluidized Bed Combustion, La Jolla.
- Varadi, T., & Grace, J. R. (1978). High pressure fluidization in a two-dimensional bed. In J. F. Davidson & D. L. Keairns (Eds.), *Fluidization* (pp. 55-58). Cambridge: Cambridge University Press.
- Vogt, C., Schreiber, R., Werther, J., & Brunner, G. (2001). Fluidization at supercritical fluid conditions. In M. Kwauk, J. Li & W. C. Yang (Eds.), *Fluidization X* (pp. 117-124). New York: United Engineering Foundation.
- Vogt, C., Schreiber, R., Werther, J., & Brunner, G. (2002). *The expansion behavior of fluidized beds at supercritical fluid conditions*. Paper presented at the World Congress on Particle Technology 4, Sydney.
- Wang, S. J., Dyakowski, T., Xie, C. G., Williams, R. A., & Beck, M. S. (1995). Real time capacitance imaging of bubble formation at the distributor of a fluidized bed. *Chemical Engineering Journal*, 56(3), 95-100.
- Wang, Y., Wei, F., Jin, Y., & Luo, T. (2001). Bed collapse behavior of primary nanoparticles. In M. Kwauk, J. Li & W. C. Yang (Eds.), *Fluidization X* (pp. 477-484). New York: United Engineering Foundation.
- Weimer, A. W. (1986). Letters to the editor. *AIChE Journal*, 32(5), 877-878.
- Weimer, A. W., & Jacob, K. V. (1986). On bed voidage and apparent dilute phase hold-up in high pressure-turbulent fluidized beds of fine powders. In K. Ostergaard & A. Sorensen (Eds.), *Fluidization V* (pp. 313-320). New York: Engineering Foundation.
- Weimer, A. W., & Quarderer, G. J. (1985). On dense phase voidage and bubble size in high pressure fluidized beds of fine powders. *AIChE Journal*, 31(6), 1019-1028.
- Wen, C. Y., & Yu, Y. H. (1966a). A generalized method for predicting the minimum fluidization velocity. *AIChE Journal*, 12(3), 610-612.
- Wen, C. Y., & Yu, Y. H. (1966b). Mechanics of fluidization. *Chemical Engineering Progress Symposium Series*, 62(62), 100-111.

- Werther, J. (1977). Stromungsmechanische Grundlagen der Wirbelschichttechnik (in German). *Chemie Ingenieur Technik*, 49(3), 193-202.
- White, F. M. (1994). *Fluid Mechanics* (3rd ed.). New York: McGraw-Hill.
- Wimam, J., & Almstedt, A. E. (1998). Influence of pressure, fluidization velocity and particle size on the hydrodynamics of a freely bubbling fluidized bed. *Chemical Engineering Science*, 53(12), 2167-2176.
- Xavier, A. M., & Davidson, J. F. (1985). Convective heat transfer in fluidized beds. In J. F. Davidson, R. Clift & D. Harrison (Eds.), *Fluidization* (2nd ed., pp. 450). London: Academic Press.
- Xavier, A. M., King, D. F., Davidson, J. F., & Harrison, D. (1980). Surface-bed heat transfer in a fluidized bed at high pressure. In J. R. Grace & J. M. Matsen (Eds.), *Fluidization* (pp. 209-216). New York: Plenum Press.
- Xianglin, S., Najun, Z., & Yiqian, X. (1991). Experimental study on heat transfer in a pressurized circulating fluidized bed. In P. Basu, M. Horio & M. Hasatani (Eds.), *Circulating Fluidized Bed Technology III* (pp. 451-456). Oxford: Pergamon Press.
- Yang, W. C. (1981). Jet penetration in a pressurized fluidized bed. *Industrial & Engineering Chemistry Fundamentals*, 20(3), 297-300.
- Yang, W. C. (1998). 30-years of industrial research on fluidization - bridging the gap between theory and practice. In L. S. Fan & T. M. Knowlton (Eds.), *Fluidization IX* (pp. 31-43). New York: Engineering Foundation.
- Yang, W. C., Chitester, D. C., Kornosky, R. M., & Keairns, D. L. (1985). A generalized methodology for estimating minimum fluidization velocity at elevated pressure and temperature. *AIChE Journal*, 31(7), 1086-1092.
- Yates, J. G. (1996). Review article number 49. Effects of temperature and pressure on gas-solid fluidization. *Chemical Engineering Science*, 51(2), 167-205.
- Yates, J. G. (1997). Experimental observations of voidage in gas fluidized beds. In J. Chaouki, F. Larachi & M. P. Duducovic (Eds.), *Non-Invasive Monitoring of Multiphase Flows* (pp. 141-160). Amsterdam: Elsevier Science.
- Yates, J. G., Bejcek, V., & Cheesman, D. J. (1986). Jet penetration into fluidized beds at elevated pressures. In K. Ostergaard & A. Sorensen (Eds.), *Fluidization V* (pp. 79-86). New York: Engineering Foundation.
- Yates, J. G., & Simons, S. J. R. (1994). Experimental methods in fluidization research. *International Journal of Multiphase Flow*, 20(Suppl.), 297-330.
- Zenz, F. A. (1997). Fluidization phenomena and fluidized bed technology. In M. E. Fayed & L. Otten (Eds.), *Handbook of Powder Science & Technology* (2nd ed.). New York: Chapman & Hall.
- Zevenhoven, R., Kohlman, J., Laukkanen, T., Tuominen, M., & Blomster, A.-M. (1999). *Near-wall particle velocity and concentration measurements in circulating fluidised*

beds in relation to heat transfer. Paper presented at the 15th International Conference on Fluidized Bed Combustion, Savannah.

Zijerveld, R. C., Johnsson, F., Marzocchella, A., Schouten, J. C., & van den Bleek, C. M. (1998). Fluidization regimes and transitions from fixed bed to dilute transport flow. *Powder Technology*, 95, 185-204.